NOVEMBER 2018 Ph.D. in Civil Engineering MOHAMMED SAKIB AL JAWAHERY

UNIVERSITY OF GAZİANTEP
GRADUATE SCHOOL OF
NATURAL & APPLIED SCIENCES

EXPERIMENTAL INVESTIGATION AND FINITE ELEMENT MODELING OF REHABILITATED AND STEEL FIBER RC MEMBERS

Ph.D THESIS

IN

CIVIL ENGINEERING

BY

MOHAMMED SHAKIB AL JAWAHERY

NOVEMBER 2018

Experimental Investigation and Finite Element Modeling of Rehabilitated and Steel Fiber RC Members

Ph.D. Thesis

in

Civil Engineering

University of Gaziantep

Supervisor
Prof. Dr. Abdulkadir ÇEVİK
Co-Supervisor
Assist. Prof. Dr. Mehmet Eren GÜLŞAN

by

Mohammed Shakib AL JAWAHERY

November 2018

REPUBLIC OF TURKEY
UNIVERSITY OF GAZİANTEP
GRADUATE SCHOOL OF NATURAL & APPLIED SCIENCES
CIVIL ENGINEERING DEPARTMENT

Name of the thesis: Experimental Investigation and Finite Element Modeling of Rehabilitated and Steel Fiber RC Members

Name of the student: Mohammed Shakib Mohammed AL JAWAHERY

Exam date: November 06, 2018

Approval of the Graduate School of Natural and Applied Sciences.

Prof. Dr. A. Necmeddin YAZICI
Director

I certify that this thesis satisfies all the requirements as a thesis for the degree of Doctor of Philosophy.

Prof. Dr. Hanifi ÇANAKCI
Head of Department

This is to certify that we have read this thesis and that in our opinion it is fully adequate, in scope and quality, as a thesis for the degree of Doctor of Philosophy.

Assist. Prof. Dr. Mehmet Eren GÜLŞAN Co. Supervisor	Prof. Dr. Abdulkadir ÇEVİK Supervisor

Examining Committee Members:	Signature
Prof. Dr. Abdulkadir ÇEVİK	………………………….
Prof. Dr. İbrahim H. GÜZELBEY	…………………………
Assoc. Prof. Dr. Amjad KHABAZ	…………………………
Assist. Prof. Dr. M. Tolga GÖĞÜŞ	…………………………
Assist. Prof. Dr. Hüseyin Çağan KILINÇ	…………………………

I hereby declare that all information in this document has been obtained and presented in accordance with academic rules and ethical conduct. I also declare that, as required by these rules and conduct, I have fully cited and referenced all material and results that are not original to this work.

Mohammed Shakib AL JAWAHERY

ABSTRACT

Experimental Investigation and Finite Element Modeling of Rehabilitated and Steel Fiber RC Members

AL JAWAHERY, Mohammed
Ph.D. Thesis in Civil Engineering
Supervisor: Prof. Dr. Abdulkadir ÇEVİK
Co. Supervisor: Assist. Prof. Dr. Mehmet Eren GÜLŞAN
November 2018
178 pages

This thesis consists of four essential parts which investigate the mechanical behavior of rehabilitated reinforced concrete haunched beams (RCHBs) and rehabilitated reinforced concrete corbels (RCCs) in addition to the behavior of steel fiber reinforced concrete haunched beams (SF RCHBs). The main objective of the first and second part are to investigate the behavior of reinforced concrete haunched beams after being rehabilitated by Basalt Fiber Fabric (BFF) and Carbon Fiber Reinforced Polymer (CFRP) Fabric. These parts consist of two studies; experimental and the finite element (FE) modeling studies. The experimental study consists of loading tests of 24 different rehabilitated RCHBs which had failed in shear and flexural mode beforehand. In the second study, a new FE based technique is proposed to form a zone that exhibits all possible load capacities of rehabilitated RCHBs. The results show that there is a nearly perfect agreement between tested RCHBs and the maximum limit of strengthened RCHBs regarding ultimate load capacity. The main objective of the third part of this thesis is to investigate the effectiveness of the steel fiber, which is used to resist shear loads instead of stirrups, on the mechanical behavior of RCHBs. Moreover, effects of main steel reinforcement, compressive strength, and the inclination angle of RCHBs on the behavior of steel fiber reinforced concrete haunched beams (SF RCHBs) are researched in this part. 81 FE models were prepared for this purpose. The parametric study was carried out to clarify the effect of each parameter on the behavior of SF RCHBs. Parametric results show that the effective inclination angle of the haunched beam is 10º regarding shear load capacity. The last part of this thesis investigates the behavior of normal and self-compacted steel fiber reinforced concrete corbels (SF RCCs) rehabilitated by Basalt Fiber Mesh (BFM) and Basalt Fiber Fabric (BFF). The experimental program includes totally 60 corbels. Test results show that there is no any increase in load capacity of the RC corbels rehabilitated by BFM without crack repair. Moreover, it can be concluded that the use of BFF is an effective and powerful technique for the rehabilitation of damaged RC corbels.

Keywords: Rehabilitation, Reinforced Concrete Haunched Beams, Reinforced Concrete Corbels, Steel Fiber, Basalt Fiber Mesh, Basalt Fiber Fabric, Finite Element Analysis.

ÖZET

REHABİLİTE EDİLMİŞ ÇELİK LİF KATKILI BETONARME ELEMANLARIN DENEYSEL ARAŞTIRMASI VE SONLU ELEMANLAR MODELLEMESİ

AL JAWAHERY, Mohammed
Doktora Tezi, İnşaat Mühendisliği
Tez Danışmanı: Prof. Dr. Abdulkadir ÇEVİK
Yardımcı Tez Danışmanı: Dr. Öğr. Üyesi Mehmet Eren GÜLŞAN
Kasım 2018
178 sayfa

Bu tez çelik lif takviyeli değişken kesitli kirişlerin mekanik davranışının yanında rehabilite edilmiş betonarme değişken kesitli kirişlerin ve rehabilite edilmiş betonarme kısa konsolların mekanik davranışını araştıran 4 önemli bölümden oluşmaktadır. Birinci ve ikinci bölümlerin asıl amaçları Bazalt Lif Takviyeli ve Karbon Lif Takviyeli Polimer kumaşlarla rehabilite edilmiş betonarme değişken kesitli kirişlerin mekanik davranışını araştırmaktır. Bu bölümler iki çalışmadan oluşmaktadır; deneysel ve sonlu elemanlar yöntemi ile modelleme çalışmaları. Deneysel çalışma daha önceden kesmeden ve eğilmeden göçmüş birbirinden farklı 24 adet rehabilite edilmiş değişken kesitli kirişin yükleme testlerinden oluşmaktadır. İkinci çalışmada, rehabilite edilmiş betonarme değişken kesitli kirişlerin bütün olası yük taşıma kapasitelerini gösteren bir bölge oluşturmak için sonlu elemanlar yöntemi tabanlı yeni bir teknik önerilmiştir. Sonuçlar test edilmiş değişken kesitli kirişlerle güçlendirilmiş değişken kesitli kirişlerin maksimum limitleri arasında nihai yük kapasitesi açısından mükemmele yakın bir uyum olduğunu göstermiştir. Tezin üçüncü bölümünün asıl amacı kesme kuvvetlerine karşı dayanım sağlayan etriye yerine çelik liflerin değişken kesitli kirişlerin mekanik davranışı üzerindeki etkinliğini araştırmaktır. Ayrıca, bu bölümde asal donatının, basınç mukavemetinin ve kiriş eğim açısının çelik lif katkılı değişken kesitli kirişlerin davranışı üzerindeki etkisi araştırılmıştır. Bu amaç için 81 adet sonlu elemanlar modeli hazırlanmıştır. Her bir parametrenin çelik lif katkılı değişken kesitli kirişler üzerindeki etkisini belirlemek için parametrik çalışma yapılmıştır. Parametrik sonuçlar kesme yükü kapasitesi bakımından en etkili eğim açısının 10^{o} olduğunu göstermiştir. Tezin son bölümü Bazalt Lif Örgü ve Bazalt Lif Takviyeli Polimer Kumaşla rehabilite edilmiş normal ve kendiliğinden yerleşen betonla üretilmiş kısa konsolların davranışını araştırmaktadır. Deney programı toplam 60 adet kısa konsolu kapsamaktadır. Test sonuçları çatlak tamiri olmaksızın sadece bazalt lif örgüsü ile rehabilite edilen kısa konsolların yük taşıma kapasitelerinde bir artış olmadığını göstermiştir. Ayrıca, bazalt lif takviyeli polimer kumaş kullanımının hasar görmüş betonarme kısa konsolların rehabilitasyonu için etkin ve güçlü bir teknik olduğu sonucuna varılmıştır.

Anahtar Kelimeler: Rehabilitasyon, Betonarme Değişken Kesitli Kiriş, Betonarme Kısa Konsol, Çelik Lif, Bazalt Lif Örgüsü, Bazalt Lif Takviyeli Polimer Kumaş, Sonlu Elemanlar Analizi.

To my family

ACKNOWLEDGEMENTS

First and foremost, I must begin by expressing my tremendous appreciation and respect for my supervisor, **Prof. Abdulkadir ÇEVİK**, Thank you for your support, guidance, and patience during my graduate studies. I am grateful to have had the opportunity to learn from your scientific experiences and invaluable help with all aspects of this thesis as well as the future possible publication of the journal paper.

Special acknowledgment to my Co-Supervisor **Assist. Prof. Dr. Mehmet Eren GÜLŞAN** for his valuable comments, helps, and suggestions during my staying at Gaziantep University.

My sincere thanks also go to the Instructors of the civil engineering department and all my friends whose helped me in all stages of my study.

I would also like to thank my committee member, **Prof. Dr. İbrahim H. Güzelbey**, **Prof. Dr. Ömer ARIÖZ** for their important comments and suggestions, as well as I would like to also thank the jury members for their participation and criticism.

Thanks to **Gaziantep University** to provide me with the opportunity to obtain a doctorate degree. Sincere thanks to **Kurdistan Region-IRAQI Ministry of Higher Education and Scientific Research** and **Duhok Polytechnic University** for their support which was the main motivation to complete my study.

A special thanks to my family with my deepest appreciation to my spirit; my father **Dr. Shakib Al JAWAHERY,** and **my mother**, for all of the sacrifices that you've made on my behalf, and who were always supporting and encouraging me with endless love. As well as I thank my brothers and my sister for their endless encouragement and motivation during the period of studying.

Last, but definitely not least, I would like to thank my wife **Huda Al SAFFAR** for continuously and patiently supporting me in every phase of the work of this thesis by dedicating the work to her.

TABLE OF CONTENTS

Page

LIST OF TABLES

Page

LIST OF FIGURES

LIST OF SYMBOLS AND ABBREVIATIONS

FRP Fiber Reinforced Polymer

BFF Basalt Fiber Fabric

BFM Basalt Fiber Mesh

BFRP Basalt Fiber Reinforcement Polymer

CFRP Carbon Fiber Reinforcement Polymer

Es Elasticity modulus of steel Reinforcement

f_c Compressive strength of concrete

f_t Tensile strength of concrete

f_{ts} Tensile strength of steel Reinforcement

f_y Reinforcement yield strength

α Inclination angle

RC Reinforced Concrete

ST Steel fiber

SFRC Steel Fiber Reinforcement Concrete

RCHBs Reinforced Concrete Haunched Beams

RCCs Reinforced Concrete Corbels

SCC Self-Compacted Concrete

SCC-SFRC Self-Compacted Concrete-Steel Fiber Reinforcement Concrete

MS-SCC Medium Strength-Self Compacted Concrete

HS-SCC High Strength-Self Compacted Concrete

CHAPTER 1

INTRODUCTION

1.1 General

During the recent years, the rehabilitation of reinforced concrete structures has become an important scientific interesting and economic field. Worldwide the investments for maintenance, repair, and restoration of the infrastructure are increasing individual solutions are required for each status of maintenance and rehabilitation of damaged reinforced concrete structure. This has led to the development of lots of different basic strategies and solutions for the repair of reinforced concrete structures. However, the new European Standard Series EN 1504 has 43 methods to repair and protect reinforced concrete structures according to altogether 11 different principles. It is the task of the designer of repair or protection works to select appropriate solutions taking the relevant technical and economic facts into account. Repairing and protection of reinforced concrete structures are complex tasks requiring special knowledge in different fields such that static and dynamic behaviors of the structures, damaged behavior with corrosion behaviour of materials, the type of rehabilitation and methods, the behaviour of materials after rehabilitation, and beside to the quality control and maintenance (Alexander *et al.* 2008).

In general, retrofitting or rehabilitation is a part of civil-mechanical engineering. In civil engineering, all types of damage such as corrosion, old RC, and any other deterioration of structures need for the rehabilitation based on the conditions of damaged. All methods of rehabilitation or retrofitting are being adapted to compatible the service level of building and increase the service life and level structures (Kumar *et al.* 2015a).

Besides that, the rehabilitation or retrofitting works are done by multi-types of techniques, like jacketing by the plate, wrapping by FRP, or near surface mounting method etc.

Nowadays one of the important material is basalt fibers which made from extremely fine fibers of basalt rocks which is consisted from the material of plagioclase, pyroxene, and olivine. To product, the basalt fiber must the basalt rocks crushed, washed and melted at temperature 1400 degree centigrade, then the melted rocks extruded from small nozzles and continuous filament of basalt are produced which is the diameters are between 9 to 13 micrometer. Basalt fibers have a better physical, mechanical properties than glass fiber, but being significantly cheaper than carbon fiber (Vora and Patel 2014).

1.2 Reinforced Concrete Haunched Beams (RCHBs)

Nowadays reinforced concrete haunched beams (RCHBs) are widely used in structural members and bridges. Especially in old bridges there is an increasing demand for repair and rehabilitation (Al-Sulaimani *et al.* 1994, Aldahdooh *et al.* 2016). As can be seen in the German Code 2001 there is lack of information about the factor of safety for several bridges due to uncertainties of the materials or geometries related to RCHBs (DIN 2001, hasssan 2015). Moreover, on the rehabilitation of RCHBs lack of information is much more critical as there are very few studies in this field.

There are relatively more studies about strengthening of reinforced concrete prismatic beams by FRP where researchers investigated the improvement of shear load capacity after retrofitting them with fiber reinforced polymers (Khalifa and Nanni 2000, Bousselham and Chaallal 2009). Moreover, other researchers investigated the performance of fiber reinforced polymer for the strengthening of reinforced concrete prismatic beams (Chajes *et al.* 1995, Khalifa *et al.* 1998, Triantafillou 1998, Triantafillon, T.C 2000, Deniaud and Cheng 2001, pellegrino C and Modena 2002, 2006, Chen and Teng 2003, Mofidi and Chaallal 2010).

Unfortunately, there is no experimental data currently available to predict the behavior of after rehabilitated by FRP. Moreover rather there are no specific recommendations for the rehabilitation of RCHBs in the state-of-the-art ACI 440.2R (ACI 440 2008). Very little published information available on the strengthening or rehabilitation of RCHBs by FRP except some studies dealing with another technology to rehabilitate or strengthen the RCHBs (Tena and Hernández 2009a).

On the other hand, limited studies focused on numerical modeling of shear strength of repaired beams using finite element method (Lee *et al.* 2000, Wong and Vecchio 2003, Godat *et al.* 2007, Al-Rousan and Haddad 2013). While many previous FE analysis studies focused on the strengthening of Reinforced concrete members with

FRP. The experimental studies show that the behavior of repaired RC members are different as compared to the behavior strengthened RC members (Sasmal *et al.* 2012, Al-Rousan and Haddad 2013).

1.3 Steel Fiber-Reinforced Concrete (SFRC)

A composite form between steel fibers and concrete, known as steel fiber-reinforced concrete (SFRC), the adding of steel fibers into the concrete matrix with random orientation improve various mechanical characteristics such as flexural and shear strength with other variables like ductility and absorption energy (Sharma 1986, Chunxiang and Patnaikuni 1999, Dinh 2009, Dinh *et al.* 2010, Aoude *et al.* 2012, Slater *et al.* 2012, Spinella *et al.* 2012, Islam and Alam 2013, Kara 2013, Lee *et al.* 2013, Michels *et al.* 2013, Sahoo and Sharma 2014, Shoaib *et al.* 2014a, Yoo *et al.* 2015, Amin and Foster 2016, Hwang *et al.* 2016). Moreover, the idea of adding steel fiber in to the concrete matrix came from old times adding of straw to the brick mud (Altun *et al.* 2006).

The performance of SFRC depends on the bonding between steel fibers and concrete which came from friction between each other, in addition to the ratio and distribution of fibers in the concrete matrix. Thus, the performance of bonding depends on the surface area of fibers which is increased when fibers have a higher surface area which respects to the volume ratio, and that led to conclude that the fibers with rectangular sections are more efficient than fibers with circular sections. Moreover, the fibers which have the same length with small diameter (higher aspect ratio) are more efficient (Altun *et al.* 2006, Dinh 2009, Dinh *et al.* 2010, Sahoo and Sharma 2014).

Some studies investigated on the material characteristics of SFRC and fiber orientation inside the concrete, while many other experimental and analytical studies implemented on the structural behavior of SFRC beam members (Romualdi and Mandel 1964, Batson *et al.* 1972, Mansur *et al.* 1986, Lim *et al.* 1987, Narayanan and Darwish 1987, Soroushian and Lee 1990, Alwan *et al.* 1991, Ashour *et al.* 1992, Faisal and Ashour 1992, Li *et al.* 1992, Song and Hwang 2004, Cucchiara *et al.* 2004, Karl *et al.* 2011, Shoaib *et al.* 2014b). Moreover, many other studies focused on the behavior of steel fibers as shear reinforcement on the SFRC beams without steel stirrups (Adebar *et al.* 1997, Casanova *et al.* 1997, Voo *et al.* 2006, Di Prisco *et al.* 2009, Dinh, Hai H and Parra-Montesinos, Gustavo J and Wight 2010, Cuenca and

Serna 2013, Sahoo and Kumar 2015). While other few studies combined between the effect of steel stirrups and steel fiber on the behavior of members against the shear strength (Cucchiara *et al.* 2004, Dancygier and Savir 2011, Aoude *et al.* 2012, Spinella *et al.* 2012).

1.4 Reinforced Concrete Corbels (RCCs)

Corbels or brackets are reinforced concrete structural members with short cantilevers, with shear span-to-depth ratios not greater than one, which are tended to act as simple trusses or deep beams. The failure modes may occur by: Shearing along the interface between the column and corbel, yielding of tension tie, crushing or splitting of the compression strut, and localized bearing or shearing failure under the loading plate (ACI Committee 318 2011).

Corbels or brackets can be used to support pre-cast structural systems like pre-cast beam and pre-stressed beam. Corbels or brackets became a standard feature in building construction and is typically cast with the column or wall members. The main function for the corbels is transferring the coming load from the beams the supporting columns or walls (Yong and Balaguru 1994, Foster *et al.* 1996, Hwang *et al.* 2000, Foster and Malik 2002, Hwang and Lee 2002, Russo *et al.* 2006, He *et al.* 2012). Structural cracks may occur in RC corbels like other structural members for several reasons. Cracks in the corbels should be strengthened or repaired before the collapse affected the members.

In general, repairing is a part of the civil engineering field, to set right the deteriorated, damaged, corroded and aged RC structures, masonry structures, and steel structures. The repairing, retrofitting, rehabilitating and strengthening processes are based on the damage conditions of the structures (Kumar *et al.* 2015b). Modern technology has developed new composite materials to increase and enhance the load carrying capacity and mechanical behavior of reinforced concrete members by increasing the flexural and shear strength and decreasing the cracks and deformations that may occur (Ivanova and Assih 2015b).

The differentiation between strengthening and repair isn't perpetually obvious. Reinforced concrete members may be damaged as a result of an overload or as a result of deficient initial capacity. In either case, cracking or other distress is obvious. Whether this is a repair or a strengthening activity depends on the source of the damage. Repairing of cracks are generally achieved by injection epoxy o fiber-reinforced mortar which is a new technique in the literature (Benyahia *et al.* 2017). If the reinforced concrete member is undamaged and the structure's live load is to be increased, then the appliance is merely for strengthening functions (Corry and Dolan 2001). Unfortunately, there is no data currently available for repair of RCCs by the Basalt fiber. A much fewer number of researchers (Corry and Dolan 2001, Assih *et al.* 2015, Ivanova and Assih 2016), dealt with CFRP for repairing damaged RCC, while a significant number of researchers (Elgwady *et al.* 2005, Erfan *et al.* 2010, Ahmad *et al.* 2013, Ivanova *et al.* 2014, 2015, Ivanova and Assih 2015a, 2015b, 2016, Shadhan, Khalid K and Kadhim 2015) used CFRP for the strengthening of RCC. Researchers found CFRP to be an effective and significant technology for strengthening and repairing RCCs.

Till date, very less research has been carried out on the strengthening of heated reinforced concrete elements (Haddad *et al.* 2007, 2008, 2011, Toumi *et al.* 2009, Yaqub *et al.* 2013, Leonardi *et al.* 2011, Yaqub and Bailey 2011a, 2011b, Yaqub *et al.* 2011, Roy *et al.* 2014, 2015). Rehabilitation of RCCs is necessary after a possible heat damage. Moreover, if corbels are both exposed to high temperature and failed about load carrying capacity, repairing of them will become more critical (Abdulhaleem *et al.* 2018).

1.5 Research objectives and aim of the study

The overall aim of this study is to investigate and gather the rehabilitation of damaged RC elements which are RCHBs and RCCs. Besides, the finite element modeling study for both the rehabilitation RCHBs and the behavior of SF RCHBs.

This study can be divided into four essential parts;

- Part one; The aims of this part are to investigate the effectiveness of BFF on rehabilitation of RCHBs and to research the efficiency of finite element modeling for predicting the mechanical behavior of rehabilitated RCHBs. A new technique is proposed to form a region that exhibits all possible load capacities of rehabilitated RCHBs via finite element modeling by ATENA-GiD 3D software program.
- Part two; This part consists of two essential parts; the experimental findings obtained from structural tests of damaged (RCHBs) after being rehabilitated by CFRP. And a new FE methodology for the simulation of the behavior of

rehabilitated RCHBs which was followed before in part one by use of ATENA-GiD 3D software program.

- Part three; analytical study of proposing finite element models of SF RCHBs which are evaluated by selected experimental data of SF RCHBs.
- Part four; The main aim of this part is to investigate the mechanical behavior of heated and non-heated damaged RCCs (with and without steel fiber) after being rehabilitated with new uses of Basalt Fiber Mesh (BFM) and Basalt Fiber Fabric (BFF). In addition to the behavior of corbels which are rehabilitated cracks only by injecting material without wrapping by any FRP. Besides, the investigation of ultimate load capacities and the failure modes before and after the rehabilitation.

For all specimens, the following tasks will be achieved in order to accomplish the objectives of this research:

- Studying the behavior of BFRP mesh and fabric.
- Studying the structural member's behavior (RCHBs, and RCCs) after rehabilitated by BFRP fabric and mesh.
- Determining the ultimate load at failure.
- Investigating the mode of failure.
- Studying the load-deflection behavior.
- Comparing the experimental cracks and corresponding cracks which are produced from Finite element modeling.
- Comparing and analyzing the experimental and corresponding finite element modeling data.
- ATENA-GiD software package will be used to develop finite element models for simulating the behavior of RC members before and after the rehabilitation by FRP. From the analysis, the (load-deflection relationships until failure, failure modes and crack patterns) will be obtained and compared with the corresponding experimental results. Proposing zone to predict the limitations of failure criteria of the members which are rehabilitated by FRP.
- ATENA-GiD software package will be used to develop finite element models for simulating the behavior of SF RCHBs, besides the parametric study of some parameters which affect the behavior of SF RCHBs.

1.6 Layout of the Thesis

The contents of this thesis are described as shown below:

Chapter 1: Provides a summary of the introduction of retrofitting by FRP materials and gives a brief information about the RCHBs, RC Corbels and the behavior of steel fiber reinforced members, as well as described brief previous studies which were implemented. The objectives and aims of the thesis also described in this chapter.

Chapter 2: Reviews the literature studies of an experimental investigation of rehabilitation damaged RCHBs, and RCCs. Furthermore, the literature review of steel fiber behavior after added to the mix of RC members.

Chapter 3: The experimental research carried out on rehabilitation of damaged RCHBs by Basalt Fiber Fabric and Carbon Fiber polymer, Also provided all the mechanical properties of the material which were used in this study and the test procedures according to corresponding specifications have been mentioned in this chapter.

Chapter 4: The experimental research carried out on rehabilitation of damaged RC Corbels by Basalt Fiber Mesh and Basalt Fiber Fabric, as well as provided all the mechanical properties of the material which were used in this study and the test procedures according to corresponding specifications have been mentioned in this chapter.

Chapter 5: The nonlinear finite element modeling of proposing models of rehabilitation RCHBs by Basalt Fiber Fabric and Carbon Fiber polymer were described in this chapter, as well as the proposing models of constitutive materials which were used in this study.

Chapter 6: The nonlinear finite element modeling of proposing models of steel fiber RCHBs, as well as discussed and expounded the experimental and corresponding FE results, and interpreted the behavior of load-displacement curves, mode of failure, and propagation of cracks. This chapter also described and discussed the results of parametric studies of steel fiber RCHBs.

Chapter 7: Provided a general summary of a conclusion that can be concluded from this research study, as well as recommended future works can be found at the end of the chapter.

CHAPTER 2

LITERATURE REVIEW

2.1 General

Many experimental and analytical works have been done by many researchers in the area of strengthening and retrofitting the structural members with composite materials. The concept of retrofitting the structural members is rapidly growing due to enable the early identification of damage and provides warning for unsafe condition. Some researchers have also investigated or work on the area of the failure mode of the FRP strengthened structural members and some are working on the strengthening of the structural members with different FRP materials.

This chapter deals with literature that must be reviewed to assess and determine the performance of the proposed research study, besides the necessary to understand what are the previous research studies reach on.

This chapter consists of three main sections: The first part of this chapter presents survey about the available previous studies which are dealing with reinforced concrete haunched beams (RCHBs) especially that studies which are dealing with the simulation of finite element analysis to predict the shear load capacity. In addition to the reviewing studies which were focused on rehabilitation by using FRP. As mentioned earlier, there are a few numbers of articles that deal with the rehabilitation of RCHBs by FRP, most of them dealing with the rehabilitation by another technology which will be showing it in this chapter.

The second part of this chapter includes reviewing the studies that treated with the evaluated the effect of steel fiber on the RC beams.

Eventually the last part of this chapter deals with reinforced concrete corbels (RCCs), and what are the technologies that used to rehabilitate it. Although there are a few types of research achieved on this topic, it will clear indicators about the behavior of RCCs after rehabilitating by FRP. The available experimental studies which are focused on RC corbels did not use Basalt Fiber Mesh to rehabilitate it and there is no article in the literature dealt with its topic.

2.2 Reinforced concrete haunched beams (RCHBs)

2.2.1 Experimental rehabilitation studies

Very little published information is available on the strengthening or rehabilitation of RCHBs by FRP, except for some studies utilizing a different method to rehabilitate or strengthen the RCHBs which are listed below:
In 2009 Tena and Hernández, used jacket technique by steel wired mesh to rehabilitating damaged haunched beams which were obtained on eight haunched beams were previously designed and tested to fail in shear. The haunched beams repaired by using a beam jacketing with a light-gauge steel wired mesh covered within 2 cm thick grout. All beams were tested under monotonic load and the results showed that the repairing by jacketing technique was effective in the higher deformation and load capacities (Tena and Hernández 2009b).

Megahid et al. in 2010, studied the behavior of damaged haunched beams after rehabilitated by the steel plate in the shear zone, high compressive strength was used to product haunched beams. The main variables were entered in this study were; geometric dimensions of steel plates, width, position and arrangements, thickness of plate bonded on both sides of shear zone of beams. The shape effect of haunches (Negative angle of haunched beams -20 degrees and positive angle of haunched beams +20 degrees) and the last variable was entered in this study was used multi-values of using concrete strength. The researchers found from the results of this study that the increase of width, position, arrangements, and thickness of plate bonded on both sides of the shear zone of haunched beams increases the ultimate capacities of the rehabilitated haunched beams, and affected of deformation and mode of failure. Moreover, the using of high compressive strength in the casting of beams decreases the relative cracks of beams and the effective shape of haunched beams was the Negative haunched beams -20 degrees which affected the ultimate load capacities (Megahid *et al.* 2010).

2.2.2 Review of the experimental and analytical studies

There is a lack of data to assist structural engineers to design RCHBs. A number of researchers studied the shear behavior of haunched beams, while other researchers focused on analytical studies using nonlinear finite element modeling. Some of these studies are reviewed below:

Debaiky and Elniema in 1982 were the first researchers focused on the shear behavior of RCHBs. This study consists of 33 RCHBs, which were divided into prismatic beams and others had varying depth. The parameters which were entered in this study were the inclination angle, shear span, concrete strength, and flexure and shear reinforcement, in addition to the geometry of the beams. The researchers found that the beams with increased depth at the support did not improve the shear capacity. Whereas, the beams were decreased depth at the support did deteriorate the shear capacity. The nominal shear contribution of the concrete and the longitudinal reinforcement were influenced by the haunch's inclination while the nominal contribution of the stirrups is not (Debaiky and Elniema 1982).

Macleod and Houmsi in 1994, investigated the behavior of shear strength of RCHBs, which was contained six full-scale RCHBs where the inclination angle of haunched beam ranged from 5 to 10 degrees. The authors concluded that the decreasing volume of concrete in the beam due to increasing slope angle improves the shear load capacity and leads the failure to be more ductile (MacLeod and Houmsi 1994).

In 2008 Tena et al., examined the behavior of 10 prototypes of simply supported reinforced concrete beams which were divided into 2 prismatic beams and 8 RCHBs. All beams were designed to fail in shear and it tested under static load. 4 haunched beams and 1 prismatic beam were designed without shear stirrups and the remain beams with shear stirrups, The depth of the beams was increased at the support. The experimental results observed that RCHBs indeed have more deformation capacity compared to the prismatic beams. However, the ultimate shear strength was developed compared to the prismatic beams (Tena-Colunga *et al.* 2008).

In 2017 Tena et al., published another paper of 5 prototypes continuous RC beams which are divided into 4 haunched beams and 1 prismatic beam, all beams were designed to fail in shear and the testing was under cyclic loading. The parameters which were taken in the account were; the inclination angle of RCHBs, the contribution of the inclined longitudinal steel reinforcement in shear, the contribution of the steel stirrups in shear strength, and the inclination angle of the main crack on the face of RCHBs. The authors concluded that haunched beams can resist similar or more than prismatic beams in the effective of shear force, especially for the negative haunched beams. Moreover, the inclined longitudinal steel reinforcement was contributed in the shear strength besides the steel stirrups of haunched beams. As a consequence of result, when the inclination angle of RCHBs increased the inclination angle of the main crack will decrease (Tena-Colunga *et al.* 2017a), in addition to the RCHBs seem to be more efficient under cyclic testing than the prismatic beams, even when they fail in shear (Tena-Colunga *et al.* 2017b).

Jolly and Vijayan in 2016 published an article which was conducted an analytical study of RCHBs behaviour in ANSYS and ETABS packages, nonlinear finite element analysis was carried out in both software. The parameters which were entered in this study were; seismic analysis of RC frames, stepped RCHBs, time period, and varying in the haunch angle. The researchers found that the RCHBs can be affected by the seismic behaviour of the frame, moreover, the RCHBs increased the lateral stiffness of buildings substantially (Jolly and Vijayan 2016).

Harba and Abdulridha in 2017 investigated the behavior of RCHBs on the cyclic response. The finite element analysis was carried out on previous experimental work which was contained 5 simply supported RC beams (4 RCHBs and 1 prismatic beam). The Abaqus software package was used for modeling the models of RCHBs. Moreover, the plastic-damage model was used for concrete developed by Lubliner and Lee & Fenves. The authors conducted that there was a good agreement between the selected experimental work and the proposed model of finite element analysis, And the variations in loading history will decrease the ultimate load and corresponding deflection with an increase in the number of cycles at ultimate load (Harba and Abdulridha 2017).

Godínez-Domínguez et al. in 2015 carried out a study of different models of nonlinear finite element analysis for 8 simply supported RCHBs designed to fail in shear failure and the testing was obtained under static load. The constitutive models of longitudinal steel reinforcement and stirrups were assessed by SAP2000 package. Besides, the software ANSYS which is used to constitute more complex (built models) of nonlinear finite element models in the case of longitudinal steel reinforcement and stirrups. Von Mises yield criteria was considered in the strain hardening of steel reinforcement, and a perfect bond between concrete and steel reinforcement. The curves of shear load-displacement were compared with obtained curves of experimental testing and both analytical and experimental crack patterns were compared in different loads steps. The authors concluded that there is a good correlation between analytical and experimental load-deformation curves which is considered more than acceptable. However, there is only a medium correlation between crack patterns of finite element models and crack patterns of experimental results, especially for beams with shear stirrups reinforcement (Godínez-Domínguez *et al.* 2015).

2.3 Steel fiber reinforced concrete beams (SFRC)

A composite form between steel fibers and concrete, known as steel fiber-reinforced concrete (SFRC), the adding of steel fibers into the concrete matrix with random orientation improve various mechanical characteristics such as flexural and shear strength with other variables like ductility and absorption energy. Below some interesting studies will be reviewing:

Naaman and Najm in 1991 studied the behavior of bond strength of steel fiber, which is increased in matrix strength resulted in an increase in bond strength. The authors concluded that when using a hooked steel fiber required a work to pulling out four times greater than the required for smooth steel fiber and the slip at peak load to pulling out the hooked fiber was up to two times greater than the smooth steel fiber (Naaman and Najm 1991).

In 1994 Banthia and Trottier studied the pullout behavior of hooked steel fiber, two types of steel fiber were used; crimped, and stranded steel fibers which are embedded in concrete matrices with different compressive strengths. The maximum aggregate size was 3/8 inches (10 mm) for the aggregates which were used in the concrete matrix. The fibers which were used were inclined from the loading direction at an angle from 0 to 90 degrees. The authors concluded that bond strength increased with respect to an increase in matrix strength, which is compatible with the concludes of Naaman and Najm in 1991. Besides, at peak load the increase of bond strength of hooked steel fibers was modest. For the normal and medium strength of concrete; a change in the angle from 0 to 15 degrees did not significantly affect the load-slip curve. And when the angle increased beyond 30 degrees, the effect of fiber inclination was more clear up to a slip of 3.5 mm (Banthia and Trottier 1994).

In 1999 Khuntia et al. investigated the predicting of shear strength of normal and high-strength steel fiber RC beams. The researchers suggested a design equation to evaluate the ultimate shear strength of FRC beams based on the shear transfer mechanisms and experimental data which were published before on concrete strength up to 100 MPa, besides the strength of concrete the influence of the fiber factors, shear span to the depth ratio, main longitudinal steel ratio, and size effect. The authors found that the modeling approach to that applied for conventional RC beams, except some modifications which were suggested, to account the effect of fibers. The comparison between computed values and experimentally values showed a validate the proposed analytical equations (Khuntia *et al.* 1999).

Dinh et al. in 2010 proposed a new simple model to predict the shear strength of steel fibers beams without stirrups reinforcement. The authors create the model depending on the basic observation of 27 large scale beams under monotonic increased concentrated load. Three types of steel fiber were evaluated in the model, one beam from all beams was failed in shear and others failed in flexural. Besides, the modeling of steel fiber RC beams was assumed to be resisting the shear stress in the compression zone and tension transferred across diagonal cracks by steel fibers. the contribution of fiber reinforcement in beam shear strength is linked to the performance of material which was obtained from an ASTM 1609 four-point bending test. The researchers concluded from the results of this study that the shear strength of steel fiber beams can be reasonably estimated assuming that the shear strength of the beam is provided over the compression zone by shear resisted and tension resisted by fibers bridging diagonal cracks, neglecting any contribution of aggregate overlap and dowel action in this zone. The estimation of average steel fiber tensile stress across the diagonal crack at shear beam failure can be equivalent to the bending strength which is calculated from ASTM 1609 four-point bending tests, the equivalent bending strength at a deflection equal to 1/24 of the fiber length, compared to a crack width equal to 5% of the fiber length, led to reasonable shear strength predictions in the test beams. In addition to that, the authors found that the shear strength models which were created by (Khuntia *et al.* 1999), were the most conservative and moderate scatter in data which means the mean and standard deviation values between predicted and experimental strength of 0.71 and 0.15, respectively. Also, the authors compared the proposed shear strength equations and they concluded that there more accurate predictions which mean (mean and standard deviation of 0.79 and 0.12, respectively) (Dinh, Hai H and Parra-Montesinos, Gustavo J and Wight 2010).

2.4 Reviews of the experimental and analytical studies of damaged reinforced concrete corbels (RCCs)

Unfortunately, there is no data currently available for repair of RCCs by the Basalt fiber. A much fewer number of researchers dealt with CFRP for repairing damaged RCCs which are listed below:

Corry and Dolan in 2001 examined rehabilitation of damaged column brackets specimens using Carbon Fiber Reinforced Polymer (CFRP). The procedure failure of samples was loaded to 75 % of its nominal capacity and then the cracked bracket was strengthened to increase the original capacity until 50 %, and then retested until failure. Fig. 1 shows the failure mode of the bracket after tested. The researchers found that strengthening must be at least two layers of CFRP to verifying the recommended load and when it uses a single layer of CFRP, the failure will be a sudden failure.

Figure 2.1 Failure of Bracket after fabric cut

Moreover, a new philosophy was proposed to simulate the require layer number of strengthening by CFRP that should be applied. In addition, to presume fabric and adhesive would be lost in a fire beside the provision and supplying a mental fabric to protect the fabric in the catastrophic failure of structure (Corry and Dolan 2001).

In 2015 Assih et al., conducted an experimental and theoretical analysis of rehabilitated damaged RCCs by carbon fiber fabrics. The researchers aimed in this study to investigate the role of strengthening on damaging RC corbels, and to propose an analytical model of RCCs. The experimental program contained 5 RCCs were tested until failure under a three-point bending up. Three of the RCCs were damaged at 45, 65 and 90 % of their ultimate load. After the specimens were repaired with carbon fiber fabrics and the failure loading was recorded. The fourth corbel which was not damaged. It was strengthened and tested until its collapse. The last corbel was put as a reference specimen corbel which was not repaired by carbon fiber. The study shows that the carbon fiber fabrics could be a convenient and effective strengthening method for concrete structures. Thus, carbon fabrics and steel reinforcement played a major role in the rehabilitation of RCCs. The role of carbon fiber fabrics increased the ultimate load from 30 to over 50 %. The mechanical damage up to 90 % affected the ultimate load (less than 20 %). After being damaged, the type of shear failure was splitting failures. Moreover, the theoretical analysis which was described the behavior of strengthened damaged RCCs by using the damage theory of RC beams (Assih *et al.* 2015).

Ivanova et al. in 2016 investigated the repairing of damaged RCCs by glued carbon fiber fabrics, 7 RCCs were tested. 2 of RCCs are made as a reference, 1 without strengthening and the other one strengthened by carbon fiber fabrics which were tested under static loading. Different levels of damaging were tested for the other three specimens at 40, 60 and 80 % of the ultimate load of reference corbel, after then they were strengthened by carbon fiber fabrics. Moreover, the last two RCCs were tested under dynamic loading, one of them without strengthening and the last one after strengthening by carbon fiber fabrics. The mechanical behavior of RCCs was investigated besides to the ultimate loads at failure. The results of rehabilitation by carbon fiber fabrics show that strengthening gives a significant improvement on the ultimate load capacities which were reached up to 82 %, as well as the increasing of RC stiffness to third (Ivanova *et al.* 2016).

CHAPTER 3

REHABILITATION OF REINFOCED CONCRETE HAUNCHED BEAMS (RCHBs)

3.1 Introduction

This chapter presents the experimental work carried out in the present research work. The program consists of two individual parts as mentioned in chapter one, in each part, there is a specific work which was done to satisfy the scientific objectives, this chapter shows all parts work as follows below:

3.2 Rehabilitation of RCHBs by Basalt Fiber Fabric (BFF)

3.2.1 Objective

The main aim of the study is to investigate the effectiveness of BFF on damaged RCHBs after being rehabilitated by BFF which was described in this chapter below.

3.2.2 Experimental work description and material properties

The haunched beams, which had been tested by (ALBEGMPRLI 2017) before, was used for the rehabilitation process. There are two groups of RCHBs. Each group has 6 RCHBs with different shape and reinforcement ratio. The first group was designed to fail in shear and the second group was designed to fail in flexure mode.

All RCHBs have the same length and width of 1700 mm and 150 mm respectively, while the height is variable. All details of geometry and steel reinforcements for the first and second groups are shown in Figures 3.1 - 3.2. The name of RCHBs contains six terms. The first term represents the sample number (HB No. # #), the second term represents the height of the haunched beam in the mid-span, the third term represents the inclination angle from the middle to the sides of haunched beams. The fourth term represents the height edges of the haunched beam, the fifth term represents the main area of steel reinforcement, and the last term represents the cylindrical compressive strength of the specimen.

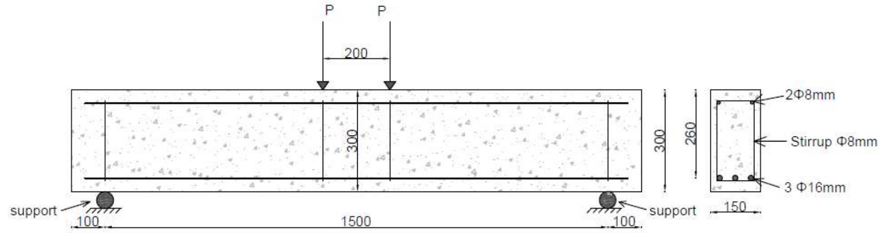

HB1-300-0-300-603-55

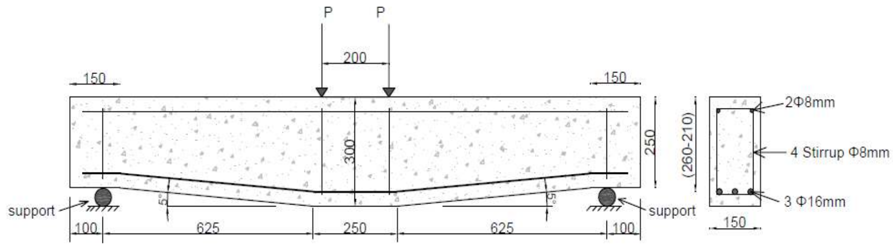

HB2-300-+5-250-603-53.5

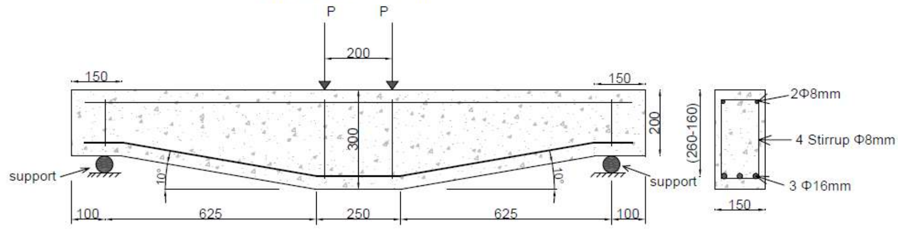

HB3-300-+10-200-603-55.1

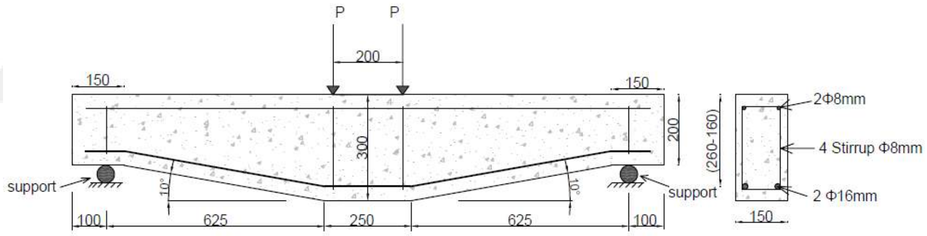

HB4-300-+10-200-402-53.9

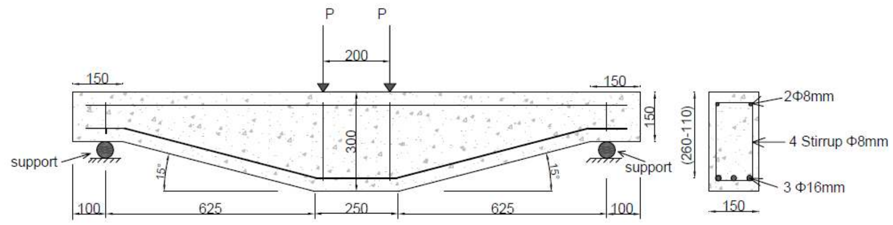

HB5-300-+15-150-603-59.5

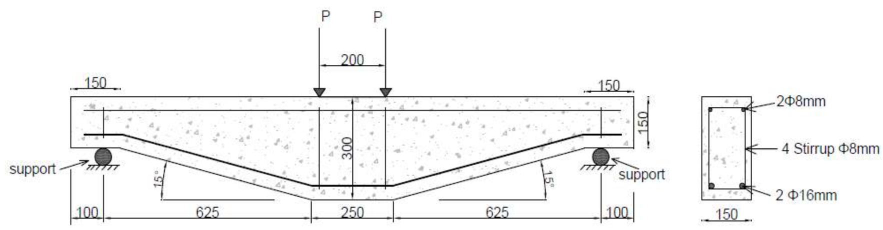

HB6-300-+15-150-402-51.5

First Group (All dimensions in the figures are in mm)

Figure 3.1 Geometries and steel reinforcement details of the first group of RCHBs

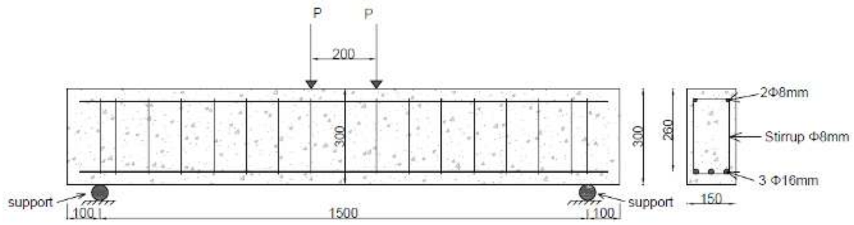

HB1-300-0-300-603-58

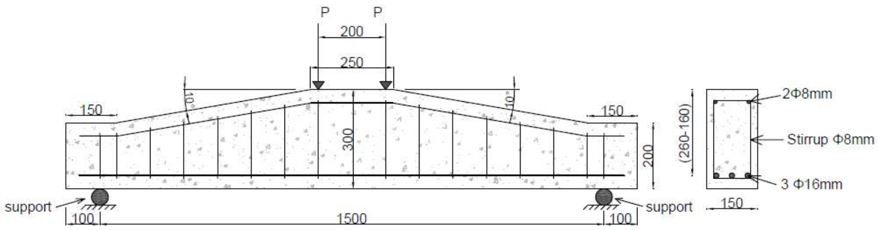

HB2-300--10-200-603-59

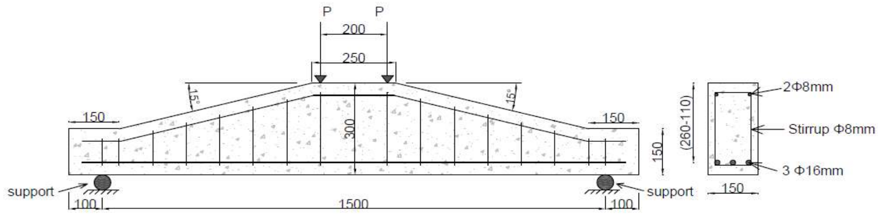

HB3-300--15-150-603-59.9

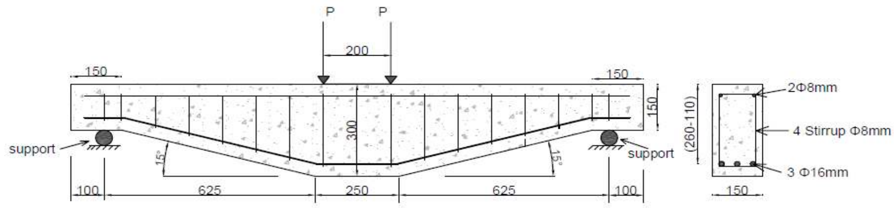

HB4-300-+15-150-603-59

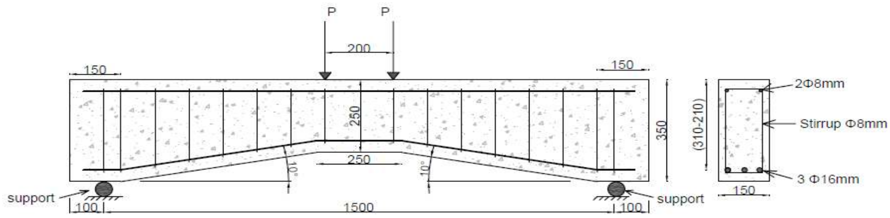

HB5-250--10-350-603-65

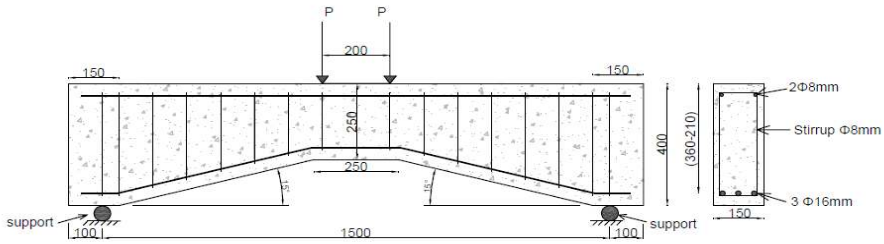

HB6-250--15-400-603-59

Second Group (All dimensions in the figures are in mm)

Figure 3.2 Geometries and steel reinforcement details of the second group of RCHBs

Mechanical properties of cylinder samples of self-compacted concrete (SCC) for both groups are given in Table 3.1. The average yield strengths for reinforcements were found to be 550 MPa and 456 MPa and average ultimate strength values were found to be 640 MPa and 560 MPa for 8 mm and 16 mm steel bars, respectively. Unidirectional Basalt Fiber Fabric (BFF) was used in this study to rehabilitate RCHBs. The mechanical properties of BFF presented in Table 3.2.

Two types of epoxy were used in this study. The first one was low viscosity epoxy resin (Sikadur 52) presented in Table 3.3 and was used to repair the cracks which had occurred as a result of the first test (ALBEGMPRLI 2017). The second one was medium viscosity- high strength epoxy adhesive (TEKNOBOND 300) presented in Table 3.4 and was used to bond the Basalt Fabric on the concrete surface.

Table 3.1 Test results of compressive strength, modulus of elasticity and splitting tensile strength of SCC

	Beam No.	f_c MPa	E_c GPa	f_{ts} MPa
Group one	HB1	55	34.1	3.9
	HB2	53.5	35.2	4.65
	HB3	55.1	50.6	4.26
	HB4	53.9	33.2	4.0
	HB5	59.5	36.38	4.36
	HB6	51.5	35	3.6
Group two	HB1	58	34.7	4.2
	HB2	59	38.2	4.1
	HB3	59.9	37	4.2
	HB4	59	40.2	4.45
	HB5	65	39	4.1
	HB6	59	40	3.7
	Av.	57.37	37.80	4.13
	S.D	3.69	4.65	0.299
	C.V%	6.43	12.299	7.269

Table 3.2 Mechanical properties of BFF

Tensile Strength (MPa)	Modulus of Elasticity (GPa)	Strain (%)	Thickness (mm)	Area weight (gm/m^2)
2100	105	2.6	0.115	300

Table 3.3 Properties of epoxy Sikadur 52 (Sika Company 2014)

Density	Part A: 1.1 kg/l (at +20°C) Part B: 1.0 kg/l (at +20°C) Part A+B mixed (2 : 1):1.1 kg/l (at +20°C)	
Viscosity	Temperature	Type Normal part A+B mixed (2: 1)
	+10°C	~ 1200 MPa_s
	+20°C	~ 430 MPa_s
	+30°C	~ 220 MPa_s
	+40°C	-
Thermal Expansion Coefficient	89 x 10-6 per °C (from -20°C to +40°C) (According to EN ISO 1770)	
Compressive Strength	52 N/mm^2 (after 7 days at +23°C) (According to ASTM D695-96)	
Flexural Strength	61 N/mm^2 (after 7 days at +23°C) (According to DIN 53452)	
Tensile Strength	37 N/mm^2 (after 7 days at +23°C) (According to ISO 527)	
Bond Strength	To concrete: (According to DafStb-Richtlinie, part 3) > 4 N/mm^2 (failure in concrete) (after 7 days at +23°C)	
E-Modulus	Flexural Strength: 1800 N/mm^2 (after 7 days at +23°C) (According to DIN 53 452)	

Table 3.4 Properties of epoxy TEKNOBOND 300 (Tekno Construction Chemicals 2016)

Color	Component A Light Brown/ Component B Transparent
Density	1.15 gr/cm^3(Component A)- 1.05 gr/cm^3(Component B)
Consumption	2.0 kg/m^2 for 1 mm thickness
Bonding strength concrete	5.3 N/mm^2
Pot life	45 minutes (at 20 ^{o}C)
Loading capability	1 day
Full strength	7 days
Application Ground Temperature	(+5 °C) - (+30 °C)

3.2.3 Rehabilitation Process

The installation procedure of FRP fabrics can vary depending on the sort and condition of the structural member and FRP. All problems related to the condition of the original concrete and substrate which compromise the integrity of the FRP system should be addressed before surface preparation. All concrete repairs ought to meet the requirements of project specifications and be compatible with the FRP system (No n.d., ACI 546 2006, ACI 440 2008). Moreover, cracks that are 0.3mm and wider will have an effect on the performance of externally bonded FRP system through delamination or fiber crushing (ACI 440 2008). Therefore, the cracks were repaired by low viscosity epoxy resin (Sikadur 52). Surface preparation demand ought to be based on the intended application of the FRP system. The application may depend on Bond-critical applications like shear or flexural strengthening of beams, slabs, columns, or walls.

These needs an adhesive bond between concrete and the FRP system, therefore, the concrete surface preparation is the critical parameter in the bond performance of epoxy adhesive materials applied to concrete. Therefore, a grinder machine was used in this study to get rid of any loose, weak, or unsound materials like oil, grease, etc…the corners of the rectangular cross sections were rounded with minimum 13 mm radius to prevent the concentrations of stress in the FRP system and voids between the FRP system and the concrete (ACI 440 2008). To avoid the decrease of strengthening system with the FRP system, the surface should be cleaned and dry as recommended by ACI 503.4 (ACI 440 2008). After the repair of cracks and surface were cleaned, the compressed air system was used to remove the remaining dust on the surface. Thereafter, the locations of the Basalt Fibers Fabric strips were determined on the concrete surface. The strips were placed on the beam surfaces according to the configuration shown in Figure 3.3. However, for all samples of group two, the horizontal strips of Basalt Fibers Fabric were located along the bottom face of the beams between two supports to increase the flexural ability of the beams.

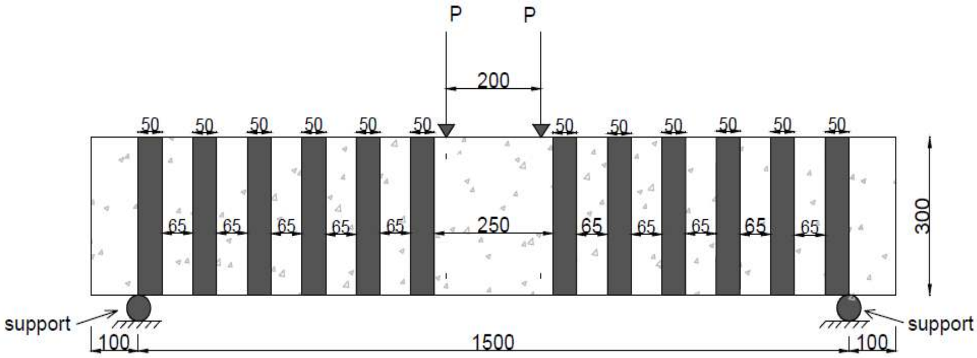

Figure 3.3 The arrangement of U strips of Basalt Fiber Fabric on the surface of samples for group one (All dimensions in mm.)

The wet lay-up method was followed to place the strips of Basalt Fiber Fabric on the surface of beams as recommended by (ACI 440 2008). This technique is usually achieved by hand using dry fibers sheets and a saturating resin. The saturating resin (epoxy) should be applied uniformly to the surfaces on which FRP sheets are to be placed. Fibers of fabrics were also impregnated by low viscosity epoxy before placement on the concrete surface to obtain perfect contact between them. The fibers should be gently pressed into the saturating resin. Any trapped air between FRP sheets and the surface should be removed or rolled out before the resin sets.

3.2.4 Test setup:

All haunched beams before and after the rehabilitation were tested under four-point load by 500 kN capacity, displacement controlled loading machine. Loading rate was 0.2 mm/min for all tests. Two linear variable displacement transducers (LVDTs) were used to record the deflections of haunched beams as shown in Figure 3.4. Loads and corresponding deflections were recorded for every 0.2 seconds continuously until the end of tests. All of the beams were loaded until failure to provide better insight of the post-peak behavior.

Figure 3.4 Test setup for four-point loading test

3.2.5 Experimental Results of RCHBs Before and After the Rehabilitation

The experimental results (ultimate load capacities and corresponding deflections at mid-span) of the haunched beams before and after the rehabilitation are shown in Table 3.5. It should be noted that all cracks were injected with epoxy (Sikadur 52) before being rehabilitated by Basalt fabric. Behavior at the ultimate shear load before the rehabilitation varied with the change of the haunched beam's inclination (column 3 in Table 3.5). Distinct behavior was observed for beams of smaller depth of the support when the other variables kept constant.

HB5 has the highest load capacity among the specimens in group 1. Also, it can be observed for samples (HB5 and HB6) that the variance of the main area of steel reinforcement affected on the value of the ultimate shear load before the rehabilitation. On the other hand, according to the load capacity of HB11 and HB12 specimens before rehabilitation, it can be concluded that RCHBs having negative inclination angle are the weakest beams regarding flexural behavior. However, the capacities of other types of RCHBs are nearly same and they exhibit nearly same behavior against the flexural behavior. The increase of ultimate shear load capacity after being rehabilitated by Basalt Fabric varies from 1.25% of HB6 to 46% of HB1 (Column 5 in Table 3.5), variation in the values depend on several variables; shape of the haunched beam, degree of damage of the haunched beam before the rehabilitation, type and amount of FRP which is used in the rehabilitation, and repair of cracks before using FRP fabric. Regarding the specimens failed in flexure before rehabilitation (group 2), distinct behaviors were observed for types of RCHBs after rehabilitation. However, all load capacities increased as compared to the original capacities.

Table 3.5 Experimental results of haunched beams before and after the rehabilitation

Names		Shape of RCHBs	Exp. Result before Rehabilitation		Exp. Result after Rehabilitation		$\frac{P_{After\ Rehab.}}{P_{Before\ Rehab.}}$	Mode of Failure	
			P_{Test} (kN)	Δ_{Test} (mm)	P_{Test} (kN)	Δ_{Test} (mm)		Before* Reh.	After** Reh.
Group one	HB1-300-0-300-603-55		110.3	2.15	160.95	5.02	1.459	F.S.C	D.F
	HB2-300-$^{+}$5-250-603-53.5		108.2	2.21	135.74	4.07	1.255	F.S.C	D.F
	HB3-300-$^{+}$10-200-603-55.1		117.07	2.69	151.86	4.22	1.297	F.S.C	D.F
	HB4-300-$^{+}$10-200-402-53.9		91	2.57	98.7	3.23	1.085	F.S.C	D.F
	HB5-300-$^{+}$15-150-603-59.5		132	4.65	147.97	5.42	1.121	D.S.F	D.F
	HB6-300-$^{+}$15-150-402-51.5	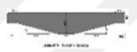	122.8	4.57	124.23	8.34	1.012	D.S.F	D.F
Group two	HB7-300-0-300-603-58		215	5.86	241.14	9.96	1.122	F.F	D.F
	HB8-300-$^{-}$10-200-603-59		215	7.77	236.78	10.13	1.101	F.F	D.F
	HB9-300-$^{-}$15-150-603-59.9		220.9	6.44	272.58	11.71	1.234	F.F	D.F
	HB10-300-$^{+}$15-150-603-59		208	8.26	235.4	10.14	1.132	F.F	D.F
	HB11-250-$^{-}$10-350-603-65		176	11.36	179.58	7.02	1.020	F.F	D.F
	HB12-250-$^{-}$15-400-603-59	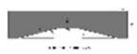	165	13.25	180.52	12.27	1.094	F.F	D.F

*F.S.C Flexural and shear cracks with shear failure; D.S.F Diagonal shear failure; F.F Flexural failure. ** D.F Debonding failure.

Comparison of load capacities of all RCHBs between before and after rehabilitation is shown in Figure 3.5. It can be observed clearly from the figure that the load capacity of all specimens before the rehabilitation increase after being rehabilitated. Figure 3.6 shows the comparison of mid-span deflection of RCHBs at ultimate load between before and after the rehabilitation. It is worth mentioning that the deflection of all specimens increases after being rehabilitated by Basalt Fabric, except the specimens HB11 & HB12. Therefore, it can be concluded that ductility of the rehabilitated RCHBs increases significantly in addition to the increase in load capacity. For HB11 & HB12, the decrease in the deflection after being rehabilitated by Basalt fabric is related to the shapes of HB11 and HB12. In these specimens, debonding of Basalt Fabric strips was observed earlier as compared to other RCHBs types.

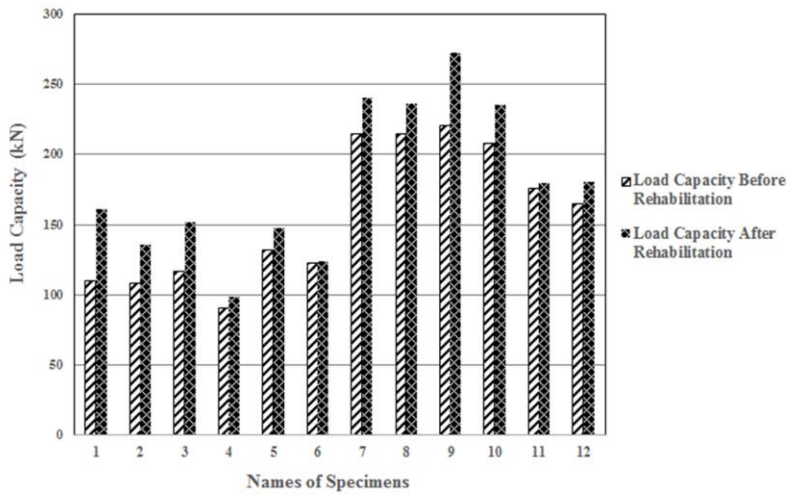

Figure 3.5 Comparison between the load capacity before and after the rehabilitation of all specimens

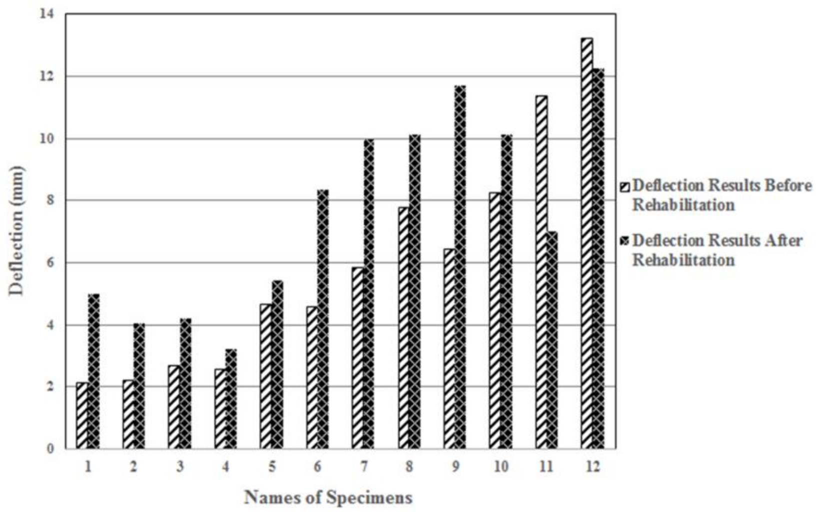

Figure 3.6 Comparison between the deflections before and after the rehabilitation of all specimens

The modes of failure of all specimens after being rehabilitated were debonding failure as mentioned in Table 3.5, while the failure modes of the specimens before the rehabilitation were variables between diagonal shear failure to the flexural failure and (flexural and shear) cracks with shear failure, depending on the shapes and details of steel reinforcement of haunched beams. The most significant and interesting outcome regarding the crack pattern of RCHBs in group one was that the failure of the haunched beams occurred at a section approximately above the kink of the major crack. These major cracks propagate upwards when the haunch's inclination increase, which can be clearly seen in Figure 3.7. In the other words, there is no noticeable increase in ultimate shear strength after being rehabilitated by

FRP strips when the angle of inclination of the haunched beams increased. Moreover, when the major crack propagates upwards, the distance from the top side to the major crack will decrease and then there is not enough distance for the strips of FRP to increase the cohesion between itself and the surface of specimens. Therefore, the amount of increase in the load shear capacity of rehabilitated prismatic beams is higher than the increase in the capacity of rehabilitated haunched beams. Load-deflection curves of all haunched beams before and after rehabilitation can be observed from Figures 3.8 and 3.9.

Tested RCHBs

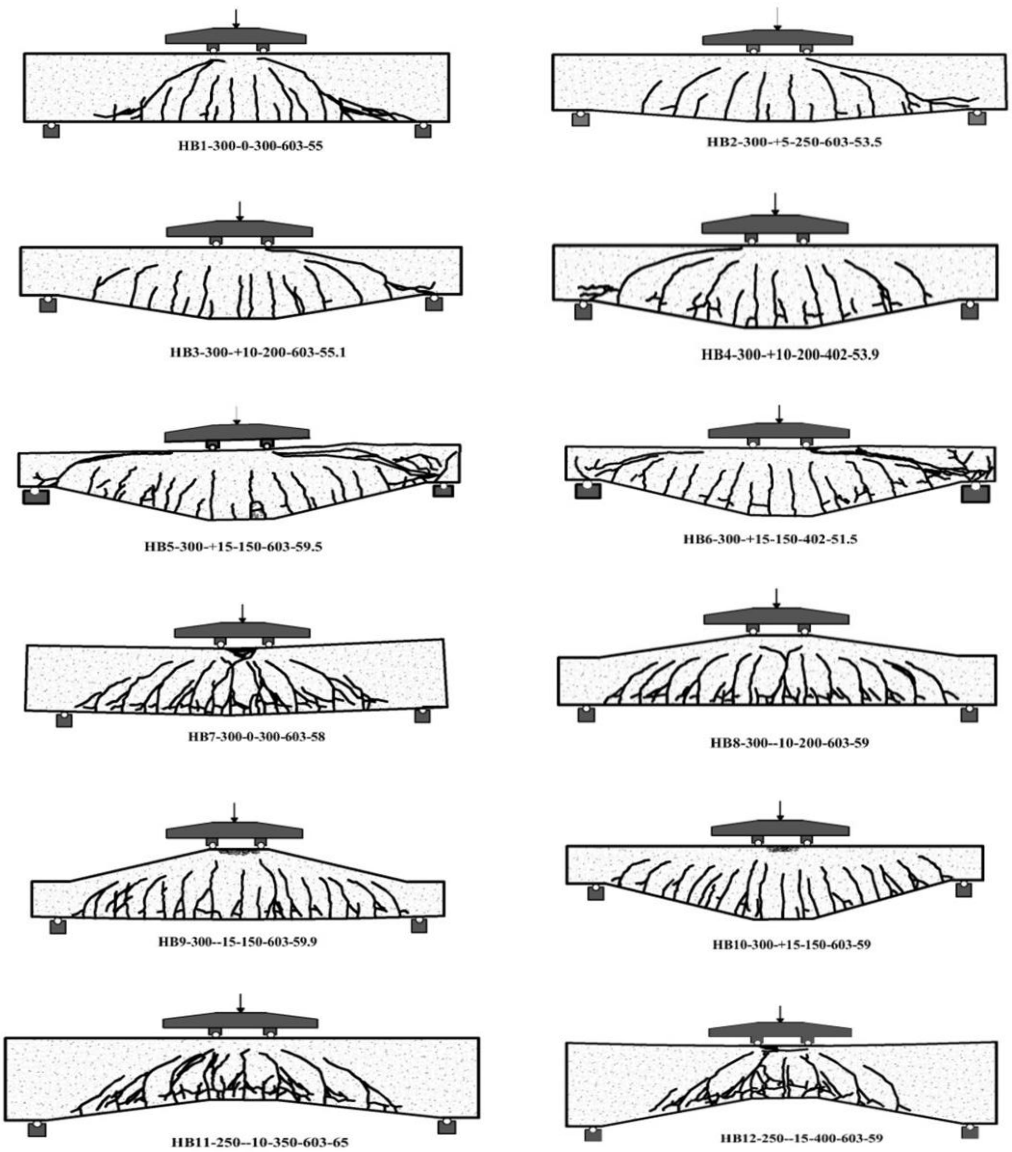

Figure 3.7 Cracks pattern of tested haunched beams (HB1-HB12)

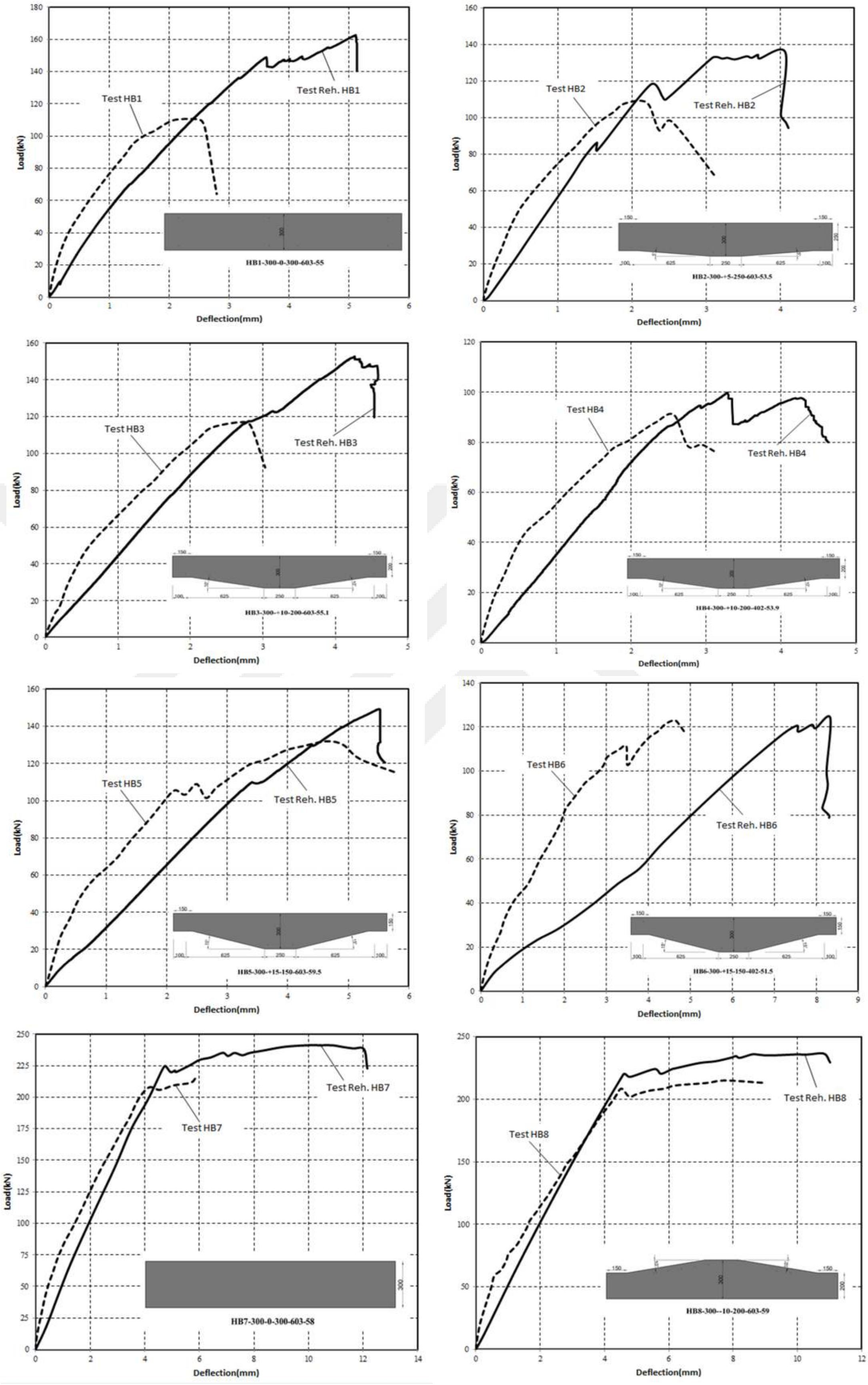

Figure 3.8 Load-Deflection curves of (HB1-HB8) for experimental test before and after the rehabilitation

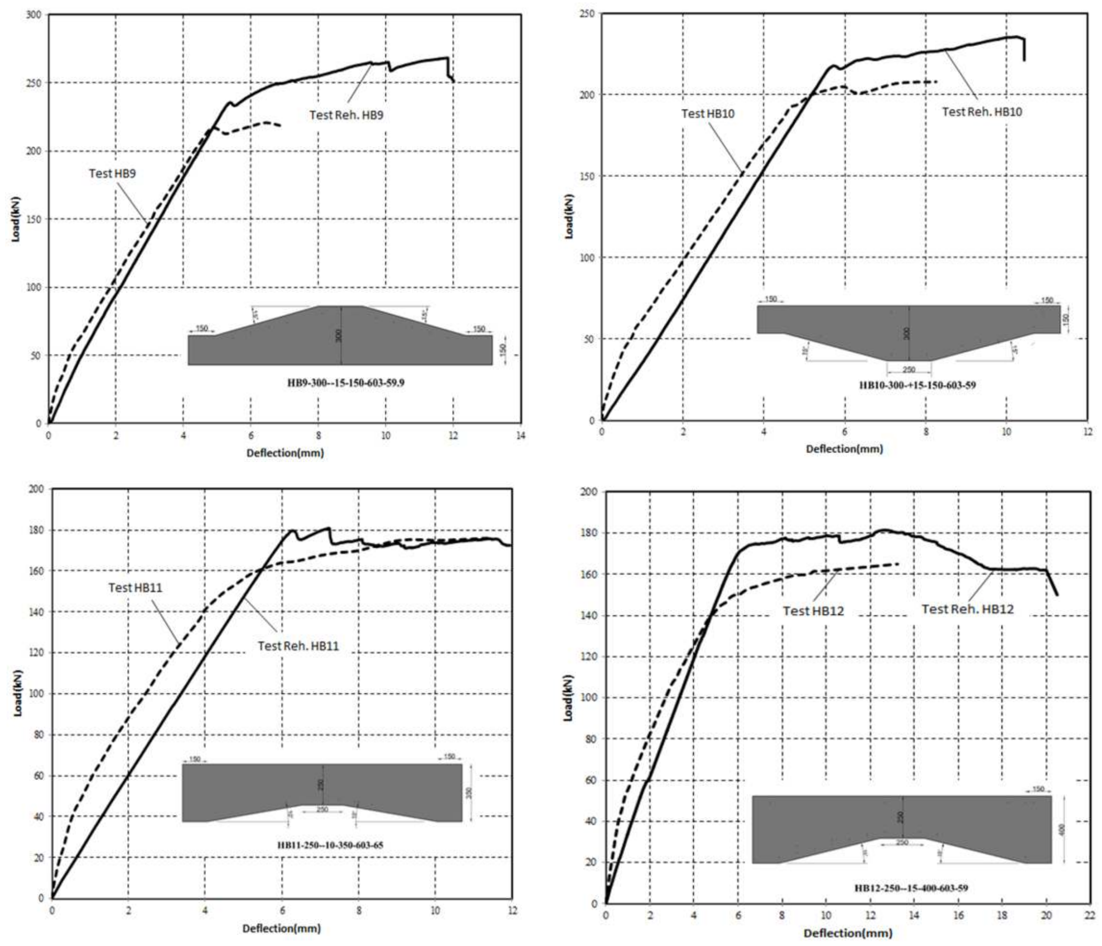

Figure 3.9 Load-Deflection curves of (HB9-HB12) for experimental test before and after the rehabilitation

3.3 Rehabilitation of RCHBs by Carbon Fibers (CFRP)

3.3.1 Description works and Objective

This study consists of two parts, the first part the experimental findings obtained from structural tests of damaged RCHBs after being rehabilitated by CFRP, which had been prepared and tested by (ALBEGMPRLI 2017, Mansoori 2017) before. The second part which will describe in chapter four was the same procedure of simulating of proposing models of part 3.2, which is following a new FE methodology for the simulation the behavior of rehabilitated RCHBs by use of ATENA-GiD 3D software package. The main aims of using and exhibiting previous experimental results of rehabilitation RCHBs by CFRP are to evaluate the effectiveness of proposing models of FE analysis which were used before.

3.3.2 Experimental Program

The experimental program consists of 12 reinforced concrete haunched beams (RCHBs). There are two types of RCHBs (A and B), each type has 6 RCHBs which were designed to fail in shear. All reinforced concrete haunched beams (RCHBs) have the same length and width of 1700 mm and 150 mm respectively, while the height is variable. The shear span of all beams is equal to 65 mm and all beams were designed without steel stirrups, except under loading points and above supports. All details of geometry and steel reinforcements for all RCHBs are shown in Table 3.6, in addition to Figures 3.10 and 3.11.

There were 8 RCHBs with different angles of inclination (10°and 15°) which were repaired by epoxy injection and strengthened with CFRP strips. The strips were placed in vertical and inclined positions that correspond to 90^o and 45^o with respect to the x-axis. There were also 2 RCHBs with an inclination angle of 5^o which were repaired by epoxy injection only. Moreover, 2 prismatic beams were included as reference beams in the experimental program. These beams were also repaired by epoxy injection and strengthened with a vertical and different width of CFRP strips.

Table 3.6 Geometries and steel reinforcement details of all RCHBs

Name of RCHB	Beam type	Type	α^o	h_f^* (mm)	h_S^* (mm)	Reinforced details			
						A_s (mm)^2	N0. Steel	$A_{s'}$ (mm)^2	N0. Steel
1	Rf1*U90	Rf	0	300	300	603	3ϕ16	100	2ϕ8
2	A1-5INJ*	A	5	300	250	603	3ϕ16	100	2ϕ8
3	A1-10U90	A	10	300	200	603	3ϕ16	100	2ϕ8
4	A2-10U45	A	10	300	200	603	3ϕ16	100	2ϕ8
5	A1-15U90*	A	15	300	150	603	3ϕ16	100	2ϕ8
6	A2-15U45	A	15	300	150	603	3ϕ16	100	2ϕ8
7	Rf2U90	Rf	0	250	250	603	3ϕ16	100	2ϕ8
8	B1-5INJ	B	-5	250	300	603	3ϕ16	100	2ϕ8
9	B1-10U90	B	-10	250	350	603	3ϕ16	100	2ϕ8
10	B2-10U45	B	-10	250	350	603	3ϕ16	100	2ϕ8
11	B1-15U90	B	-15	250	400	603	3ϕ16	100	2ϕ8
12	B2-15U45	B	-15	250	400	603	3ϕ16	100	2ϕ8

INJ*: repaired with epoxy injection only; **Rf1***: first reference beam (prismatic); **A or B**: Beam type; **5, 10 or 15**: angle inclination of haunched beams; **U**: shape of wrapping; **45° or 90°**: angle inclination of CFRP strips with respect to the x-axis; h_f: depth at the middle; h_s: depth at the supports .

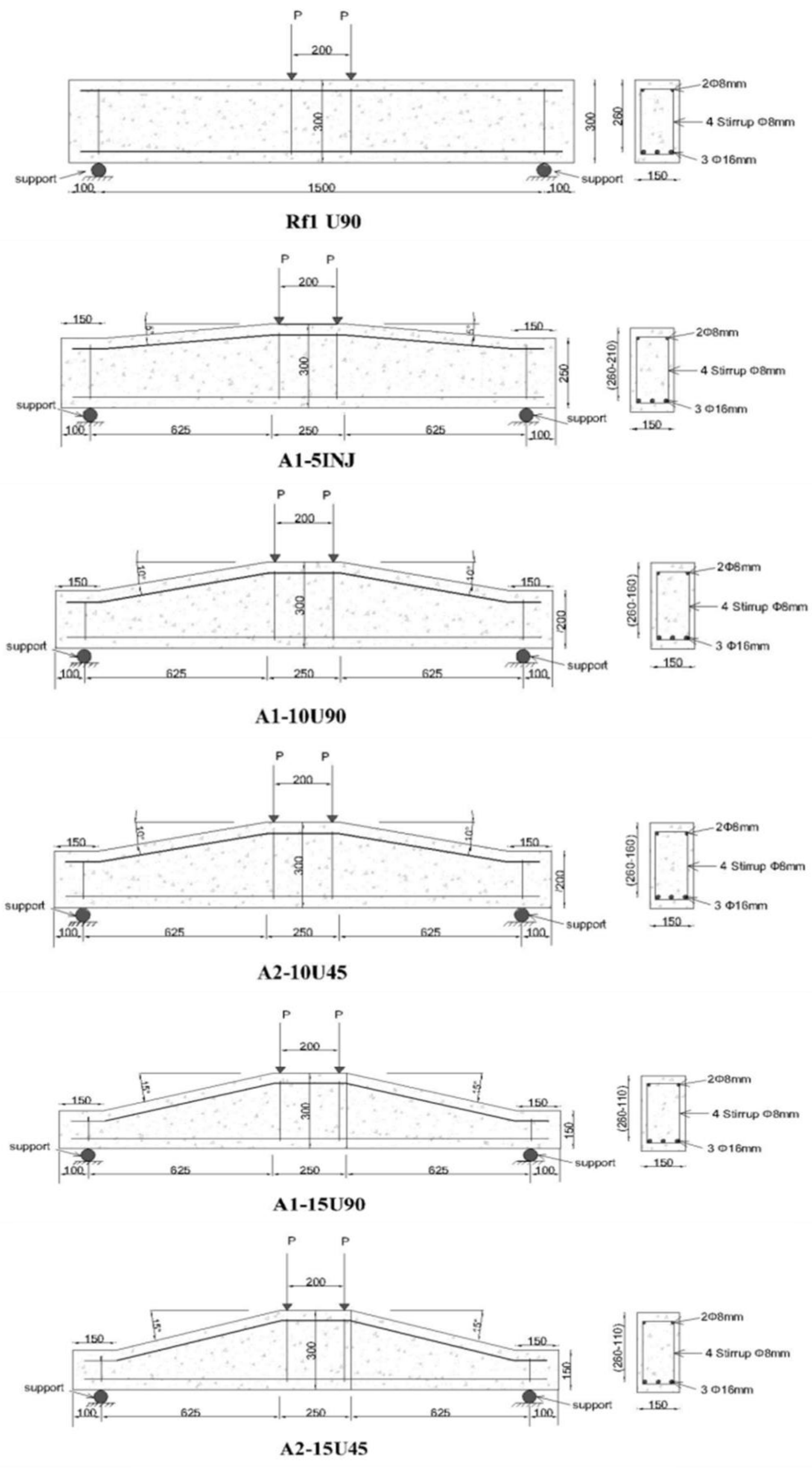

Type A (All dimensions in the figures are in mm)

Figure 3.10 Geometries and steel reinforcement details of RCHBs type A

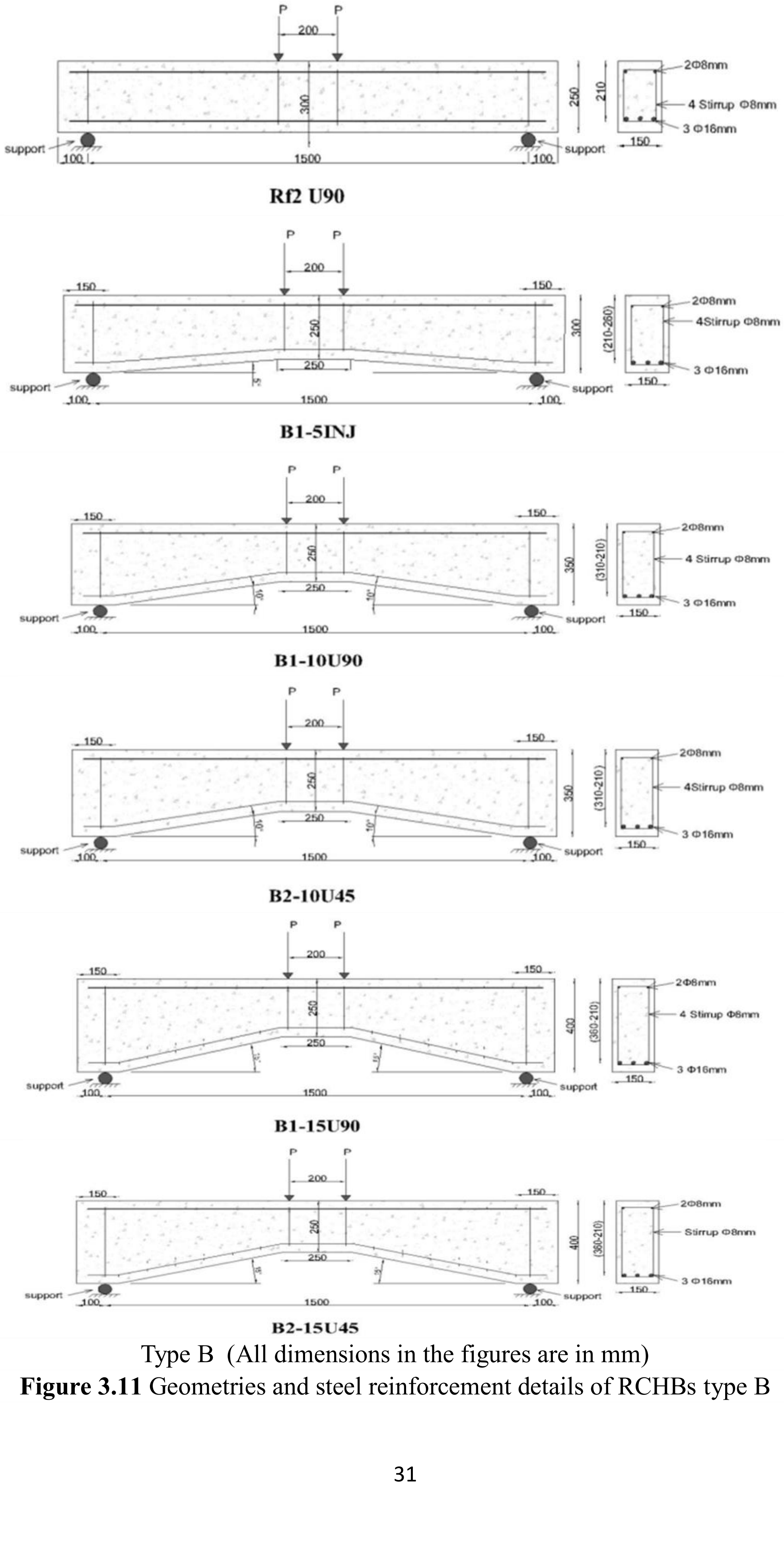

Type B (All dimensions in the figures are in mm)

Figure 3.11 Geometries and steel reinforcement details of RCHBs type B

3.3.3 Materials Properties

3.3.3.1 Concrete

CEM I 32.5 R type Portland cement, silica fume, and fly ash type F were utilized for producing self-compacting concrete (SCC). Trial batches were produced for the SCC mixture to fulfill EFNARC (European Federation for Specialist Construction Chemicals and Concrete Systems) fresh properties limitations (The European Project Group 2005). Moreover, 28 days compressive strength ranged from 44.2 to 62 MPa. The details of mixture proportions are given in Table 3.7. Mechanical properties of cylinder samples of self-compacted concrete (SCC) used for production of all RCHBs are given in Table 3.8.

Table 3.7 Details of mix proportion in kg/m^3

Cement	Silica Fum	Fly Ash	Water	Coarse Aggregate	Sand	Super Plasticizer
250	35	215	150	680	1100	5

Table 3.8 Test results of compressive strength, modulus of elasticity and splitting tensile strength of SCC

Name of RCHB	Beam code	Type	$F_{c\ (MPa)}$	$E_{C\ (GPa)}$	f_{ts} (MPa)
1	Rf1*U90	Rf	44.5	34.2	3.72
2	A1-5INJ*	A	60	37	4.4
3	A1-10U90	A	49	35.26	4.04
4	A2-10U45	A	51.5	33.2	4.3
5	A1-15U90*	A	42.5	34	3.7
6	A2-15U45	A	60	37.2	4.15
7	Rf2U90	Rf	60.7	34.2	3.87
8	B1-5INJ	B	58.5	37.26	4.01
9	B1-10U90	B	44	33.1	3.69
10	B2-10U45	B	61	37	4.3
11	B1-15U90	B	62	37.4	4.35
12	B2-15U45	B	50.1	32.74	4.3

3.3.3.2 Steel Reinforcement

Three sizes of steel reinforcement were used. The diameters of steel reinforcement were (8, 10 and 16) mm. The yield strength of the bars was 550, 485 and 456 MPa, respectively; the ultimate strength was 640, 595 and 560 MPa, respectively.

3.3.3.3 Epoxy Injection

In this study, Sikadur 52 epoxy was used which consists of two-components A and B. These two components were mixed in a ratio of 2:1 by an electric mixer (drill) with slow rotation (maximum 250 RPM) for 3 minutes to get a homogeneous mixture according to the manufacturer's recommendations. The properties of epoxy resin (Sikadur 52) were shown in Table 3.3.

3.3.3.4 Adhesive and CFRP Sheet Material

The epoxy adhesive used in this study was (Teknobond 300 Tix). It consists of two-component A and B, mixed with a ratio of 1:4 by an electric mixer (drill) with a speed of 400 RPM for 2-3 minutes to get a homogeneous mixture according to manufacturer's recommendation. Table 3.9 shows the properties of (Teknobond 300 Tix). Table 3.10 shows the general properties for the CFRP.

Table 3.9 General properties of TEKNOBOND 300 TIX

TYPE	TEKNOBOND 300 TIX
Pot life at 20C° (Minutes)	30
Flexural Strength7 days (N/mm^2)	≥ 25
Compressive Strength7 days (N/mm^2)	≥62.5
Bond Strength 7 days (N/mm$^{2)}$	≥3
Mixing ratio	4:1
Elastic Modules 7 days (GPa)	>20
Color (A + B)	Off-white
Fluid density (Kg. /Lt.)	1,02 ± 0,02

Table 3.10 Properties of Carbon Fiber Reinforced Polymer Fabric

Type	Pattern	Tensile Strength (MPa)	Tensile Modulus (GPa)	Strain (%)	Density g/m^2	Thickness (mm)	Yarn	Weft
SPN U 300	Unidirectional	4900	240	2	300 ±%3	0.3±%10	12K DOWAKSA CARBON (800 TEX)	1/cm Glass hot melts

3.3.4 The procedure of Rehabilitation and Strengthening

3.3.4.1 Repairing Cracks by Injection Epoxy

The cracks were cleaned by using compressed air to remove dust and loose materials, which are affected by the efficiency of bonding as shown in Figure 3.12 (A). The cracks wider than 0.3 mm should be pressure injected with epoxy before FRP installation which affect the performance of the externally bonded FRP system through delamination or fiber crushing accordance with ACI 440.2R and ACI 224.1R (ACI 224 2008, ACI 440 2008).

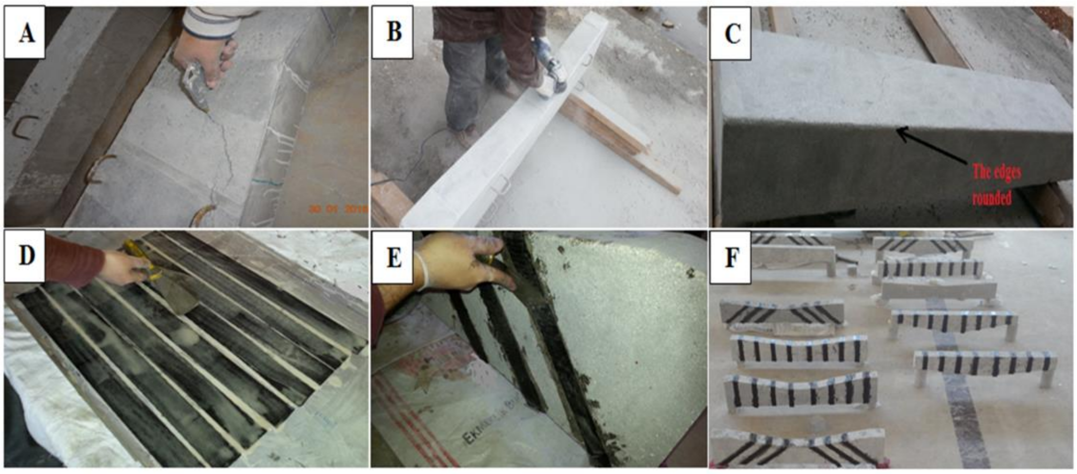

Figure 3.12 Photos show some steps of rehabilitation and strengthening

The injection process includes creating an entry at a distance of (15cm) along cracks. The cracks were sealed on three faces of the beam by using a high viscosity epoxy (Teknobond 200) to keep up the low viscosity epoxy (Sikadur 52) from leaking out. The two components of high viscosity epoxy A+B were mixed with a proper amount with a ratio of 2:1 by using an electric mixer (drill) with a speed of 250 RPM for three minutes. When the mixture became ready, it was used to seal cracks. After this procedure, we wait and finally start the injection process. All cracks were injected by low viscosity epoxy (Sikadur 52). The injection was done by gravity.

3.3.4.2 Surface Preparation

Previous research has shown the importance of bond strength between the concrete surface and CFRP strips. Concrete grinder with rotating disk was used to prepare the concrete surface to remove a laitance layer and roughen the surface of concrete (Hollaway and Teng 2008).

Figure 3.12 (B, C) shows the use of a concrete grinder to clean and roughen the surface of beams. The bottom edges of beams were rotated with a radius about (0.5 in) according to ACI 440.2R (ACI 440 2008), to avoid the concentration of stresses which lead to premature rupture of the CFRP strips.

3.3.4.3 Installation of CFRP Sheet

Before proceeding with the installation of CFRP strips, the concrete surface was cleaned again by using compressed air to remove any remaining dust that results from surface grinding. Lines are then drawn on the surface of the concrete to specify the locations of CFRP strips. All CFRP strips were cut into proper lengths to avoid wasting in quantity of the carbon sheet. After cutting the CFRP sheet, it was started the processes of mixing with a suitable amount of two components of epoxy (A+B) with a ratio 4:1. The epoxy was mixed using the electric mixer (drill) with a speed of 250 RPM for three minutes. The installation of CFRP sheet was by Wet Lay-up method (ACI 440 2008), which requires starting with impregnation of CFRP sheet with epoxy for two faces to make sure that the process of fiber saturation with epoxy is sufficient as shown in Figure 3.12 (D). The sheets become ready to be installed onto the surface of the beam. The CFRP strips were compressed carefully to expel air bubbles as shown in Figure 3.12 (E, F). The width, spacing, and configuration between CFRP strips were listed in Table 3.11.

Table 3.11 Configuration of CFRP strips

Name of RCHB	Beam code	Strengthening scheme	$W_{f\ (mm)}$	$S_{f\ (mm)}$	$t_{f\ (mm)}$
1	Rf1U90		80	180	0.3
2	A1-5INJ	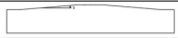	-	-	-
3	A1-10U90		50	200	0.3
4	A2-10U45		50	200	0.3
5	A1-15U90		50	200	0.3
6	A2-15U45		50	200	0.3
7	Rf2U90		50	200	0.3
8	B1-5INJ		-	-	-
9	B1-10U90		50	200	0.3
10	B2-10U45		50	200	0.3
11	B1-15U90		50	200	0.3
12	B2-15U45		50	200	0.3

W_f: Width of CFRP strips. S_f: Spacing between CFRP strips. t_f: Thickness of CFRP strips.

3.3.5 Experimental Results of RCHBs Before and After the Rehabilitation

All beams have been repaired by epoxy injection and rehabilitated by CFRP strips except two beams with the angle of inclination equal to 5°, which were just repaired by epoxy injection to check the efficiency of epoxy injection for restoring the load capacities of haunched beams.

The test results of all beams are listed in Table 3.12. The results include the ultimate load capacities and the corresponding deflections at mid-span with the failure mode before and after the rehabilitation. The ultimate shear load capacities before the rehabilitation varied according to haunch beam types. Better mechanical behaviors were observed for the beams that have smaller depths at the supports. HB5-A1-15U90 and HB6-A2-15U45 beams appeared to have higher shear load capacities as compared to other RCHBs. Also, it can be seen from the results obtained before rehabilitation that beams of type A can carry higher loads as compared to beams of type B Moreover, the stiffness of beams of type B is smaller than beams of type A leading to higher deflection values at maximum loads for beams of type B.

On the other hand, ultimate load capacities recovered after being rehabilitated by CFRP changes between 131% and 149% of the corresponding original capacity of the beams of type A. However, the recovering amount is between 115% and 131% of the original capacity for the beams of type B. Moreover, the recovered capacities of tested prismatic beams are 142% and 210% of the original capacities after being rehabilitated by CFRP fabrics.

The important variable which affects the ultimate shear capacity after rehabilitation is the degree of damage of the haunched beams before rehabilitation, besides, shape of haunched beam, type and ratio of FRP fabrics and the quality of cracks repair before strengthening with the fabrics affect the load capacity of the rehabilitated beams. For instance, load capacities of HB2-A1-5INJ and HB8-B1-5INJ beams increased after rehabilitation as amount of 104% and 141% of their original capacities even they were rehabilitated only by crack repair epoxy.

Figure 3.13 shows the ultimate shear load capacities of all RCHBs before and after being rehabilitated with CFRP. The failure modes of RCHBs which were rehabilitated with CFRP fabrics were debonding of the fabric, as shown in Table 3.12, while the failure mode of all samples was shear failure before the rehabilitation. Furthermore, it can be concluded that strengthening with vertical CFRP strips is more efficient than strengthening with the inclined strips for all types of beams.

Figures 3.14, and 3.15 represent the load-deflection behavior with resulting crack patterns of all RCHBs before and after the rehabilitation. As can be seen from the figures that the stiffness of haunched beams after being rehabilitated are less than the stiffness before rehabilitation. Moreover, the paths of crack patterns after the rehabilitation are different than the paths before the rehabilitation which proves the efficiency of the crack repair epoxy before strengthening.

Table 3.12 Results of experimental tests

Name of RCHB	Beam code	Strengthening scheme	Experimental					Mode of failure	
			$^*P_{Bef.}$ (kN)	$\Delta_{Bef.}$ (mm)	$^{*1}P_{Aft.}$ (kN)	$\Delta_{Aft.}$ (mm)	$P_{Aft.}/P_{Bef}$	Before Repairing	After Repairing
1	Rf1U90		107	1.51	225	9.65	2.10	Shear	*[2]D.F
2	A1-5INJ		113.5	2.217	118.2	3.401	1.04	Shear	Shear
3	A1-10U90		114.5	2.51	170.5	4.572	1.49	Shear	D.F
4	A2-10U45		115.3	2.72	160	4.413	1.39	Shear	D.F
5	A1-15U90		121	2.535	158	4.407	1.31	Shear	D.F
6	A2-15U45		113.2	2.48	164	4.192	1.45	Shear	D.F
7	Rf2U90		94.4	2.618	134	5.29	1.42	Shear	D.F
8	B1-5INJ		108	5.554	152.8	7.555	1.41	Shear	Shear
9	B1-10U90		101.5	6.219	130.8	5.673	1.29	Shear	D.F
10	B2-10U45		91	7.2	110	7.71	1.21	Shear	D.F
11	B1-15U90		104	5.328	136	5.389	1.31	Shear	D.F
12	B2-15U45		95.5	8.362	110	10.64	1.15	Shear	D.F

$^*P_{Bef.}$=Ultimate load capacity before rehabilitation (kN); $^{*1}P_{Aft.}$=Ultimate load capacity after rehabilitation (kN); *[2]D.F= Debonding failure in CFRP.

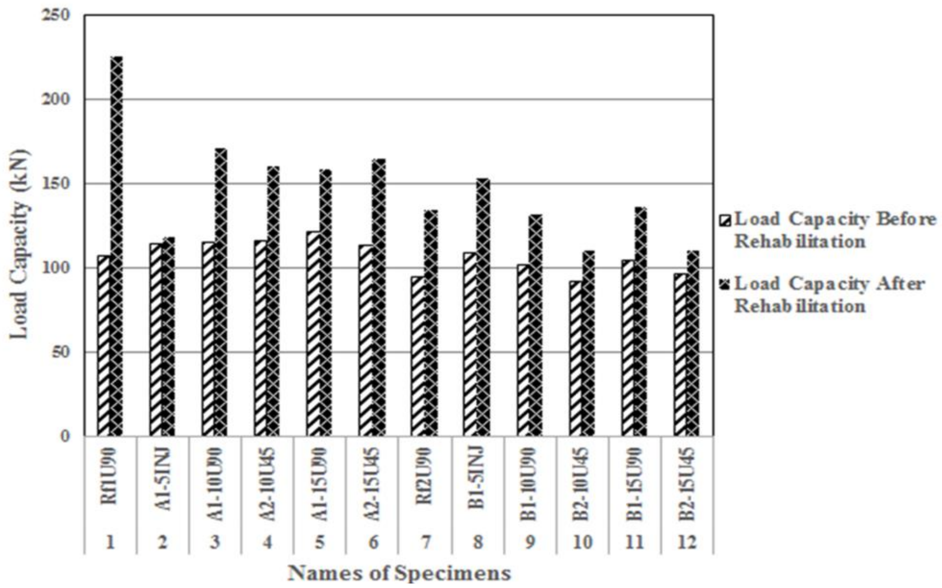

Figure 3.13 Comparison between the load capacity before and after the rehabilitation of all specimens of hunched beams

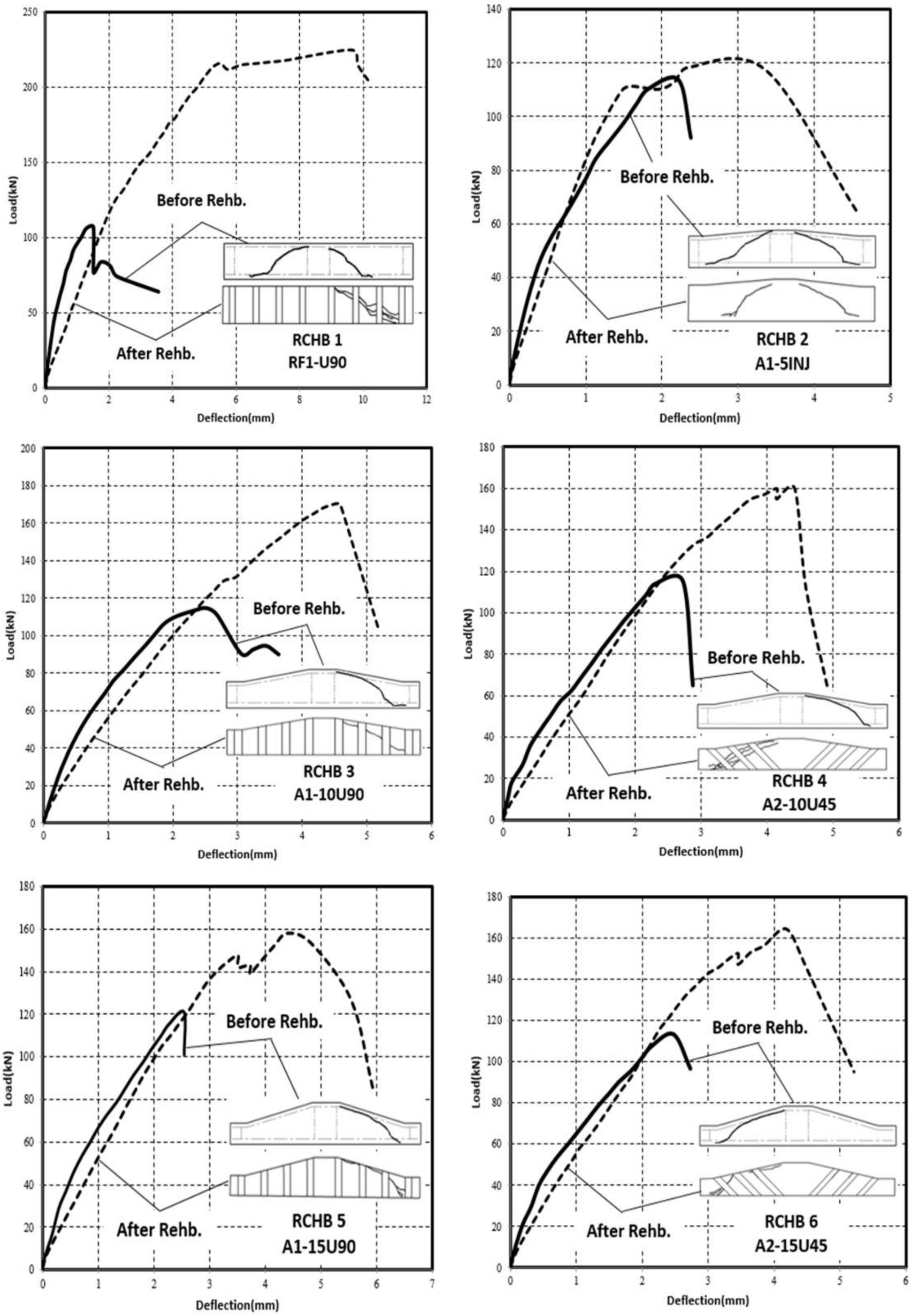

Figure 3.14 Load-Deflection curves of experimental test with cracks pattern before and after the rehabilitation for HB1 to HB6

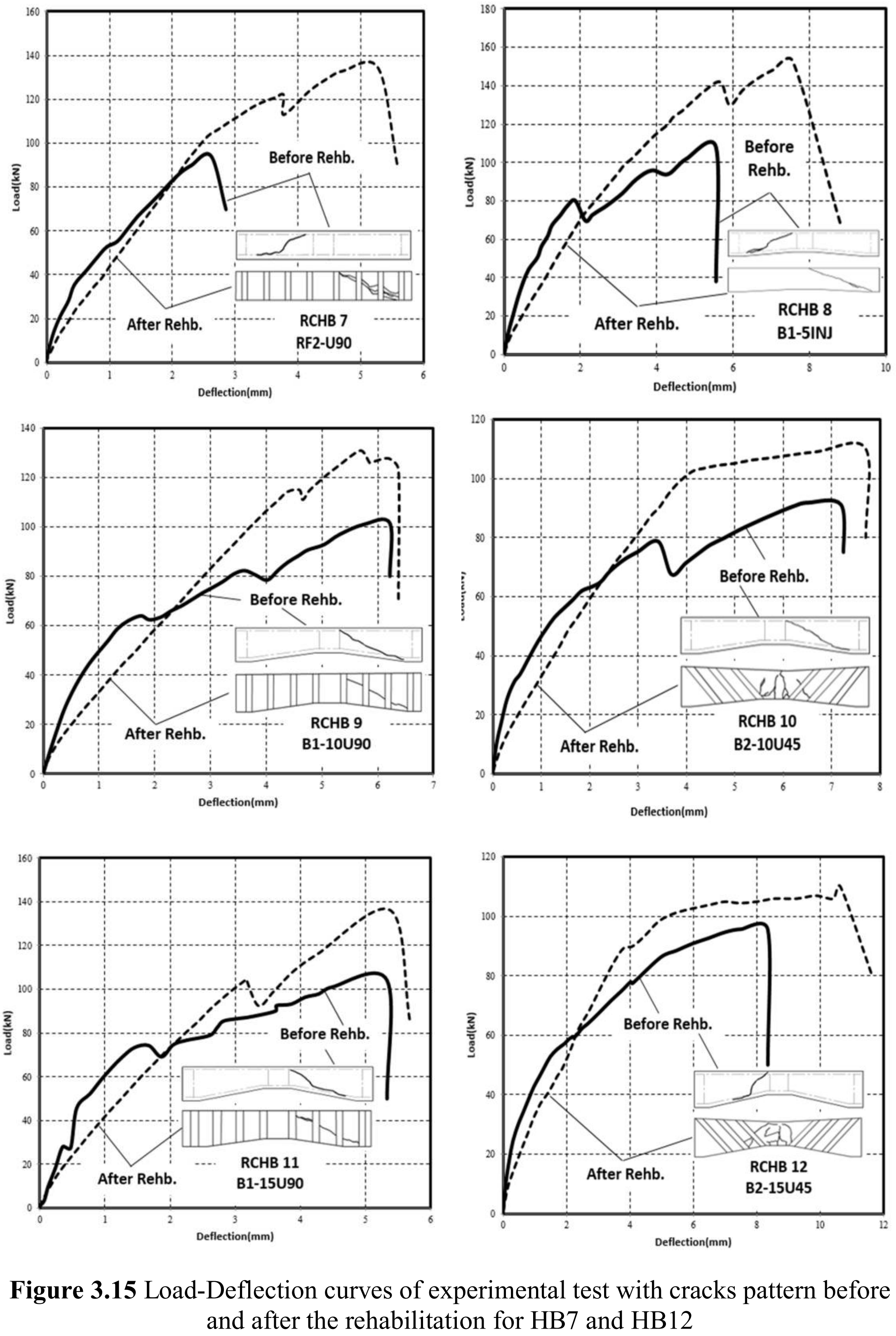

Figure 3.15 Load-Deflection curves of experimental test with cracks pattern before and after the rehabilitation for HB7 and HB12

CHAPTER 4

REHABILITATION OF REINFORCED CONCRETE CORBELS

4.1 Objectives

The main aim of this study is to investigate the mechanical behavior of heated and non-heated, damaged reinforced concrete corbels (with and without steel fiber) after being rehabilitated with new uses of Basalt Fiber Mesh (BFM) and Basalt Fiber Fabric (BFF). In addition to the behavior of corbels which are rehabilitated cracks only by injecting material without wrapping by any FRP. Moreover, to investigate the ultimate load capacities and the failure modes before and after the rehabilitation.

4.1.1 Experimental Work Description

In this study, two groups of corbels consisting of 60 specimens, which had been prepared and tested by (Abdulhaleem 2018) before. For first group having 24 corbels which are rehabilitated by BFM with two parts, for each part having 12 corbels with different parameters (normal concrete for the first part, and self-compacted concrete for the second part, two values of compressive strength, steel reinforcement ratio which was one value for the first part and two values for the second part, three volumetric values of steel fiber ratio and two values of shear span distance), which will be described in detail as follow below. For the second group, having 36 corbels with two parts, for each part having 18 corbels. the first part was repaired with epoxy resin injection only without wrapping by any FRP and the second part was strengthened with BFF beside the injection material in cracks. The rehabilitation of the second group had been repaired and tested by (ALSHAWAF 2017, Hussein 2017). The second group was mentioned in this chapter to compare the results of it with the results of first group. The corbels of group two had been constructed and heated up to three different temperature levels of 250°C, 500°C, and 750°C before the first failure and tested under vertical loading until failure. The concrete was self-compacting concrete (SCC) with two values of compressive strength, two values of steel reinforcement ratio, three volumetric values of steel fiber ratio and two values of shear span distance, which was described in detail as follows:

4.1.2 Corbel Details

All corbels have the same geometry and the steel reinforcement arrangement which is shown in Figure 4.1. The cross-sections of the column and corbels (150mm x 150mm), 4-φ10mm steel bars for longitudinal bar reinforcement of the column, and of 4-φ8mm for stirrups. For the main reinforcement of corbel, two sizes of bars were used: 2-φ10mm and 2-φ14mm.

4.1.3 Material properties

The properties of materials that are used in this experimental work are as follows:

- Ordinary Portland cement was used in all mixes, which corresponded to ASTM type II cement, with specific gravity and fineness, 3.12 and 295 m^2/kg respectively.
- Coarse aggregate used in the first group was crushed gravel with a maximum size of 10 mm, and for the second group, was crushed limestone with a maximum size of 11 mm.

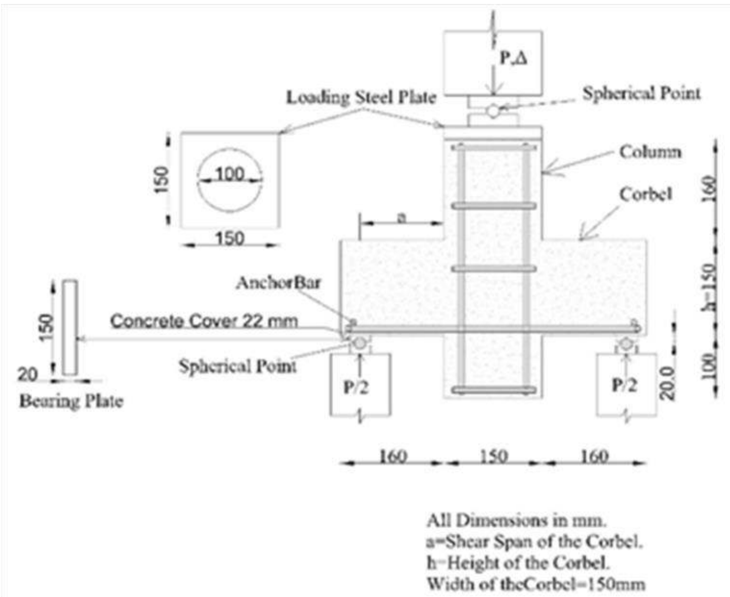

Figure 4.1 Corbels details

- The specific gravity for all coarse and fine aggregates was 2.65.

- Average yield strengths for reinforcement of the first part of group one were found to be 491 MPa, and 560 MPa, and average ultimate strength values were found to be 614 MPa, and 678 MPa, for 8 mm and 10 mm steel bars, respectively.
- In the second group and second part of group one, average yield strengths for reinforcement were found to be 550 MPa, 455 MPa, and 480 MPa, and average ultimate strength values were found to be 640 MPa, 588 MPa, and 595 MPa, for 8 mm, 10 mm and 14 mm steel bars, respectively.
- In the first part of group one, the steel fibers (SF) used were of hooked end, 30 mm length, 0.55 mm diameter, and 54.5 aspect ratio; with 3 different percentages (0%, 1%, and 1.5% steel fiber).
- In the second group and second part of group one, the steel fibers used were hooked end of 30 mm length, of 0.75 mm diameter, and 40 aspect ratio; with 3 different percentages (0%, 0.5%, and 1.0% steel fiber). Polypropylene fibers (PP) of 12 mm length, 0.2 mm diameter, 0.91 g/cm^3 density, and 450 N/mm^2 tensile strength with a percentage of 0.1% of concrete volume were added in the second group.
- For normal concrete, which was used with two values of compressive strengths (30 MPa and 50 MPa). The amount of ingredients for 1 m^3 of normal concrete was illustrated in Table 4.1 for both values of compressive strength.

Table 4.1 Ingredient amount for 1 m^3 of normal concrete

Value of f_{cu}	Cement (kg)	coarse Agg. (kg)	Fine Agg. (kg)	Water (kg)	W/C ratio
f_{cu}= 30MPa	400	1110	600	220	0.55
f_{cu} =50MPa	400	1110	600	190	0.48

- For Self-compacted concrete (SCC) which was used with two values of compressive strength, medium and high strength (MS-SCC and HS-SCC) around 53 MPa and 82 MPa respectively. The amount of ingredients for 1 m^3 of SCC concrete for both values of compressive strength was illustrated in Table 4.2.

Table 4.2 Ingredient amount for 1 m^3 of SCC

Value of f_{cu}	Cement (kg)	Fine Agg. (kg)	Coarse Agg. (kg)	Fly ash (kg)	Silica fume (kg)	Water (kg)	W/C ratio	Super plasticizer (% binder volume)
MS-SCC 53 MPa	250	1000	667	215	35	170	0.55	1.0
HS-SCC 82MPa	450	1000	667	50	35	160	0.36	1.2

- TEKNOBOND 200 is the epoxy used for bonding the Basalt Fiber Mesh (BFM) on concrete. Table 4.3 shows the properties of the epoxy used.

Table 4.3 Properties of epoxy TEKNOBOND 200 (Tekno Construction Chemicals 2016)

Color	Gray
Density	1.5 gr/cm^3
Consumption	1.5 kg/m^2 for 1 mm thickness
Bonding strength concrete	4.0 N/mm^2 (7 days) (TS EN 1542)
Pot life	30 minutes (at 20^o C)
Loading capability	1 day
Full strength	7 days
Application Ground Temperature	(+5° C) - (+30° C)

- Sikadur 52 is the epoxy used for repair damaged specimens by injection in cracks. Table 3.3 shows the properties of the epoxy used which was mentioned in section 3.2.2.
- TEKNOBOND 300 is the epoxy used for bonding the Basalt Fiber Fabric (BFF) on concrete. Table 3.4 shows the properties of the epoxy used which was aforementioned in section 3.2.2.
- Basalt Fiber Mesh (BFM) was used in this study and had a 10 x 10 mm spaced mesh geometry. The mechanical specifications of the basalt fiber mesh are given in Table 4.4.

Table 4.4 Mechanical specifications of BFM

Modulus of elasticity (GPa)	Mesh size (mm x mm)	Tensile Strength (MPa)	Rupture Strain	Design thickness (mm)
32	10 x 10	1600	0.05	0.035

- Unidirectional Basalt Fiber Fabric (BFF) was used for strengthening of some of the corbels. The mechanical properties of the fabric are specified in Table 4.5.

Table 4.5 Properties of BFF

Tensile Strength (MPa)	Tensile Modulus of elasticity (GPa)	Elongation (%)	Thickness (mm)	Polyester Yarn Density (tex)	Area weight (g/m^2)
2100	105	2.6	1.15	5.25	300

4.1.4 Description of Rehabilitation

4.1.4.1 Corbels with BFM

The surface preparation was of primary importance and called for care. Preparation of concrete should be meted out to get rid of any loose or weak material, oil, grease, etc. Therefore a grinder machine was used. The four corners of the corbels were rounded with minimum 13 mm radius to cut back a decrease in the strength and to forestall tearing of the FRP as recommended by ACI 440.2R-08 (ACI 440 2008). Step 1 in Figure 4.2 shows the corbel after being surface prepared.

Preparation of the surface should be meted out before the bonding operation to forestall any contamination. To avoid contamination, the glue was applied to the concrete and BFM with a brush or trowel, pressure was applied to squeeze out excess glue and hold the BFM in place until the glue had hardened. Resin and hardened glue are simply mixed before the gluing operation, epoxy is applied on concrete with a brush or trowel, and then BFM is placed on the epoxy. Steps 2 and 3 show how the glue was placed on the surface of the corbel (Ivanova and Assih 2015a).

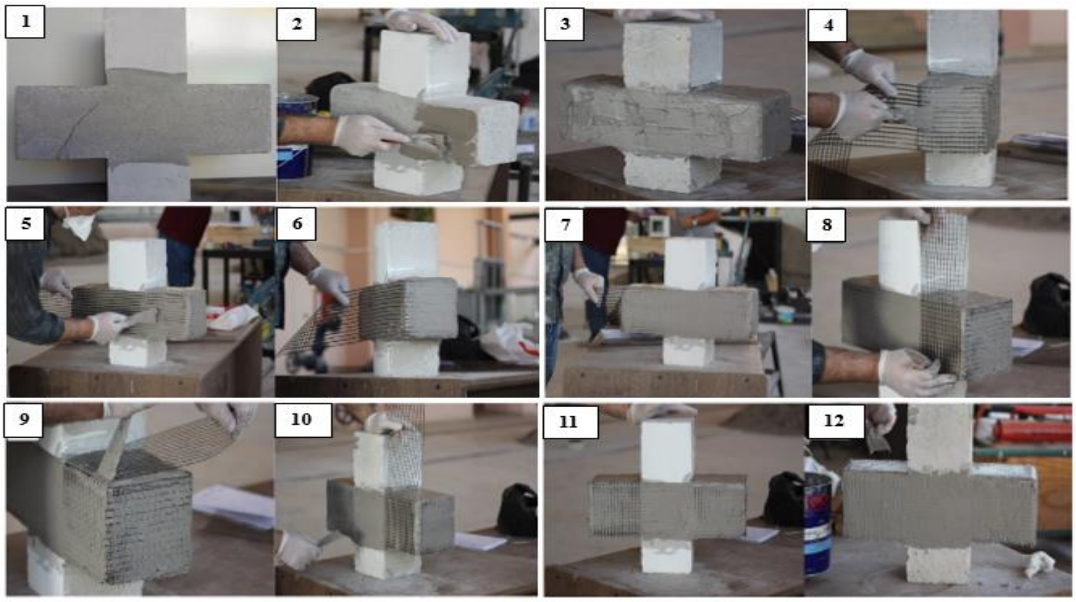

Figure 4.2 Configuration steps of the bonding surface and applying the Basalt Fiber Mesh with epoxy to the damaged corbel from 1 to 12 steps

Four U strips of the BFM were placed on the four positions of the corbel for all specimens to rehabilitate the damaged corbels. The 1st U strip was placed on the front face of corbel as illustrated in steps 4 and 5 in Figure 4.2. The 2nd U strip was placed on the back face of corbel as the 1st U strip was placed on the front face of corbel as illustrated in steps 4 and 5. The 2nd U strip was placed on the back face of corbel as illustrated in step 6 and 7 in Figure 4.2. The positions of the 3rd, and 4th, U strips of BFM were placed on the bottom face of the corbel as illustrated in step 8, 9, 10 and 11 in Figure 4.2. For every strip of BFM after being placed on the first coat of epoxy; a second coat of epoxy was rolled over the BFM. Step 12 in Figure 4.2 illustrates the final shape of rehabilitation by BFM for all samples of corbels.

4.1.4.2 Corbels with Injection Material

First of all, surfaces of corbels were cleaned with the same details in the part 3.5.5.1. The high viscosity epoxy was used as a replacing material for loosing parts of the concrete, and this epoxy was also used in order to prevent the leaking of crack repairing epoxy whose viscosity is very low. The crack repairing epoxy was injected into the cracks by injection syringe. Injection of the epoxy was implemented until ensuring the filling of all cracks. The steps of repairing with epoxy injection are shown in Figure 4.3. All of the corbels strengthened with BFF were also subjected to these methods before gluing the BFF. After injection process, the corbels were left for 7 days for curing of the epoxy in order to obtain the target strength of the epoxy. Eventually, grinder machine was used to level the bottom surface of the all corbel beams as shown in step 7 in Figure 4.3, in order to provide the appropriate setup on the supports of the testing machine.

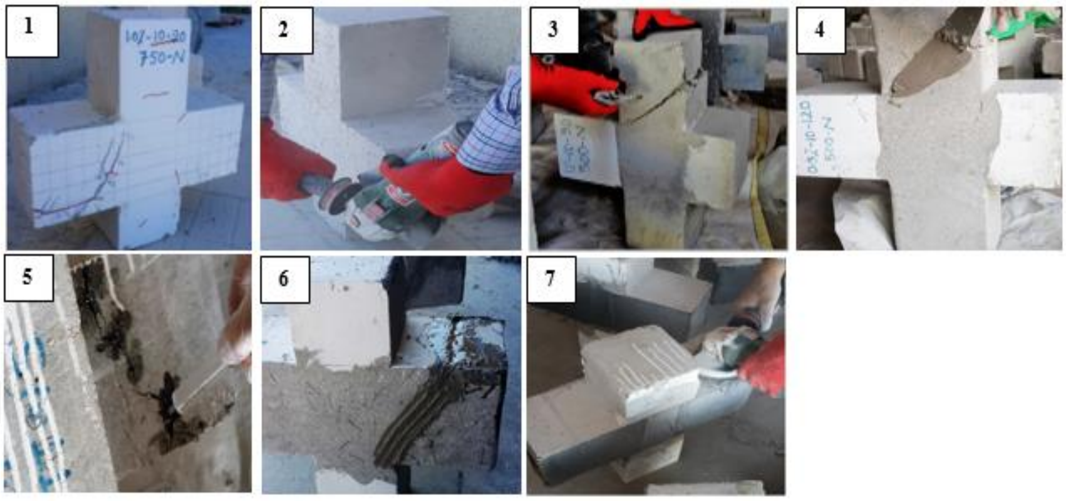

Figure 4.3 Configuration steps of the preparation surface and injection of crack repairing epoxy

4.1.4.3 Corbels with BFF

The second part of group two of corbels was strengthened with BFF in addition to repairing of cracks. The wet lay-up method was followed to replace the strips of BFF which is recommended by ACI 440.2R-08 (ACI 440 2008). Three strips of the BFF were prepared in specific dimensions that are compatible with the corbel dimensions. The components of crack repairing epoxy (epoxy hardener and resin) were mixed by an electric drill machine according to datasheet of the repairing epoxy. Then the BFF was saturated with the lower viscosity epoxy for gluing process. The saturated BFF were glued bi-directionally onto the corbels to achieve better resistance to the combination of vertical and horizontal stresses. Therefore, one layer of the fabric was placed parallel to the corbel axis, and the other layer was wrapped transversally to the corbel surface. Afterward, a trowel was used to eliminate air voids and to achieve perfect adhesion between the fabric and corbel surface. At last, grinder machine was used again for leveling bottom surface of corbels to provide successful simultaneous load transfer mechanism up to both of the supports. The steps of strengthening with BFF are illustrated in Figure 4.4.

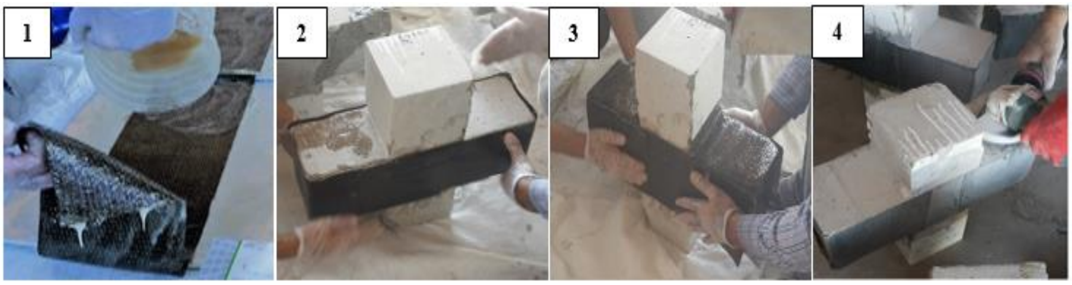

Figure 4.4 Configuration steps of bonding surface and applying the BFF with epoxy

4.1.5 Test Setup

The values of compressive strength were determined as average of three cylindrical samples (150 *300) mm according to ASTM C39 specification. All corbels before and after the rehabilitation were tested under a three-point load (Figure 4.1). The maximum load capacity of the machine used was 500 kN. The loading rate displacement controlled (0.2 mm/min), the datasets were recorded every 0.2 s. Two LVDTs were used to record the deflections of corbels as shown in Figure 4.5.

Figure 4.5 Corbel Setup on the test machine

4.2 Results and Discussion of RC Corbels

The results and discussions of experimental work are listed below:

4.2.1 Experimental Results of First Group-Part one

The test results of part one of first group normal concrete corbels which are rehabilitated by BFM are shown in Table 4.6.

Table 4.6 Part one of first group normal concrete corbels rehabilitated by BFM

Type of Concrete and Rehabilitation	Specimen Index	Comp. Strength (f_c) (MPa)	Ultimate Load Capacity before Reh. (kN)	Ultimate Load Capacity After Reh. (kN)	% Recovered of Ultimate Load Capacity after Reh.	Deflection		Mode of Failure	
						Before Reh. δmax (mm)	After Reh. δmax (mm)	Before Reh.	After Reh.
Normal Concrete / Rehabilitation By BFM	C1-50-0.0-10-100	39	151.44	124.4	82.145	1.46	5.35	Shear failure	BFM rupture
	C2-50-0.0-10-130	39	114.013	87.077	76.375	0.863	1.634	Diagonal splitting	BFM rupture
	C3-50-1.0-10-100	40	242.095	188.03	77.668	2.918	6.161	Flexural failure	BFM rupture
	C4-50-1.0-10-130	40	176.77	128.034	72.430	2.489	3.552	Flexural /shear failure	BFM rupture
	C5-50-1.5-10-100	42.5	253.43	188.04	74.198	4.588	8.453	Flexural failure	BFM rupture
	C6-50-1.5-10-130	42.5	171.209	132.332	77.293	1.55	5.378	Shear failure	BFM rupture
	C7-30-0.0-10-100	24	125.7	102.8	81.782	1.134	5.674	Diagonal splitting	BFM rupture
	C8-30-0.0-10-130	24	98.3	78.14	79.491	0.812	3.48	Shear failure	BFM rupture
	C9-30-1.0-10-100	22.3	145.6	120.034	82.441	2.312	5.096	Shear failure	BFM rupture
	C10-30-1.0-10-130	22.3	111.108	86.323	77.693	2.12	5.92	Diagonal splitting	BFM rupture
	C11-30-1.5-10-100	25.5	158.25	119.98	75.817	2.821	6.96	Diagonal splitting	BFM rupture
	C12-30-1.5-10-130	25.5	115.18	96.25	83.565	1.873	5.715	Diagonal splitting	BFM rupture

In Table 4.6, the first and second columns contain the designation of part one of first group with all related values. The first term of specimen index represents the name of the sample (Corbel No. # #), the second term represents the cubic compressive strength of the sample, the third term represents the steel fiber ratio, the fourth term represents the diameter of the main reinforcement, and the last term represents the shear span that will be applied to test the corbels. For all corbels of part one, no injection material was used to repair the cracks in the corbels to investigate the performance of the BFM to rehabilitate the corbels without internal epoxy injection. The third column of Table 4.6 contains all relevant cylindrical compressive strength of corbels. The fourth column of Table 4.6 represents the ultimate load capacity of the corbels before the rehabilitation. It can be concluded from the test results that when the shear span increases, the value of ultimate load capacity decreases for all corbels. Indeed, the increase of compressive strength from 30 MPa to 50 MPa also increases the ultimate load for all corbels as expected. The addition of steel fibers (SF) on the concrete mix enhances the ultimate load and the ductility of each corbel (Fattuhi 1990). The fifth column of Table 4.6 presents the ultimate load capacity of corbels after rehabilitation, and these values are less than the original values. The percentage recovered of load capacity after rehabilitating can be observed in the sixth column of Table 4.6.

It can be summarized from Table 4.6 that the percentage recovered of ultimate load capacity after being rehabilitated for all corbels were found to be variable from 72.430% of C4 until 83.565% of C12 from the original load capacity before rehabilitation, Figure 4.6 shows all values of ultimate load capacity before and after the rehabilitation for all corbels. It can be concluded from the results that the value of rehabilitation depends on the damage degree of corbel before the rehabilitation, which affects results of rehabilitation.

It can be concluded after rehabilitation by BFM led to a significant increase in the maximum deflection which is led to a significant increase in the ductility. The values of δmax for all corbels of part one of first group can be seen in the curves of Load-Deflection behavior as shown in Table 4.7. Obviously, it can be seen from the relation of Load-Deflection that the slope of the curves decreased after rehabilitated by BFM, which means the stiffness of corbels decreased after being rehabilitated by BFM.

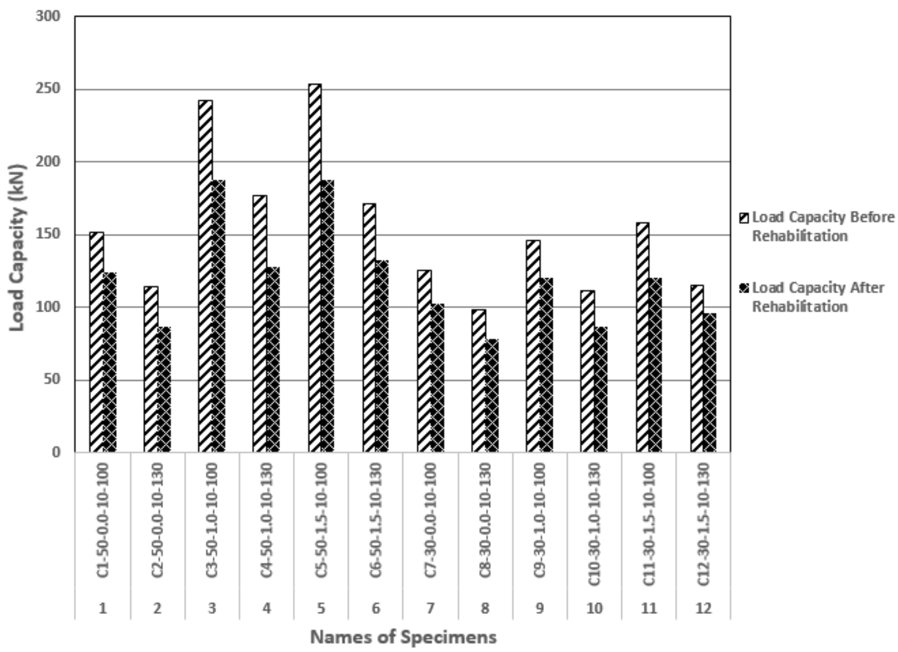

Figure 4.6 Ultimate Load capacity of all corbels before and after the rehabilitation by BFM

The failure modes of the corbels before and after rehabilitation are summarized in Table 4.7. The modes of failure for the corbels before the rehabilitation; flexural failure, shear failure, flexural/shear failure and diagonal splitting failure (Fattuhi 1990). Obviously, the mode of failure after rehabilitation was simply ruptured in the BFM for all corbels and no other type of a failure like a de-bonding failure was observed in the BFM. This type of failure (rupture in the BFM) was a most significant and interesting outcome of this study. Figure 4.7 shows the failure in BFM after being tested for four selected corbels, which is occurred in all samples of part one of first group. Moreover, summary of all results of the corresponding corbels were given in Table 4.7.

Figure 4.7 The mode of failure in the Basalt Fiber Mesh (Rupture in the Fibers)

Table 4.7 Summary of mechanical behavior of corbels for C1 to C12

			Mode of failure		Load-Deflection Relationship
Normal Concrete / Rehabilitation By BFM	C1-50-0.0-10-100	Before Reh.	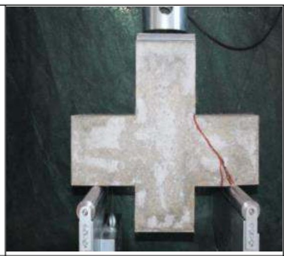	Shear failure	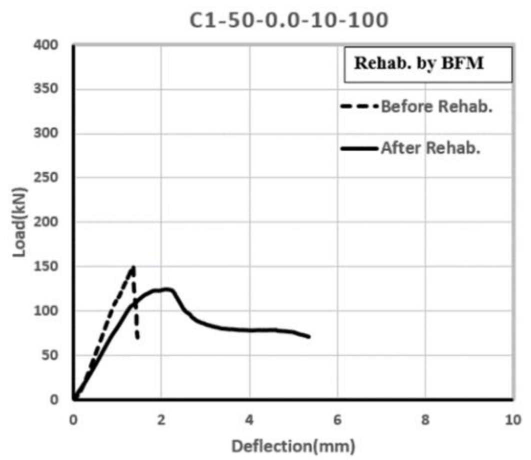
		After Reh.		BFM rupture	
	C2-50-0.0-10-130	Before Reh.		Diagonal splitting	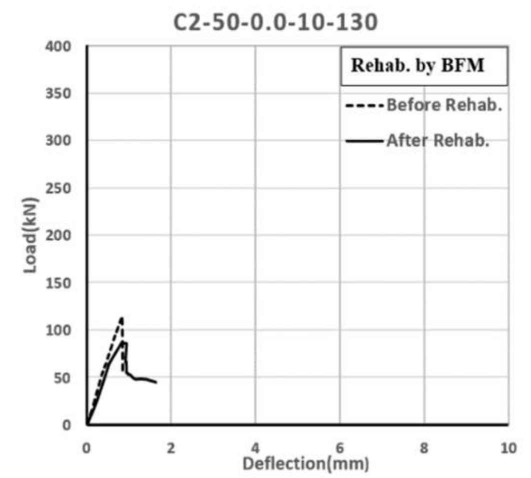
		After Reh.		BFM rupture	
	C3-50-1.0-10-100	Before Reh.		Flexural failure	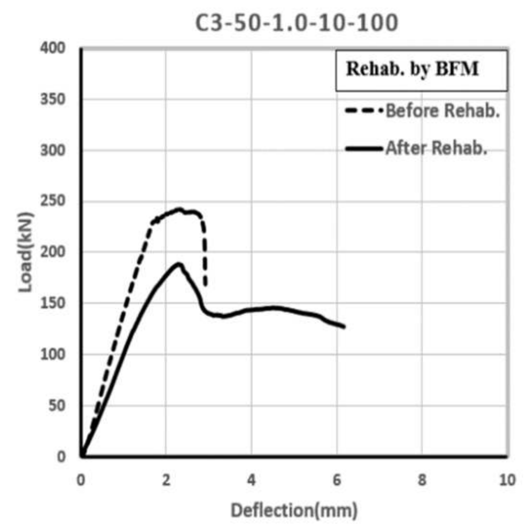
		After Reh.		BFM rupture	

<table>
<tr><td rowspan="7">Normal Concrete / Rehabilitation By BFM</td><td></td><td colspan="2">Mode of failure</td><td></td><td>Load-Deflection Relationship</td></tr>
<tr><td rowspan="2">C4-50-1.0-10-130</td><td>Before Reh.</td><td>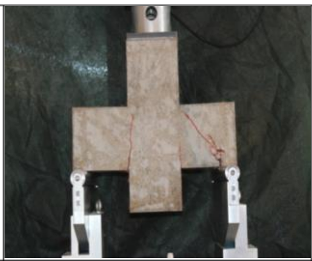</td><td>Flexural /shear failure</td><td rowspan="2">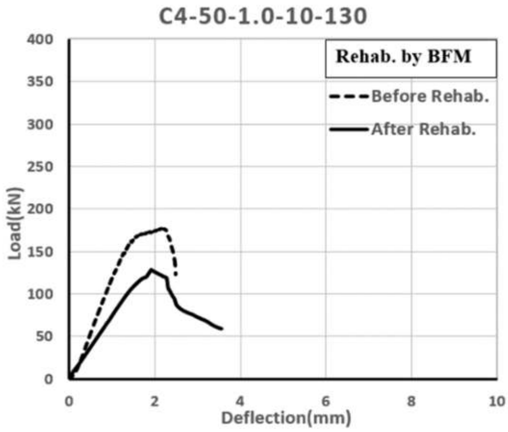</td></tr>
<tr><td>After Reh.</td><td></td><td>BFM rupture</td></tr>
<tr><td rowspan="2">C5-50-1.5-10-100</td><td>Before Reh.</td><td>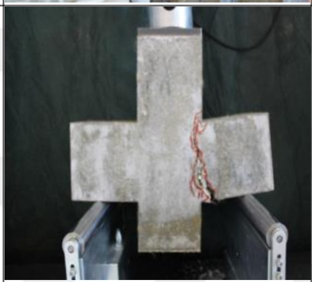</td><td>Flexural failure</td><td rowspan="2">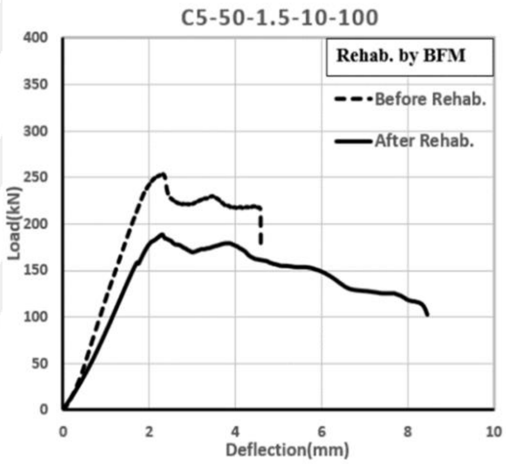</td></tr>
<tr><td>After Reh.</td><td></td><td>BFM rupture</td></tr>
<tr><td rowspan="2">C6-50-1.5-10-130</td><td>Before Reh.</td><td></td><td>Shear failure</td><td rowspan="2">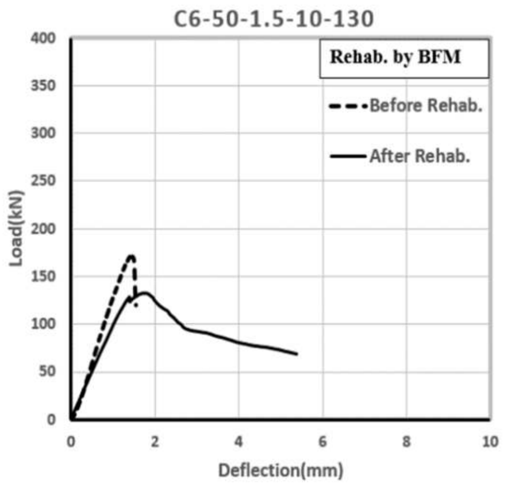</td></tr>
<tr><td>After Reh.</td><td></td><td>BFM rupture</td></tr>
</table>

			Mode of failure		Load-Deflection Relationship
Normal Concrete / Rehabilitation By BFM	C7-30-0.0-10-100	Before Reh.	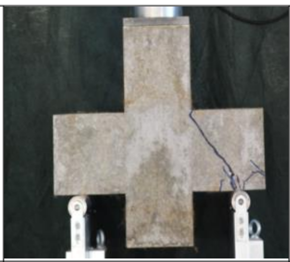	Diagonal splitting	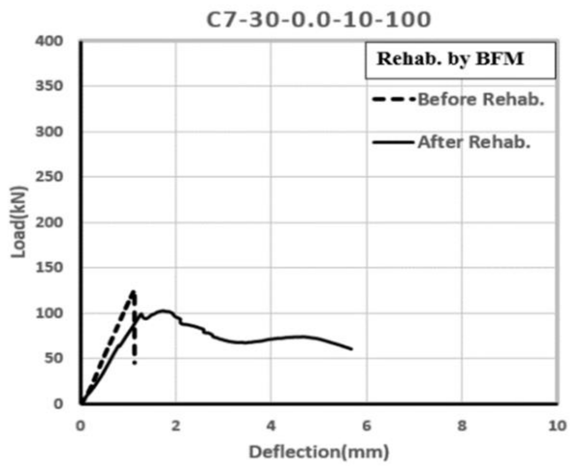
		After Reh.		BFM rupture	
	C8-30-0.0-10-130	Before Reh.		Shear failure	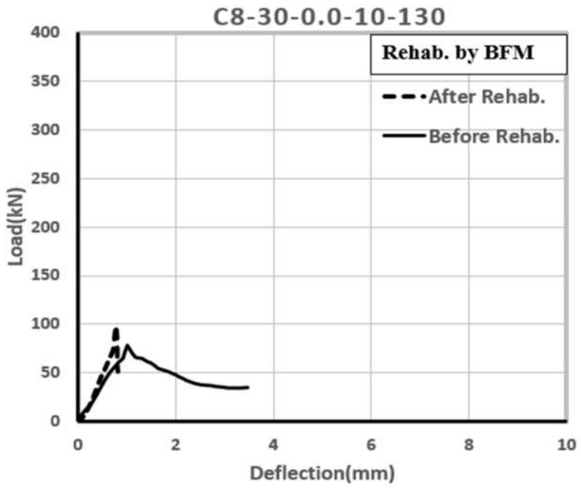
		After Reh.		BFM rupture	
	C9-30-1.0-10-100	Before Reh.		Shear failure	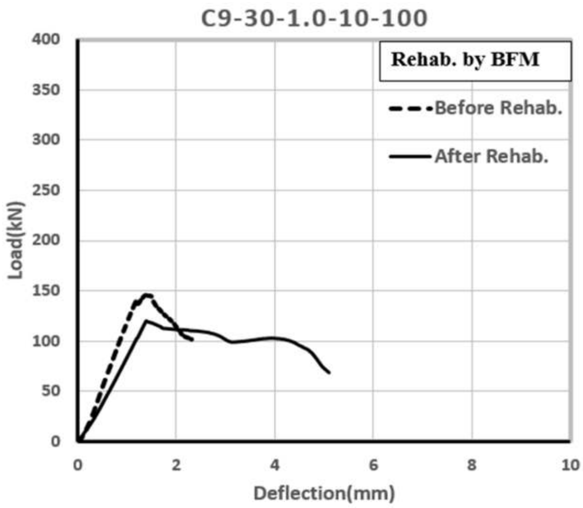
		After Reh.	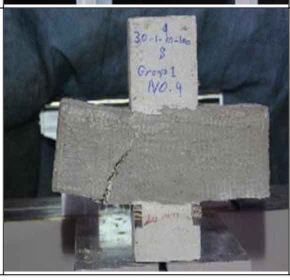	BFM rupture	

<table>
<tr><td rowspan="7">Normal Concrete / Rehabilitation By BFM</td><td></td><td colspan="3">Mode of failure</td><td>Load-Deflection Relationship</td></tr>
<tr><td rowspan="2">C10-30-1.0-10-130</td><td>Before Reh.</td><td></td><td>Diagonal splitting</td><td rowspan="2">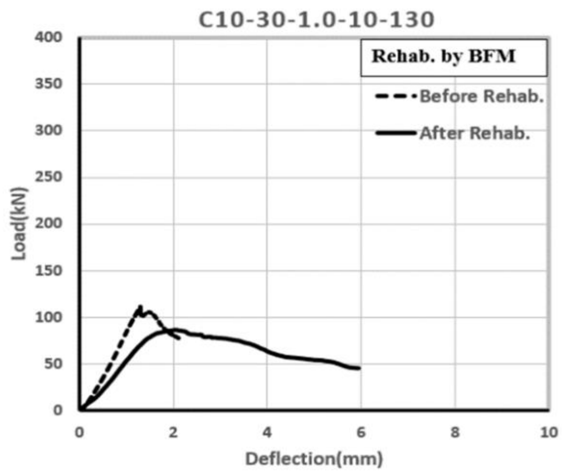
</td></tr>
<tr><td>After Reh.</td><td></td><td>BFM rupture</td></tr>
<tr><td rowspan="2">C11-30-1.5-10-100</td><td>Before Reh.</td><td></td><td>Diagonal splitting</td><td rowspan="2">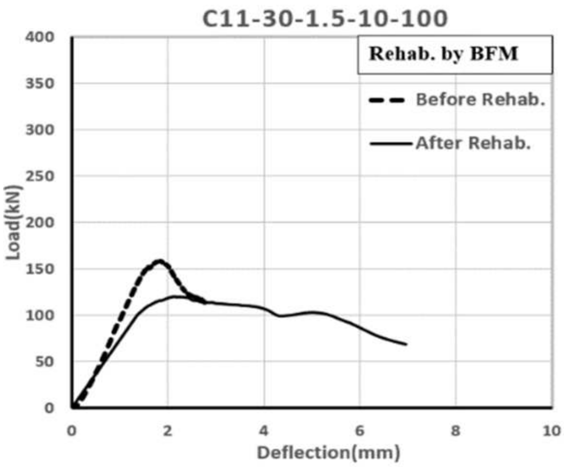
</td></tr>
<tr><td>After Reh.</td><td></td><td>BFM rupture</td></tr>
<tr><td rowspan="2">C12-30-1.5-10-130</td><td>Before Reh.</td><td></td><td>Diagonal splitting</td><td rowspan="2">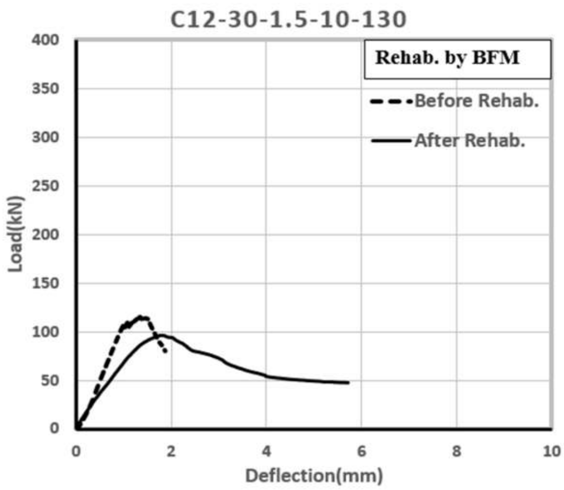
</td></tr>
<tr><td>After Reh.</td><td></td><td>BFM rupture</td></tr>
</table>

4.2.2 Experimental Results of First Group-Part Two

The test results with all details of self-compacted concrete (SCC) corbels belonging to part two of first group which are rehabilitated by BFM are shown in Table 4.8. Varying parameters of corbels in part two were shear span (120 mm and 90 mm), steel fiber ratio (0.0%, 0.5%, and 1.0%) and compressive strength (53 MPa and 82 MPa). Low viscosity epoxy was injected into some corbels to show the effect of internal epoxy injection in rehabilitation. The third column of Table 4.8 contains all relevant cylindrical compressive strength of corbels. It can be observed the detail values of corbels (C13, C19, C14, and C20), 53 MPa cubic compressive strength, 0.0% and 0.5% steel fiber ratio, no injection material was used in these corbels. The percentage recovered of ultimate load capacity after being rehabilitated by BFM was found to be started from 57.432% of C19 until 81.272% of C13 from the origin load capacity before rehabilitation. The ductility was increased after rehabilitation, by comparing the maximum deflection before and after the rehabilitation. However, the stiffness of these corbels decreased, and it is obvious to see that by comparing the slope of load-deflection curves in (Table 4.9) before and after using the BFM. The mode of failure after rehabilitation was ruptured in the fiber for all corbels of self-compacted concrete corbels. C15 and C21 were injected by low viscosity epoxy to repair the internal cracks. The percentage recovered of ultimate load capacity was found to be a 106.421% and 136.428% for C15 and C21 respectively of the original load capacity before the rehabilitation.

In general, when the shear span to the depth (a/h) ratio is decreased, the ultimate load will be increased when the other variables are kept constant. Actually, it is observed that the value of increase load capacity after rehabilitation of C15 equal to 6.24% and for C21 equal to 36.43% of original load capacity were used 90mm & 120mm as a shear span respectively. When it is focused on the result of these corbels; the result was opposite of the general concept of shear spans, and to conclude the reason; first of all, must be observed the mode of failure for both corbels. the first corbel (C15) was failed as a diagonal splitting failure and the second corbel (C21) was failed as a flexural failure (Figure 4.8). For a diagonal splitting failure; the bond between main bars reinforcement and surrounding concrete covers were damaged, therefore, the reinforcement of the main bars cannot be working correct status. While the failure of C21 was less damaged than the diagonal splitting.

Table 4.8 Part two of first group SCC corbels rehabilitated by BFM

Type of Concrete and Rehabilitation	Specimen Index	Comp. Strength (f_c) (MPa)	Ultimate Load Capacity before Reh. (kN)	Ultimate Load Capacity After Reh. (kN)	% Recovered of Ultimate Load Capacity after Reh.	Injection Status	Deflection		Mode of Failure	
							Before Reh. δmax (mm)	After Reh. δmax (mm)	Before Reh.	After Reh.
Self-Compacted Concrete/ Rehabilitation By BFM	C13-53-0.0-10-90	52.9	202.1	164.25	81.272	Without injection	0.75	2.607	Shear failure	BFM rupture
	C19-53-0.0-10-120	52.9	90.6	52.033	57.432	Without injection	0.88	3.399	Diagonal splitting	BFM rupture
	C14-53-0.5-10-90	51.1	217.3	170.635	78.525	Without injection	2.546	8.682	Shear failure	BFM rupture
	C20-53-0.5-10-120	51.1	140.2	87.3	62.268	Without injection	2.2	2.85	Diagonal splitting	BFM rupture
	C15-53-1.0-10-90	50.8	230.5	245.3	106.421	injected	0.592	3.944	Diagonal splitting	BFM rupture
	C21-53-1.0-10-120	50.8	156.2	213.1	136.428	injected	1.347	6.504	flexural failure	BFM rupture
	C16-82-0.0-10-90	83.3	235.2	186.55	79.315	Without injection	0.935	4.953	Shear failure	BFM rupture
	C17-82-0.5-10-90	79.5	281.3	186.5	66.299	Without injection	2.339	6.26	Flexural / shear failure	BFM rupture
	C18-82-1.0-10-90	79.8	327.1	180.5	55.182	Without injection	2.504	7.07	Flexural/ shear failure	BFM rupture
	C22-82-0.0-14-90	83.3	264.82	265.3	100.181	injected	1.72	4.66	Diagonal splitting	BFM rupture
	C23-82-0.5-14-90	79.5	285.6	130.12	45.560	Without injection	0.46	3.1	Diagonal splitting	BFM rupture
	C24-82-1.0-14-90	79.8	334.402	136.3	40.759	Without injection	4.596	4.71	Diagonal splitting	BFM rupture

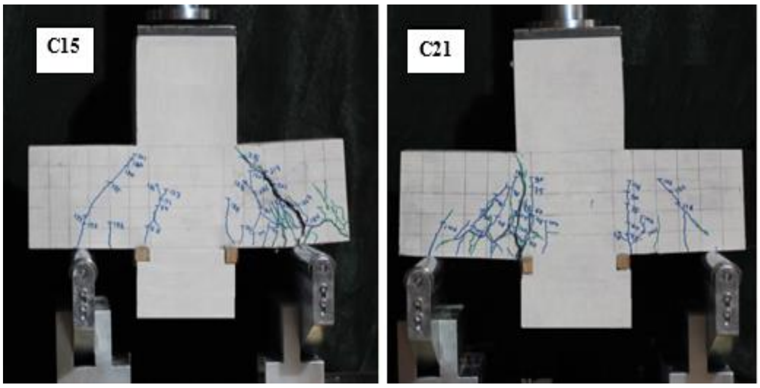

Figure 4.8 Mode of failure of C15 was Diagonal splitting failure and C21 was flexural failure

Therefore, the reinforcement of the main bars will work better than the first case of failure. The results are shown in Table 4.8 that when the self-compacted concrete corbels had a diagonal splitting failure, the result after rehabilitated by BFM will be less than another type of failure. On the other hand, the performance of rehabilitation depends on the damaged degree of the specimen before the rehabilitation, which is controlled in the result of strengthening after rehabilitation.

Unfortunately, the result showed that the self-compacted concrete corbels that had a high compressive strength in Table 4.8, had low values after rehabilitation by BFM. The percentage recovered of ultimate load capacity for C16, C17, and C18 which were rehabilitated by BFM without injection epoxy in cracks were found to be 79.315%, 66.299%, and 55.182% respectively from the original load capacities before rehabilitation. The increases of ductility of these samples were variable depending on the maximum deflection before and after the rehabilitation., in addition to the decreasing of the stiffness of these corbels which are concluded by comparing the slope of load-deflection curves before and after the rehabilitation as shown in (Table 4.9).

The other samples of high compressive strength C22, C23, & C24 were rehabilitated by BFM, C22 was injected by low viscosity epoxy to repair the cracks, the result showed that the percentage recovered of ultimate load capacity after rehabilitated was 100.181% of original load capacity. The mode of failure was a diagonal splitting failure before the rehabilitation. The samples C23 & C24 were rehabilitated by BFM without injection epoxy, which is no reliability between the BFM and high compressive self-compacted concrete, and the percentage recovered of ultimate load capacity of C23 and C24 were about 45.560% and 40.759% respectively, from original value before the rehabilitation. The increase of ductility can be concluded from the results of maximum deflection before and after the rehabilitation and the decrease of stiffness can be seen in the behaviour of load-deflection curves in Table 4.9.

Figure 4.9 shows the mode of failure of several selected corbels after rehabilitation (ruptured in BFM), which is the same mode in all corbels of part two. Figure 4.10 shows the ultimate load capacities of part two of second group before and after the rehabilitation which are recorded as values in Table 4.8. Moreover, summary of all results of the corresponding corbels were given in (Table 4.9).

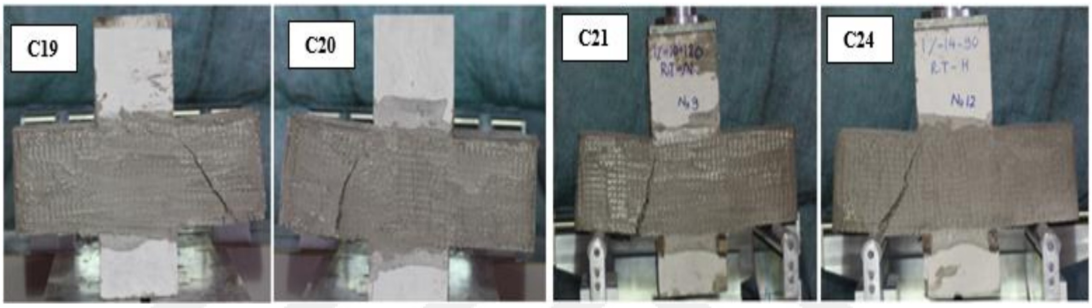

Figure 4.9 Failure mode of Basalt Fiber Mesh in several corbels of part two of second group (Ruptured in BFM)

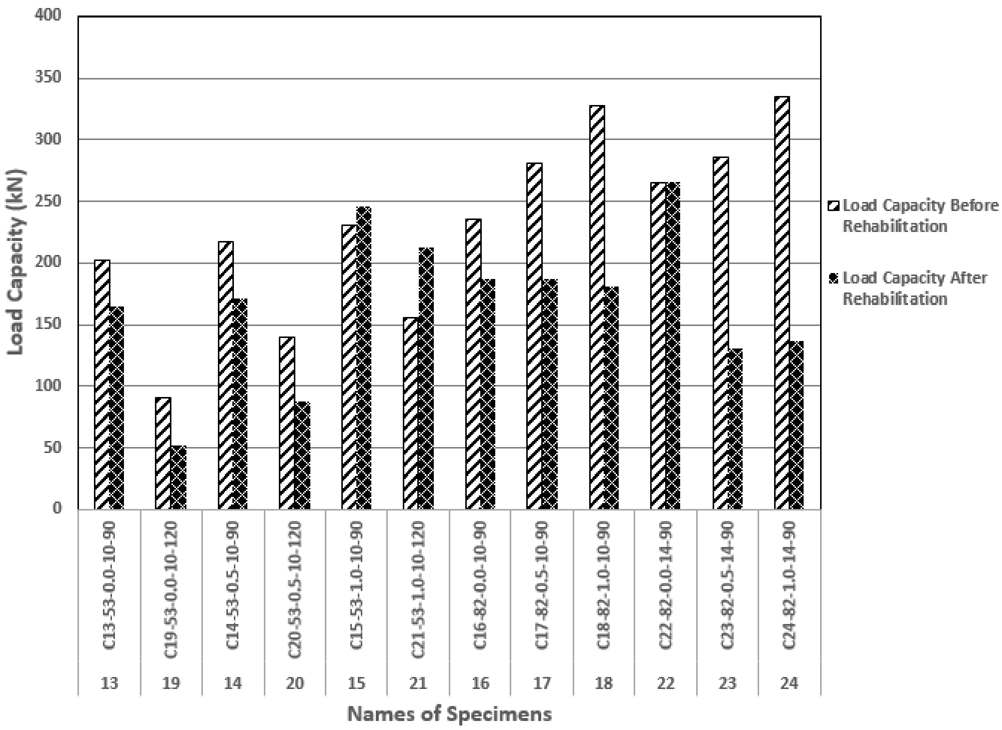

Figure 4.10 The behaviour of part two of second group after rehabilitation by BFM with respect to the ultimate load capacity

Table 4.9 Summary of mechanical behavior of corbels for C13 to C24

		Mode of failure			Load-Deflection Relationship
Self-Compacted Concrete/ Rehabilitation By BFM	C13-53-0.0-10-90	Before Reh.	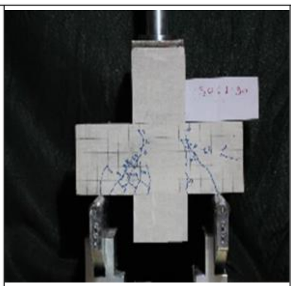	Shear failure	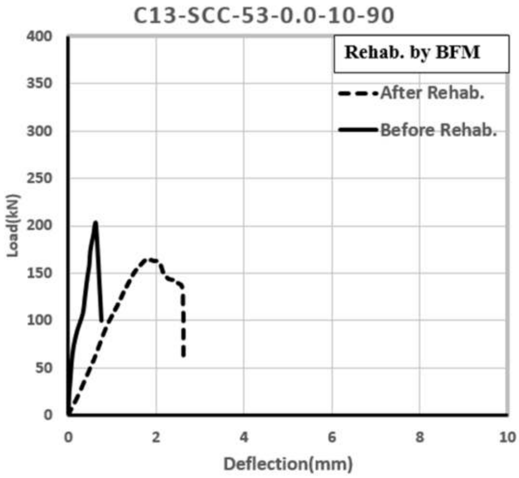
		After Reh.		BFM rupture	
	C14-53-0.5-10-90	Before Reh.	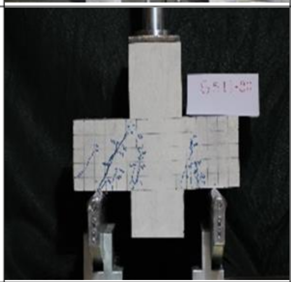	Shear failure	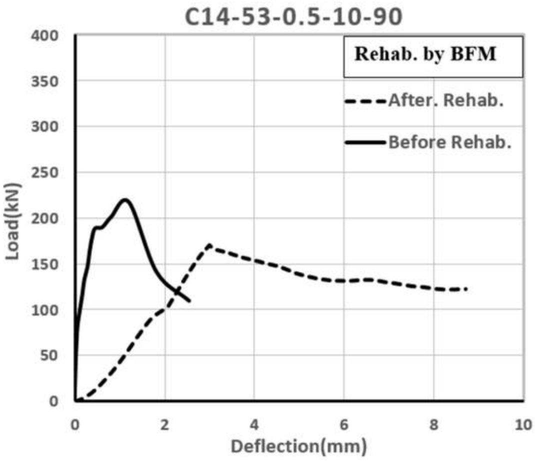
		After Reh.		BFM rupture	
	C15-53-1.0-10-90	Before Reh.	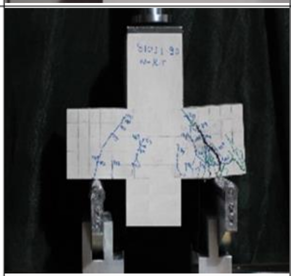	Diagonal splitting	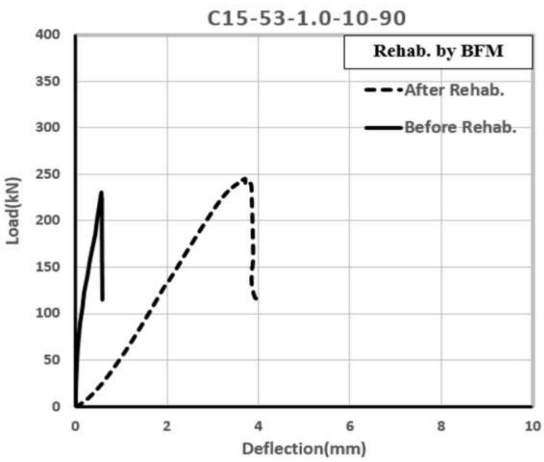
		After Reh.		BFM rupture	

<table>
<tr><th rowspan="7">Self-Compacted Concrete/ Rehabilitation By BFM</th><th></th><th colspan="3">Mode of failure</th><th>Load-Deflection Relationship</th></tr>
<tr><td rowspan="2">C16-82-0.0-10-90</td><td>Before Reh.</td><td>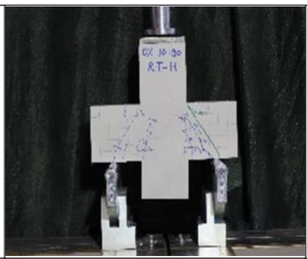</td><td>Shear failure</td><td rowspan="2">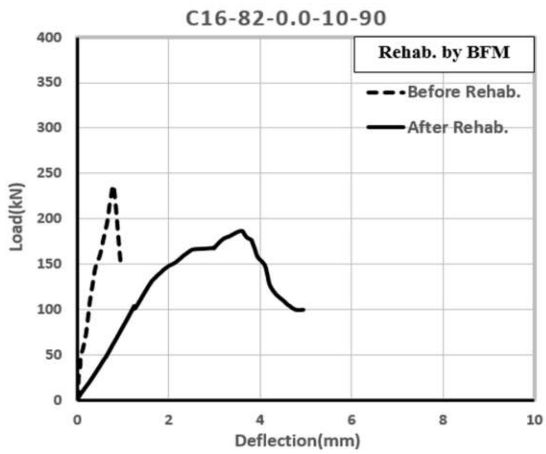
</td></tr>
<tr><td>After Reh.</td><td></td><td>BFM rupture</td></tr>
<tr><td rowspan="2">C17-82-0.5-10-90</td><td>Before Reh.</td><td>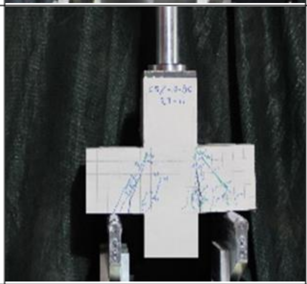</td><td>Flexural/ shear failure</td><td rowspan="2">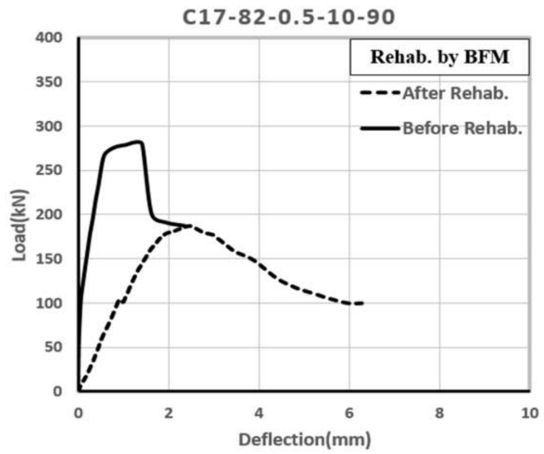
</td></tr>
<tr><td>After Reh.</td><td></td><td>BFM rupture</td></tr>
<tr><td rowspan="2">C18-82-1.0-10-90</td><td>Before Reh.</td><td>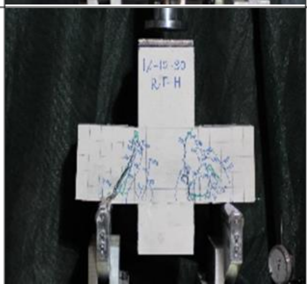</td><td>Flexural/ shear failure</td><td rowspan="2">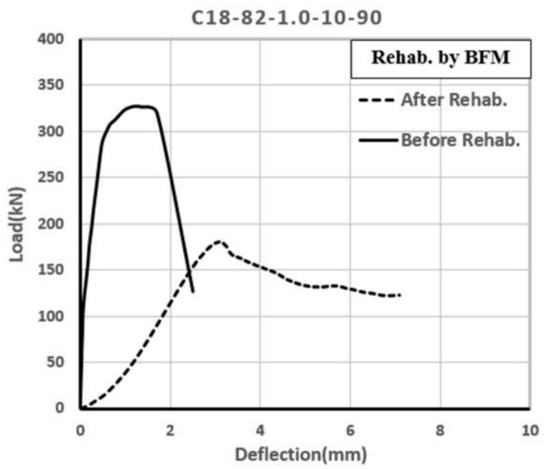
</td></tr>
<tr><td>After Reh.</td><td></td><td>BFM rupture</td></tr>
</table>

		Mode of failure			Load-Deflection Relationship
Self-Compacted Concrete/ Rehabilitation By BFM	C19-53-0.0-10-120	Before Reh.	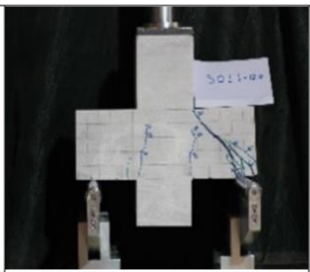	Diagonal splitting	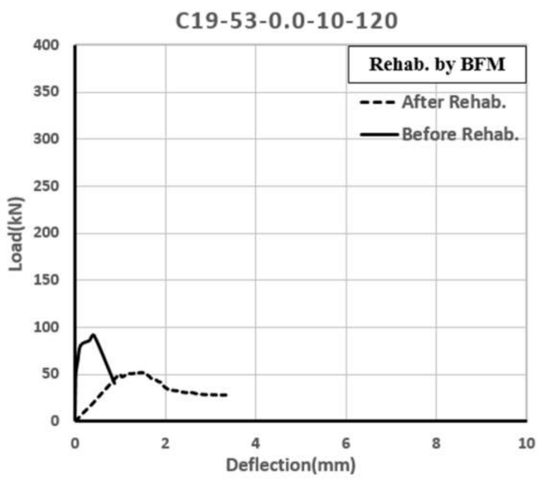
		After Reh.	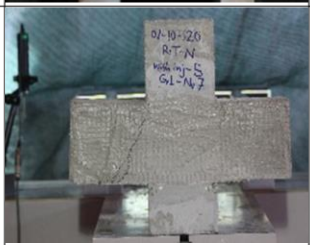	BFM rupture	
	C20-53-0.5-10-120	Before Reh.		Diagonal splitting	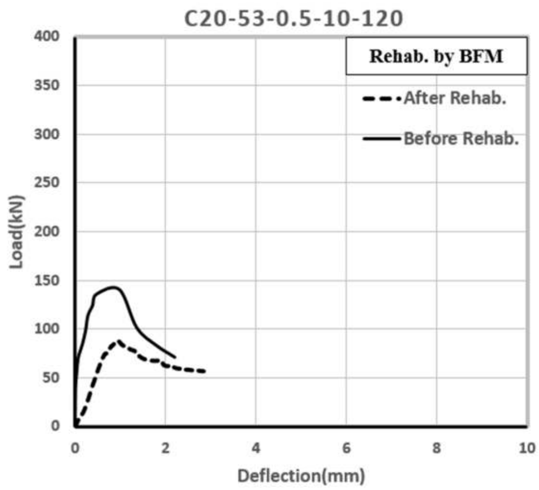
		After Reh.		BFM rupture	
	C21-53-1.0-10-120	Before Reh.	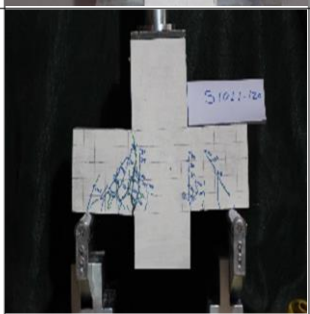	flexural failure	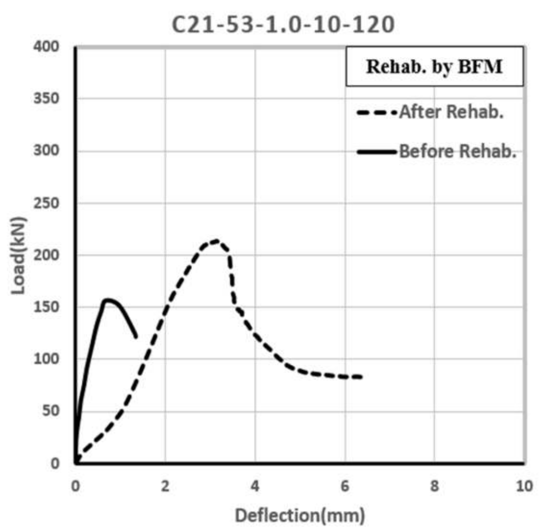
		After Reh.	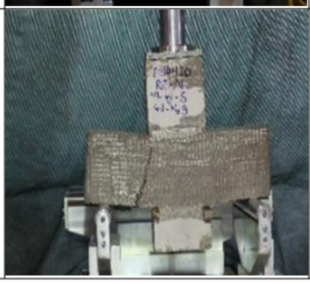	BFM rupture	

<table>
<tr><th rowspan="7">Self-Compacted Concrete/ Rehabilitation By BFM</th><th></th><th colspan="3">Mode of failure</th><th>Load-Deflection Relationship</th></tr>
<tr><td rowspan="2">C22-82-0.0-14-90</td><td>Before Reh.</td><td>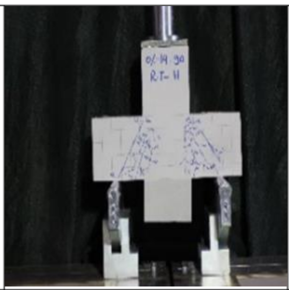</td><td>Diagonal splitting</td><td rowspan="2">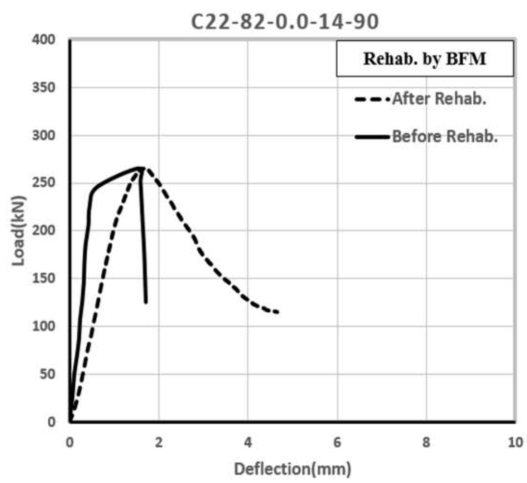
</td></tr>
<tr><td>After Reh.</td><td></td><td>BFM rupture</td></tr>
<tr><td rowspan="2">C23-82-0.5-14-90</td><td>Before Reh.</td><td>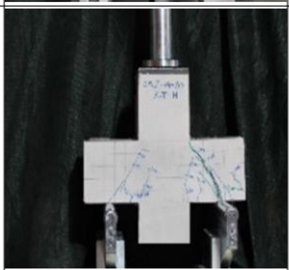</td><td>Diagonal splitting</td><td rowspan="2">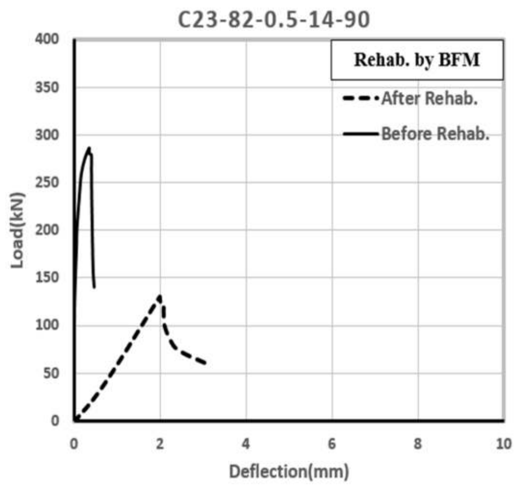
</td></tr>
<tr><td>After Reh.</td><td></td><td>BFM rupture</td></tr>
<tr><td rowspan="2">C24-82-1.0-14-90</td><td>Before Reh.</td><td>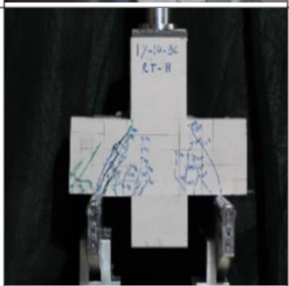</td><td>Diagonal splitting</td><td rowspan="2">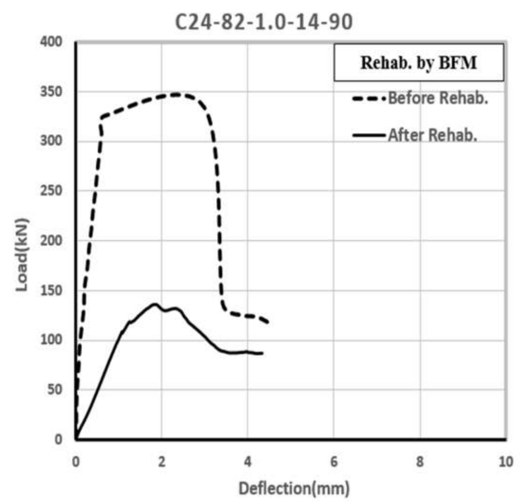
</td></tr>
<tr><td>After Reh.</td><td></td><td>BFM rupture</td></tr>
</table>

4.2.3 Experimental Results of Second Group-Part one

Eighteen damaged corbels were repaired by (ALSHAWAF 2017, Hussein 2017) with only crack repair material in order to investigate the efficiency of epoxy injection for restoring the capacity of the corbels after heated up to three different temperature levels of 250°C, 500°C, and 750°C before the first failure and tested under vertical loading until failure. The results of these rehabilitated corbels are listed in Table 4.10.

Again the designation of corbel is the same as it explained before, except it is added term before the last term which is represented to the degree of heating. The ultimate load capacities before repairing were affected by various parameters, especially the heating degree and steel fiber ratio. While increasing the temperature adversely affected the capacity. The addition of steel fiber increased ultimate load capacity and ductility as well.

It is observed that the result of percentage recovered of ultimate load capacity after rehabilitation varies from 43.172% to 127.5% depending on the mode of failure before the rehabilitation which determines the damaged degree of the specimen and the existence of cracks and micro-cracks. Micro-cracks width which is less than 0.3mm cannot be repaired by low-viscosity epoxy which sufficiently influences adversely to the effectiveness of rehabilitation process (ACI 224 2008, ACI 440 2008). Again it can be concluded from the result in Table 5.31 that when the self-compacted concrete corbels had a diagonal splitting failure, the result after rehabilitated by injection epoxy will be less than another type of failure, especially for the high compressive strength of self-compacted concrete corbels (C34 until C38), the rehabilitation by repairing cracks only cannot be restoring the strength to the original value of load capacity before the rehabilitation, which is restored about 43.172% from C34 until 99.574% from C38. It can be seen in the Figure 4.11 the mode of failure of several selected corbels which is recorded in Table 4.10. Table 4.11 shows the load-deflection behavior of all corbels of part one of second group with all details.

Table 4.10 Part one of second group SCC heated corbels rehabilitated by injection epoxy

Type of Concrete and Rehabilitation	Specimen Index	Comp. Strength (f_c) (MPa)	Ultimate Load Capacity before Reh. (kN)	Ultimate Load Capacity After Reh. (kN)	% Recovered of Ultimate Load Capacity after Reh.	Deflection		Mode of Failure	
						Before Reh. δmax (mm)	After Reh. δmax (mm)	Before Reh.	After Reh.
Self-Compacted Concrete/ Rehabilitation By Injection	C25-53-0.0-10-250-120	53.3	130	150	115.385	0.736	2.523	Shear failure	Shear failure
	C26-53-0.0-10-500-120	48.8	80	102	127.500	0.697	1.057	Shear failure	Diagonal splitting
	C27-53-0.0-10-750-120	21.1	51	43	84.314	1.085	1.672	Diagonal splitting	Diagonal splitting
	C28-53-0.5-10-250-120	54.8	201	135	67.164	1.718	1.628	Diagonal splitting	Shear failure
	C29-53-0.5-10-500-120	50.5	117	132	112.821	0.682	0.765	Shear failure	Shear failure
	C30-53-0.5-10-750-120	25.4	88	80	90.909	2.083	2.157	Diagonal splitting	Diagonal splitting
	C31-53-1.0-10-250-120	57.1	212	190	89.623	1.221	1.094	Diagonal splitting	Shear failure
	C32-53-1.0-10-500-120	51.1	136	157	115.441	1.723	2.621	Shear failure	Shear failure
	C33-53-1.0-10-750-120	27.9	99	80	80.808	1.852	2.868	Diagonal splitting	Diagonal splitting
	C34-82-0.0-10-250-90	77.8	227	98	43.172	0.551	1.116	Diagonal splitting	Diagonal splitting
	C35-82-0.0-10-500-90	70.6	195	90	46.154	1.147	1.348	Diagonal splitting	Diagonal splitting
	C36-82-0.0-10-750-90	28.8	107	59	55.140	0.979	0.954	Diagonal splitting	Diagonal splitting
	C37-82-0.5-10-250-90	72.7	280	150	53.571	1.63	3.927	Diagonal splitting	Diagonal splitting
	C38-82-0.5-10-500-90	71.4	235	234	99.574	1.19	3.131	Diagonal splitting	Diagonal splitting
	C39-82-0.5-10-750-90	38.6	267	231	86.517	1.816	2.849	Shear failure	Shear failure
	C40-82-1.0-10-250-90	74.8	317	293	92.429	1.022	3.522	Flexural/ shear failure	Diagonal splitting
	C41-82-1.0-10-500-90	72.2	267	231	86.517	2.432	1.883	Flexural failure	Shear failure
	C42-82-1.0-10-750-90	40.3	171	169	98.830	1.645	3.593	Shear failure	Diagonal splitting

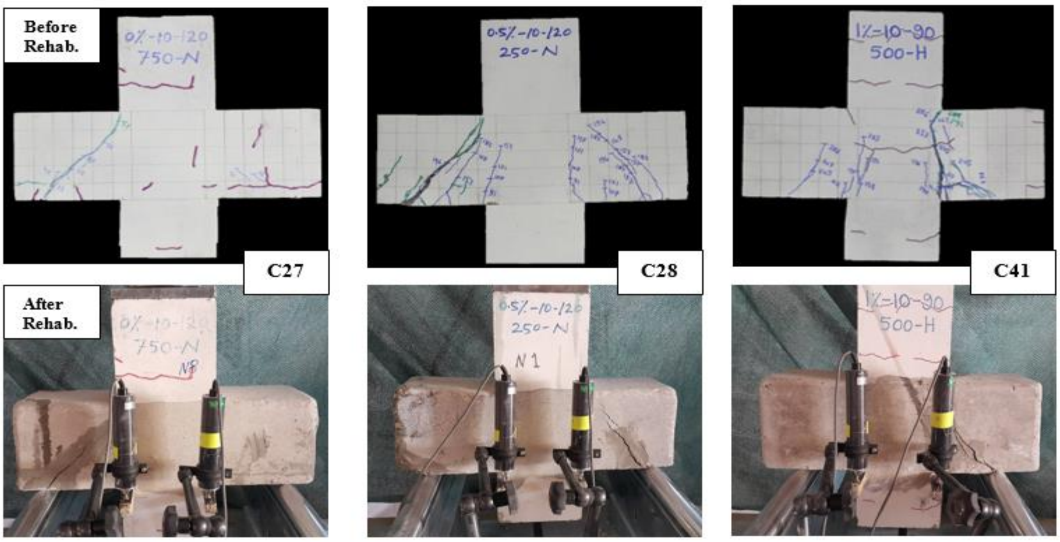

Figure 4.11 Mode of failure for several corbels before and after the rehabilitation

4.2.4 Experimental Results of Second Group-Part Two

The part two of second group contains eighteen damaged corbels were rehabilitated by (ALSHAWAF 2017, Hussein 2017) with crack repair epoxy and wrapped with BFF after heated up to three different temperature levels of 250°C, 500°C, and 750°C before the first failure and tested under vertical loading until failure. The main purpose of this part is to investigate the effectiveness of the use of epoxy injection and BFF together on the serviceability of reinforced concrete corbels. Test results with all details are listed in Table 4.12. It can be noticed from Table 4.12 that use of BFF to strengthen the corbels leads to a significant increase in the load capacity for all types of corbels. The percentage recovered of load capacity after rehabilitation varied from 102.459% of C60 until 151.208% of C50 from the original value of load capacity before the rehabilitation. This increment of load capacity depends on the type of failure of specimen before the rehabilitation which determines the damage degree of the specimen. Again, it can be concluded from Table 4.12 that the failure diagonal splitting was the worst type which affects the performance of load capacity after the rehabilitation more than other types of failure before the rehabilitation.

Table 4.11 Summary of mechanical behavior of corbels C25 to C42

<table>
<tr><th rowspan="7">Self-Compacted Concrete/ Rehabilitation By Injection</th><th rowspan="3">C25-53-0.0-10-250-120</th><th colspan="3">Mode of failure</th><th>Load-Deflection Relationship</th></tr>
<tr><td>Before Reh.</td><td>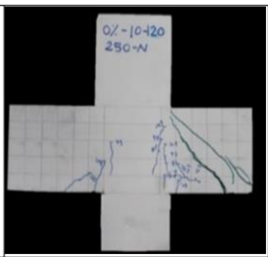</td><td>Shear failure</td><td rowspan="2">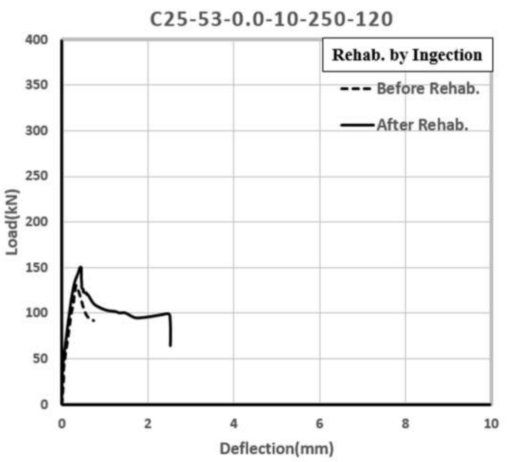</td></tr>
<tr><td>After Reh.</td><td></td><td>Shear failure</td></tr>
<tr><td rowspan="2">C26-53-0.0-10-500-120</td><td>Before Reh.</td><td>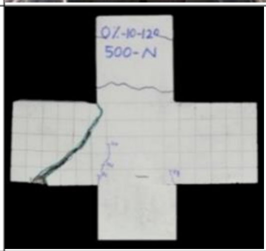</td><td>Shear failure</td><td rowspan="2">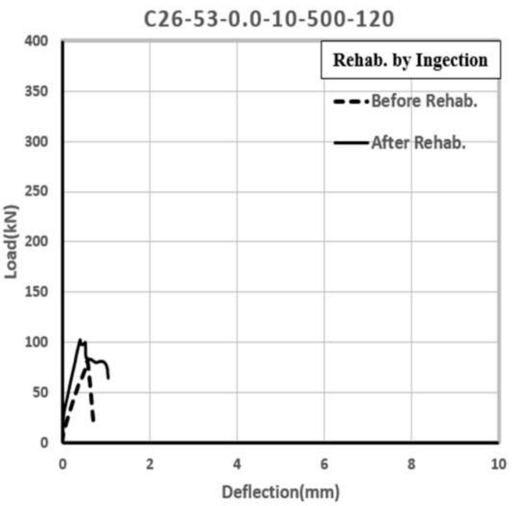</td></tr>
<tr><td>After Reh.</td><td></td><td>Diagonal splitting</td></tr>
<tr><td rowspan="2">C27-53-0.0-10-750-120</td><td>Before Reh.</td><td>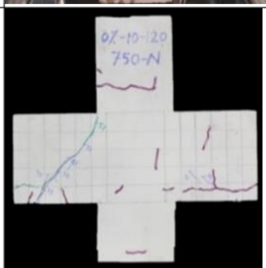</td><td>Diagonal splitting</td><td rowspan="2">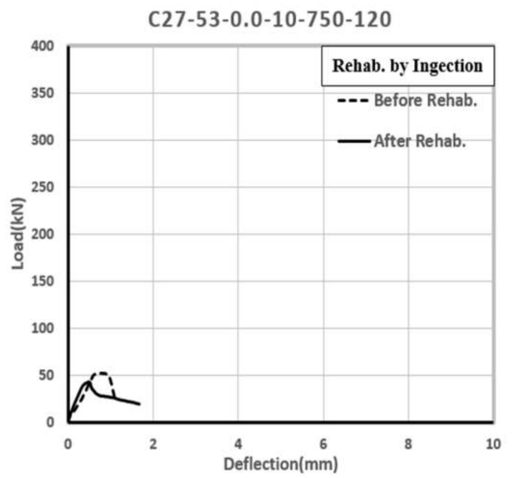</td></tr>
<tr><td>After Reh.</td><td></td><td>Diagonal splitting</td></tr>
</table>

<table>
<tr><td rowspan="7">Self-Compacted Concrete/ Rehabilitation By Injection</td><td></td><td colspan="3">Mode of failure</td><td>Load-Deflection Relationship</td></tr>
<tr><td rowspan="2">C28-53-0.5-10-250-120</td><td>Before Reh.</td><td>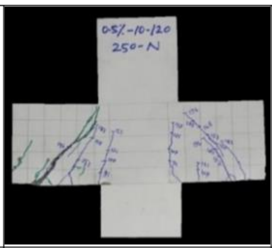</td><td>Diagonal splitting</td><td rowspan="2">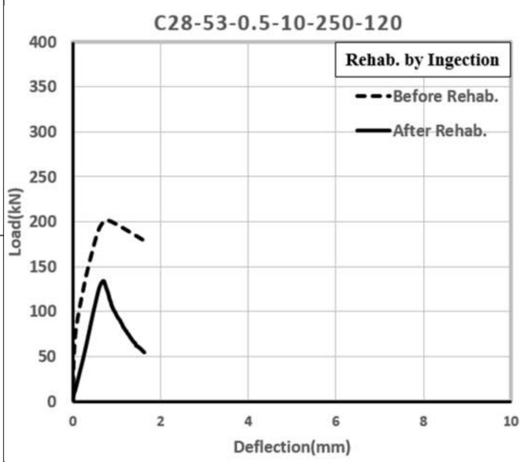</td></tr>
<tr><td>After Reh.</td><td></td><td>Shear failure</td></tr>
<tr><td rowspan="2">C29-53-0.5-10-500-120</td><td>Before Reh.</td><td>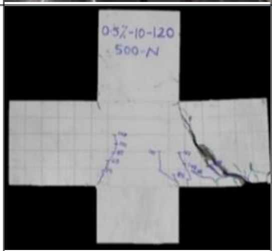</td><td>Shear failure</td><td rowspan="2">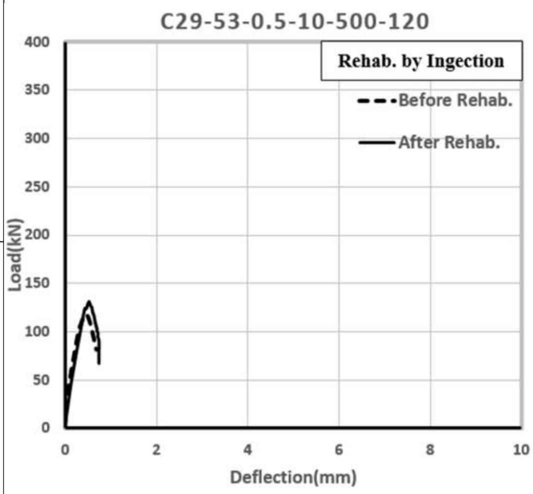</td></tr>
<tr><td>After Reh.</td><td></td><td>Shear failure</td></tr>
<tr><td rowspan="2">C30-53-0.5-10-750-120</td><td>Before Reh.</td><td>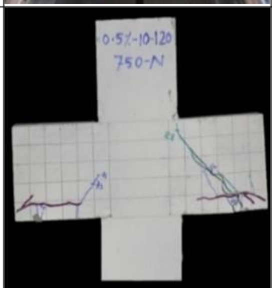</td><td>Diagonal splitting</td><td rowspan="2">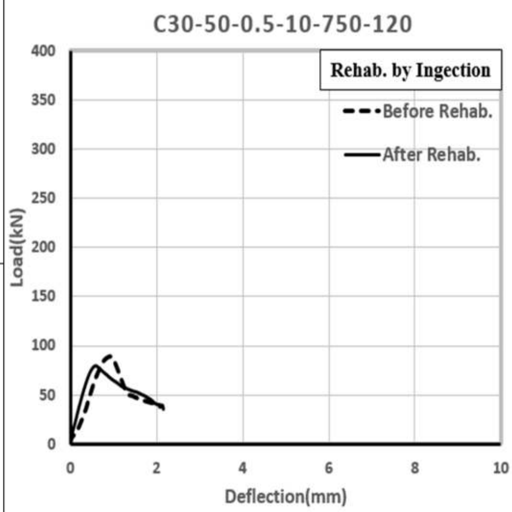</td></tr>
<tr><td>After Reh.</td><td></td><td>Diagonal splitting</td></tr>
</table>

<table>
<tr><th rowspan="7">Self-Compacted Concrete/ Rehabilitation By Injection</th><th rowspan="1"></th><th colspan="3">Mode of failure</th><th>Load-Deflection Relationship</th></tr>
<tr><td rowspan="2">C31-53-1.0-10-250-120</td><td>Before Reh.</td><td>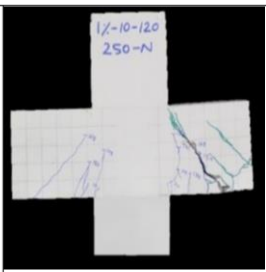
</td><td>Diagonal splitting</td><td rowspan="2">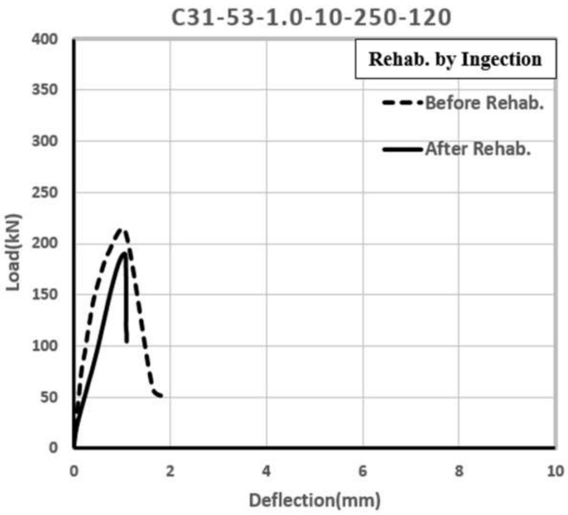
</td></tr>
<tr><td>After Reh.</td><td>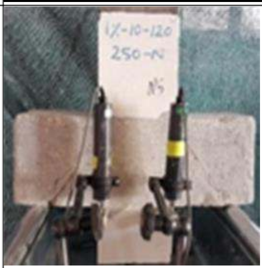
</td><td>Shear failure</td></tr>
<tr><td rowspan="2">C32-53-1.0-10-500-120</td><td>Before Reh.</td><td>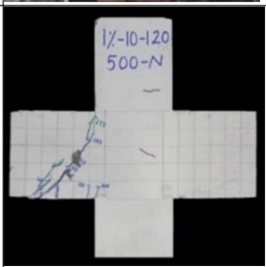
</td><td>Shear failure</td><td rowspan="2">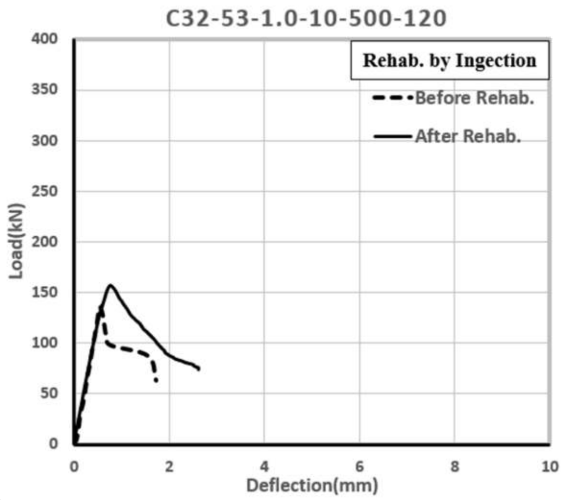
</td></tr>
<tr><td>After Reh.</td><td>
</td><td>Shear failure</td></tr>
<tr><td rowspan="2">C33-53-1.0-10-750-120</td><td>Before Reh.</td><td>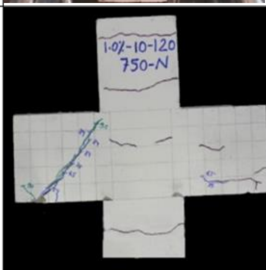
</td><td>Diagonal splitting</td><td rowspan="2">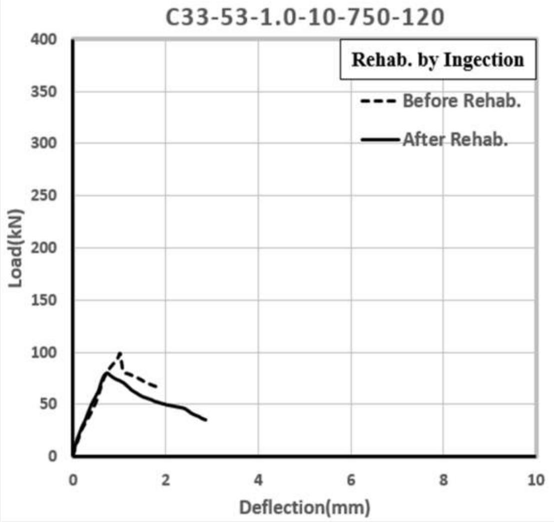
</td></tr>
<tr><td>After Reh.</td><td>
</td><td>Diagonal splitting</td></tr>
</table>

			Mode of failure		Load-Deflection Relationship
Self-Compacted Concrete/ Rehabilitation By Injection	C34-82-0.0-10-250-90	Before Reh.	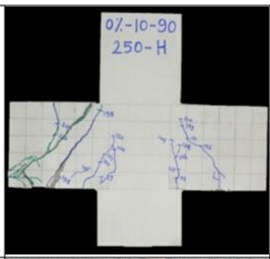	Diagonal splitting	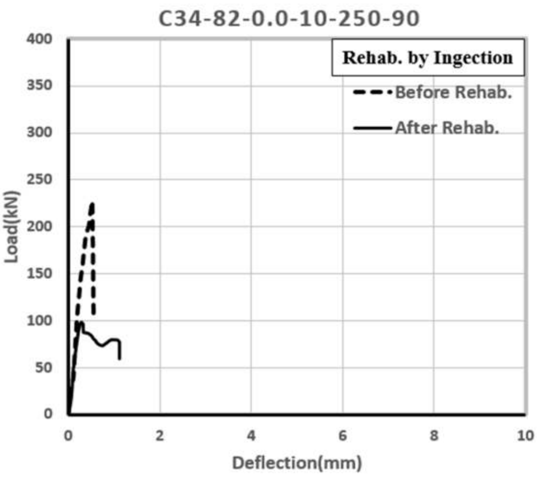
		After Reh.		Diagonal splitting	
	C35-82-0.0-10-500-90	Before Reh.	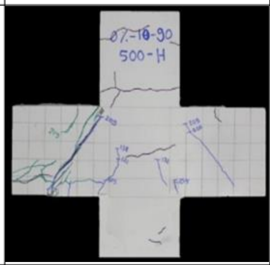	Diagonal splitting	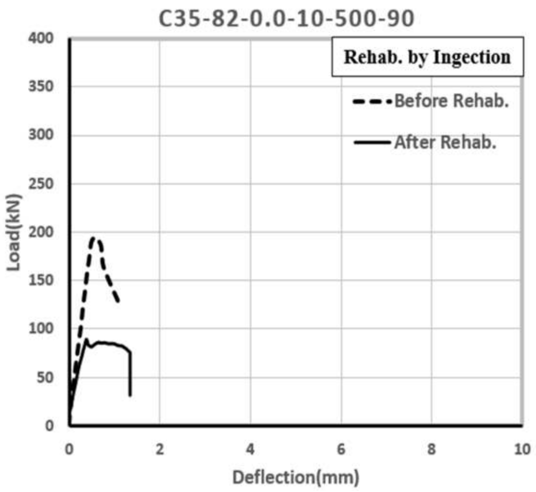
		After Reh.		Diagonal splitting	
	C36-82-0.0-10-750-90	Before Reh.	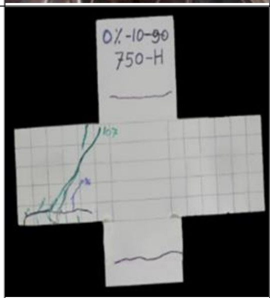	Diagonal splitting	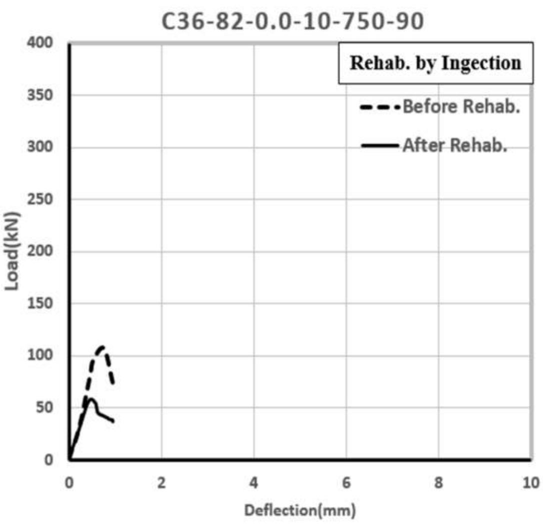
		After Reh.		Diagonal splitting	

<table>
<tr><td rowspan="7">Self-Compacted Concrete/ Rehabilitation By Injection</td><td></td><td colspan="3">Mode of failure</td><td>Load-Deflection Relationship</td></tr>
<tr><td rowspan="2">C37-82-0.5-10-250-90</td><td>Before Reh.</td><td>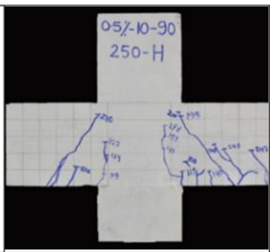</td><td>Diagonal splitting</td><td rowspan="2">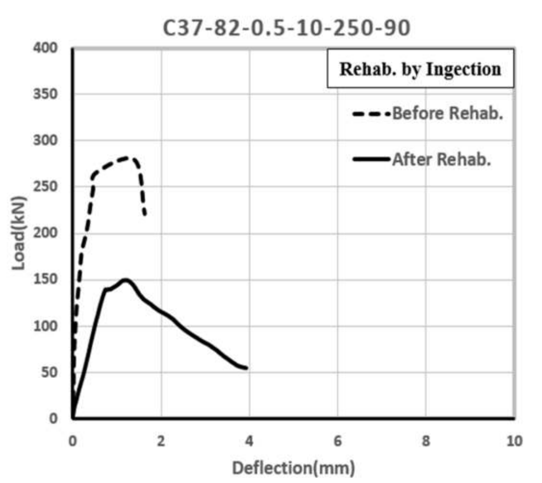</td></tr>
<tr><td>After Reh.</td><td></td><td>Diagonal splitting</td></tr>
<tr><td rowspan="2">C38-82-0.5-10-500-90</td><td>Before Reh.</td><td>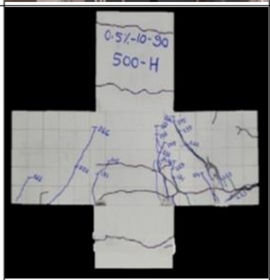</td><td>Diagonal splitting</td><td rowspan="2">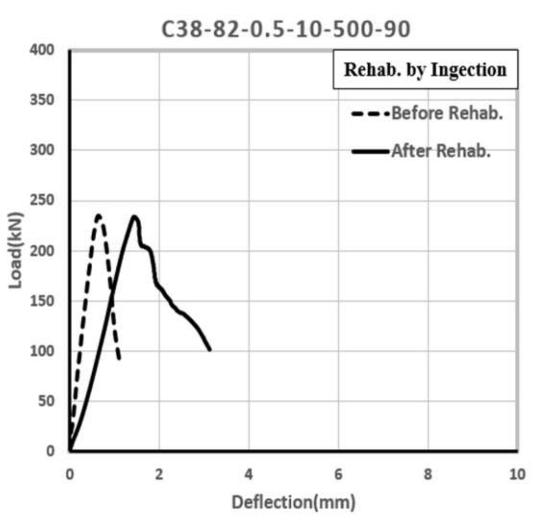</td></tr>
<tr><td>After Reh.</td><td></td><td>Diagonal splitting</td></tr>
<tr><td rowspan="2">C39-82-0.5-10-750-90</td><td>Before Reh.</td><td>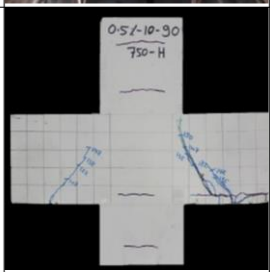</td><td>Shear failure</td><td rowspan="2">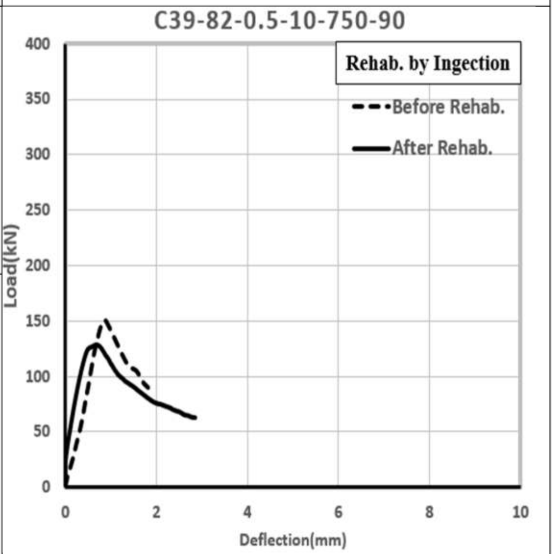</td></tr>
<tr><td>After Reh.</td><td></td><td>Shear failure</td></tr>
</table>

		Mode of failure			Load-Deflection Relationship
Self-Compacted Concrete/ Rehabilitation By Injection	C40-82-1.0-10-250-90	Before Reh.	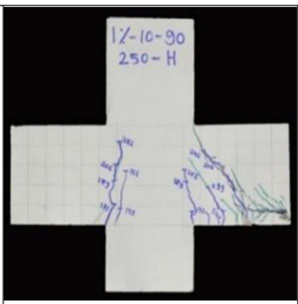	Flexural / shear failure	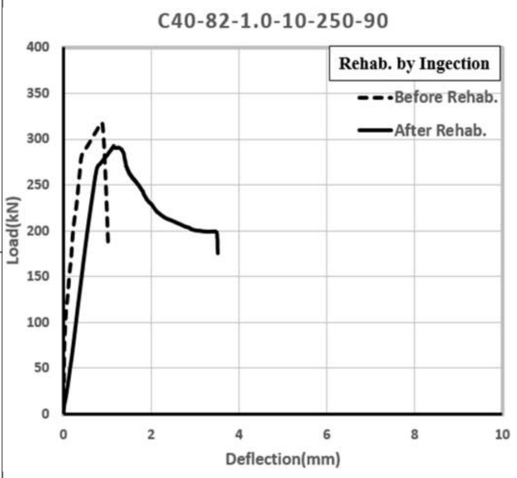
		After Reh.		Diagonal splitting	
	C41-82-1.0-10-500-90	Before Reh.	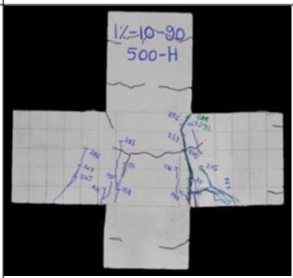	Flexural failure	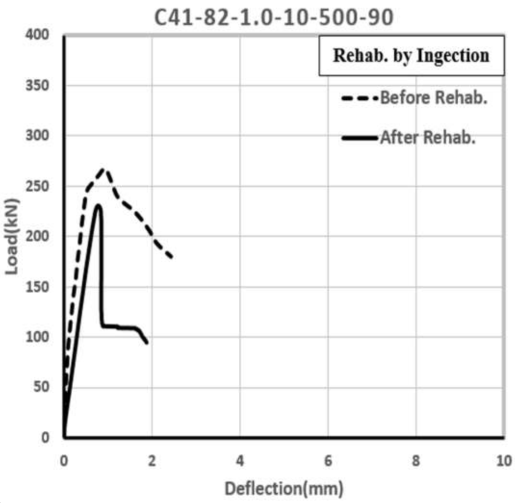
		After Reh.	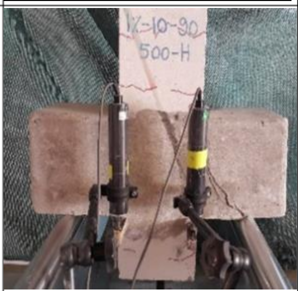	Shear failure	
	C42-82-1.0-10-750-90	Before Reh.	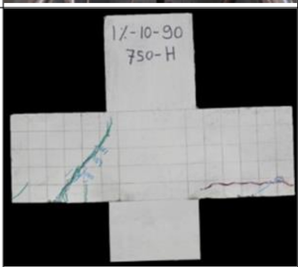	Shear failure	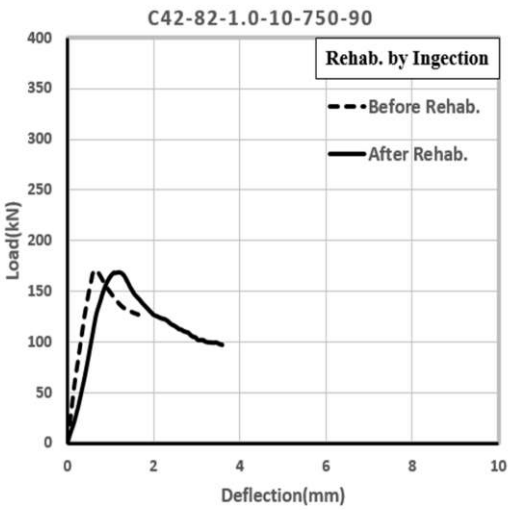
		After Reh.		Diagonal splitting	

Table 4.12 Part two of second group SCC heated corbels rehabilitated by injection epoxy beside to BFF

Type of Concrete and Rehabilitation	Specimen Index	Comp. Strength (f_c) (MPa)	Ultimate Load Capacity before Reh. (kN)	Ultimate Load Capacity After Reh. (kN)	% Recovered of Ultimate Load Capacity after Reh..	Deflection		Mode of Failure	
						Before Reh. δmax (mm)	After Reh. δmax (mm)	Before Reh.	After Reh.
Self-Compacted Concrete/ Rehabilitation By BFF & Injection	C43-53-0.0-10-250-90	53.3	208	256.2	123.173	1.186	4.897	Diagonal splitting	De-bonding
	C44-53-0.0-10-500-90	48.8	175	227	129.714	1.102	3.125	Shear failure	De-bonding
	C45-53-0.0-10-750-90	21.1	82	123.8	150.976	1.102	3.125	Shear failure	De-bonding
	C46-53-0.5-10-250-90	54.8	243	278	114.403	1.936	5.51	Diagonal splitting	De-bonding
	C47-53-0.5-10-500-90	50.5	193	260	134.715	0.913	7.437	Shear failure	De-bonding
	C48-53-0.5-10-750-90	25.4	119	142	119.328	1.591	6.158	Diagonal splitting	De-bonding
	C49-53-1.0-10-250-90	57.1	247	269	108.907	1.71	2.442	Diagonal splitting	De-bonding
	C50-53-1.0-10-500-90	51.1	207	313	151.208	1.884	6.769	Shear failure	De-bonding
	C51-53-1.0-10-750-90	27.9	132	185	140.152	1.74	7.034	Shear failure	De-bonding
	C52-82-0.0-14-250-90	77.8	268	292.5	109.142	0.744	4.443	Diagonal splitting	De-bonding
	C53-82-0.0-14-500-90	70.6	210	246.5	117.381	1.654	3.6	Diagonal splitting	De-bonding
	C54-82-0.0-14-750-90	28.8	113	150	132.743	1.231	7.583	Diagonal splitting	De-bonding
	C55-82-0.5-14-250-90	72.7	370	399.6	108.000	1.6	7.3	Diagonal splitting	De-bonding
	C56-82-0.5-14-500-90	71.4	251	262	104.382	2.309	6.292	Diagonal splitting	De-bonding
	C57-82-0.5-14-750-90	38.6	134	201	150.000	1.654	3.69	Shear failure	De-bonding
	C58-82-1.0-14-250-90	74.8	382	430.3	112.644	2.048	6.125	Diagonal splitting	De-bonding
	C59-82-1.0-14-500-90	72.2	294	306	104.082	2.329	3.805	Diagonal splitting	De-bonding
	C60-82-1.0-14-750-90	40.3	183	187.5	102.459	1.68	6.886	Diagonal splitting	De-bonding

Moreover, strengthening with BFF enhances the ductility of corbels noticeably. Therefore, a preferable seismic performance of reinforced concrete corbels can be achieved with BFF even they are damaged due to either fire or overloading. All of corbels were covered with unidirectional BFF in two directions, this operation makes the fabric to possess much more strength as compared to adhesive epoxy resin. Therefore, all of the failure modes were a de-bonding failure, which occurred between the BFF and concrete surface (see Figure 4.12).

The Load-Deflection relationships of BFF-strengthened corbels are shown in Table 4.13. The corbels numbered C43 to C51 represent normal strength concrete corbels and remaining ones (C52 to C60) refer to high strength concrete corbels. Moreover, it can be concluded from the results of second group (Table 4.10 and 4.12) that the damaged due to the high level heated degree 750°C adversely affected the compressive strength of concrete as can be seen in the results of cylindrical compressive strength beside to the capacity of corbels. Summary of all behaviour of the corresponding corbels were given in Table 4.13.

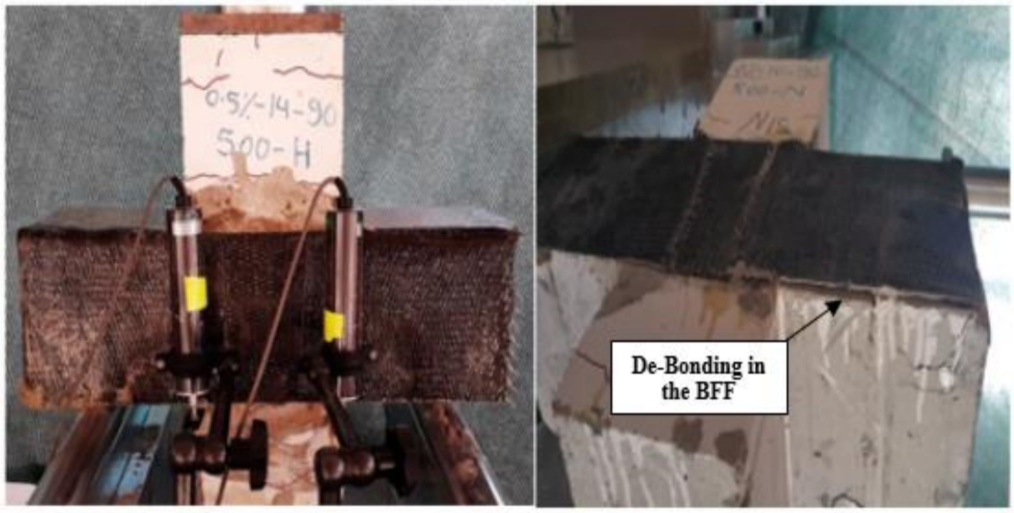

Figure 4.12 BFF-strengthened specimen with de-bonding failure

Table 4.13 Summary of mechanical behavior of corbels C43 to C60

			Mode of failure		Load-Deflection Relationship
Self-Compacted Concrete/ Rehabilitation By BFF & Injection	C43-53-0.0-10-250-90	Before Reh.	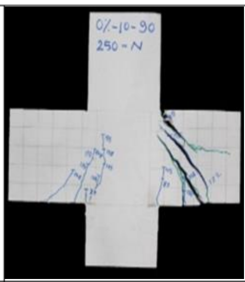	Diagonal splitting	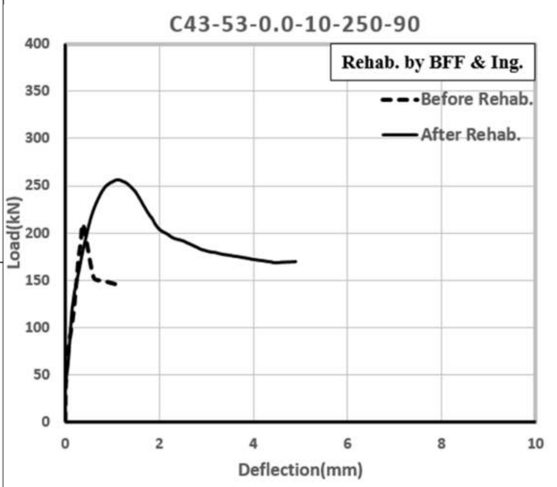
		After Reh.		De-bonding	
	C44-53-0.0-10-500-90	Before Reh.		Shear failure	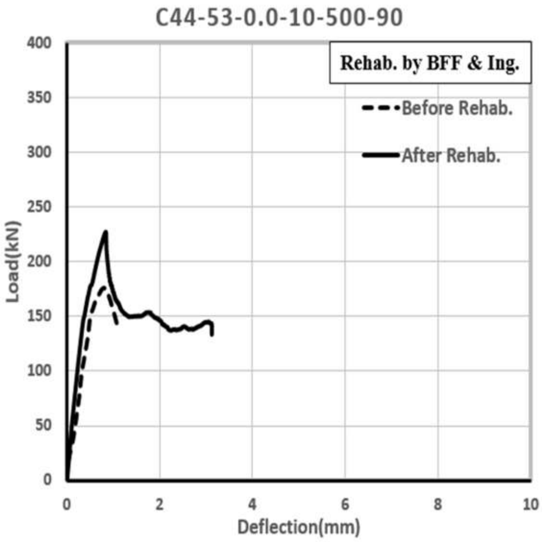
		After Reh.		De-bonding	
	C45-53-0.0-10-750-90	Before Reh.	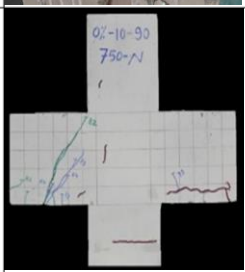	Shear failure	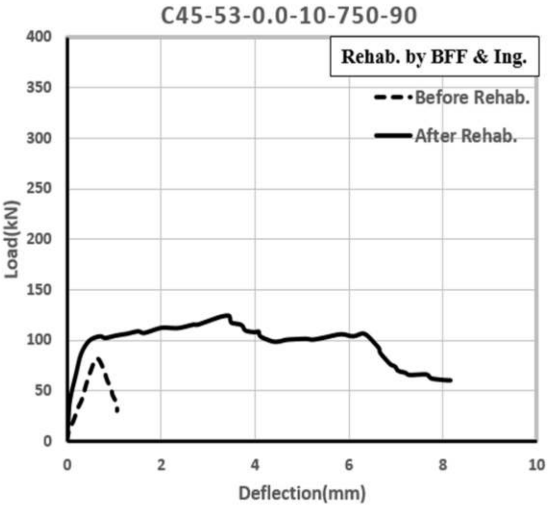
		After Reh.		De-bonding	

<table>
<tr><td rowspan="7">Self-Compacted Concrete/ Rehabilitation By BFF & Injection</td><td></td><td colspan="3">Mode of failure</td><td>Load-Deflection Relationship</td></tr>
<tr><td rowspan="2">C46-53-0.5-10-250-90</td><td>Before Reh.</td><td>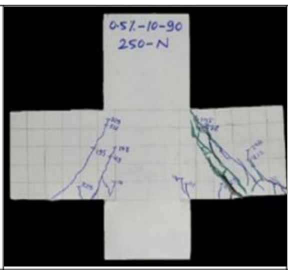
</td><td>Diagonal splitting</td><td rowspan="2">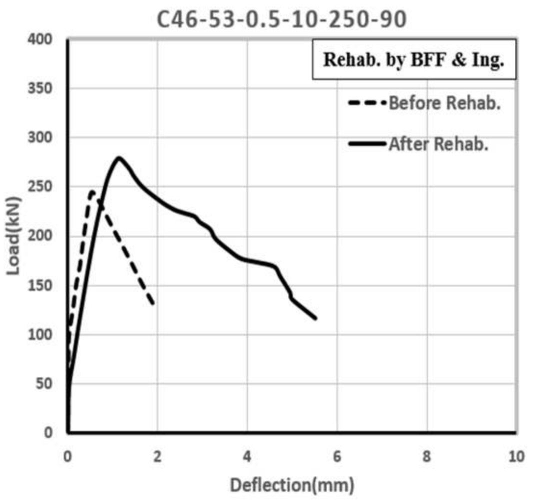
</td></tr>
<tr><td>After Reh.</td><td></td><td>De-bonding</td></tr>
<tr><td rowspan="2">C47-53-0.5-10-500-90</td><td>Before Reh.</td><td>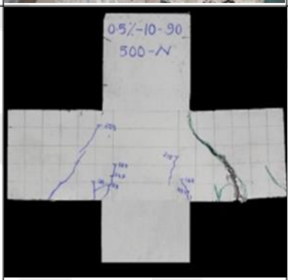
</td><td>Shear failure</td><td rowspan="2">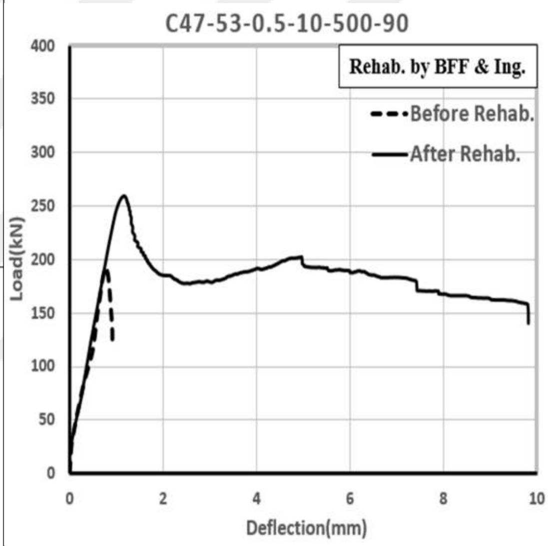
</td></tr>
<tr><td>After Reh.</td><td></td><td>De-bonding</td></tr>
<tr><td rowspan="2">C48-53-0.5-10-750-90</td><td>Before Reh.</td><td>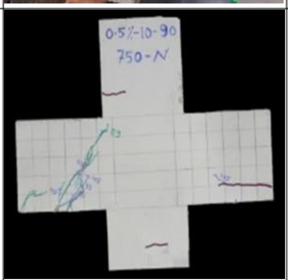
</td><td>Diagonal splitting</td><td rowspan="2">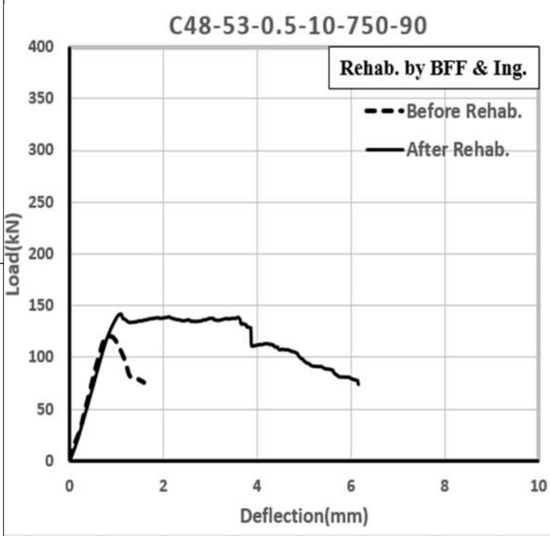
</td></tr>
<tr><td>After Reh.</td><td></td><td>De-bonding</td></tr>
</table>

		Mode of failure			Load-Deflection Relationship
Self-Compacted Concrete/ Rehabilitation By BFF & Injection	C49-53-1.0-10-250-90	Before Reh.	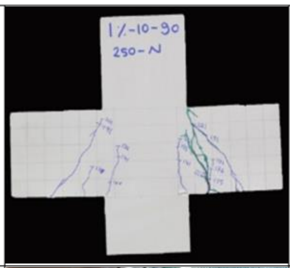	Diagonal splitting	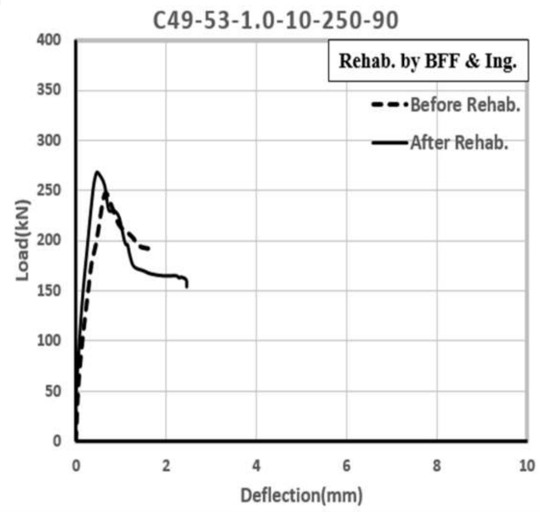
		After Reh.		De-bonding	
	C50-53-1.0-10-500-90	Before Reh.	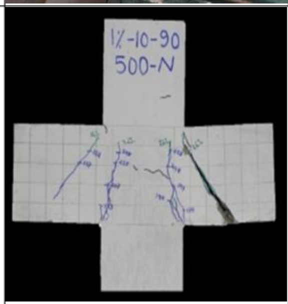	Shear failure	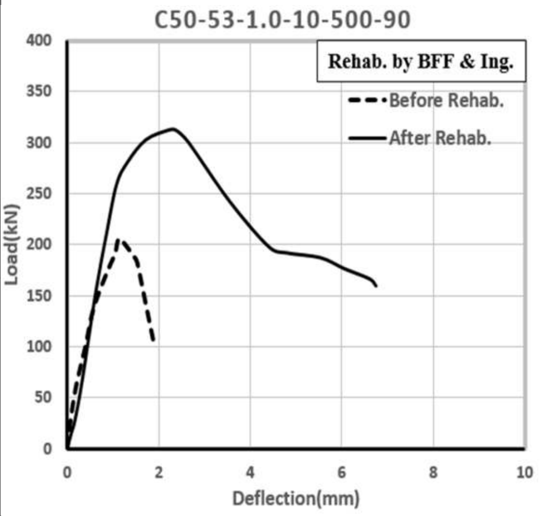
		After Reh.		De-bonding	
	C51-53-1.0-10-750-90	Before Reh.	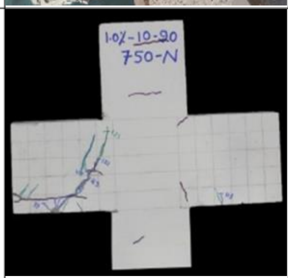	Shear failure	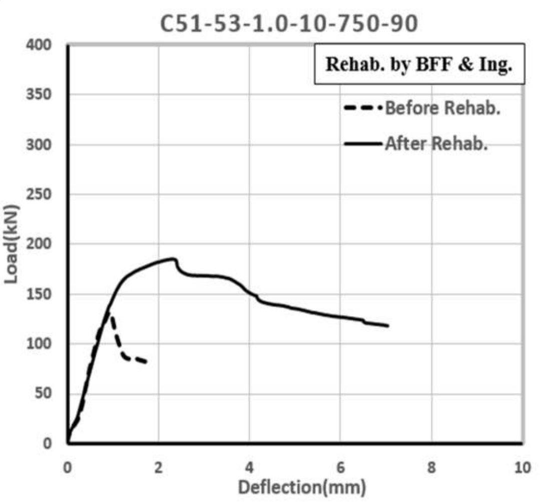
		After Reh.		De-bonding	

Self-Compacted Concrete/ Rehabilitation By BFF & Injection			Mode of failure		Load-Deflection Relationship
	C52-82-0.0-14-250-90	Before Reh.	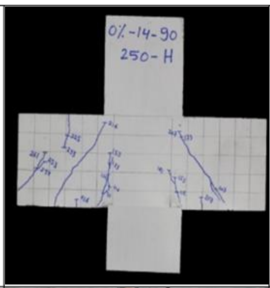	Diagonal splitting	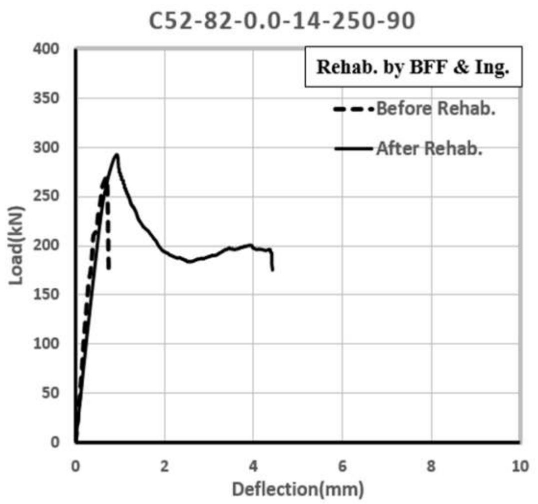
		After Reh.		De-bonding	
	C53-82-0.0-14-500-90	Before Reh.	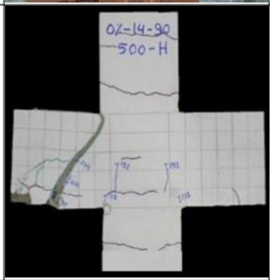	Diagonal splitting	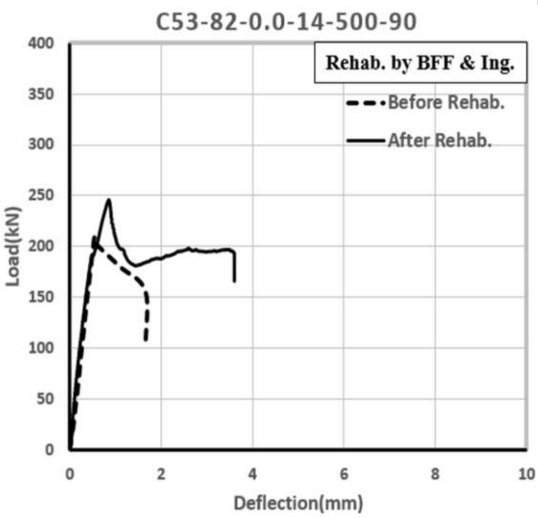
		After Reh.		De-bonding	
	C54-82-0.0-14-750-90	Before Reh.	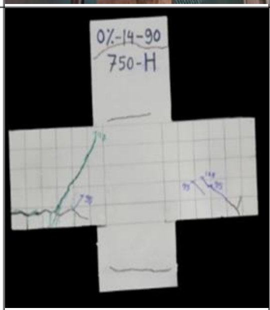	Diagonal splitting	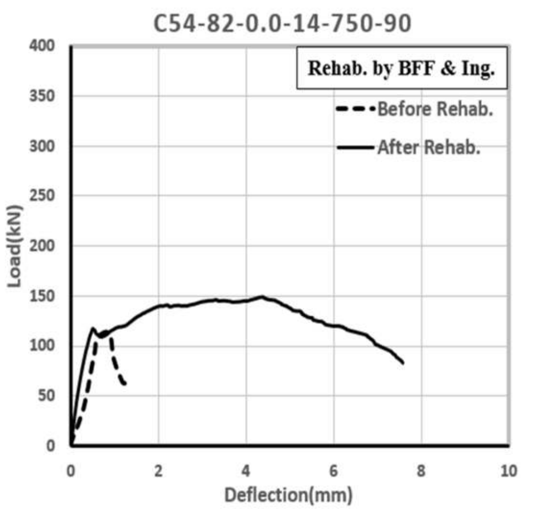
		After Reh.		De-bonding	

<table>
<tr><td rowspan="7">Self-Compacted Concrete/ Rehabilitation By BFF & Injection</td><td></td><td colspan="3">Mode of failure</td><td>Load-Deflection Relationship</td></tr>
<tr><td rowspan="2">C55-82-0.5-14-250-90</td><td>Before Reh.</td><td>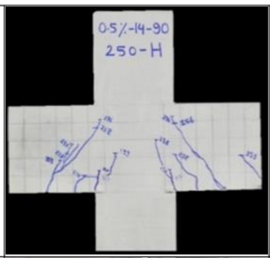
</td><td>Diagonal splitting</td><td rowspan="2">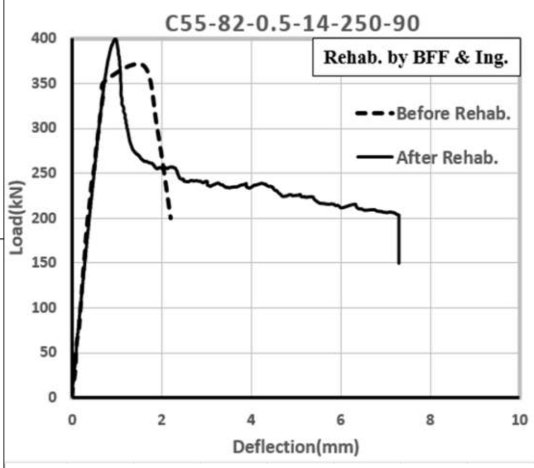
</td></tr>
<tr><td>After Reh.</td><td></td><td>De-bonding</td></tr>
<tr><td rowspan="2">C56-82-0.5-14-500-90</td><td>Before Reh.</td><td>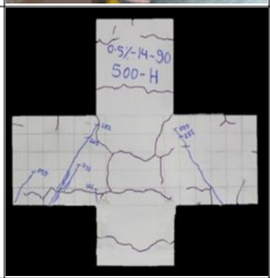
</td><td>Diagonal splitting</td><td rowspan="2">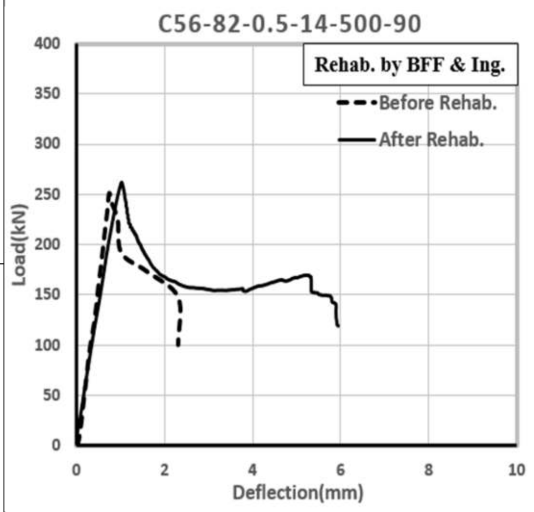
</td></tr>
<tr><td>After Reh.</td><td></td><td>De-bonding</td></tr>
<tr><td rowspan="2">C57-82-0.5-14-750-90</td><td>Before Reh.</td><td>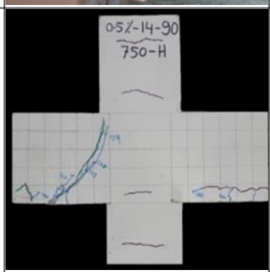
</td><td>Shear failure</td><td rowspan="2">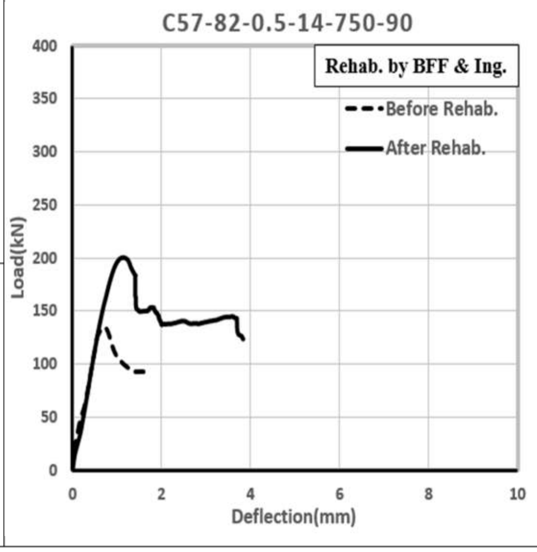
</td></tr>
<tr><td>After Reh.</td><td></td><td>De-bonding</td></tr>
</table>

			Mode of failure			Load-Deflection Relationship
Self-Compacted Concrete/ Rehabilitation By BFF & Injection	C58-82-1.0-14-250-90	Before Reh.	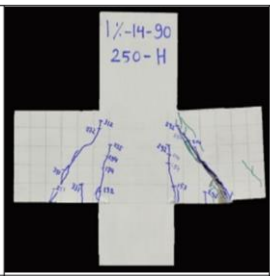	Diagonal splitting		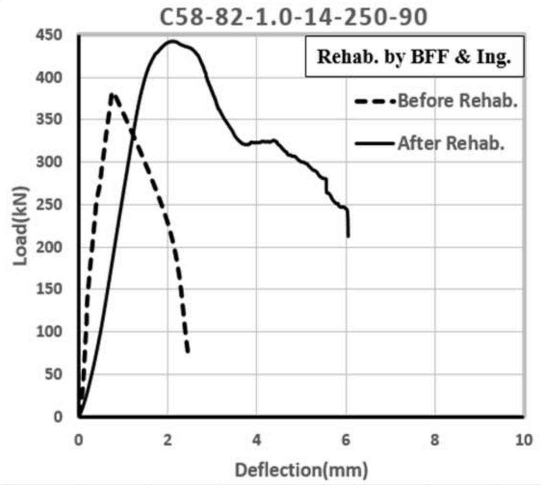
		After Reh.		De-bonding		
	C59-82-1.0-14-500-90	Before Reh.	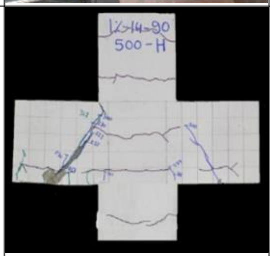	Diagonal splitting		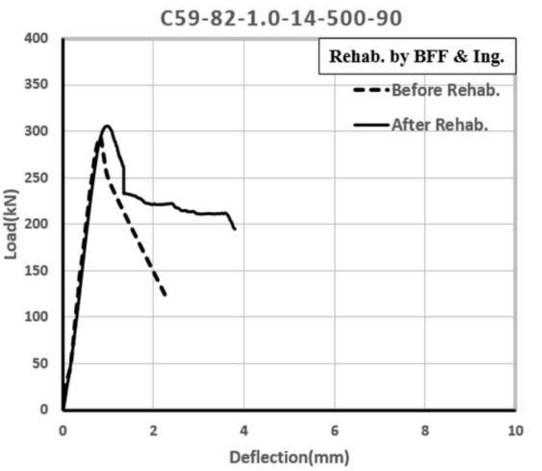
		After Reh.		De-bonding		
	C60-82-1.0-14-750-90	Before Reh.	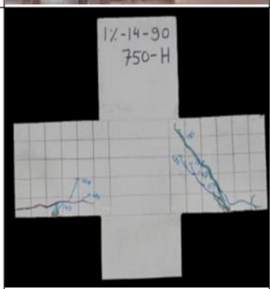	Diagonal splitting		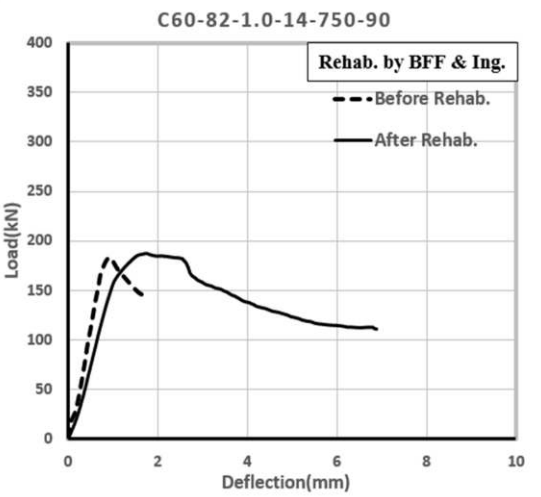
		After Reh.		De-bonding		

4.3 Conclusions

Reinforced concrete corbels play an important role in precast constructions, particularly in industrial buildings. Therefore, the functionality of the corbels is very important for the service life of these types of structures. In this study, a new technique is investigated for the rehabilitation of damaged normal and self-compacted steel fiber reinforced concrete (SCC-SFRC) corbels for the first time in literature via Basalt Fabric and Mesh. The experimental program includes two types of concrete: normal concrete, and self-compacted concrete. For the normal, 12 corbels were rehabilitated by BFM without injection material (epoxy) in cracks, with two values of compressive strength, three ratios of steel fiber (SF), and two values of shear span. For SCC-SFRC, 48 corbels were rehabilitated with different parameters. 12 corbels were rehabilitated by BFM with and without epoxy injection, 18 heated corbels with three different temperatures were rehabilitated by epoxy injection only, and 18 heated corbels with different three temperatures were rehabilitated by epoxy injection and wrapping by BFF. All 48 corbels have two values of compressive strength, three ratios of steel fiber (SF), and two values of shear span.

Following conclusions can be drawn according to results of experimental study;

- For both types of concrete corbels (Normal and Self-Compacting Concrete); BFM cannot improve the ultimate load capacity without epoxy injecting.
- For normal concrete corbels, the percentage recovered of ultimate load capacities after rehabilitation by BFM for all corbels were found to be ranging from 72.430% until 83.565% from the original load capacity before rehabilitation. However, the mode of failure for normal concrete corbels before the rehabilitation did not affect the result of rehabilitation too much.
- For self-compacted concrete corbels with normal compressive strength and without epoxy injection, the percentage recovered of ultimate load capacity after rehabilitation by BFM were found to be ranging from 57.432% until 81.272% from the original load capacity before rehabilitation. On the other hand, for high compressive strength and without epoxy injection, the percentage recovered of ultimate load capacity after rehabilitation by BFM were found to be ranging from

40.759% to 79.315% from the original load capacity before rehabilitation which are depending on mode of failure before the rehabilitation. For normal and high-compressive strength self-compacted concrete corbels which are injected by low viscosity epoxy in the cracks, the ultimate load capacities after rehabilitation by BFM are retained to the original values.

- For both types of concrete (normal and SCC), the mode of failure of BFM was observed to be rupture of Basalt Mesh which is considered to be the most important and significant failure mode for FRP.
- Test results showed that it is not reliable to use BFM alone without injection epoxy in high-compressive strength SCC-SFRC corbels for rehabilitation.
- In general, rehabilitation with only epoxy injection gives better results for medium strength corbels as compared to high strength corbels.
- It can be concluded that use of epoxy and BFF together for the rehabilitation of damaged reinforced or steel fiber reinforced concrete corbels increases the original load capacity and ductility considerably.
- Rehabilitation with only epoxy injection is not sufficient for medium strength corbels that had been damaged due to an elevated temperature (750°C or higher degrees) and overloading. Therefore, extra measures need to be considered in addition to crack repairing to achieve effective rehabilitation.
- The existence of steel fiber plays an important role in both of the investigated rehabilitation techniques for both medium strength and high strength concrete corbels. It increases the effectiveness of the rehabilitation due to partial restoring of bridging effect of steel fibers. Moreover, the possibility of restoring the original load capacity by repairing with only epoxy injection increases for steel fiber reinforced concrete corbels. This situation leads to an economical alternative for rehabilitation.
- Rehabilitation with BFF can provide the serviceability and functionality of reinforced concrete corbels again, even they are damaged due to elevated temperature and overloading.
- The high tensile strength of BFF and bidirectional placement of the fabric

on corbel surfaces make it more powerful as compared to the adhesive epoxy leading to de-bonding failure for all of the corbels strengthened with BFF.

- For SCC, the mode of failure before the rehabilitation considerably affects the rehabilitation performance. Moreover, the diagonal splitting failure is observed to be the worst failure type for corbels which is concluded from the results.
- Structural engineers consider ductility to be one of the most important and significant parameters for safety. In this study, it is observed that ductility of rehabilitated corbels depends primarily on the type of concrete, compressive strength, steel fiber ratio, shear span, and type of Fiber Reinforcement.

CHAPTER 5

FINITE ELEMENT MODELING OF REHABILITATED RCHBs

5.1 Introduction

The nonlinear finite element analysis is the most efficient approaches as a potential numerical method to predict the reinforced concrete fracture behavior in the last decades. In this research study, finite element analysis was carried out via ATENA-GiD software. GiD program is used for data preparation and mesh generation of models and ATENA program is used for the analysis. ATENA is a specialized software for nonlinear finite element analysis of RC-Structures which is developed by Cervenka Consulting (Cervenka *et al.* 2017). In this chapter, the nonlinear finite element modeling described the proposing models of rehabilitation of RCHBs by BFF and CFRP. All analysis carried out in a three-dimensional manner in order to approach the real behavior of the beams. Furthermore, crushing and cracking of the concrete, yielding of the reinforcement were taken into account in all analyses. The aim of this chapter is to verify the numerical modeling with the corresponding experimental results of RCHBs which were obtained and discussed in the results of this chapter.

5.2 Nonlinear finite element analysis of Rehabilitated RCHBs by FRP

The nonlinear finite element modeling consisted of three parts; firstly. i) modeling of undamaged RCHBs to check the sufficiency of finite element modeling for further analyses ii) modeling of undamaged RCHBs strengthened by BFF and CFRP which represents the maximum load that can be gained from rehabilitation (ideal case regarding load capacity of rehabilitated RCHBs and crack repair epoxy), iii) modeling of damaged RCHBs rehabilitated by BFF and CFRP, but without crack repair epoxy which represents the minimum load that can be obtained as a result of rehabilitation process (worst case regarding load capacity of rehabilitated RCHBs). All analysis were carried out in a three-dimensional manner in order to approach the real behavior of the beams. Furthermore, crushing and cracking of the concrete, yielding of the reinforcement were taken into account in all analyses.

In all damaged members; it cannot be predicted the exact dimensions and location of cracks, therefore, it cannot be simulated the exact locations and dimensions of injection epoxy to represent the reality of rehabilitation and that lead to probabilistic values of ultimate load of rehabilitation. In this study, load-deflection graphs of rehabilitated RCHBs resulted from the experimental study were compared with the same graphs of the ideal case and the worst case of rehabilitated RCHBs which were obtained from FE results.

5.2.1 Constitutive Models

5.2.1.1 Concrete Constitutive Model

The constitutive models for tensile (fracturing) and compressive (plastic) behavior was the fracture-plastic model combines and it is based on the classical orthotropic smeared crack formulation and cracks band model. It employs Rankine failure criterion, exponential softening, and it can be used as rotated or fixed crack model. The hardening-softening plasticity model is based on Menétrey-Willam failure surface. The fracture-plastic model can be used to simulate concrete cracking, crushing under high confinement, and crack closure due to crushing in other material directions. The model differs from another model by the ability to handle also physical changes like for example crack closure, and it is not restricted to any particular shape of hardening-softening laws (Menetrey and Willam 1995, Cervenka *et al.* 2016), Figure 5.1 shows the model 3D failure surface by (Menetrey and Willam 1995).

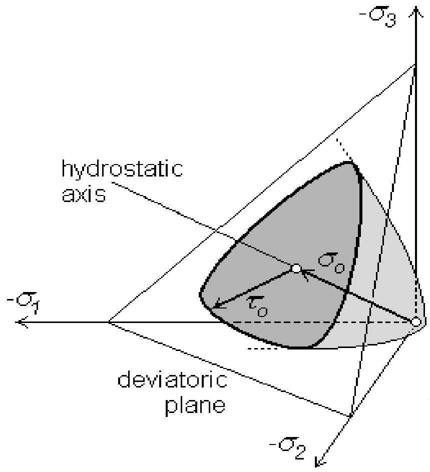

Figure 5.1 Menétrey-Willam model of 3D failure surface (Menetrey and Willam 1995)

5.2.1.2 Steel Reinforcement Constitutive Model

Two distinct forms can be used to model the reinforcement (discrete and smeared). Discrete reinforcement is modeled by truss elements as a form of reinforcing bars and the smeared reinforcement is a component of composite material and can be considered either as a single (only one-constituent) material in the element under consideration or as one of the more such constituents. The former case can be a special mesh element (layer), while the later can be an element with concrete containing one or more reinforcements. In either case, the reinforcement stress-strain relationship can be defined by one of the following laws (Cervenka *et al.* 2016):

1-Bilinear Law: elastic-perfectly plastic, is assumed as shown in Figure 5.2. The initial elastic part has the elastic modulus of steel Es. The second line represents the plasticity of the steel with hardening and its slope is the hardening modulus Esh. In case of perfect plasticity Esh =0. Limit strain represents limited ductility of steel.

2-Multi-Line Law – Figure 5.3 shows the multi-linear law consists of four lines. This law allows to model all four stages of steel behavior: elastic state, yield plateau, hardening, and fracture. The multi-line is defined by four points, which can be specified by the input.

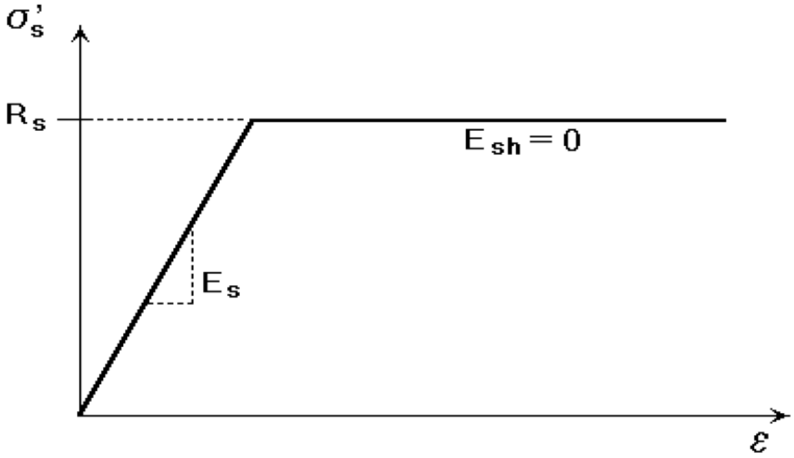

Figure 5.2 The bilinear stress-strain law for reinforcement (Cervenka *et al.* 2016)

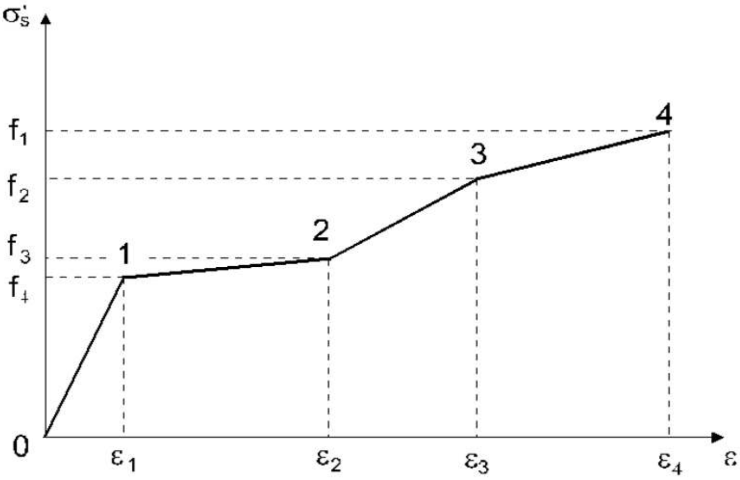

Figure 5.3 The multi-linear stress-strain law for reinforcement (Cervenka *et al.* 2016)

5.2.1.3 Crack Opening Constitutive Model:

The crack-normal stress components are related to cracking strains corresponding to opening of multiple and localized cracks by piecewise linear relations depicted in Figure 5.4. For multiple cracks, it's assumed that they do not close unless exposed to crack-normal compression (plasticity-like unloading) while a localized crack is assumed to close so that normal stress decreases linearly to reach zero (Cervenka *et al.* 2016).

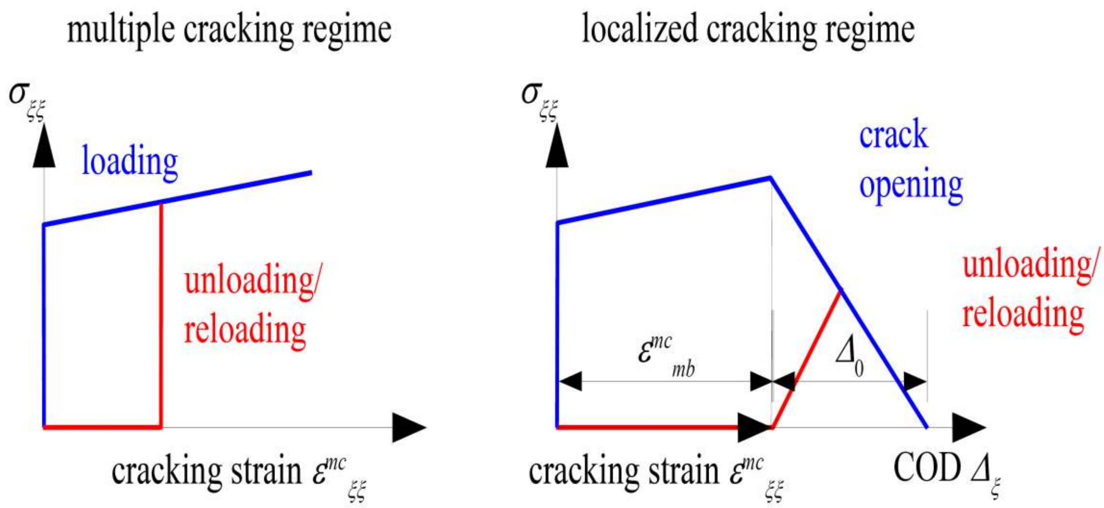

Figure 5.4 Stress vs. cracking strain relations in crack-normal direction (Cervenka *et al.* 2016)

5.2.1.4 Interface Material Constitutive Model

To simulate contact between two materials such as for instance a construction joint between two concrete segments or a contact between foundation and concrete structure the interface material model can be used. Mohr-Coulomb criterion with tension cut off the interface material is based on it. The constitutive relation for a general three-dimensional case is given in terms of tractions on interface planes and relative sliding and opening displacements (Cervenka *et al.* 2016).

$$\begin{pmatrix} \tau_1 \\ \tau_2 \\ \sigma \end{pmatrix} = \begin{pmatrix} k_{tt} & 0 & 0 \\ 0 & k_{tt} & 0 \\ 0 & 0 & k_{tt} \end{pmatrix} \begin{pmatrix} \Delta_{v_1} \\ \Delta_{v_2} \\ \Delta_u \end{pmatrix} \tag{4.1}$$

The initial failure surface depends on the Mohr-Coulomb condition (5.2-5.3) with ellipsoid in tension regime. This surface collapses to a residual surface which corresponds to dry friction after stresses violate this condition.

$$|\tau| \le c - \sigma.\phi, \sigma \le 0$$

$$\tau = \tau_0 \sqrt{1 - \frac{(\sigma - \sigma_c)^2}{(f_t - \sigma_c)^2}}, \tau_0 = \frac{c}{\sqrt{1 - \frac{\sigma_c^2}{(f_t - \sigma_c)^2}}} \quad (4.2)$$

$$\sigma_c = -\frac{f_t^2 \phi}{c - 2 f_t \phi}, 0 < \sigma \le f_t \quad (4.3)$$

$$\tau = 0, \sigma > f_t$$

The failure criterion is replaced by an ellipsoid in tension region, which intersect the normal stress axis at the value of f_t with the vertical tangent and the shear axis is intersected at the value of c (i.e. cohesion) with the tangent equivalent to $-\emptyset$, as depicted in Figure 5.5 (Cervenka *et al.* 2016).

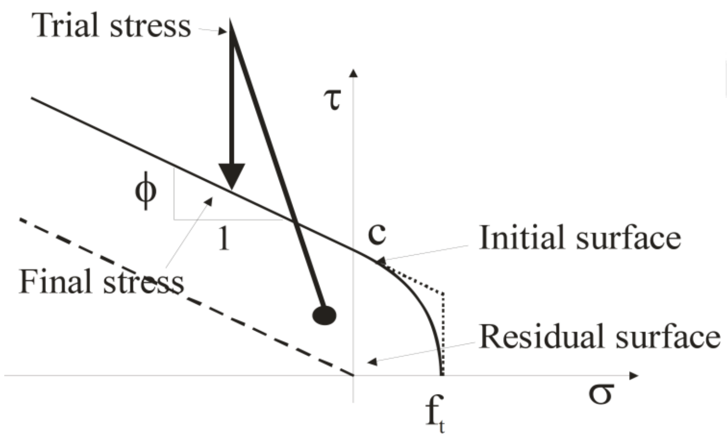

Figure 5.5 Failure surface for interface elements (Cervenka *et al.* 2016)

5.2.2 Finite Element Geometries

Truss 3D Linear and quadratic line elements with 3 nodes (CCIsoTruss<xxx>) are utilized to model the steel reinforcement bars. The 3D solid linear and quadratic Hexahedron (CCIsoBrick<xxxxxxxx>) elements with 8 nodes are used for modeling concrete.

The 3D solid linear and quadratic Tetrahedral 4-nodes (CCIsoTetra<xxxx>) are used to model the loading plate and supports. Plane Quadrilateral linear and quadratic elements 4-nodes (CCIsoQuad<xxxx>) are used to model the FRP. And finally the interface elements (CCIsoGao<xxxxxxxxxxxx> are used to model a contact between two surfaces. Figure 5.6 shows all geometries of finite elements that used in this study (Cervenka *et al.* 2016, 2017, Janda *et al.* 2016, Sajdlová 2016).

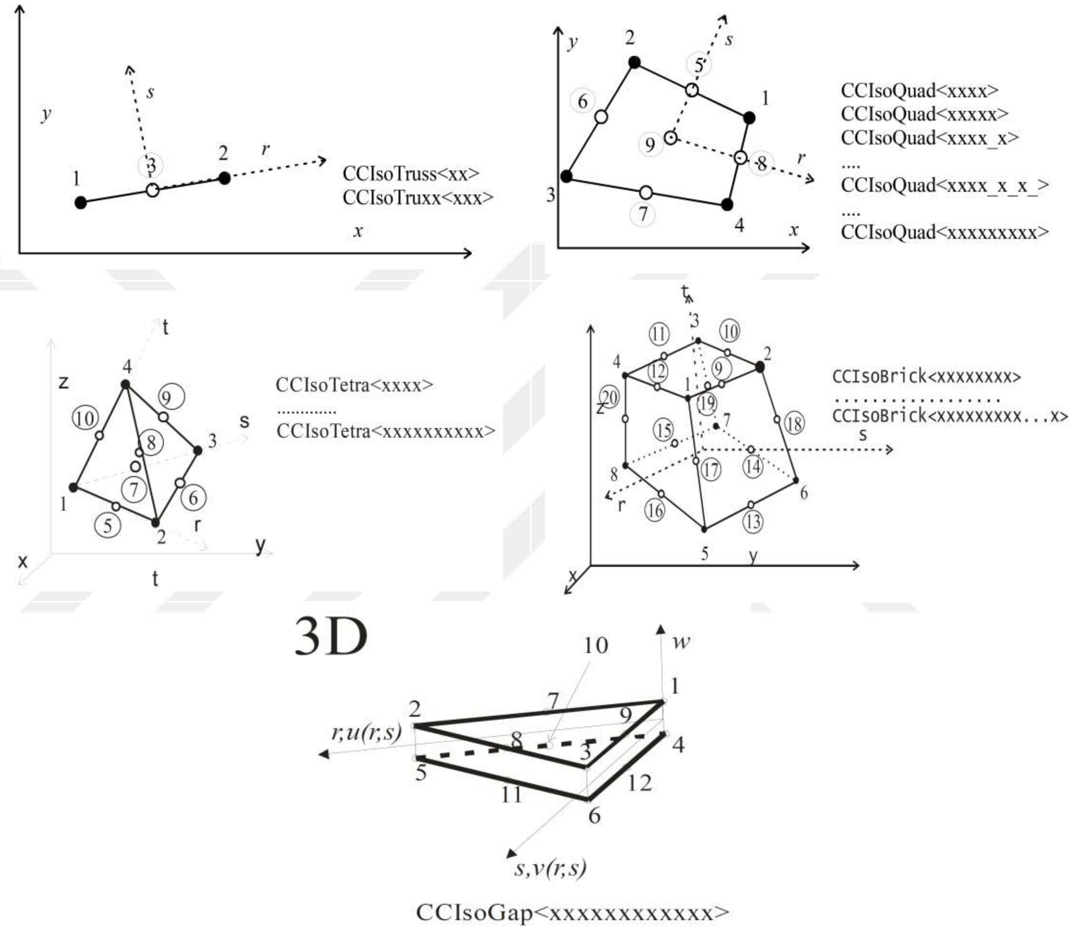

Figure 5.6 Geometries of finite elements that utilized in the analysis (Cervenka *et al.* 2016)

5.2.3 Finite Element Modeling of Haunched Beams

GiD program was used for the preparation of all finite element models and mesh generation, and then; ATENA was used for the analysis. Due to the symmetry of RCHBs in the longitudinal direction, only half of them was modeled to reduce analysis time. All boundary conditions that surrounding the test were assumed to simulate the reality of the test. A specialized material model in the software named as, "**2D Membrane Elements with Composite Material**" was followed to model BFF and CFRP strips (Sajdlová 2016). Configurations of FE modeling of RCHBs are shown in Figures 5.7-5.9; the Figure 5.7 is a specimen with all boundary conditions, the Figure 5.8 represents a specimen with FE mesh and the Figure 5.9 shows the FE model of a specimen rehabilitated by BFF or CFRP strips.

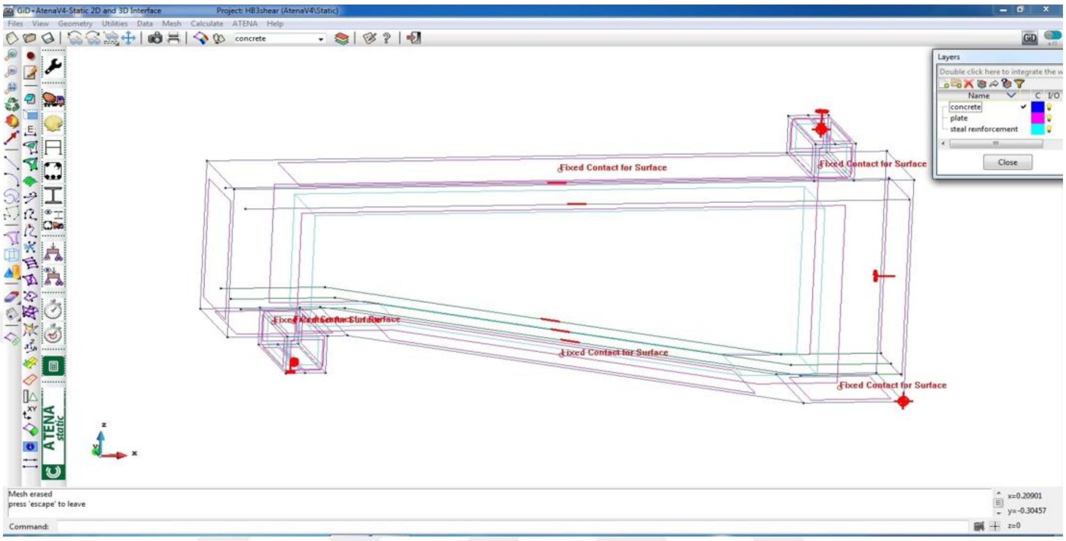

Figure 5.7 Studio of GiD-ATENA interface with boundary conditions of the specimen

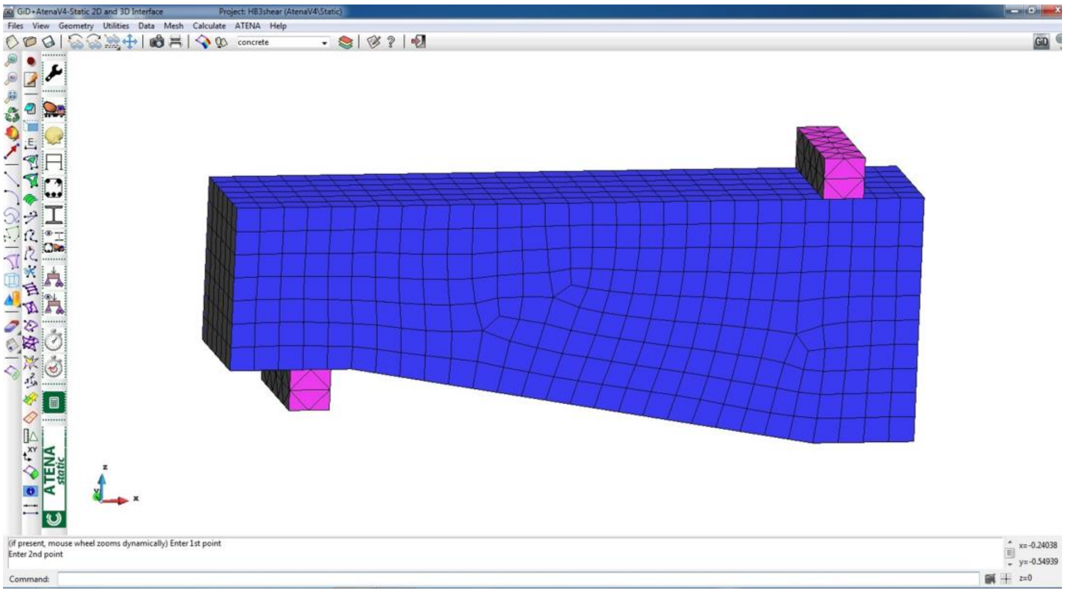

Figure 5.8 Studio of GiD-ATENA interface with FE mesh

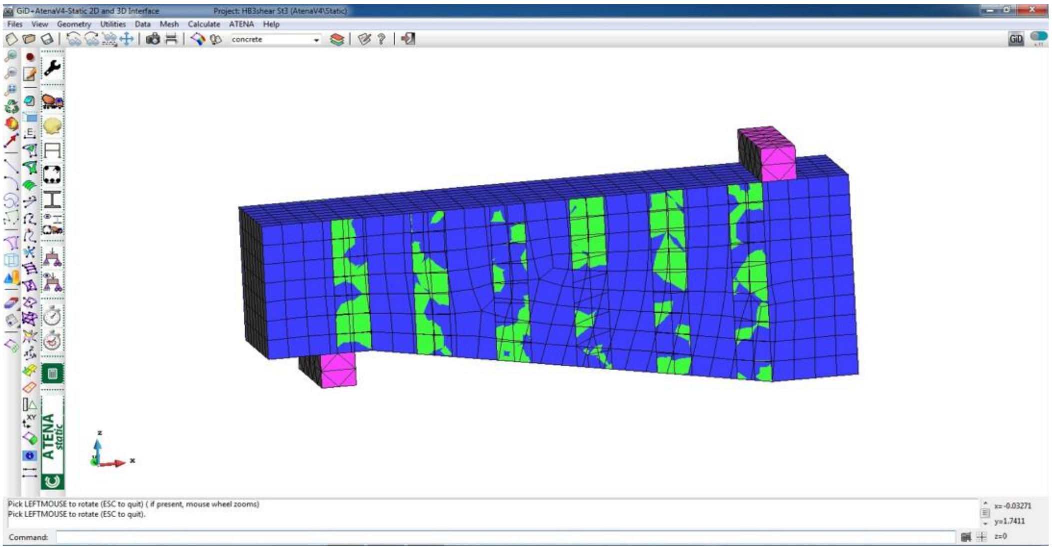

Figure 5.9 Studio of GiD-ATENA interface with FE mesh of FRP strips

5.3 Results of Rehabilitation RCHBs by Basalt Fiber Fabric (BFF)

The experimental work of this section was described in chapter three sections 3.2. The results of experimental work and FE analysis are shown below:

5.3.1 Matching of Experimental and FE Results of RCHBs Before the Rehabilitation

Maximum load capacities and corresponding deflections at mid-span of RCHBs resulting from experimental studies and finite element analyses are given in Table 5.1. Types of all RCHBs are also shown in the table. According to Table 5.1, it can be concluded that there is a good agreement between experimental results and FE analyses. Figures 5.10-5.11 show the correlation between experimental and nonlinear FE results of load capacity and deflection with correlation coefficients of $R^2 = 0.9689$ and $R^2 = 0.9652$ respectively.

Consistency between two results was also examined via statistical analysis. A statistically significant t-test was used to compare the resulting ultimate load capacity and deflection between the experimental test and nonlinear FE analysis (Ayyub and McCuen 2011). Tables 5.2-5.3 show the results of t-test statistical analysis on the results of experimental and nonlinear FE analysis regarding load and deflection, respectively.

Table 5.1 Ultimate load capacity (P) and deflection (Δ) of tested RCHBs regarding nonlinear FE analysis and experimental test results

	Name	Shape of Haunched Beam	P_{Test} (KN)	P_{ATENA} (KN)	Δ_{Test} (mm)	Δ_{ATENA} (mm)
Group one	HB1-300-0-300-603-55		110.3	115.3	2.15	1.51
	HB2-300-$^{+}$5-250-603-53.5		108.2	113.55	2.21	1.48
	HB3-300-$^{+}$10-200-603-55.1	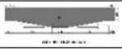	117.07	121.18	2.69	1.88
	HB4-300-$^{+}$10-200-402-53.9		91	102.5	2.57	1.66
	HB5-300-$^{+}$15-150-603-59.5		132	124.95	4.65	2.1
	HB6-300-$^{+}$15-150-402-51.5		122.8	124.84	4.57	2.75
Group two	HB7-300-0-300-603-58		215	215.92	5.86	4.22
	HB8-300-$^{-}$10-200-603-59		215	248.67	7.77	7.45
	HB9-300-$^{-}$15-150-603-59.9		220.9	225.98	6.44	5.72
	HB10-300-$^{+}$15-150-603-59		208	214.65	8.26	6.69
	HB11-250-$^{-}$10-350-603-65		176	189.33	11.36	9.66
	HB12-250-$^{-}$15-400-603-59	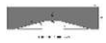	165	169.56	13.25	12.97

P_{Test} (kN): The ultimate load capacity of RCHBs obtained from experimental study.
P_{ATENA}(KN): The ultimate load capacity of RCHBs obtained from FE analyses.
Δ_{Test} (mm): The deflection at midspan of RCHBs obtained from experimental study.
Δ_{ATENA} (mm): The deflection at midspan of RCHBs obtained from FE analyses.

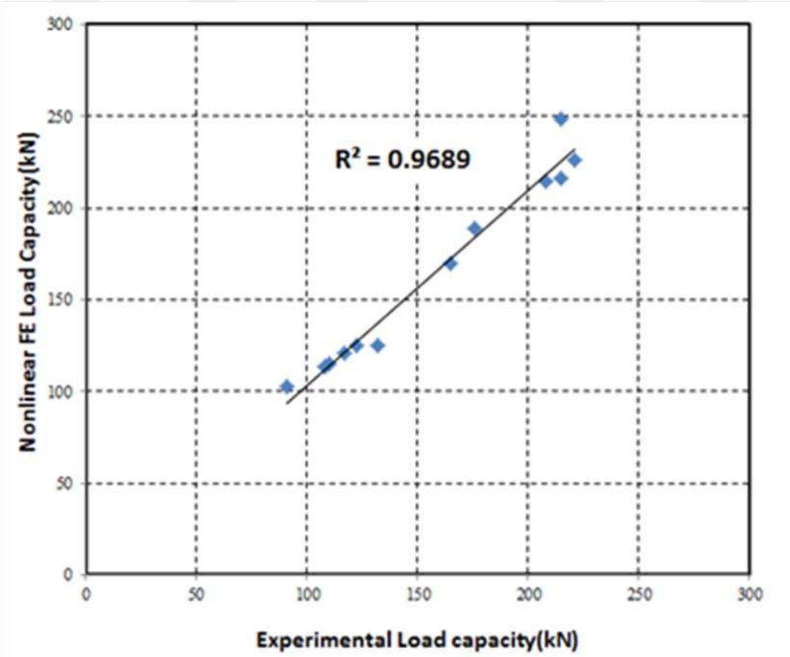

Figure 5.10 The experimental results versus the nonlinear FE analysis results of load capacity

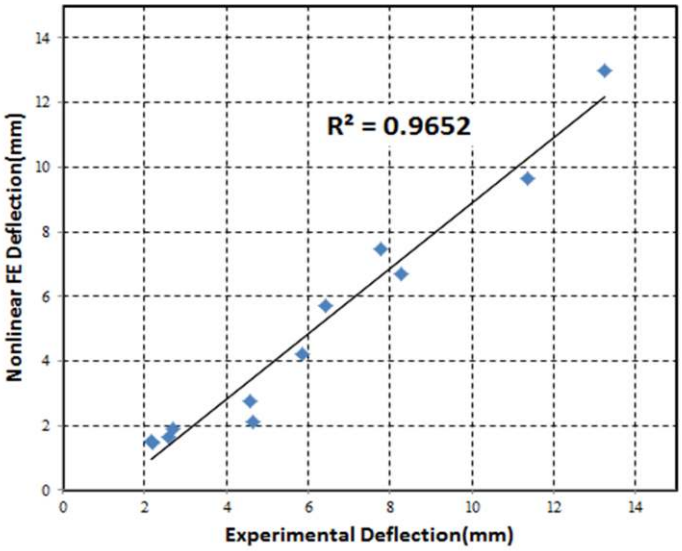

Figure 5.11 The experimental results versus the Nonlinear FE analysis results of Deflection

Table 5.2 T-Test Two-Sample of Loads; Experimental and nonlinear FE analysis

	P_{Test} (kN)	P_{ATENA} (kN)
Mean	156.7725	163.8691667
Variance	2376.723984	2775.91439
Observations	12	12
Hypothesized Mean Difference	0	
df	22	
t Stat	-0.342476044	
P(T<=t) one-tail	0.367621553	
t Critical one-tail	1.717144374	
P(T<=t) two-tail	0.735243107	
t Critical two-tail	2.073873068	

Table 5.3 T-Test:Two-Sample of deflections; experimental and nonlinear FE analysis

	δ_{TEST} (mm)	δ_{ATENA} (mm)
Mean	5.981666667	4.840833333
Variance	13.22879697	13.9864447
Observations	12	12
Hypothesized Mean Difference	0	
df	22	
t Stat	0.75754202	
P(T<=t) one-tail	0.228381589	
t Critical one-tail	1.717144374	
P(T<=t) two-tail	0.456763178	
t Critical two-tail	2.073873068	

Obviously, it can be seen from the results of t-test that the value of t Stat is less than t Critical two-tail for both results. Therefore, there are no significant differences between the results of the experimental test and the nonlinear FE analysis. In other words, there is no clear difference in the credibility of nonlinear FE analysis results, data points do not lie in the rejection region and it tends to be close to the experimental results.

The load-deflection curves obtained from the experimental study and nonlinear FE analysis are shown in the Figures 5.12-5.13. It can be also observed from these graphs that there is a good correlation between experimental and FE analysis results regarding load-deflection behavior. Furthermore, it can be concluded not only before-peak mechanical behavior, but also post-peak behavior can be predicted by FE analyses.

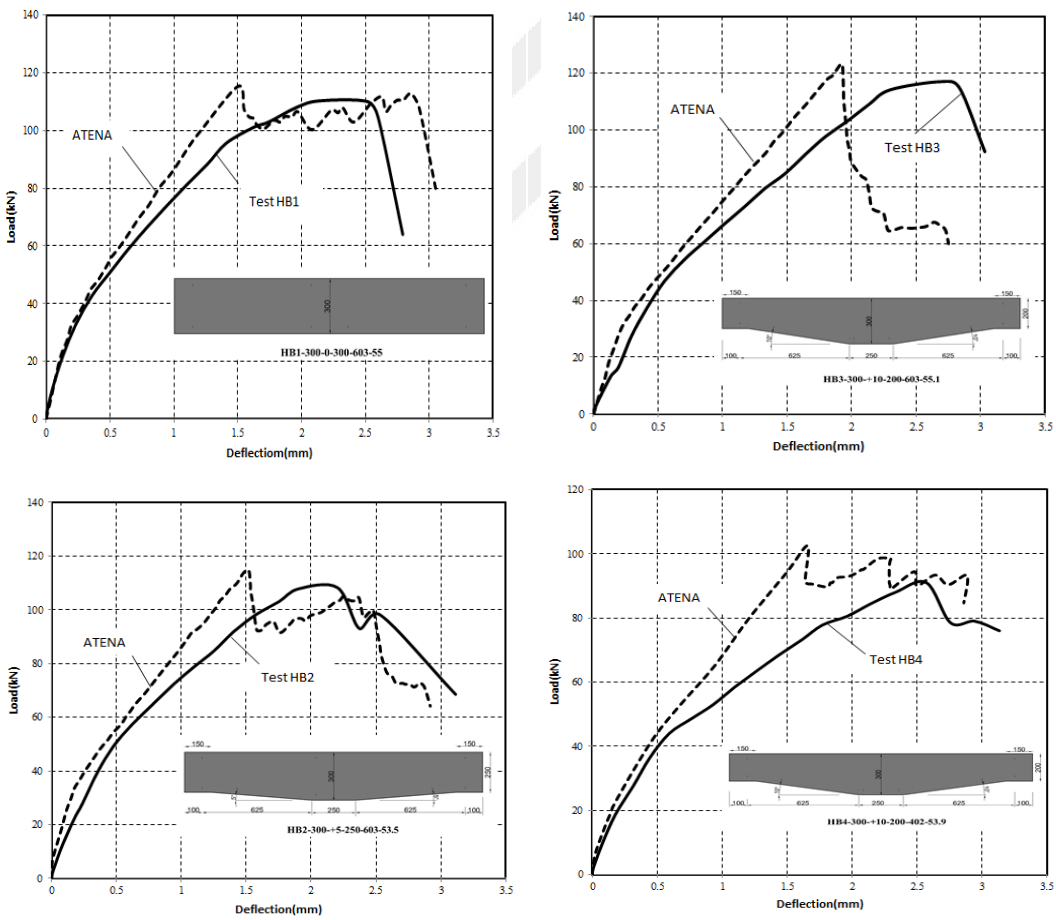

Figure 5.12 Load-Deflection curves of experimental test and nonlinear FE analysis from HB1 to HB4

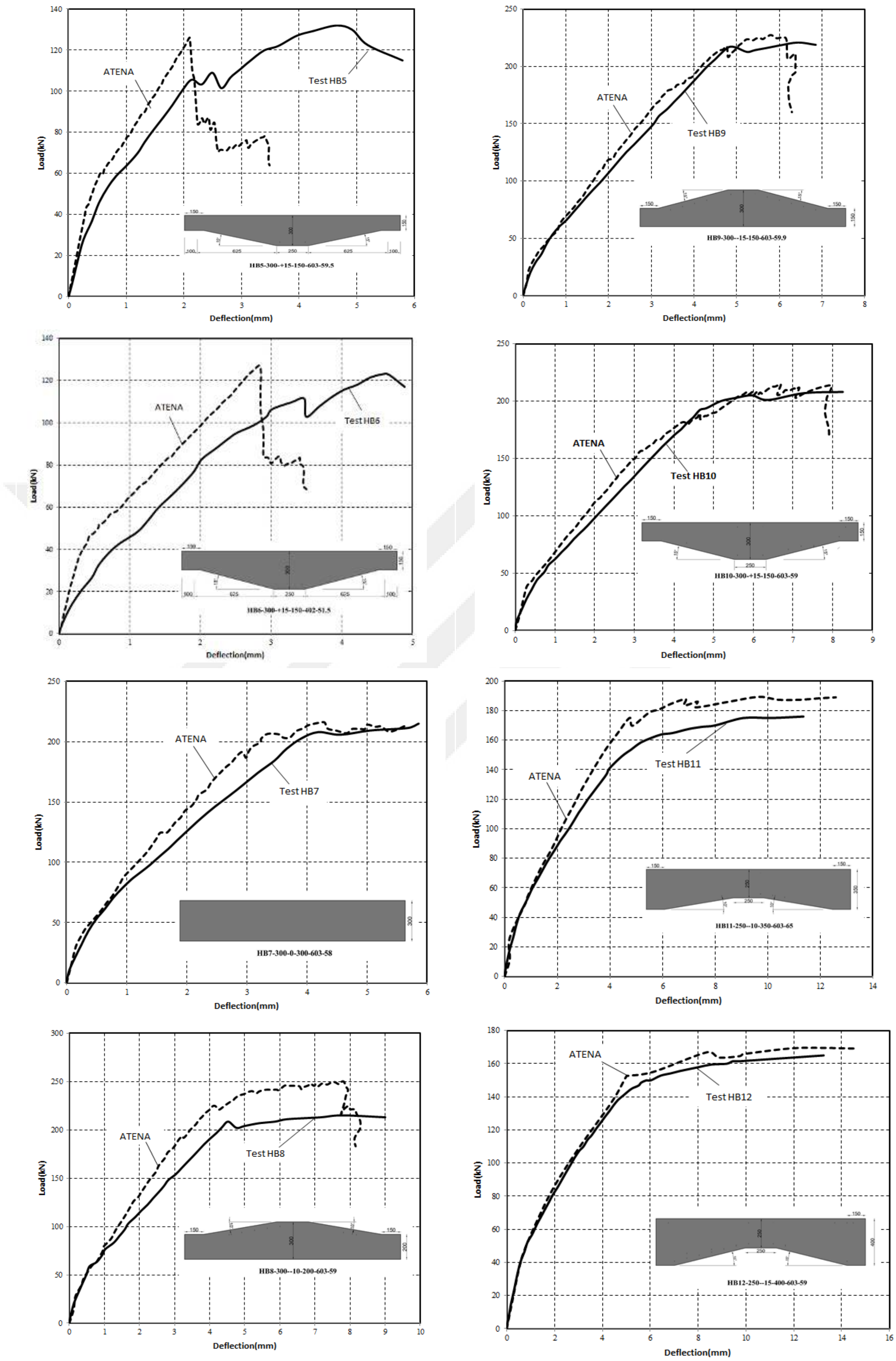

Figure 5.13 Load-Deflection curves of experimental test and nonlinear FE analysis from HB5 to HB12

5.3.1.1 Cracks Pattern of Tested and FE modeled haunched Beams before Rehabilitation:

Figures 5.14-5.15 show crack patterns resulting from the experimental study and nonlinear FE analyses. It can be observed from figures that there is a good agreement between FE analysis and experimental results with respect to the crack location, crack patterns and inclination of flexural and shear cracks.

For the shear failure, it is very important to note that the failure region of prismatic beams is about close to the position of applied load, while the region of failure of RCHBs is near to the support, this experimental result is also validated by FE analysis results. Therefore, it can be concluded that FE modeling can be preferred for further analysis of RCHBs, like modeling of rehabilitated haunched by FRP fabrics.

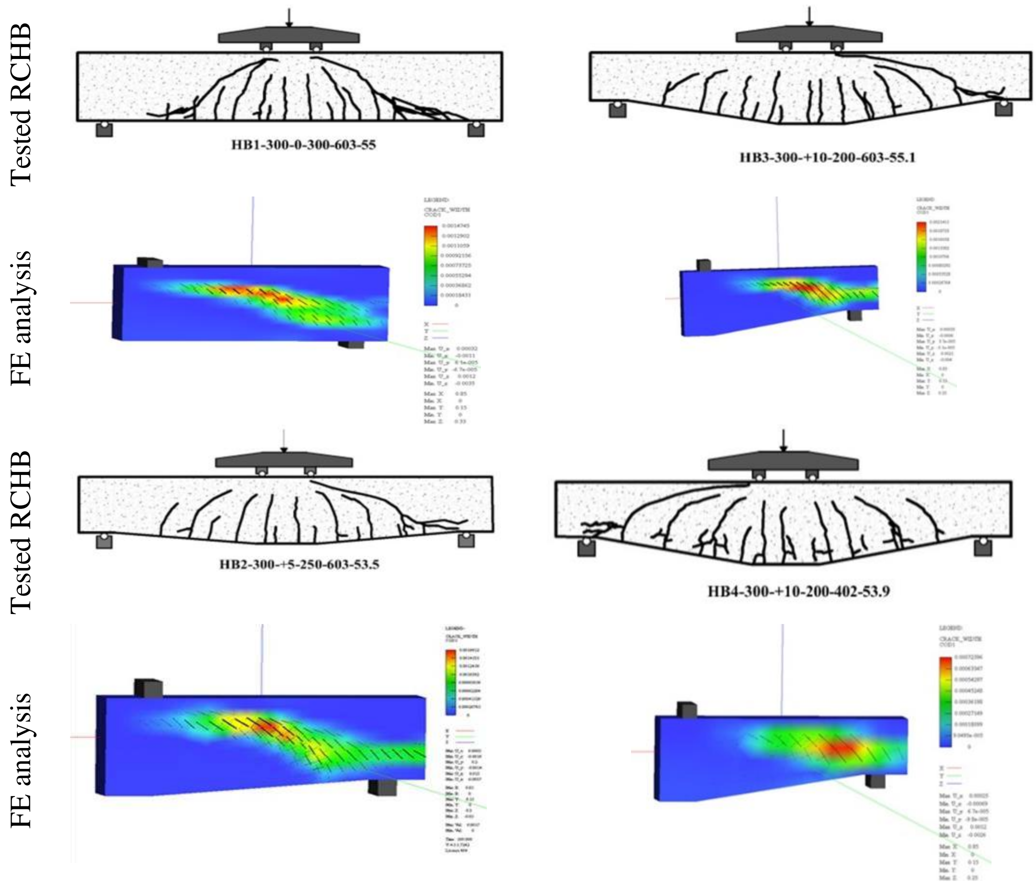

Figure 5.14 Cracks pattern of tested haunched beams (HB1-HB4) compared with corresponding FE analysis

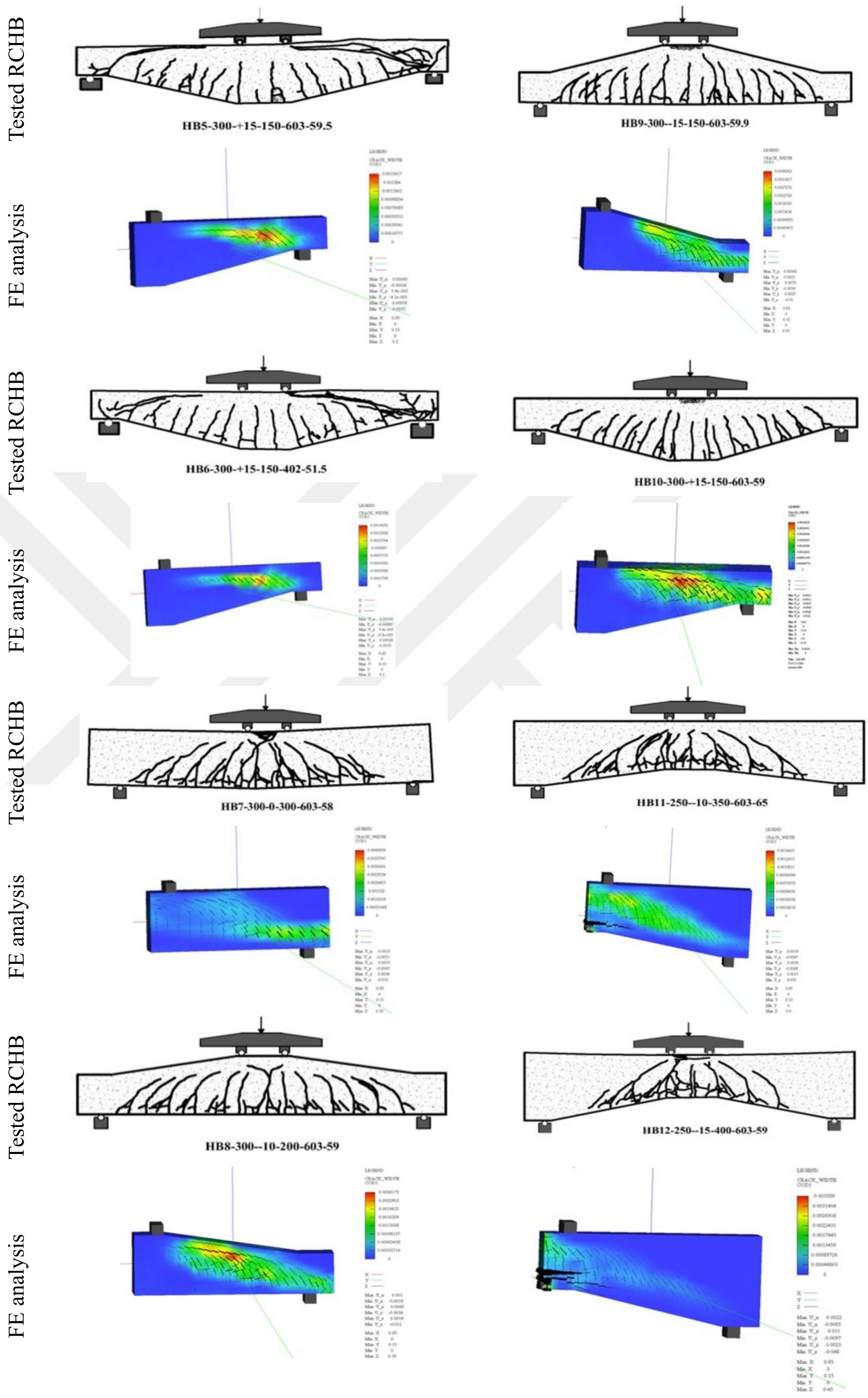

Figure 5.15 Cracks pattern of tested haunched beams (HB5-HB12) compared with corresponding FE analysis

5.3.2 Experimental and FE Results of RCHBs After the Rehabilitation

This part presents finite element analysis results of rehabilitated haunched beams after specified damage levels. Table 5.4 shows maximum and minimum limits of load capacities of rehabilitated haunched beams resulted from FE analyses. Load capacities of the same haunched beams obtained from the experimental study are also compared with maximum and minimum limits in the table. Maximum limit represents the strengthening of undamaged haunched beams by Basalt Fabric, while minimum limit represents the strengthening of cracked (damaged) haunched beams by Basalt Fabric. The levels of damage in the FE models were determined based on of haunched beams resulting from the experimental study. All details related to the production of minimum limits are specified in section 5.3.3. When the results are carefully scrutinized, the conclusion is that the variance of the experimental results of load capacities lies between the two ranges of nonlinear FE analysis and it clearly appears when the results represented by a graph as shown in Figure 5.16.

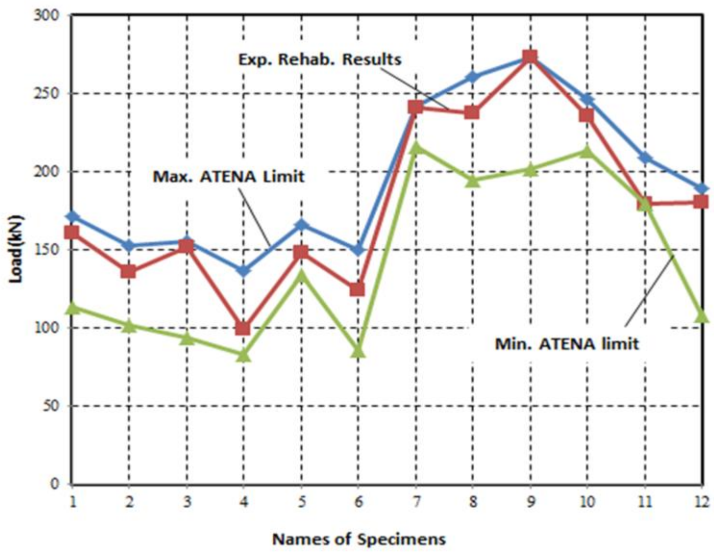

Figure 5.16 Comparison between the experimental rehabilitated results of RCHBs with the two ranges results of nonlinear FE analysis

The range of values between the maximum and minimum limits of a rehabilitated haunched beam represents all possible load capacities of the beam that can be achieved. Therefore, it can be concluded that each interval serves as a safety zone for a rehabilitated haunched beam. The experimental values of rehabilitation results that may be located between them or reach the maximum or minimum limitations of FE analysis. The locations of experimental values in the range depending on several parameters, the important point, the ratio of rehabilitating the cracks of specimens before using the FRP, also the damage ratio in the specimens will affect on the results of rehabilitation and the stiffnesses of specimens. It can be seen from Table 5.4 and Figure 5.16 that most experimental results of rehabilitation haunched beams tend to be close to the maximum limit of FE analysis. When the injection material was entered in all most available cracks in the specimen, the results of rehabilitation will be close to the maximum limit of FE analysis of the strengthening undamaged models. Moreover, load capacities of all of the repaired and strengthened beams lie between the minimum and maximum limits of FE analysis results showing the efficiency of crack repair.

Figures 5.18-5.19 show the curves of load-mid span deflection of all specimens of haunched beams, by comparing the experimental rehabilitation curves and the limitation curves of nonlinear FE analysis curves. It can be noted that the stiffness of experimental curves is less than the stiffness of upper limits of nonlinear FE analysis curves of all specimens of haunched beams, and that returned to the damaged of haunched beams. In the other meaning, the value of load capacity of the damaged specimen may be close after rehabilitation to the value of load capacity of strengthening specimen, but the value of stiffness will not be reached the value of stiffness of strengthening undamaged specimen and that may be considered the main difference between the rehabilitation of damaged specimens and the strengthening of the undamaged specimens.

Figure 5.17 shows the correlation between the experimental rehabilitation results (load & deflection) with a maximum limit of nonlinear FE analysis results (load & deflection) with correlation coefficients of $R^2 = 0.9616$ of loads and $R^2 = 0.8231$ of deflections respectively, also the correlation between the experimental rehabilitation results (load & deflection) and minimum limit of nonlinear FE analysis results (load & deflection) with correlation coefficients of $R^2 = 0.829$ and $R^2 = 0.462$ respectively.

It can be concluded from Figure 5.17 that the load capacities of rehabilitation damaged haunched beams with injection material in the cracks tended to be close the load capacities of strengthening undamaged haunched beams with a very good correlation coefficient and with less correlation coefficient with respect to the deflections.

On the other hand, it can be examined the experimental loads of rehabilitated damaged haunched beams with a comparing of the nonlinear FE analysis loads of strengthening undamaged haunched beams (max. Limit) by statistical significant t-test to see whenever there are any significant differences between them. Table 5.5 shows the result of t-test that the (t Stat) is less than the (t Critical two-tail) and it can be concluded that there are no significant differences between loads of the experimental test and loads of nonlinear FE analysis (max. limit), and the results tended to be close to each other.

Table 5.4 Experimental rehabilitation results and the range of nonlinear FE analysis results

Name		Shape of Haunched Beam	Max. Limit		Exp. Rehab. Results		Min. Limit	
			$P_{ATENA\ Max}$ (KN)	$\Delta_{ATENA\ Max.}$ (mm)	$P_{Test\ Reh.}$ (KN)	$\Delta_{Test\ Reh.}$ (mm)	$P_{ATENA\ Min.}$ (KN)	$\Delta_{ATENA\ Min.}$ (mm)
Group one	HB1-300-0-300-603-55	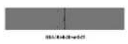	171.6	4.26	160.95	5.02	113.3	3.86
	HB2-300-$^{+}$5-250-603-53.5		152.88	3.94	135.74	4.07	101.78	2.04
	HB3-300-$^{+}$10-200-603-55.1		155.3	4.70	151.86	4.22	93.73	2.2
	HB4-300-$^{+}$10-200-402-53.9		136.17	4.1	98.7	3.23	83.16	2.4
	HB5-300-$^{+}$15-150-603-59.5	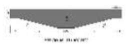	165.5	4.76	147.97	5.42	133.92	5.8
	HB6-300-$^{+}$15-150-402-51.5	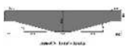	150.01	4.75	124.23	8.34	85.56	5.83
Group two	HB7-300-0-300-603-58		241.78	7.04	241.14	9.96	215.6	4.54
	HB8-300-$^{-}$10-200-603-59		260.2	10.76	236.78	10.13	194.4	6.53
	HB9-300-$^{-}$15-150-603-59.9		273.02	10.88	272.58	11.71	201.63	5.13
	HB10-300-$^{+}$15-150-603-59	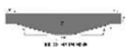	245.76	9.945	235.4	10.14	212.78	6.37
	HB11-250-$^{-}$10-350-603-65		208.55	6.03	179.58	7.02	179.21	9.23
	HB12-250-$^{-}$15-400-603-59	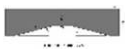	189.25	12.69	180.52	12.27	108.1	11.48

Table 5.5 T-Test Two-Sample of Loads; Experimental rehabilitated damaged RCHBs loads and nonlinear FE analysis loads of strengthening undamaged RCHBs

	$P_{\text{Test after Rehab. (kN)}}$	$P_{\text{ATENA Max. (kN)}}$
Mean	180.4541667	195.835
Variance	2950.897227	2324.042555
Observations	12	12
Hypothesized Mean Difference	0	
df	22	
t Stat	-0.733604077	
P(T<=t) one-tail	0.235468108	
t Critical one-tail	1.717144374	
P(T<=t) two-tail	0.470936216	
t Critical two-tail	2.073873068	

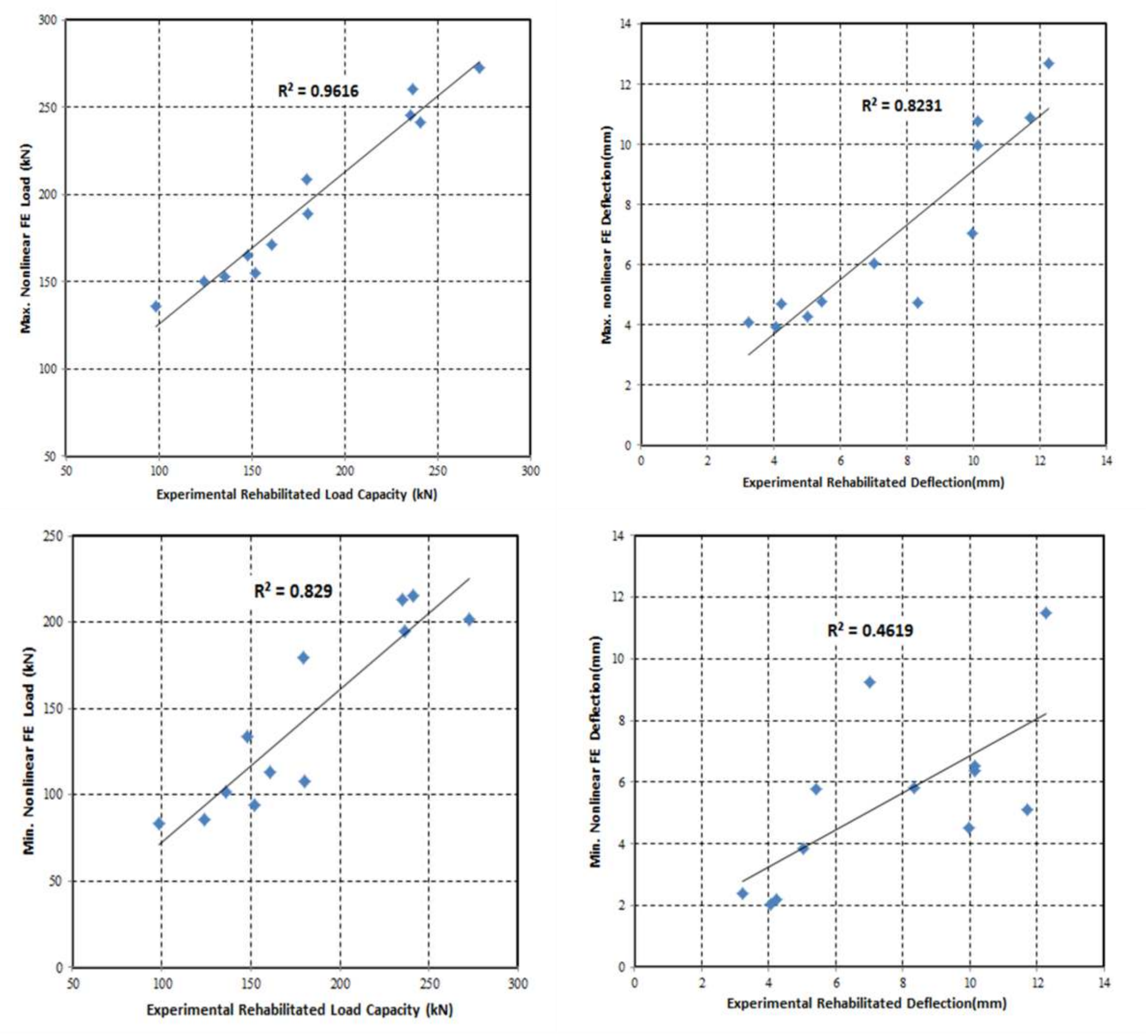

Figure 5.17 The experimental results versus the max. and min. of Nonlinear FE analysis limits of Load and Deflection respectively

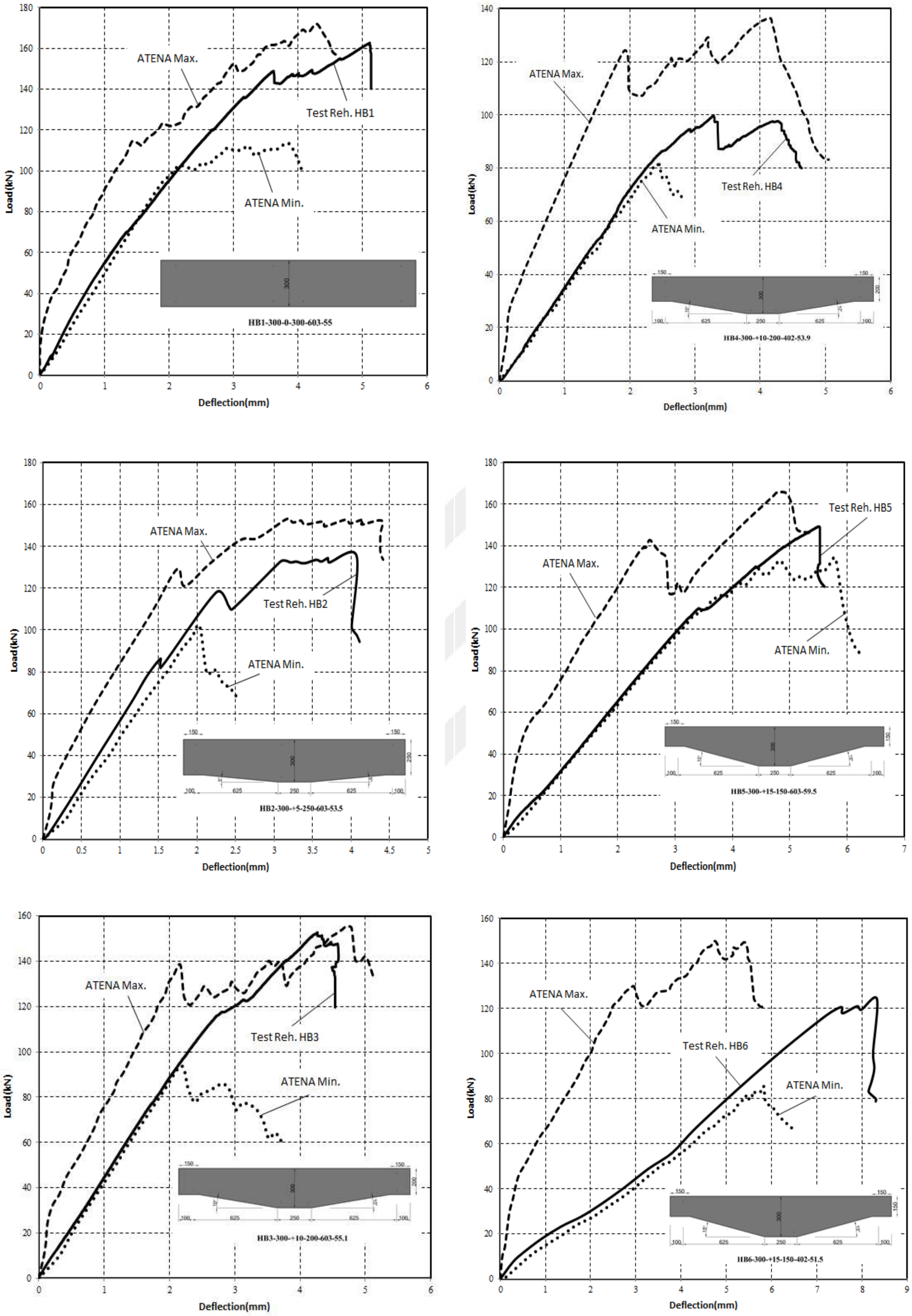

Figure 5.18 Load-deflection curves of experimental rehabilitation curves with comparing of limitations of nonlinear FE analysis curves of RCHBs from HB1 to HB6

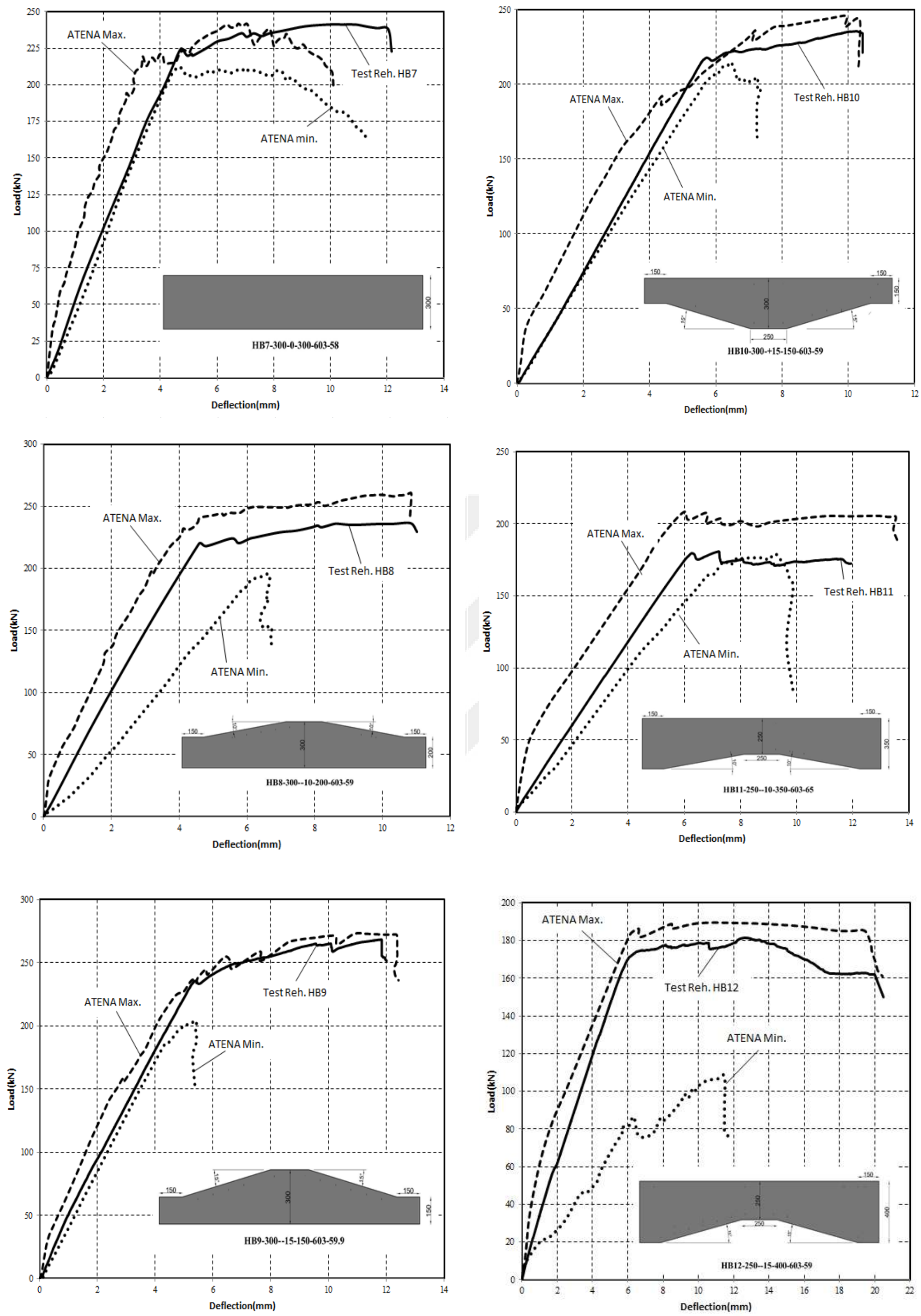

Figure 5.19 Load-deflection curves of experimental rehabilitation curves with comparing of limitations of nonlinear FE analysis curves of RCHBs from HB7 to HB12

5.3.2.2 Cracks Pattern and Mode of Failure of Rehabilitated RCHBs

Figures 5.20-5.21 show the cracks patterns of strengthening nonlinear FE haunched beams corresponding to the testing haunched beams and rehabilitated hunched beams. It can be observed from the figures, the mode of failure of rehabilitated haunched beams were a debonding failure in all specimens of haunched beams. Obviously, there is an acceptable agreement between the crack patterns of FE analysis models and the cracks patterns of rehabilitated haunched beams. According to the simplifications and the assumptions of using Finite Element analysis, it seems unattainable to get crack patterns as precisely as the experimental test, this may be due to several reasons; the main reason is due to heterogeneous natures of concrete material and the differences of FE model (half of the real specimen) from the real experimental testing. However, it can be observed from the figures 5.14, 5.15, 5.20, and 5.21 that the nonlinear FE models can predict well the inception and the spread of cracks also the region of failure where the critical crack occurs, some main features of a critical crack such as inclination, direction, and crack pattern, which are proportional similar with those from the experimental tests (Nghiep 2011, ALBEGMPRLI 2017).

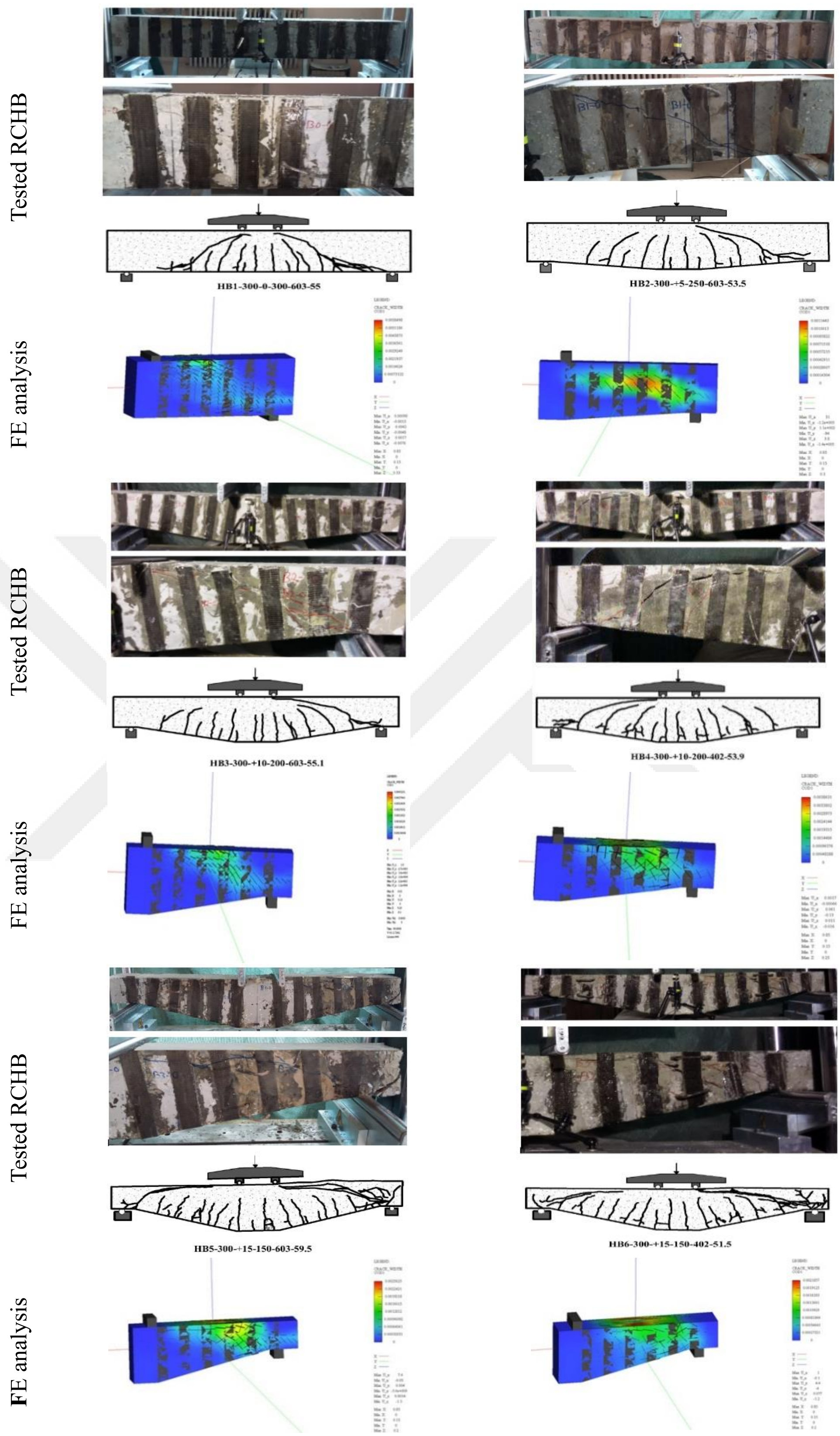

Figure 5.20 Cracks pattern with the mode of failure of testing haunched beams HB1-HB6 with relevant strengthening FE analysis cracks

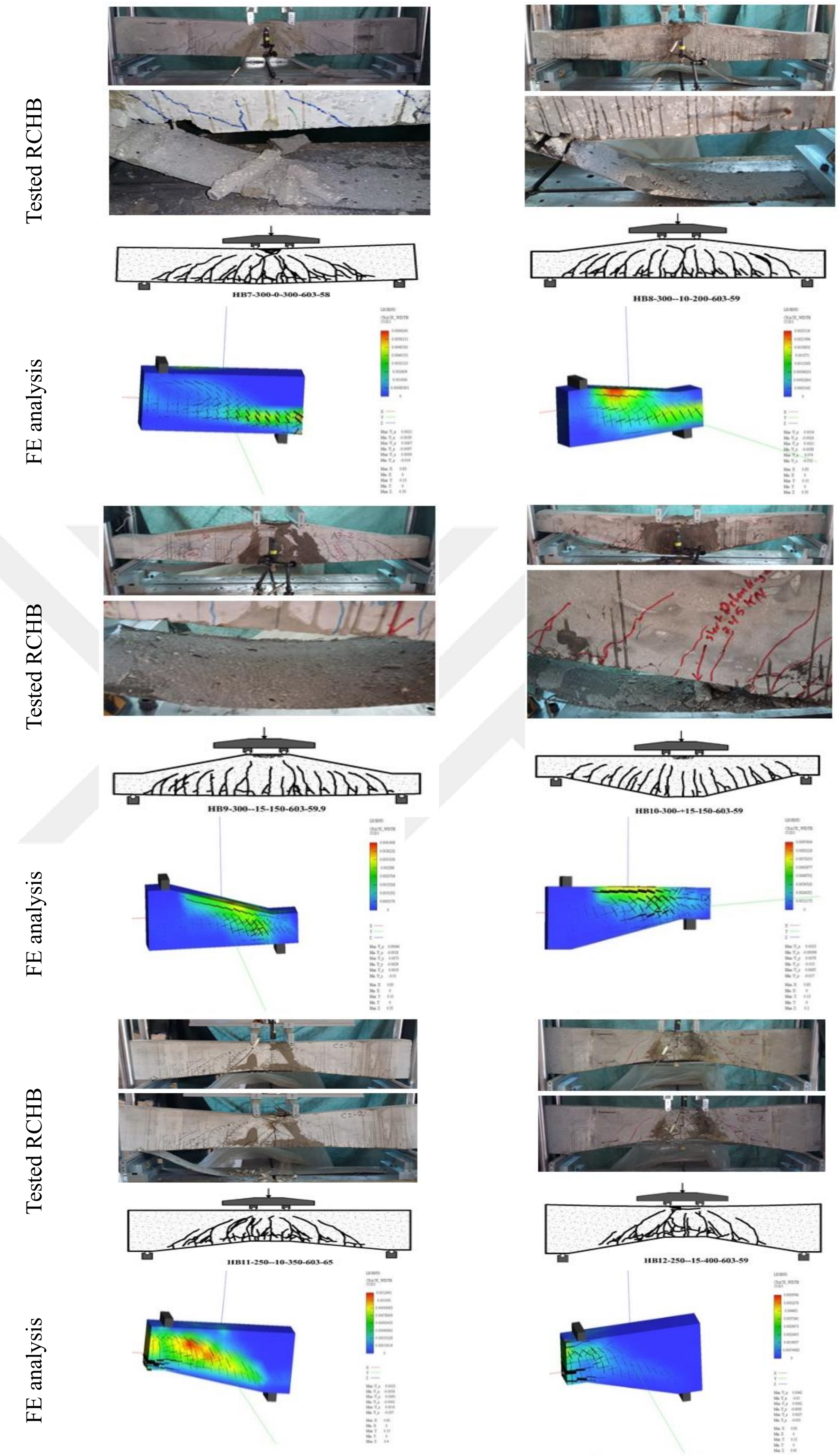

Figure 5.21 Cracks pattern with the mode of failure of testing haunched beams HB7-HB12 with relevant strengthening FE analysis cracks

5.3.3 Production of Minimum Limits

This part presents the procedure for the achievement of the minimum limit of rehabilitated RCHBs via FE modeling and analysis. Minimum limit represents the mechanical behavior of damaged haunched beams rehabilitated only by Basalt Fabric without repairing cracks. It's worth to mention that analyses can be carried out in a displacement controlled mode in ATENA-GiD software. This feature makes this software capability to estimate the mechanical behavior of the hunched beams after peak load. Judging from this feature, the level of load after the peak load can be predicted which represents the damage level of the beam. Figure 5.22 shows the damage levels of the beams that may occur after peak load.

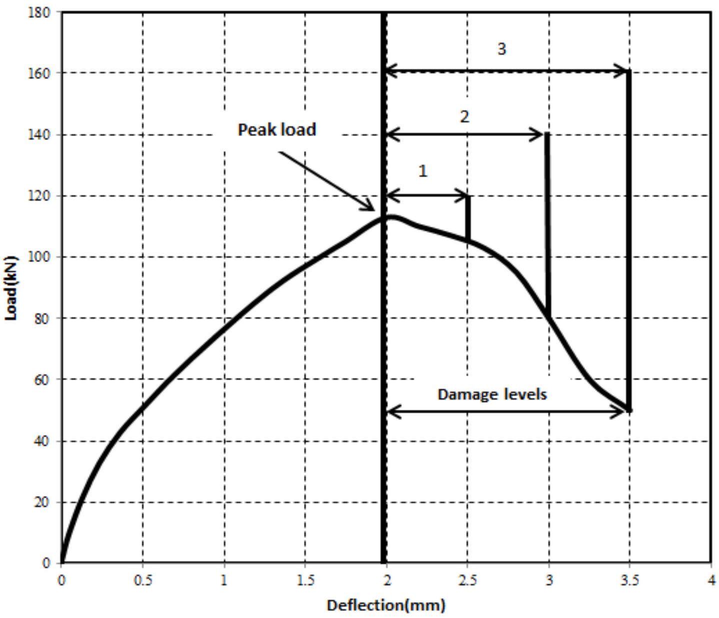

Figure 5.22 Conception of damaging levels after the peak load

The curve of load-deflection may be continued until collapse failure after the peak load, every point of the curve after the peak load represented the specific level of damage of the beam, for example, in the Figure 5.22 explained three levels of damage that may occur in the testing of the specimen, the level 3 represents more damaged degree than 2 and 1, which is represented more propagation of cracks and crack width than level 2 and 1.

In order to model the minimum limit of FE analysis, damage level of the experimental haunched beam before the rehabilitation should be determined. It can be done by calculating the ultimate deflection divided by the deflection which is corresponding to the maximum load. The result must be multiplied by the deflection which is corresponding to the maximum load of the relevant FE model before the rehabilitation(Δ_{ATENA},) after then, it can be entered the design displacement Δ_{Design} in the data simulation of the program to create the design minimum limit of the load-deflection curve of relevant haunched beam Table 5.6 shows all details of how to calculate the deflection (Δ_{Design}) that use to construct the minimum limit of FE analysis. (Δ_{Design}) was used in the program to construct the damaged level of haunched beam by applying the load until the (Δ_{Design}), then the program will unload until zero load to represent the real case of haunched beam before the rehabilitation, after then the strengthening of Basalt Fabric will apply on the haunched beam. The last step, the program will apply the load until the haunched beam fails. Finally, the results will represent the minimum limit of FE analysis models.

Δ_{Design} of HB1 equal 1.96mm as shown in table 5.6, it was used to construct the damaged level of HB1 and then the minimum limit of FE analysis, it can be observed in the Figure 5.23 several independent values of deflections that used to construct the damage levels of HB1 and then the minimum limit of haunched beam.

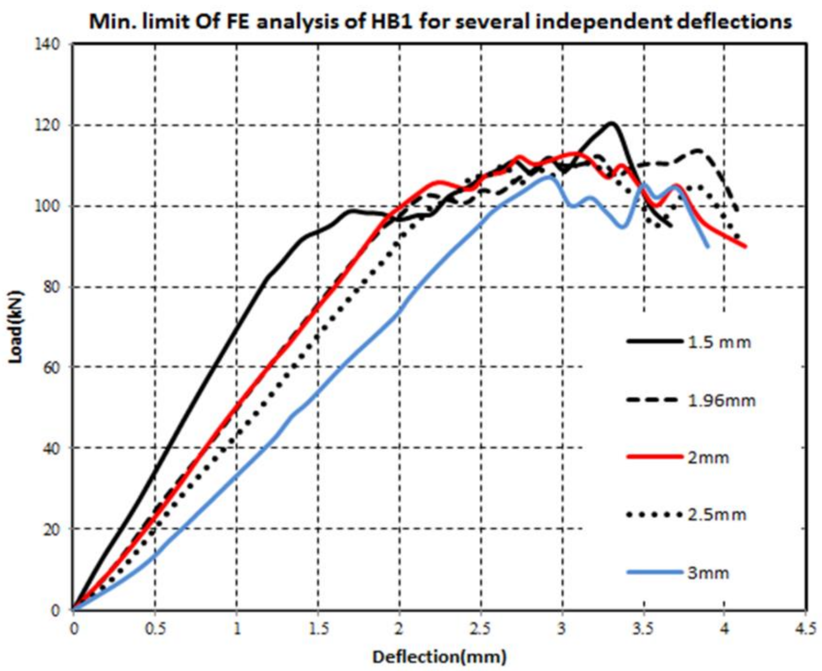

Figure 5.23 Shows several curves of minimum limit of FE analysis of HB1 depending on several independent values of deflection that used to construct the damage levels of HB1

It can be seen in the Figure 5.18; the Maximum load capacity of minimum limit which depend on Δ_{Design} =3.0 mm less than other values of minimum limit curves which depend on less values of Δ_{Design}, and that lead to conclude that the increasing value of Δ_{Design} will affect the load-displacement relationship, and that increasing of Δ_{Design} represent more damage of haunched beam before the rehabilitation and will affect the value of the ultimate load capacity and the stiffness of the specimen after being rehabilitated.

Table 5.6 Shows how to calculate the Δ_{Design} that use to construct the min. limit of FE analysis models

Names		Shape of Haunched Beam	Exp. Result before Rehabilitation		$\frac{\Delta_{UltimateDeflection}}{\Delta_{PeakLoad}}$	Δ_{ATENA} (mm)	Δ_{Design} (mm)
			Δ Peak Load (mm)	Δ Ultimate Deflection (mm)			
Group one	HB1-300-0-300-603-55	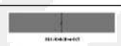	2.15	2.793	1.30	1.51	1.96
	HB2-300-$^{+}$5-250-603-53.5		2.21	3.113	1.41	1.48	2.08
	HB3-300-$^{+}$10-200-603-55.1		2.69	3.039	1.13	1.88	2.12
	HB4-300-$^{+}$10-200-402-53.9		2.57	3.133	1.22	1.66	2.02
	HB5-300-$^{+}$15-150-603-59.5		4.65	5.795	1.25	2.1	2.62
	HB6-300-$^{+}$15-150-402-51.5		4.57	4.888	1.07	2.75	2.94
Group two	HB7-300-0-300-603-58		5.86	5.86	1.00	4.22	4.22
	HB8-300-$^{-}$10-200-603-59		7.77	9.005	1.16	7.45	8.63
	HB9-300-$^{-}$15-150-603-59.9	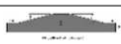	6.44	6.85	1.06	5.72	6.08
	HB10-300-$^{+}$15-150-603-59	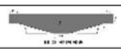	8.26	8.26	1.00	6.69	6.69
	HB11-250-$^{-}$10-350-603-65	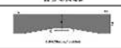	11.36	11.36	1.00	9.66	9.66
	HB12-250-$^{-}$15-400-603-59	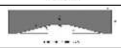	13.25	13.25	1.00	12.97	12.97

5.4 Rehabilitation Results of RCHBs by Carbon Fiber Reinforcement Polymer (CFRP)

The experimental work of this section was described in chapter three section 3.3. The results of experimental work and FE analysis are shown below:

5.4.1 Matching of Experimental and FE Results of RCHBs Before the Rehabilitation

Table 5.7 shows the ultimate load capacities and corresponding deflections at mid-span of RCHBs foretold by ATENA with corresponding of experimental results. The ultimate load capacities are determined as the highest values of the load during the procedure of analysis which are corresponding the deflections at mid-span of haunched beams. The results of ATENA show an acceptable matching with the experimental results of haunched beams; Figure 5.24 shows the correlation between experimental and nonlinear FE results of load and deflection with correlation coefficients of $R^2 = 0.8349$ and $R^2 = 0.7923$ respectively. Its worth to mention that can be examined the results of experimental and FE results by statistic hypothesis to see whenever is there any significant differences between them. A statistically significant t-test is used to exam the results of ultimate load capacities that came from the experimental test and nonlinear FE analysis, in addition to the result of deflections experimental and nonlinear FE analysis (Ayyub and McCuen 2011). Tables 5.8 and 5.9; show the results of t-test statistical analysis.

Table 5.7 Ultimate load capacity P and deflection Δ of haunched beams from both Nonlinear FE Analysis and experimental test results before the rehabilitation

Name of RCHB	Beam code	Shape of Haunched Beam	Experimental		Finite Element	
			${}^{*}P_{Bef.}$ (kN)	${}^{*1}\Delta_{Bef.}$ (mm)	${}^{*2}P_{ATENA}$ (kN)	${}^{*3}\Delta_{ATENA}$ (mm)
1	Rf1U90	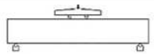	107	1.51	113.46	3.32
2	A1-5INJ	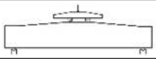	113.5	2.217	-	-
3	A1-10U90		114.5	2.51	114.83	2.54
4	A2-10U45	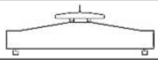	115.3	2.72	123.35	2.61
5	A1-15U90	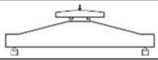	121	2.535	123.04	2.16
6	A2-15U45	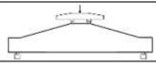	113.2	2.48	117.23	1.98
7	Rf2U90	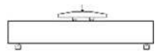	94.4	2.618	105.07	2.53
8	B1-5INJ	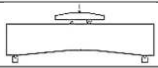	108	5.554	-	-
9	B1-10U90	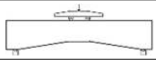	101.5	6.219	103.56	6.31
10	B2-10U45	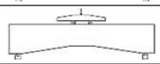	91	7.2	103.68	6.59
11	B1-15U90	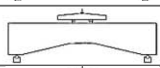	104	5.328	106.55	7.45
12	B2-15U45	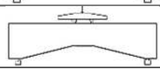	95.5	8.362	100.57	6.03

${}^{*}P_{Bef.}$(kN): The ultimate load capacity of haunched beam from experimental test before the rehabilitation.
${}^{*1}\Delta_{Bef.}$(mm): The deflection at midspan of haunched beam from experimental test before the rehabilitation.
${}^{*2}P_{ATENA}$(KN): The ultimate load capacity of haunched beam from results of ATENA.
${}^{*3}\Delta_{ATENA}$ (mm): The deflection at midspan of haunched beam from results of ATENA.

Table 5.8 T-Test Two-Sample of Loads; Experimental and nonlinear FE analysis

	$P_{Bef.}$ (kN)	P_{ATENA} (kN)
Mean	105.74	111.134
Variance	103.3293333	69.94736
Observations	10	10
Pooled Variance	86.63834667	
Hypothesized Mean Difference	0	
df	18	
t Stat	-1.295808625	
P(T<=t) one-tail	0.105706119	
t Critical one-tail	1.734063607	
P(T<=t) two-tail	0.211412239	
t Critical two-tail	2.10092204	

Table 5.9 T-Test: Two-Sample of deflections; experimental and nonlinear FE analysis

	$\Delta_{Bef.}$(mm)	Δ_{ATENA}(mm)
Mean	4.1482	4.152
Variance	5.795567	4.665507
Observations	10	10
Pooled Variance	5.230537	
Hypothesized Mean Difference	0	
df	18	
t Stat	-0.00372	
P(T<=t) one-tail	0.498538	
t Critical one-tail	1.734064	
P(T<=t) two-tail	0.997076	
t Critical two-tail	2.100922	

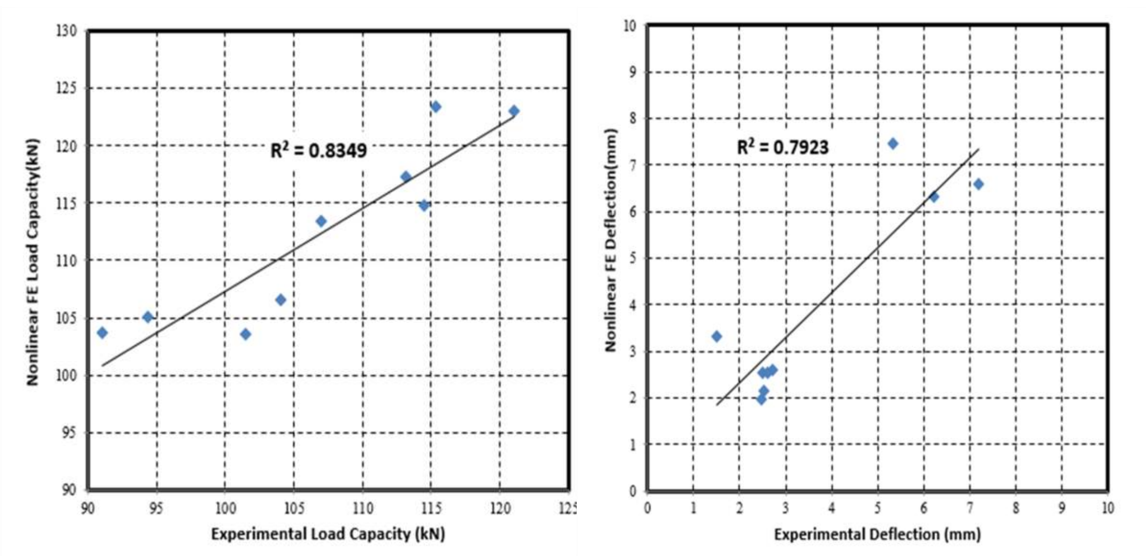

Figure 5.24 The experimental results versus the Nonlinear FE analysis results of Load and Deflection respectively

Obviously, it can be seen from the results of t-test; the value of (t Stat) is less than (t Critical two-tail) for both tests of loads and deflections, and that lead to conclude: there are no significant differences between the results of the experimental test and the nonlinear FE analysis. In other words, there is no clear difference in the credibility of nonlinear FE analysis results, data points do not lie in the rejection region and it tends to be close to the experimental results. The load-deflection curves of two groups of experimental test results and nonlinear FE analysis results are shown in the Figures5.25 and 5.26. Again, it can be observed from the figures that there is an acceptable agreement between the shapes of the load-deflection curves regarding of the ATENA results and experimental test results.

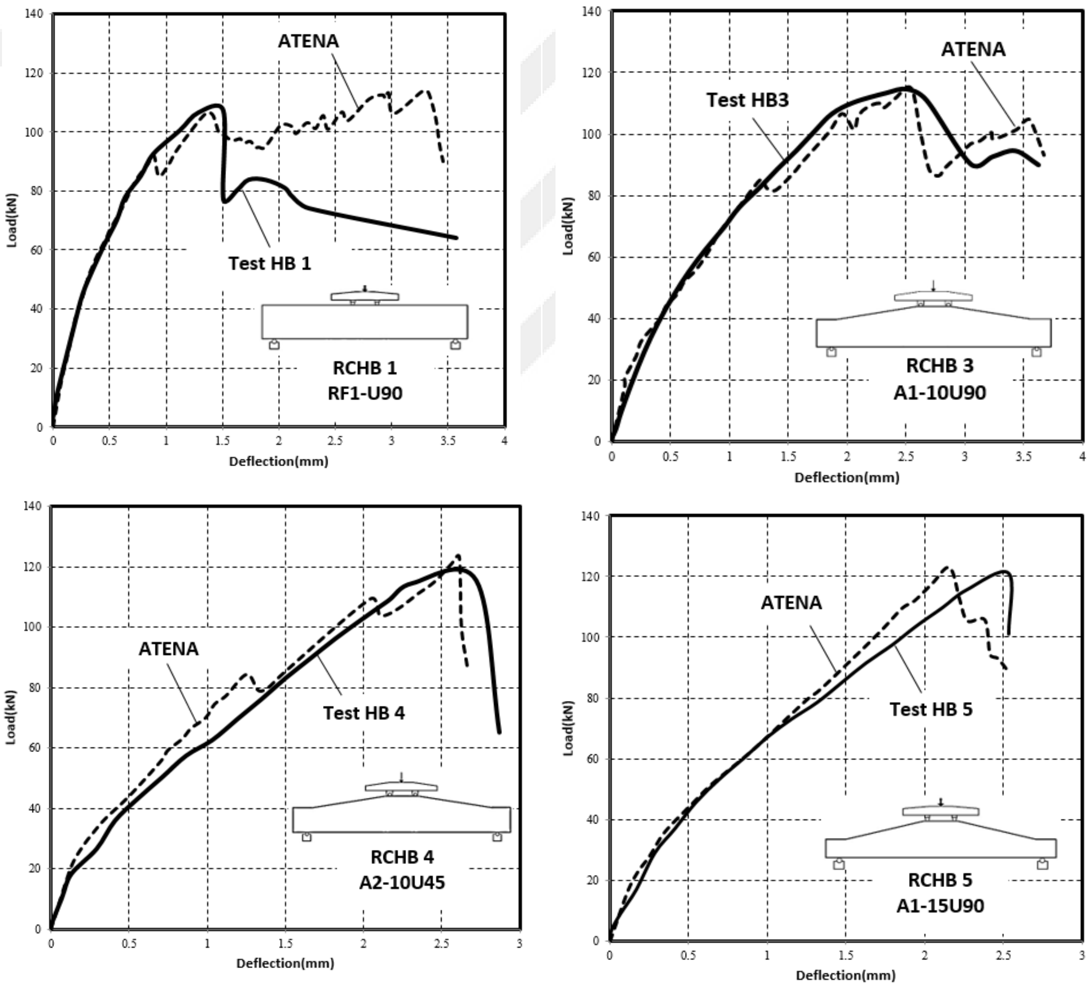

Figure 5.25 Load-Deflection curves of experimental test and nonlinear FE analysis from HB1, HB3 to HB5

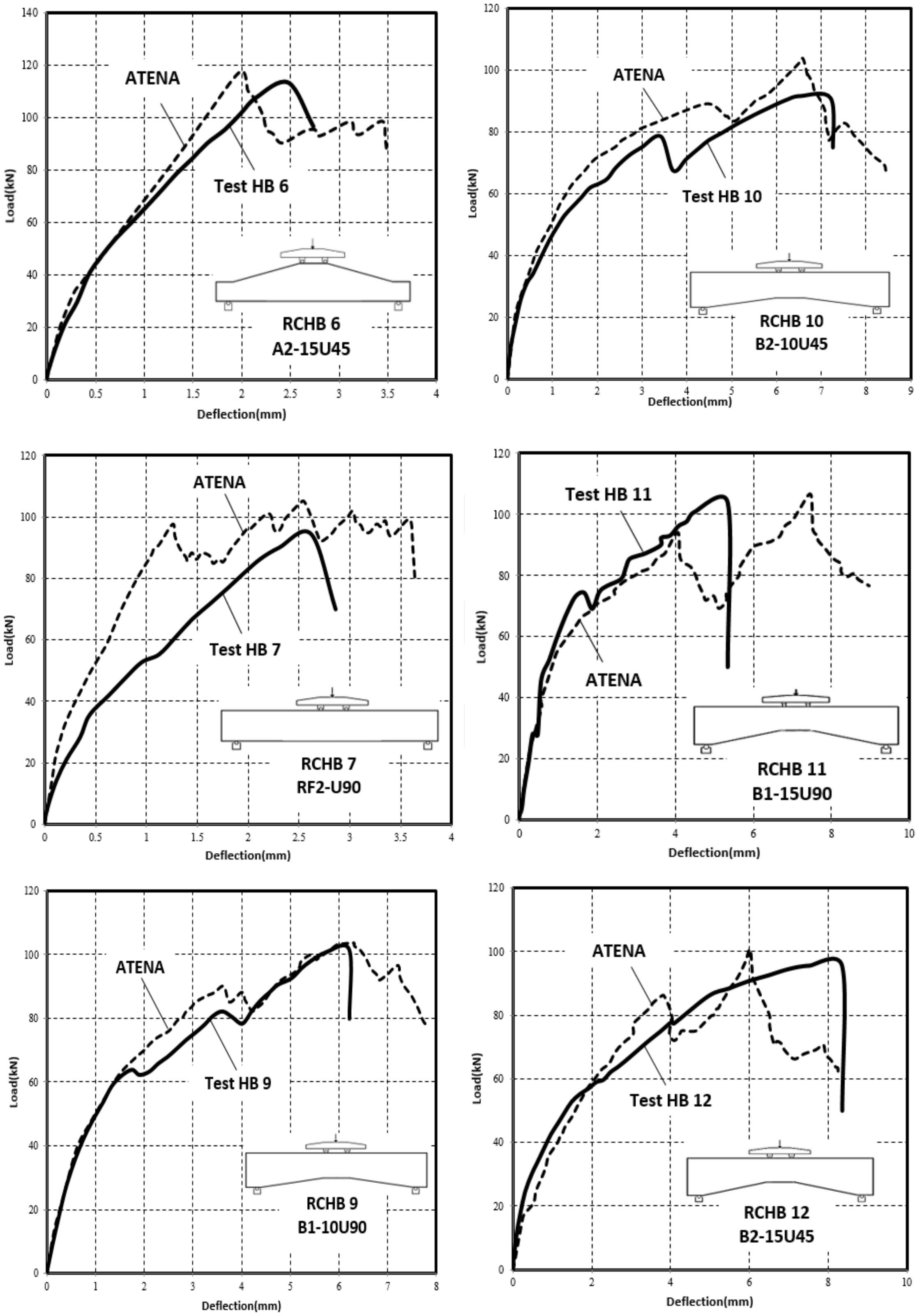

Figure 5.26 Load-Deflection curves of experimental test and nonlinear FE analysis from HB6 to HB12

5.4.1.1 Cracks Pattern Experimental and FE Results of RCHBs Before the Rehabilitation

Table 5.10 shows cracks pattern of nonlinear FE haunched beams corresponding to the testing haunched beams. It can be observed from figures that there is a good agreement between the FE analysis and the experimental results with respect to the crack location, spacing, patterns and inclination of relevant shear cracks, Form figures of shear failure, it is very interesting to find out that each nonlinear FE results and experimental test results expected quite accurately that the failure region of prismatic beams is about close to the position of load application, while the region of failure of haunched beams is near to the reaction of support, and that other confirmation of accuracy of the proposed model of FE analysis by GiD-ATENA.

Table 5.10 Cracks pattern of testing haunched beams with relevant FE analysis cracks for HB1 until HB12

Name of RCHB	Beam code	Experimental	Finite Element
1	Rf1U90	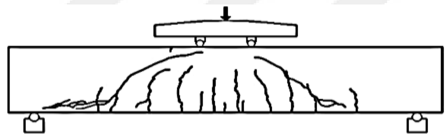	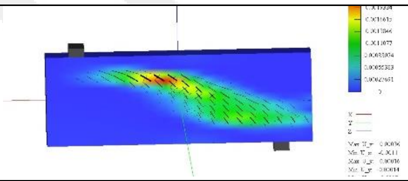
2	A1-5INJ	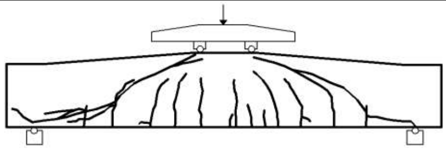	---
3	A1-10U90	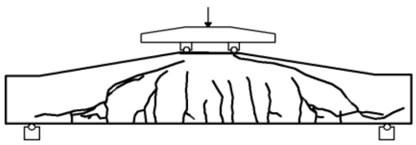	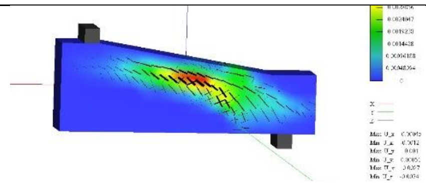
4	A2-10U45	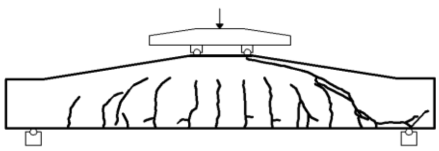	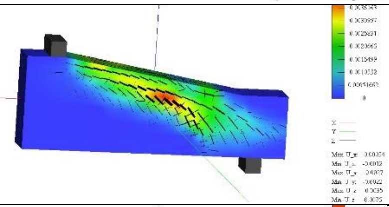
5	A1-15U90	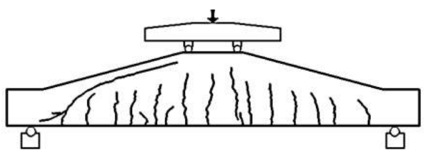	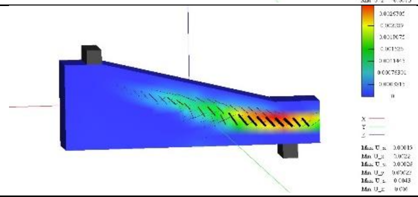

6	A2-15U45	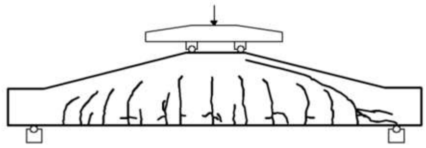	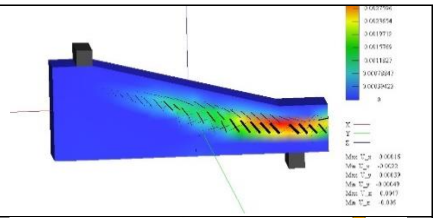
7	Rf2U90	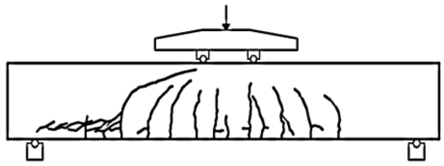	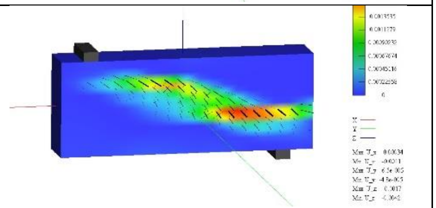
8	B1-5INJ	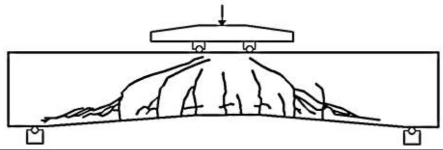	------------------------------------
9	B1-10U90	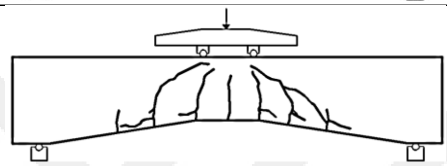	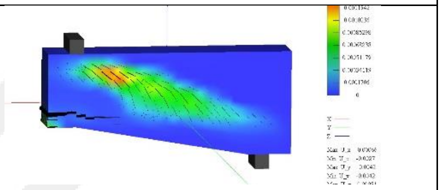
10	B2-10U45	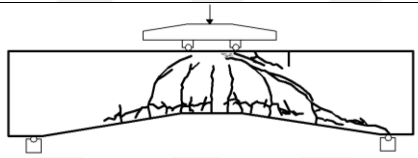	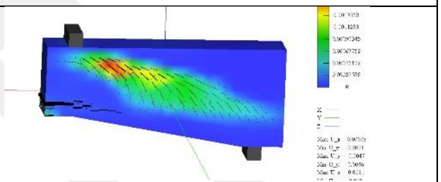
11	B1-15U90	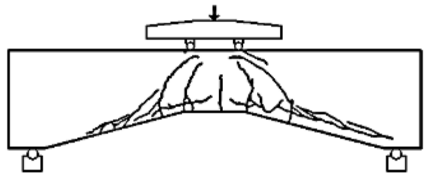	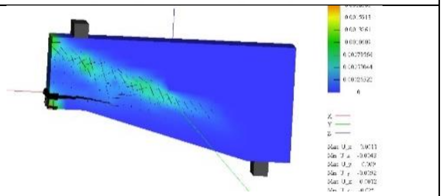
12	B2-15U45	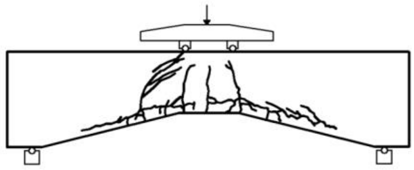	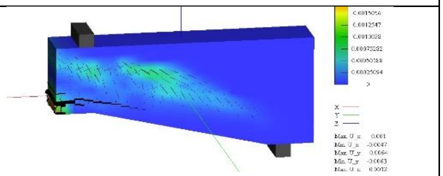

5.4.2 Experimental and FE Results of RCHBs After the Rehabilitation

This part presents the comparison between experimental and FE modeling results regarding the haunched beams rehabilitated by CFRP fabrics. Table 5.11 shows the comparison of the experimental capacity results with the maximum and minimum capacity values resulted from FE analyses. Maximum limit represents the strengthening of undamaged models of haunched beams by CFRP fabrics, while minimum limit represents the strengthening of damaged models of haunched beams by the fabric. The proportion of damage in the models were determined by taking the damage of experimentally tested haunched beams into consideration in order to approach real cases. (all details of how to produce the minimum limit in section 5.4.3.). When the results are carefully scrutinized; the conclusion is that the variance of the experimental results of load capacities lies between the two ranges of nonlinear FE analysis and it clearly appears when the results represented by a graph as shown in Figure 5.27. The range values between the maximum and minimum limits represent the values of rehabilitation results that may be located between them. The locations of experimental values depend on several points, the important point, the ratio of rehabilitating cracks of specimens before using the FRP, also the damage ratio in the specimens will affect the results of rehabilitation and the stiffnesses of specimens. It can be seen from Table 5.11 and Figure 2.27; that most experimental results of rehabilitation haunched beams tend to be close to the maximum limit of FE analysis. When the injection material was entered in all most available cracks in the specimen, the results of rehabilitation must be close to the maximum limit of FE analysis of the strengthening undamaged models.

Table 5.11 Experimental rehabilitation results and the range of nonlinear FE analysis results

No. RCHBs	Beam code	Strengthening scheme	Max. Limit		Experimental		Min. Limit	
			$P_{ATENA\,Max}$ (kN)	$\Delta_{ATENA\,Max.}$ (mm)	$P_{Aft.}$ (kN)	$\Delta_{Aft.}$ (mm)	$P_{ATENA\,Min.}$ (kN)	$\Delta_{ATENA\,Min.}$ (mm)
1	Rf1U90		233.224	7.43	225	9.65	86.02	2.787
2	A1-5INJ		----	----	118.2	3.401	------	-------
3	A1-10U90		173.21	4.045	170.5	4.572	125.46	5.86
4	A2-10U45		171.523	3.185	160	4.413	116.624	6.26
5	A1-15U90		171.445	4.11	158	4.407	135.225	2.965
6	A2-15U45		168.149	3.56	164	4.192	130.90	2.628
7	Rf2U90		163.157	2.342	134	5.29	115.98	3.255
8	B1-5INJ		----	-----	152.8	7.555	-------	---------
9	B1-10U90		140.049	5.434	130.8	5.673	119.145	8.48
10	B2-10U45		153.45	4.29	110	7.71	109.03	6.69
11	B1-15U90		140.74	6.136	136	5.389	102.40	9.385
12	B2-15U45		119.664	7.99	110	10.64	94.189	8.69

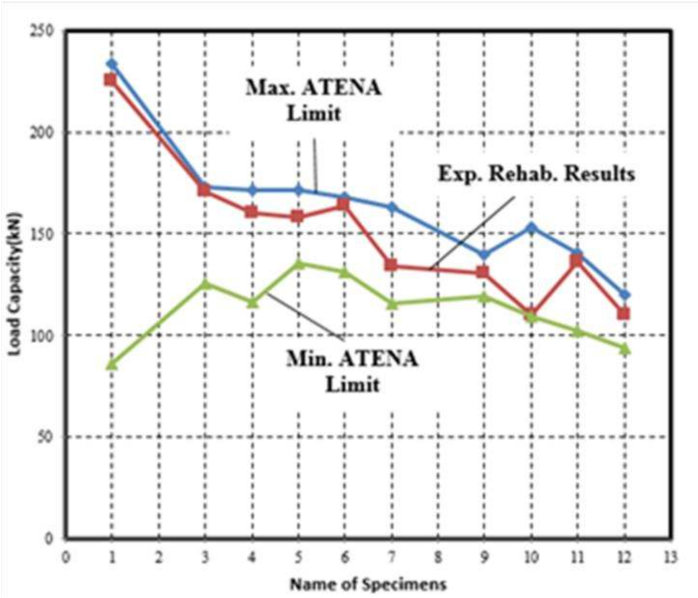

Figure 5.27 Comparison between the experimental rehabilitated results of RCHBs with the two ranges results of nonlinear FE analysis

The effect of injection material on the load capacity started from the minimum limit of nonlinear FE analysis of the damaged unrepaired cracks models to the maximum limit of nonlinear FE analysis of strengthening undamaged models, and that depends on the ratio of repairing of cracks.

Figures 5.28 and 5.29 show the curves of load-mid span deflection of all RCHBs by comparing the corresponding results of experimental study and nonlinear FE modeling. It can be noted that the stiffnesses of experimental curves are less than the stiffnesses of maximum limits of FE analysis curves for all haunched beams, which is due to the damage of haunched beams. This means that stiffness of the undamaged and strengthened RCHBs cannot be achieved even their load capacities can be approached for the rehabilitated beams. However, it is believed that this condition does not lead to undesirable results regarding seismic performance, since main function of the beams is to resist vertical loads.

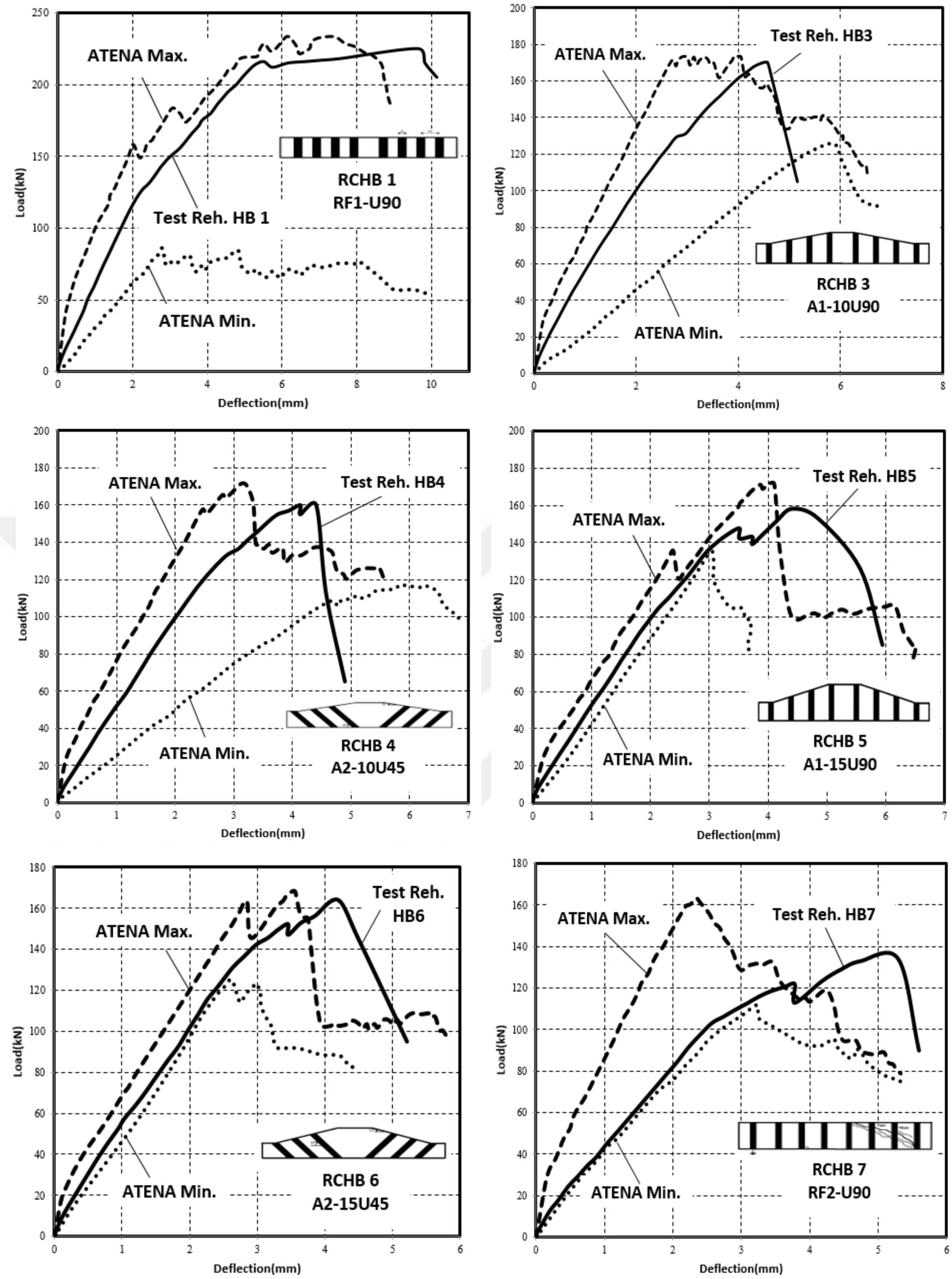

Figure 5.28 Load-deflection curves of experimental rehabilitation curves with comparing of limitations of nonlinear FE analysis curves of RCHBs from HB1, HB3 to HB7

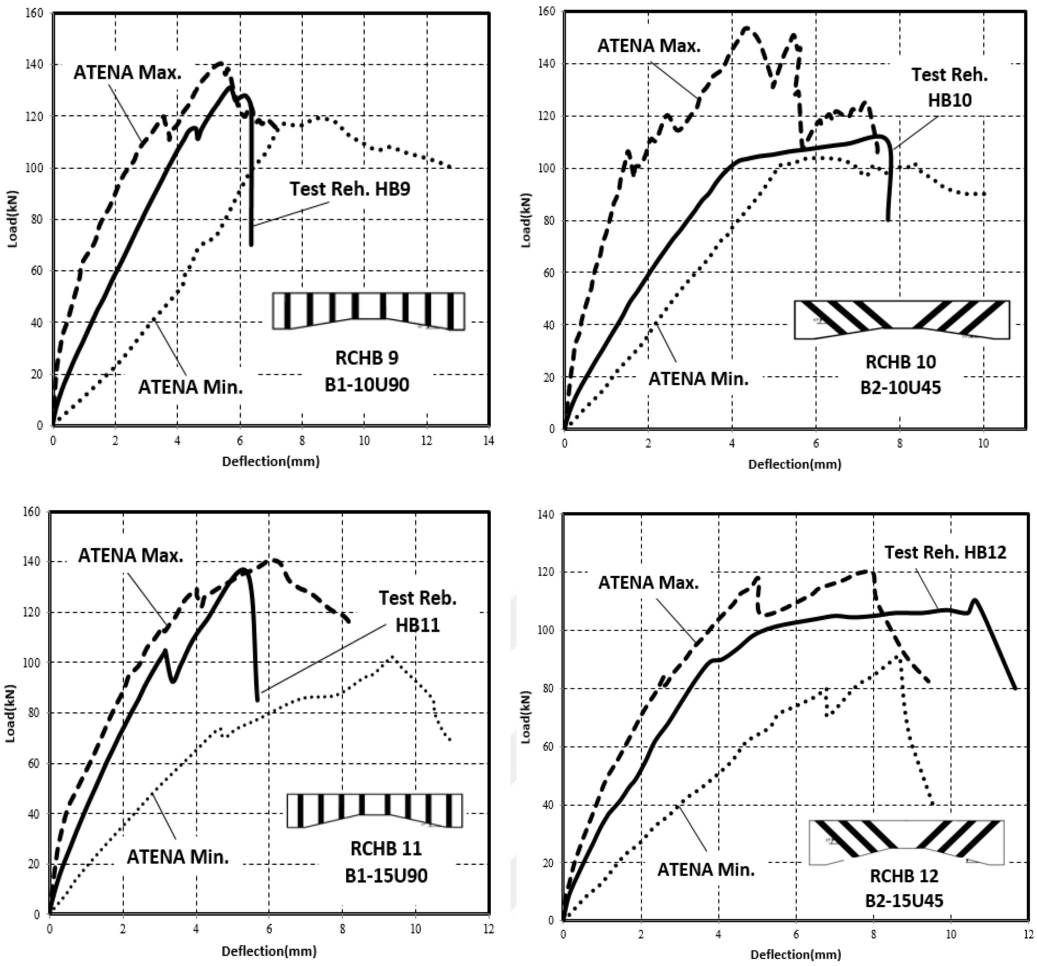

Figure 5.29 Load-deflection curves of experimental rehabilitation curves with comparing of limitations of nonlinear FE analysis curves of RCHBs from HB9 to HB12

Figure 5.30 shows the correlation between experimental results and maximum limits FE analyses regarding load capacities and corresponding deflections of the RCHBs rehabilitated with CFRP fabric. The resulting correlation coefficients (R^2) are 0.859 and 0.6466 for the load capacity and deflection, respectively. As expected higher correlation is obtained between experimental and FE analysis results for the load capacity. The less correlation regarding the deflection is due to differences in the stiffnesses between damaged-rehabilitated and undamaged-strengthened RCHBs.

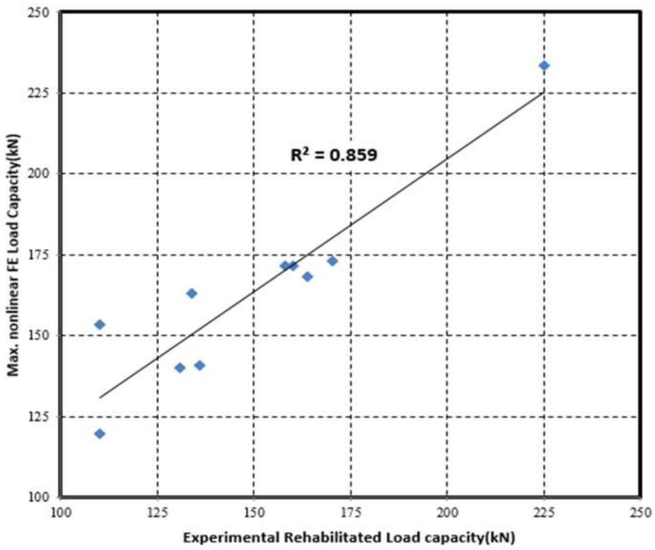

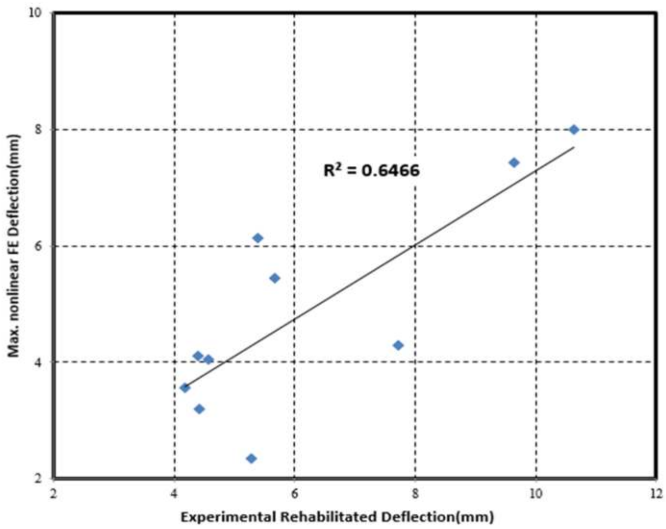

Figure 5.30 The experimental results versus the maximum Nonlinear FE analysis limits of Load and Deflection respectively

On the other hand, Table 5.12 shows the results of statistical significant t-test show that t Stat value is less than t Critical two tail value, when the load capacity results are examined. Therefore, it can be concluded that there are no significant differences between experimental and FE analysis results for the RCHBs rehabilitated with CFRP fabric.

Table 5.12 T-Test Two-Sample of Loads; Experimental rehabilitated damaged RCHBs loads and nonlinear FE analysis loads of strengthening undamaged RCHBs

	***$P_{Aft.}$ (kN)**	***[1]$P_{ATENA\ Max}$ (kN)**
Mean	149.83	163.4611
Variance	1158.4	910.6102
Observations	10	10
Pooled Variance	1034.505	
Hypothesized Mean Difference	0	
df	18	
t Stat	-0.94765	
P(T<=t) one-tail	0.177928	
t Critical one-tail	1.734064	
P(T<=t) two-tail	0.355856	
t Critical two-tail	2.100922	

*$P_{Aft.}$ (kN): The ultimate load capacity of haunched beam after rehabilitation by CFRP.
*[1]$P_{ATENA\ Max}$ (KN): The ultimate load capacity of haunched beam from results of ATENA Maximum limits.

5.4.2.1 Cracks Patterns and Mode of Failure of Experimental Rehabilitated RCHBs via FE Analysis of Strengthening RCHBs

Tables 5.13 and 5.14 show figures of cracks patterns of strengthening nonlinear FE hunched beams corresponding to the testing rehabilitated hunched beams. It can be observed from the figures, the mode of failure of rehabilitated haunched beams were a debonding failure in all specimens of haunched beams. Obviously, there is an acceptable agreement between the cracks pattern of FE analysis models and the cracks patterns of rehabilitated haunched beams. According to the simplifications and the assumptions of using Finite Element analysis, it seems unattainable to get crack patterns as precisely as the experimental test, this may be due to several reasons; the main reason is due to heterogeneous natures of concrete material and the differences of FE model (half of the real specimen) from the real experimental testing (Nghiep 2011, ALBEGMPRLI 2017). However, it can be observed from the tables 5.11, 5.13, and 5.14, that the nonlinear FE models can predict well the inception and the spread of cracks also the region of failure where the critical crack occurs, some main features of a critical crack such as inclination, direction, and crack pattern, which are proportional similar with those from the experimental tests.

Table 5.13 Cracks pattern of testing rehabilitated haunched beams via FE analysis of strengthening hunched beam cracks for HB1 untill HB7

Name of RCHB	Beam code	Experimental	Finite Element
1	Rf1U90	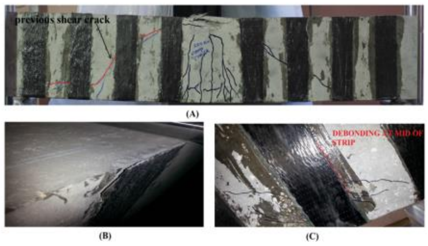	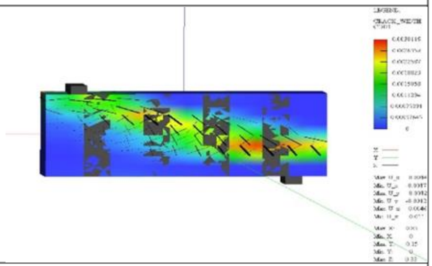
2	A1-5INJ		---
3	A1-10U90	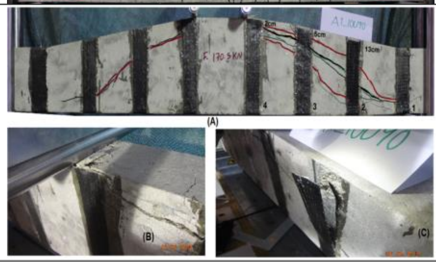	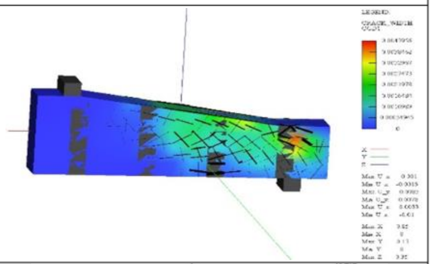
4	A2-10U45	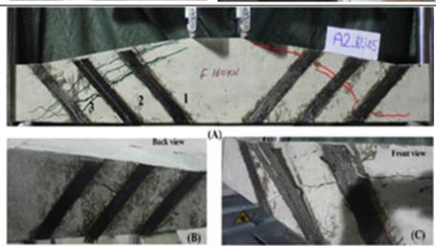	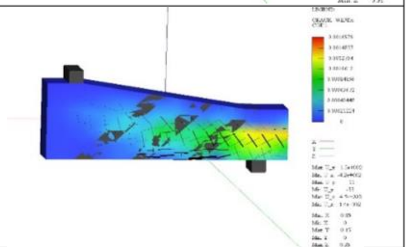
5	A1-15U90	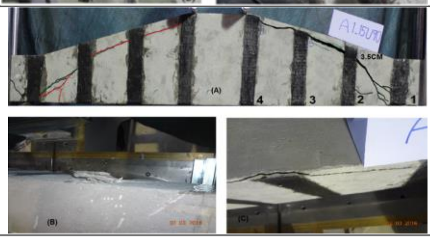	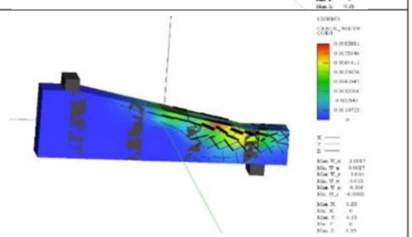
6	A2-15U45	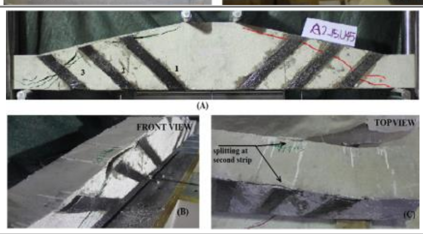	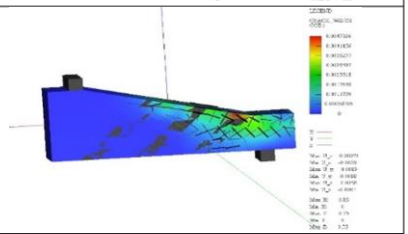
7	Rf2U90	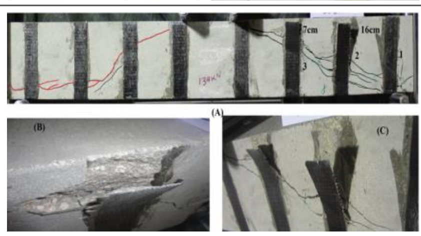	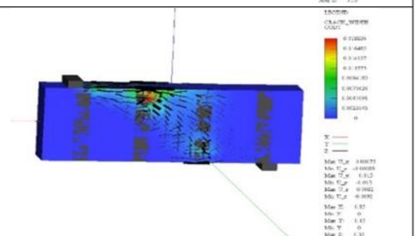

Table 5.14 Cracks pattern of testing rehabilitated haunched beams via FE analysis of strengthening hunched beam cracks for HB8 until HB12

Name of RCHB	Beam code	Experimental	Finite Element
8	B1-5INJ	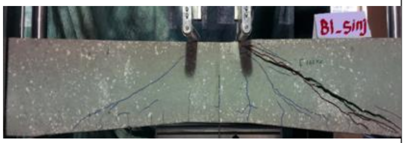	------------------------------------
9	B1-10U90	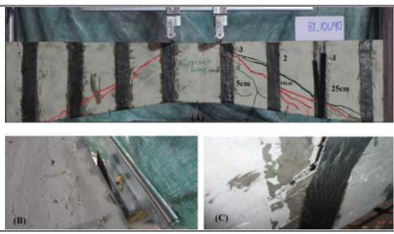	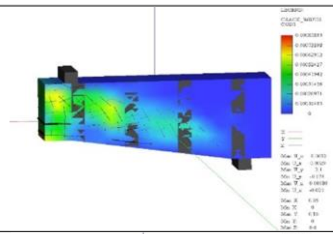
10	B2-10U45		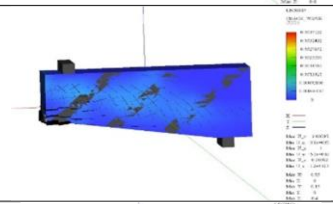
11	B1-15U90	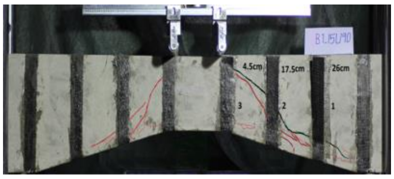	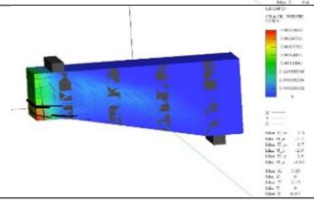
12	B2-15U45		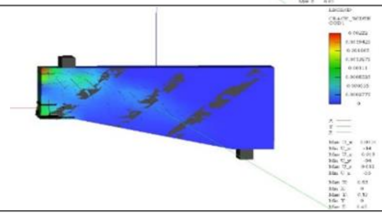

5.4.3 Production of Minimum Limits

This part presents the procedure for the achievement of the minimum limit of rehabilitated haunched beams via FE modeling analysis, which was explained in section 5.3.3 before. It can be explained again. Minimum limit represents the mechanical behavior of damaged haunched beams rehabilitated only by CFRP, that is to say without repair of cracks.

It's worth to mention that the analysis can be carried out in a displacement controlled mode in ATENA-GiD software programs. This feature makes this software capable to estimate the mechanical behavior of the haunched beams after peak load of the load-deflection curve. Judging from this feature, every point on the curve after the peak load can be represented by a specific damage level of the beam.

For example, as can be seen in Figure 5.31 that there are three points after the peak load on the load-deflection graph. Each point represents a different damage level. It can be said that the damage level of the third point is greater than the level of the second point, and the damage level of second point is greater than the level of the first point.

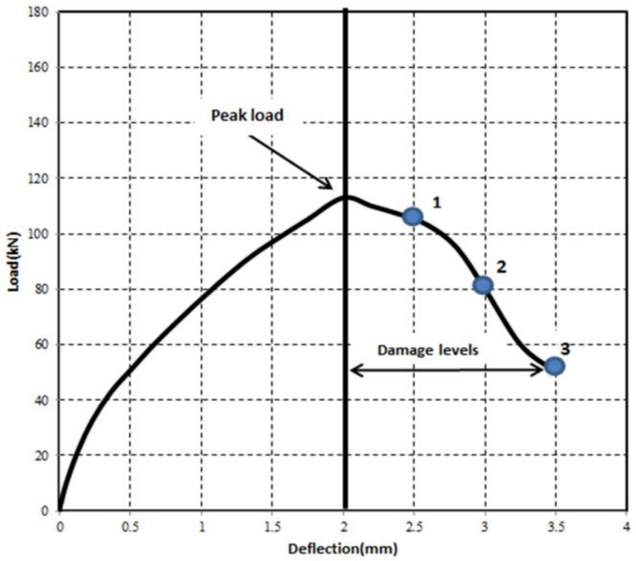

Figure 5.31 Conception of damaging levels after the peak load

Consequently, in order to obtain the minimum limit of an FE model, damage level of the experimentally tested haunched beam before the rehabilitation should be determined and transferred to the corresponding FE model. In order to obtain damage level, firstly maximum deflection value ($\Delta_{\text{Ultimate deflection}}$) is divided by the deflection corresponding to the peak load ($\Delta_{\text{def.at peak load}}$) by taking experimental load-deflection curve of RCHBs before rehabilitation into consideration. This result is multiplied by the deflection which corresponds to the maximum load of the related FE model of RCHBs before rehabilitation ($\Delta_{\text{ATENA at peak load}}$,). This operation produces the design displacement (Δ_{Design}). Thereafter, design displacement value is entered into the FE models as representative displacement value after which the rehabilitation is assumed to be started.

Table 5.15 shows all details regarding the calculation of the design deflection (Δ_{Design}). Once the deflection reaches to the design displacement, RCHBs are assumed to be damaged sufficiently so that there is no load on them. Therefore, RCHBs are unloaded to zero after this displacement which represents the real case of the damaged RCHBs before rehabilitation. Then, the application of CFRP is activated in the FE model and FE analysis of rehabilitated RCHBs are continued until failure. Finally, the load-deflection curve obtained after CFRP activation in the FE model represents the minimum limit of FE analysis of rehabilitated RCHBs with CFRP fabrics.

Table 5.15 Shows how to calculate the Δ_{Design} that use to construct the min. limit of FE analysis models

Name of RCHB	Beam code	Strengthening scheme	Exp. Result before Rehabilitation		$\frac{\Delta_{Ultimate deflection}}{\Delta_{Peakload}}$	$\Delta_{ATENA\ at}$ peak load (mm)	Δ_{Design} (mm)
			Δ peak load (mm)	Δ Ultimate deflection (mm)			
1	Rf1U90		2.27	2.27	1.00	3.32	3.32
2	A1-5INJ		---	---	---	---	---
3	A1-10U90		2.51	3.053	1.22	5.81	7.07
4	A2-10U45		2.72	2.868	1.05	6.022	6.35
5	A1-15U90		2.535	2.535	1.00	2.1574	2.16
6	A2-15U45		2.48	2.737	1.10	1.982	2.19
7	Rf2U90		2.618	2.857	1.09	2.564	2.80
8	B1-5INJ		----	---	-----	----	---
9	B1-10U90		6.219	6.219	1.00	6.31	6.31
10	B2-10U45		7.401	7.45	1.01	6.554	6.60
11	B1-15U90	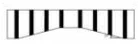	5.328	5.328	1.00	7.45	7.45
12	B2-15U45		7.52	8.362	1.11	6.03	6.71

5.5 Conclusions

5.5.1 Conclusions of Rehabilitatiom of RCHBs By Basalt Fiber Fabric (BFF)

This study has pointed out the need to improve the knowledge of the load-deflection behavior of damaged RCHBs after being rehabilitated by Basalt Fiber Fabric. Two programs were performed; the first one, the experimental program includes two groups: the first group has six samples with a different shape designed to fail in shear, and the second group has six samples with a different shape designed to fail in flexural. Both of them were injected by low viscosity epoxy to repair the cracks before being wrapped by Basalt Fabric. The second program, the nonlinear FE analysis program has been performed by ATENA-GiD programs to approach the verifying the load-deflection behavior of damaged RCHBs after being rehabilitated by Basalt Fiber Fabric and to see the effect of injected material in the cracks on the load-deflection behavior. To figure out the conception of rehabilitated damaged RCHBs, two methods of simulation of nonlinear FE analysis were performed, the first simulation models were performed on strengthening undamaged RCHBs by Basalt Fabric, the second simulation models were performed on strengthening damaged RCHBs by Basalt Fabric without injection material in the cracks.

From the experimental test and nonlinear FE analysis results presented, the following conclusion can be drawn:

- Basalt Fiber Fabric material appeared to perform well to rehabilitate the shear and flexural strength. After being damaged; in which the rehabilitated of RCHBs increase the shear and flexural capacities as compared to the original values.
- For the first group, the increase of the ultimate shear load of rehabilitated haunched beams varied with the change of the haunch's inclination. However, the range of increasing the ultimate shear load started from 1.25% of HB6 to 30% of HB3 comparing to HB1 46% (prismatic beam).
- The most significant and interesting outcome of the crack pattern of group one was when the depth of haunched beams decreases at support, the major crack will propagate upward leading to a decrease in the requirement of the distance of FRP strips above the major crack (requirement of less distance to ensure the bonding between FRP and the surface of the sample). Therefore, the bond of

strips on the surface of the sample will decrease, leading to a reduction in ultimate shear capacity when compared with prismatic beams. However, the failure of Basalt Fiber Fabric was a debonding failure for both groups. While the position of debonding failure of Basalt Fiber Fabric in the second group depended on the shape of the haunched beam.

- In the second group, the ultimate flexural loads increased after being rehabilitated by Basalt Fiber Fabric. However, the range of increasing the ultimate flexural load started from 2% of HB11 to 23% of HB9 comparing to HB7 12% (prismatic beam).
- HB11 and HB12 had a weak behavior to bear the flexural strength before and after the rehabilitation.
- In general, the rehabilitation by using Basalt Fabric in addition to repair of cracks will return the load capacity value (shear or flexural) at least to the original load capacity.
- The nonlinear FE models by ATENA-GiD programs predicted quite precisely the behavior of load-deflection of the all tested pre-rehabilitated haunched with correlation coefficient R^2 = 0.9689 between experimental load capacity and nonlinear FE load capacity, the correlation coefficient of experimental deflection and nonlinear FE deflection R^2 = 0.9652.
- All values of load capacity of experimental haunched beams after being rehabilitated by Basalt Fabric located between the values of strengthening nonlinear FE analysis of undamaged haunched beams (max. limit) and the values of strengthening nonlinear FE analysis of damaged haunched beams (min. limit) without injection material in the cracks. And the experimental rehabilitated haunched beams loads suffered a small deviation from the max. limit with correlation coefficient R^2 = 0.9616, and more deviation between the experimental rehabilitated deflection and the max. limit deflection with correlation coefficient R^2 = 0.8231.
- In general, there is an acceptable agreement between the cracks pattern of nonlinear FE analysis and the cracks pattern of an experimental test of haunched beams which is consider the second confirmation of accuracy of the proposed model of FE analysis by ATENA-GiD.
- The nonlinear FE analysis models of rehabilitated haunched beams will help

the structural engineers to figure out and predict the behavior of rehabilitated damaged haunched beams with the effect of injection material in the cracks.

5.5.2 Conclusions of Rehabilitation of RCHBs by CFRP

The present study has pointed out the need to improve the knowledge about the mechanical behavior of damaged RCHBs after being rehabilitated by unidirectional Carbon Fiber Reinforced Polymer strips (CFRP). This study consists of two parts. The first part is a comprehensive experimental study carried out on ten RCHBs being designed to fail in shear with two different types (A and B) and three different angles of inclination (5^o, 10° and 15°). Besides, there were two prismatic beams which were repaired by epoxy injection and strengthened with vertical CFRP strips. All RCHBs were repaired by epoxy injection and strengthened with CFRP strips in two configurations; vertical angle (90°) and the inclined angle (45°) with respect to the x-axis of beams. Moreover, two of RCHBs, whose angle of inclination is 5o, were rehabilitated by only crack repair epoxy in order to investigate the effect of crack repair before strengthening with CFRP strips.

The second part of the study is the nonlinear FE modeling of rehabilitated RCHBs. A new FE methodology is proposed to form a zone that exhibits all possible load capacities of rehabilitated RCHBs via FE analyses. This zone consists of two limits; maximum and minimum limits which are obtained by FE analyses. FE modeling of the haunched beams which are undamaged and strengthened with CFRP strips represents the maximum limit, while FE modeling of the damaged beams rehabilitated by only CFRP strips without crack repair epoxy represents the minimum limit.

From the experimental test and nonlinear FE analysis results, the following conclusions can be drawn:

- Carbon Fiber Reinforced Polymer (CFRP) fabrics appeared to perform very well regarding the rehabilitation of damaged RCHBs.
- In general, before and after the rehabilitation; RCHBs belonging to type B showed a worse mechanical behavior as compared to type A.
- The most important point about crack pattern is that when the depth of haunched beams at the support decreases, the major crack propagates upward.

- The most significant and interesting outcomes of rehabilitation of RCHBs which were repaired only by epoxy without CFRP strips is that the ultimate shear capacities were found to be higher than the original values.
- Ultimate load capacities recovered after being rehabilitated by CFRP changes between 131% and 149% of the corresponding original capacity of the beams type A. However, the recovering amount is between 115% and 131% of the original capacity for the beams type B. Moreover, the recovered capacities of tested prismatic beams are 141% and 210% of the original capacities after being rehabilitated by CFRP fabrics.
- Placement of CFRP strips in vertical position is more efficient than the placement in inclined position regarding the ultima load capacity. Moreover, failure mode of all RCHBs rehabilitated by CFRP strips was debonding of the strips.
- The nonlinear FE models which depend on the fracture-plastic model, predicted the mechanical outputs of undamaged and/or rehabilitated RCHBs including load capacity, load-deflection curve and crack pattern sufficiently well. Therefore, it can be said that decisions and evaluations regarding design of undamaged and/or rehabilitated RCHBs can be made by taking FE analysis results into consideration.
- All load capacity values of RCHBs which were experimentally rehabilitated with CFRP strips located between the resulted minimum and maximum limits of FE analyses. Moreover, load capacities of the rehabilitated beams exhibit good correlation with the capacity results of maximum limit (R^2 = 0.859). This result emphasizes the importance necessity of repair of cracks before strengthening with CFRP strips.
- The interval of all possible load capacities of rehabilitated RCHBs obtained by nonlinear FE analysis models will help the structural engineers to figure out and predict the mechanical behavior of rehabilitated and/or strengthened haunched beams beside the effect of crack repair epoxy on the quality of rehabilitation.

CHAPTER 6

Parametric Study of Steel Fibers Reinforced Concrete Haunched Beams (SF RCHBs) via FE Modeling

6.1 Description Works and Objective

The work objective is to clarify the effect of steel fiber on the behavior of RCHBs without shear reinforcement via Finite Element based analyses and parametric analysis. Parameters including main reinforcement area, compressive strength, inclination angle and steel fiber ratio are taken into account to conclude comprehensive results. The modeling and analysis were carried out by FE software package called Atena-GiD 3D. The program of this study consists of two-part; part one; nine results of experimental SF RCHBs samples which had been tested by (AL-DARRAJI 2018) before, were used to identifying the accuracy of FE models. Part two consists of 81 FE proposed models which were described this chapter below.

6.2 Description of Experimental Data

The experimental haunched beams, which had been tested by (AL-DARRAJI 2018) before, were used in this study to verify the models of finite element analysis. There are 9 samples of SF RCHBs were designed to fail in shear. All SF RCHBs have the same length and width of 1200mm and 120mm respectively, while the height is variable. Figures 6.1-6.3 show the details of geometry and steel arrangement of all samples which were tested before.

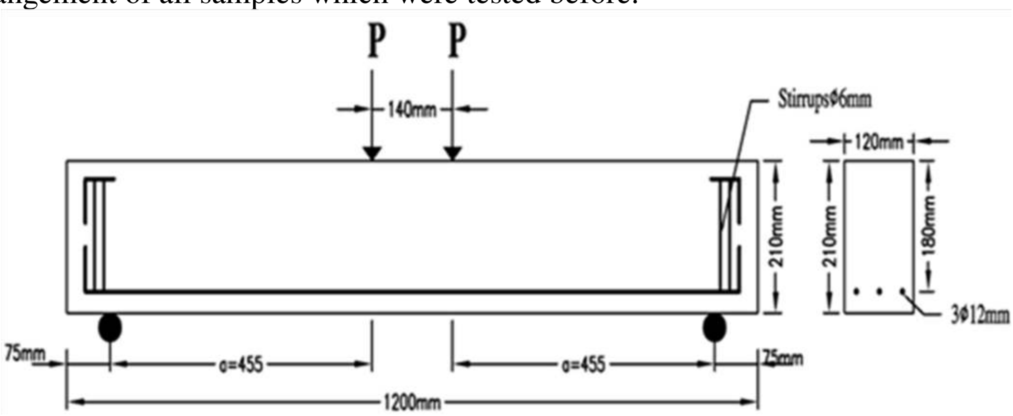

Figure 6.1 Geometry of Prismatic Beams

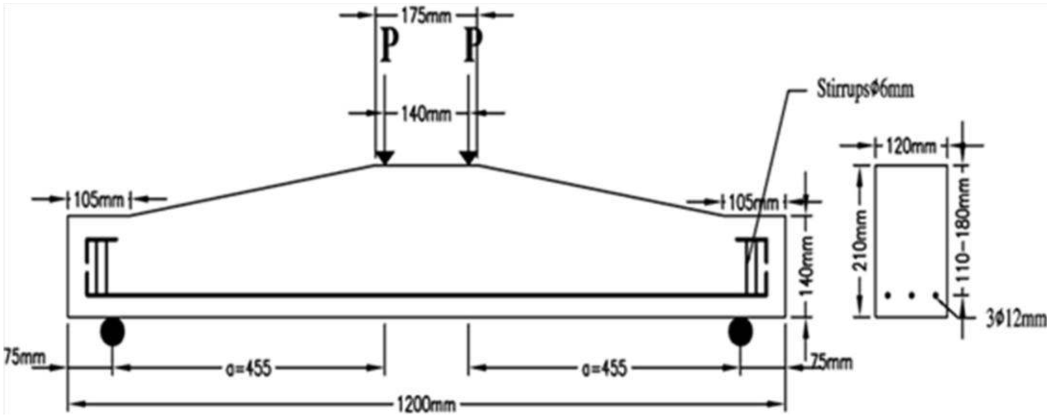

Figure 6.2 Geometry of Haunched Beams (Angle 10°)

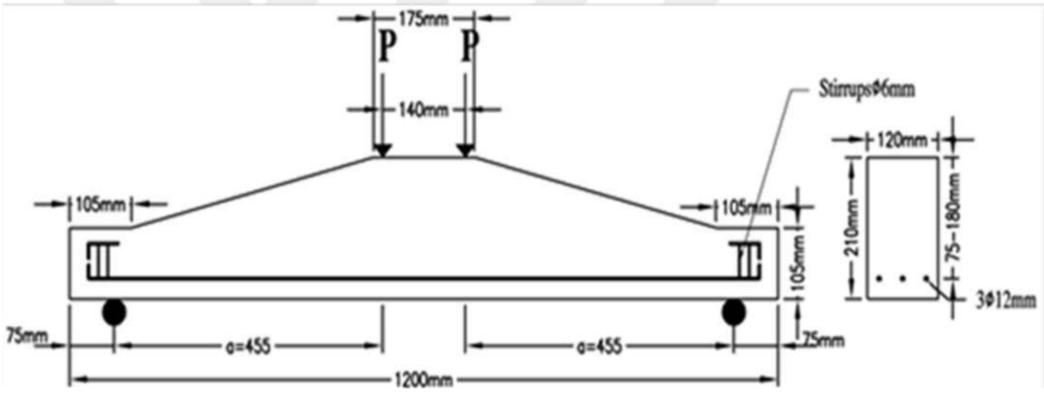

Figure 6.3 Geometry of Haunched Beams (Angle 15°)

Table 6.1 shows the experimental properties of all tested steel fiber haunched beams. The designation of RCHBs contains three terms. The first term represents the sample number (B No.), the second term represents the shape of beam: prismatic beams (P) or haunched beam (H) with an angle degree (H10 or H15) of haunched beams, the third term represents the steel fiber ratio which is used in the mix of sample. Table 6.2 shows the mechanical properties of steel fibers which were used in the mix of samples.

Table 6.1 Experimental properties of all Steel fiber RCHBs

Beam Code	α°	h_f (mm)	h_S (mm)	Steel Reinfor-cement	Area of Steel A_s (mm^2)	Steel Fiber Ratio (V_f) %
B1-P-0	0	210	210	3ϕ12	340	0
B2-H10-0	9.74	210	140	3ϕ12	340	0.5
B3-H15-0	14.45	210	105	3ϕ12	340	1
B4-P-0.5	0	210	210	3ϕ12	340	0
B5-H10-0.5	9.74	210	140	3ϕ12	340	0.5
B6-H15-0.5	14.45	210	105	3ϕ12	340	1
B7-P-1	0	210	210	3ϕ12	340	0
B8-H10-1	9.74	210	140	3ϕ12	340	0.5
B9-H15-1	14.45	210	105	3ϕ12	340	1

α°: Inclination angle of hanched beam, h_f: Depth of beam at the Middle, h_s: Depth of beam at the Supports

Table 6.2 Mechanical properties of steel fibers

Fiber Type	DRAMIX 3D 45 /35 BL
Length (I)	35mm
Diameter (d)	0.75mm
Aspect Ratio (I / d)	45
Tensil Strength	1,225N/mm^2
Young's Modulus	± 210.000 N/mm^2
Fiber Network	7.814 fibres/kg

6.3 Nonlinear Finite Element Analysis of SF RCHBs Description

The nonlinear finite element models consist of 81 SF RCHBs models with three groups in the same shape and dimensions of experimental samples, Analysis of them were carried out via ATENA-GiD software. GiD program is used for data preparation and mesh generation of models and ATENA program is used for the analysis, all details of related to ATENA-GiD software were mentioned before.

Due to the symmetry of RCHBs in the longitudinal direction, only half of them was modeled to reduce analysis time. All boundary conditions that surrounding the test were assumed to simulate the reality of the test.

The nonlinear finite element modeling consisted of three groups, for each group has 27 samples with four variables which are main steel ratio (A_s), compressive strength

(f_c), steel fiber ratio (Vf%), and shape angle of haunched beams (α°). Table 6.3 shows all variables that entered into the modeling of each group. The difference between each group was the number of steel bars of main reinforcement which are $2\phi12$=226 mm^2 for first group, $3\phi12$=340 mm^2 for second group, and $2\phi18$=509 mm^2 for the third group. It can be seen that the designation of finite element models is the same with the designation of experimental beams which is described before, except the fourth term representing the compressive strength.

Table 6.3 Variables entered in the modelling of each group of FE analysis of SF RCHBs

f_c (MPa)	Vf %	$\alpha = 0.0$	$\alpha = 10.0$	$\alpha = 15.0$
20	0.0	B1-P-0-20	B10-H10-0-20	B19-H15-0-20
	0.5	B2-P-0.5-20	B11-H10-0.5-20	B20-H15-0.5-20
	1.0	B3-P-1-20	B12-H10-1.0-20	B21-H15-1.0-20
40	0.0	B4-P-0-40	B13-H10-0.0-40	B22-H15-0-40
	0.5	B5-P-0.5-40	B14-H10-0.5-40	B23-H15-0.5-40
	1.0	B6-P-1.0-40	B15-H10-1.0-40	B24-H15-1.0-40
60	0.0	B7-P-0-60	B16-H10-0-60	B25-H15-0-60
	0.5	B8-P-0.5-60	B17-H10-0.5-60	B26-H15-0.5-60
	1.0	B9-1.0-60	B18-H10-1.0-60	B27-H15-1.0-60

6.3.1 Constitutive models of finite element analysis

The fracture-plastic model is used to simulate concrete cracking, crushing under high confinement, and crack closure due to crushing in other material directions. All details of constitutive concrete were mentioned before. The CCCombinedMaterial model was used for constitutive steel fiber reinforcement in concrete. Elastic-perfectly plastic (bilinear) model was used for steel reinforcement modeling as shown before. The initial elastic part has the elastic modulus of steel Es. The second line represents the plasticity of the steel with hardening and its slope is the hardening modulus $E_{sh.}$. In case of perfect plasticity (E_{sh} =0) limit strain represents limited ductility of steel. The 3D solid linear and quadratic Hexahedron (CCIsoBrick<xxxxxxxx>) elements with 8 nodes are used for modelling the concrete. Besides the Truss 3D Linear and quadratic line elements with 3 nodes (CCIsoTruss<xxx>) are utilized to model the steel reinforcement bars. The 3D solid linear and quadratic Tetrahedral 4-nodes (CCIsoTetra<xxxx>) are used to model the loading plate and supports (Janda *et al.* 2016, Cervenka *et al.* 2017). Figure 6.4 shows all geometries of finite elements that used in this study.

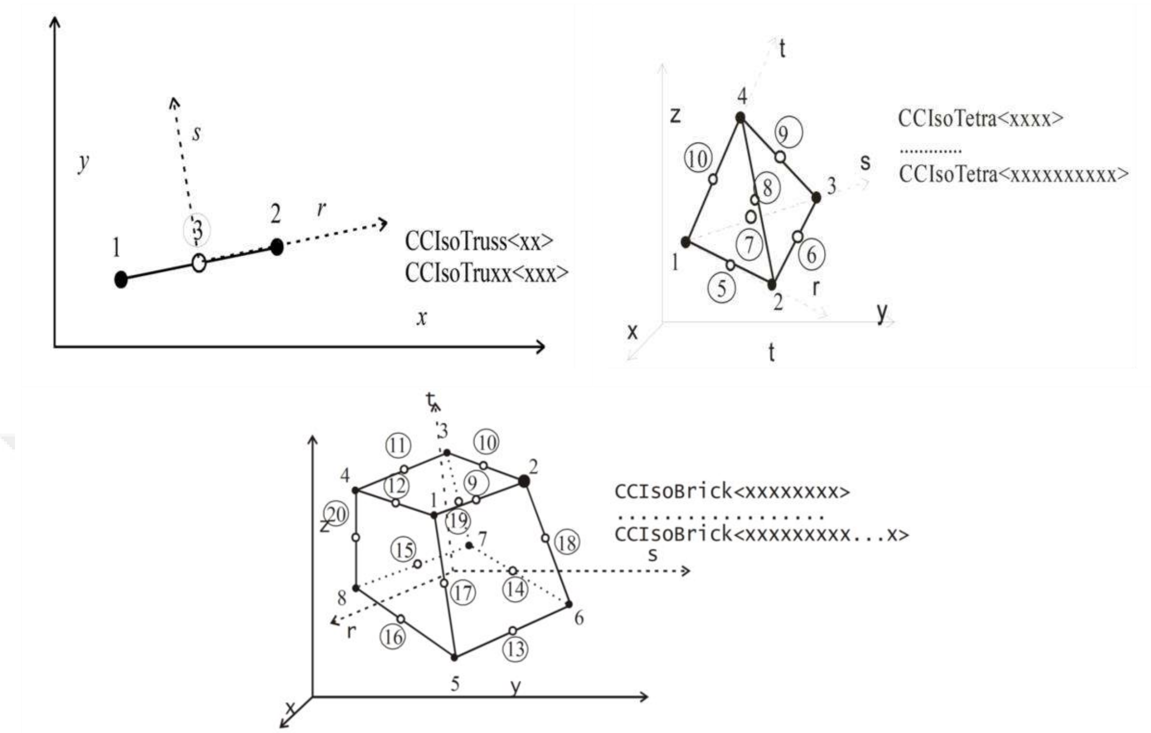

Figure 6.4 Geometries of finite elements that used in the analysis (Cervenka *et al.* 2017)

6.4 Results and Discussion of SF RCHBs

The results of experimental work and FE modeling are shown below:

6.4.1 Experimental via FE analysis of SF RCHBs

Maximum load capacities at mid-span of SF RCHBs resulted from the experimental study and finite element analyses are given in Table 6.4. According to Table 6.4, it can be concluded that there is a good agreement between experimental results and FE analyses with respect to the load capacity and mode of failure of all samples. Figure 6.5 shows the correlation between experimental and nonlinear FE results of load capacity. As shown in the figure, the correlation coefficient between FE analysis and experimental result regarding the load capacity is 0.9793 which also proves the accuracy of the FE models. Moreover, Table 6.5 shows comparison between the results of experimental SF RCHBs and nonlinear finite element analysis results with respect to the load-deflection relationship, cracks pattern and failure mode. It can be also observed from these graphs that there is a good fit between experimental and FE analysis results regarding load-deflection relationships.

Table 6.4 Ultimate load capacity of experimental and nonlinear FE analysis results of SF RCHBs

Beam Code	Experimental Results				Atena Results	
	f_c (MPa)	f_{ct} (MPa)	Max. Load (kN)	Failure Mode	Max. Load (kN)	Failure Mode
B1-P-0	47.96	3.82	54.34	S	59.62	S
B2-H10-0	46.9	3.97	57.5	S	60.6	S
B3-H15-0	44.50	3.77	49.56	S	64.60	S
B4-P-0.5	45.44	4.45	104.2	S	104.11	S
B5-H10-0.5	39.50	4.53	109.6	S	120.83	S
B6-H15-0.5	39.0	4.49	103.6	S	117.92	S
B7-P-1	39.60	5.05	134.3	F	143.13	F
B8-H10-1	40.0	5.10	140.5	F	144.72	F
B9-H15-1	40.5	5.03	138.3	F	142.20	F

*S: Shear failure. *F:Flexural failure.

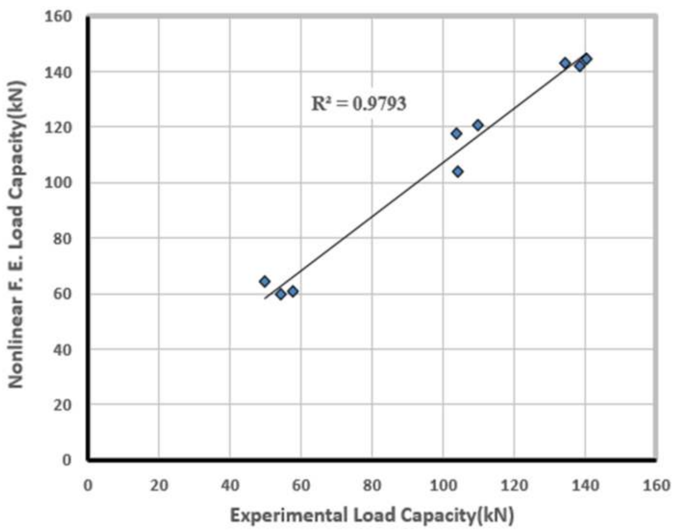

Figure 6.5 The experimental results versus the nonlinear FE analysis results of load capacities

Obviously, it is important to note that there is an acceptable agreement between the crack patterns of FE analysis models and the crack patterns of SF RCHBs. Due to the simplifications and the assumptions of using finite element analysis, it seems unattainable to get cracking patterns as precise as the experimental test. These small differences may be due to several reasons. The main reasons are due to heterogeneous natures of concrete material and the differences of FE model (half of the real specimen) from the real experimental testing. However, it can be observed from the Table 6.5 that the nonlinear FE models can be well predicted the inception and the spread of cracks besides, the region of failure in where the critical crack occurs, some main features of a critical crack such as inclination, direction, and crack pattern, which are proportionally similar to those from the experimental tests (Nghiep 2011, ALBEGMPRLI 2017).

Table 6.5 Load-deflection relationship of experimental samples vie FE models with the failure mode and failure type

Name	Load-deflection Relationship	Mode of failure		Failure Type
B1-P-0	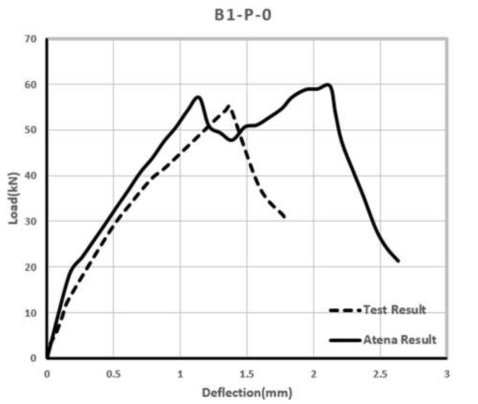	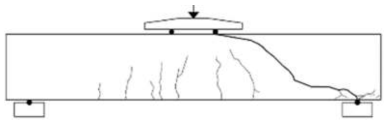	Test Result	Shear Failure
		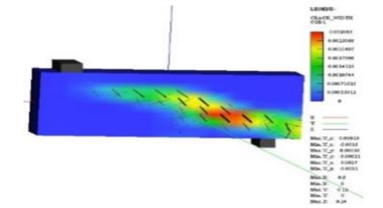	Atena Result	Shear Failure
B2-H10-0	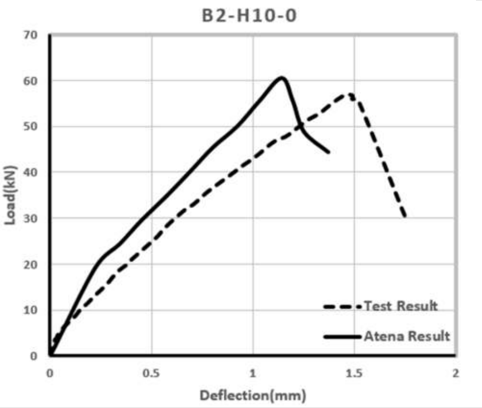	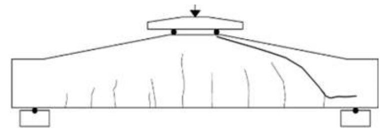	Test Result	Shear Failure
		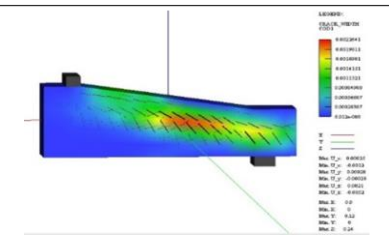	Atena Result	Shear Failure
B3-H15-0	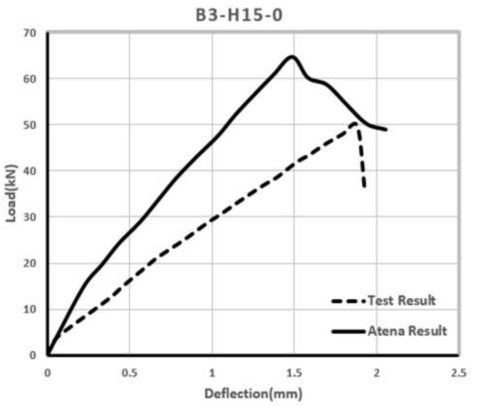	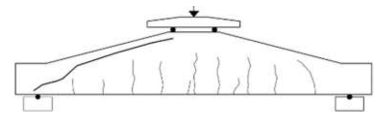	Test Result	Shear Failure
		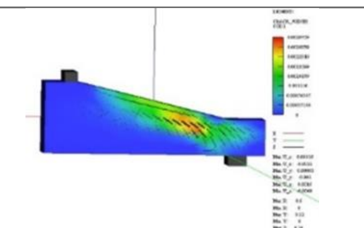	Atena Result	Shear Failure

<table>
<tr><td rowspan="2">B4-P-0.5</td><td rowspan="2">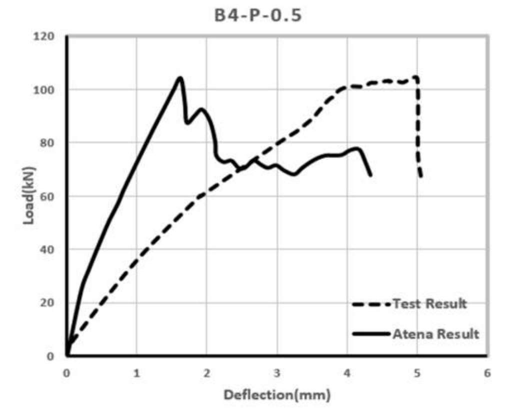
</td><td>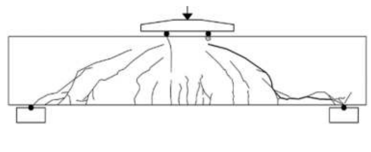</td><td>Test Result</td><td>Shear Failure</td></tr>
<tr><td>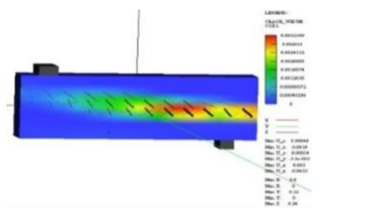</td><td>Atena Result</td><td>Shear Failure</td></tr>
<tr><td rowspan="2">B5-H10-0.5</td><td rowspan="2">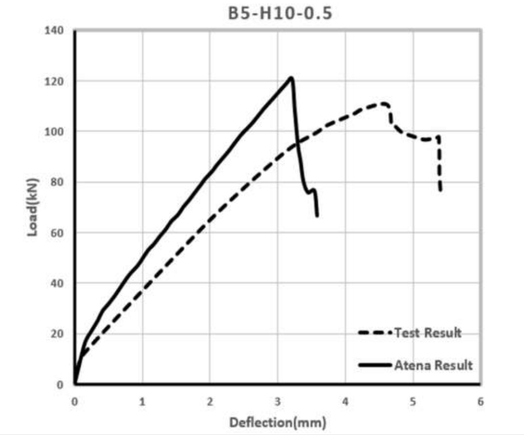
</td><td>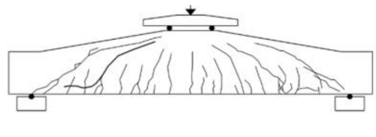</td><td>Test Result</td><td>Shear Failure</td></tr>
<tr><td>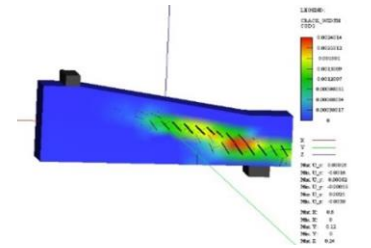</td><td>Atena Result</td><td>Shear Failure</td></tr>
<tr><td rowspan="2">B6-H15-0.5</td><td rowspan="2">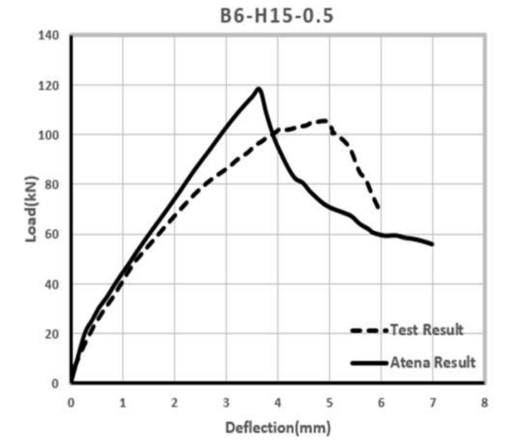
</td><td>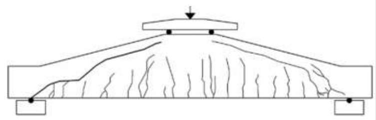</td><td>Test Result</td><td>Shear Failure</td></tr>
<tr><td>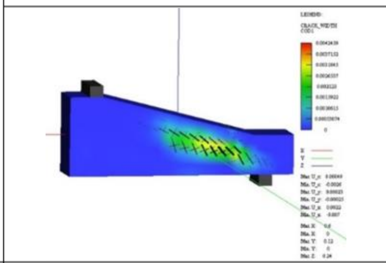</td><td>Atena Result</td><td>Shear Failure</td></tr>
<tr><td rowspan="2">B7-P- 1</td><td rowspan="2">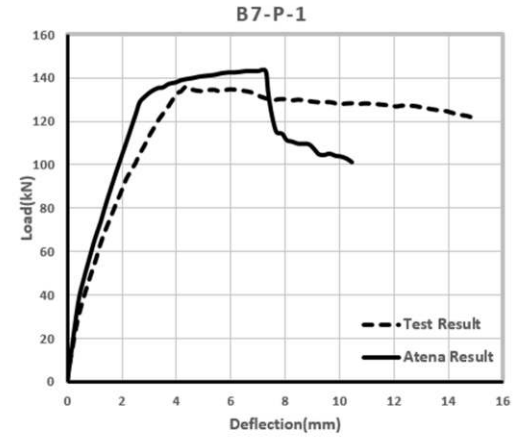
</td><td>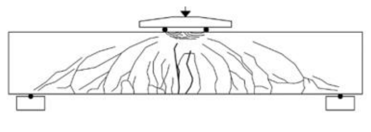</td><td>Test Result</td><td>Flexural Failure</td></tr>
<tr><td>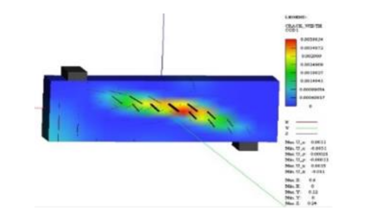</td><td>Atena Result</td><td>Flexural Failure</td></tr>
</table>

B8-H10-1	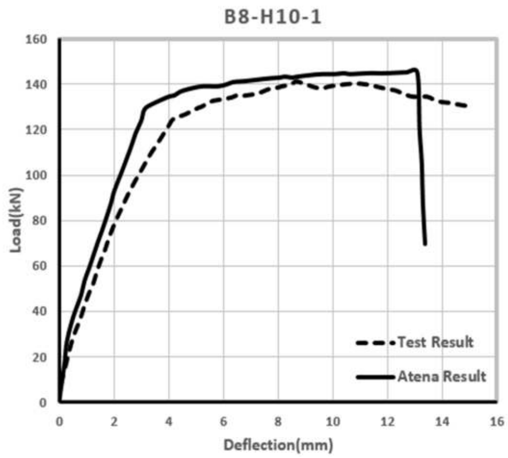	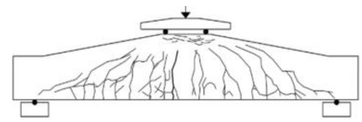	Test Result	Flexural Failure
		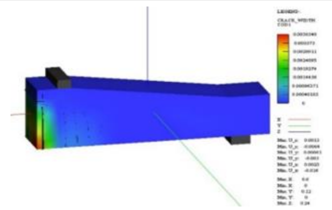	Atena Result	Flexural Failure
B9-H15-1	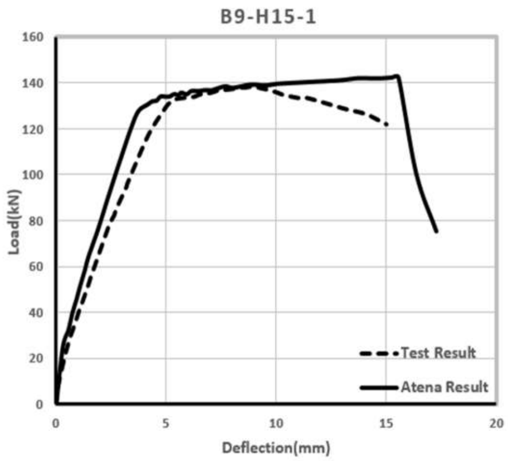	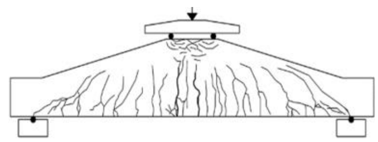	Test Result	Flexural Failure
		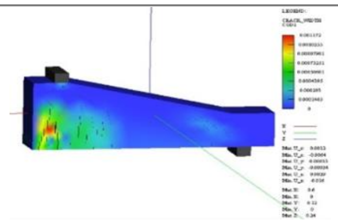	Atena Result	Flexural Failure

6.4.2 Finite Element Results of SF RCHBs

Tables 6.6-6.8 show the results of nonlinear finite element analysis of specific proposed groups of steel fiber RCHBs which are described before. It can be seen in Table 6.9 load-deflection relationship, cracks pattern and failure mode of all specific supposing groups of steel fiber RCHBs.

Table 6.6 Nonlinear finite element analysis of ultimate load capacity (kN) of first group for main reinforcement $2\phi12 = 226$ mm^2 of SF RCHBs

f_c MPa	Vf%	$\alpha = 0.0$	$\alpha = 10.0$	$\alpha = 15.0$
20	0.0	B1=57.34	B10=71.2	B19=73.58
	0.5	B2=81.52	B11=86.36	B20=81.20
	1.0	B3=93.16	B12=90.42	B21=86.84
40	0.0	B4=75.66	B13=90.48	B22=91.74
	0.5	B5=89.36	B14=97.72	B23=98.62
	1.0	B6=105.5	B15=103.02	B24=101.38
60	0.0	B7=89.28	B16=97.76	B25=106.96
	0.5	B8=87.66	B17=99.66	B26=101.36
	1.0	B9=106.26	B18=104.14	B27=103.8

Table 6.7 Nonlinear finite element analysis ultimate load capacity (kN) of second group for main reinforcement $3\phi12 = 339$ mm^2 of SF RCHBs

f_c MPa	Vf%	$\alpha = 0.0$	$\alpha = 10.0$	$\alpha = 15.0$
20	0.0	B1=57.36	B10=72.92	B19=75.12
	0.5	B2=85.85	B11=93.4	B20=87.4
	1.0	B3=105.75	B12=100.104	B21=94.6
40	0.0	B4=71.44	B13=93.8	B22=95.96
	0.5	B5=97.3	B14=119.30	B23=115.94
	1.0	B6=142.54	B15=145.72	B24=141.34
60	0.0	B7=84.18	B16=100.36	B25=106.64
	0.5	B8=105.8	B17=121.45	B26=121.34
	1.0	B9=155.44	B18=150.25	B27=149.056

Table 6.8 Nonlinear finite element analysis of ultimate load capacity (kN) of third group for main reinforcement $2\phi18 = 509$ mm^2 of SF RCHBs

f_c MPa	Vf%	$\alpha = 0.0$	$\alpha = 10.0$	$\alpha = 15.0$
20	0.0	B1=60.72	B10=73.8	B19=79.54
	0.5	B2=89.36	B11=97.36	B20=93.46
	1.0	B3=109.5	B12=106.54	B21=100.74
40	0.0	B4=70.66	B13=93.3	B22=101.88
	0.5	B5=101.4	B14=122.80	B23=122.94
	1.0	B6=153.178	B15=165.86	B24=167.14
60	0.0	B7=88.14	B16=102.94	B25=114.64
	0.5	B8=100.74	B17=125.48	B26=126.60
	1.0	B9=171.0	B18=192.32	B27=193.54

Table 6.9 Effect of different quantity of steel reinforcement on Load-deflection relationship of proposed models of SF RCHBs with all relevant failure mode and failure type

Name	Load-deflection Relationship	Mode and Type of Failure		
		2ϕ 12	3ϕ 12	2ϕ 18
B1-P-0-20	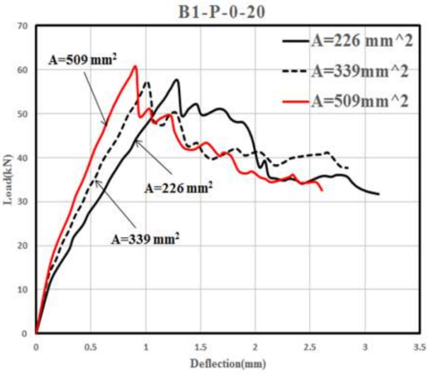	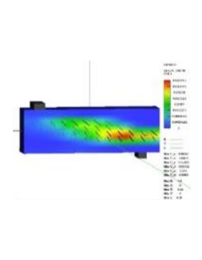	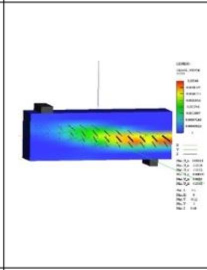	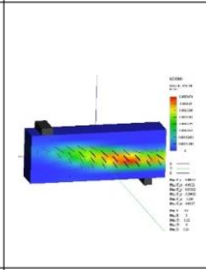
		Shear Failure	Shear Failure	Shear Failure
B2-P-0.5-20	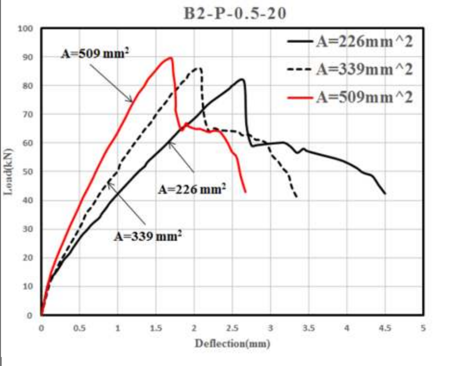	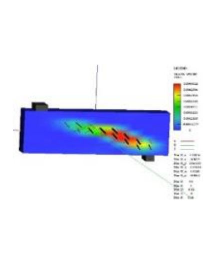	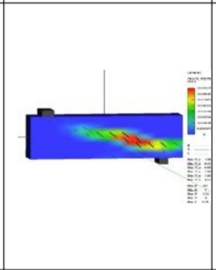	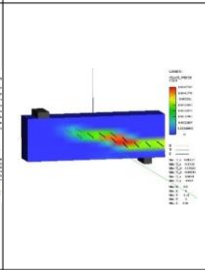
		Shear Failure	Shear Failure	Shear Failure
B3-P-1.0-20	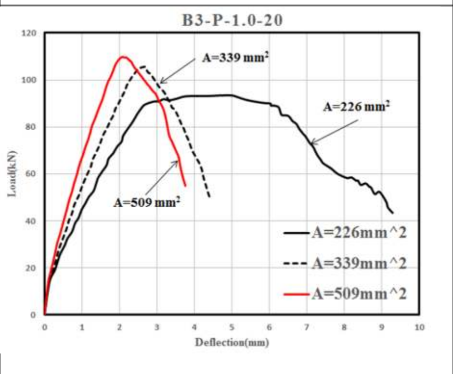	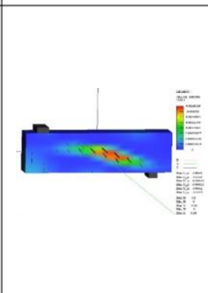	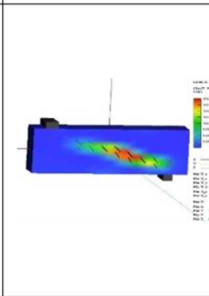	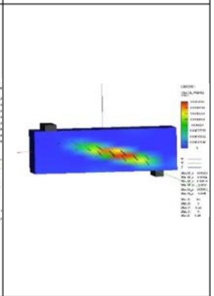
		Shear Failure	Shear Failure	Shear Failure
B4-P-0-40	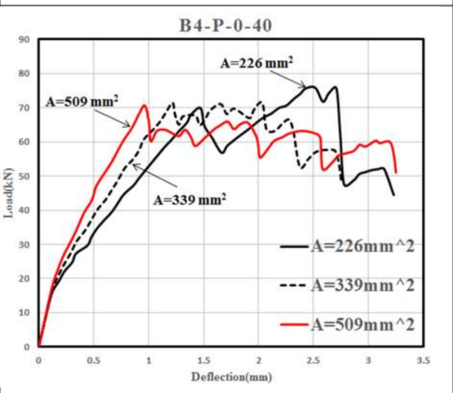	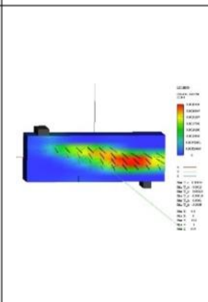	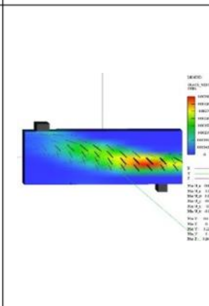	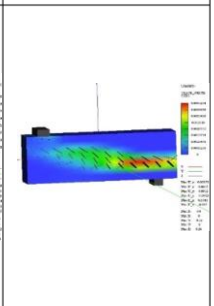
		Shear Failure	Shear Failure	Shear Failure

<table>
<tr><th rowspan="2">Name</th><th rowspan="2">Load-deflection Relationship</th><th colspan="3">Mode and Type of Failure</th></tr>
<tr><th>2 ϕ 12</th><th>3 ϕ 12</th><th>2 ϕ 18</th></tr>
<tr><td rowspan="2">B5-P-0.5-40</td><td rowspan="2">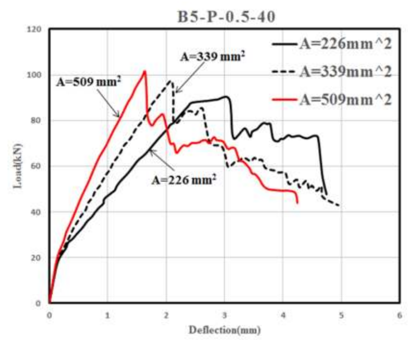</td><td>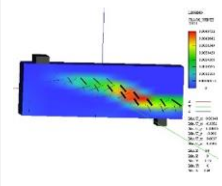</td><td>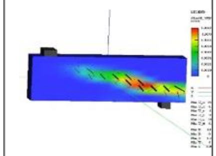</td><td>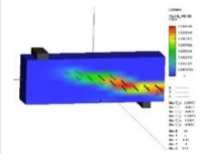</td></tr>
<tr><td>Shear Failure</td><td>Shear Failure</td><td>Shear Failure</td></tr>
<tr><td rowspan="2">B6-P-1.0-40</td><td rowspan="2">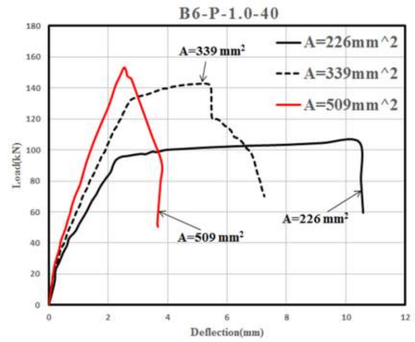</td><td>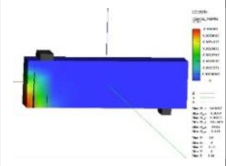</td><td>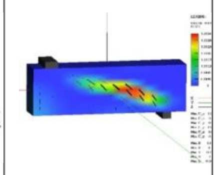</td><td></td></tr>
<tr><td>Flexural Failure</td><td>Shear Failure</td><td>Shear Failure</td></tr>
<tr><td rowspan="2">B7-P-0-60</td><td rowspan="2">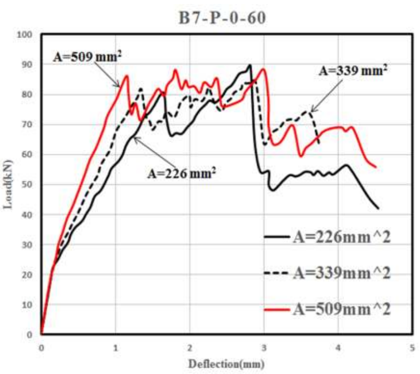</td><td>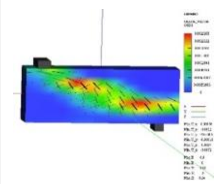</td><td>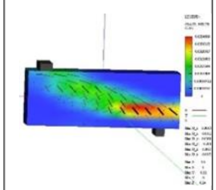</td><td>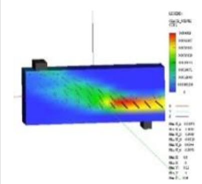</td></tr>
<tr><td>Shear Failure</td><td>Shear Failure</td><td>Shear Failure</td></tr>
<tr><td rowspan="2">B8-P-0.5-60</td><td rowspan="2">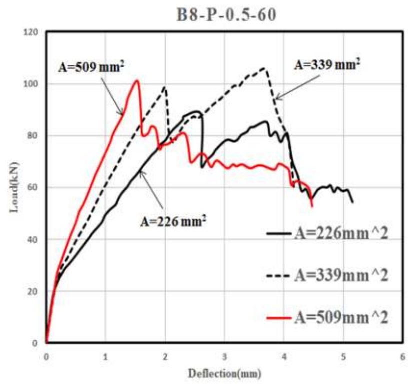</td><td>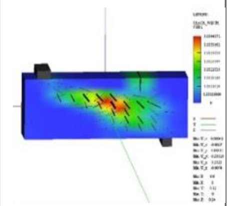</td><td>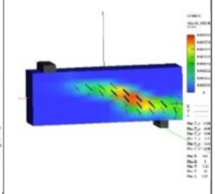</td><td>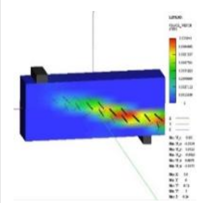</td></tr>
<tr><td>Shear Failure</td><td>Shear Failure</td><td>Shear Failure</td></tr>
</table>

Name	Load-deflection Relationship	Mode and Type of Failure		
		2ϕ 12	3ϕ 12	2ϕ 18
B9-P-1-60	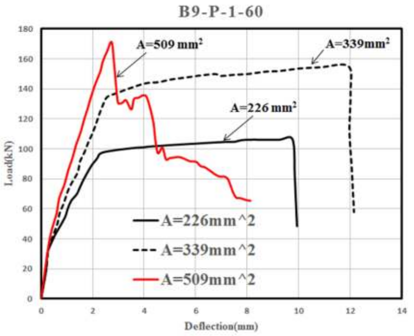	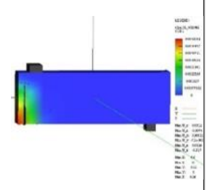 Flexural Failure	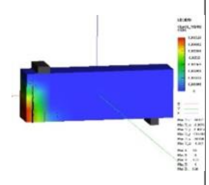 Flexural Failure	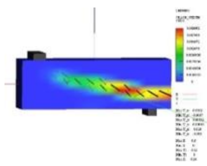 Shear Failure
B10-H10-0-20	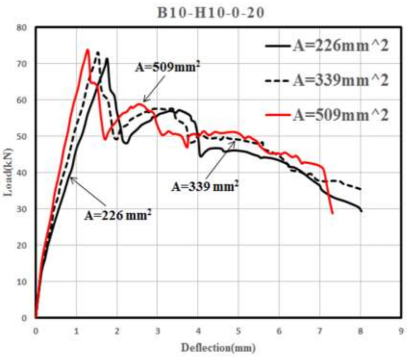	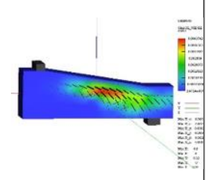 Flexural Failure	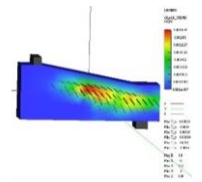 Shear Failure	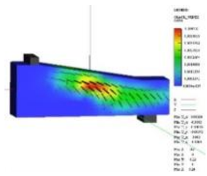 Shear Failure
B11-H10-0.5-20	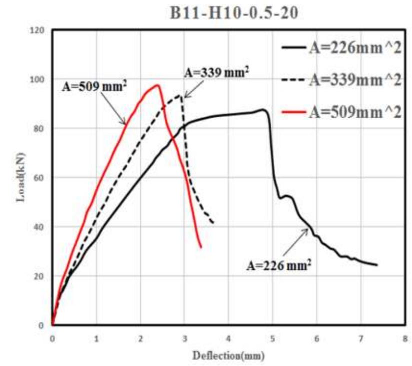	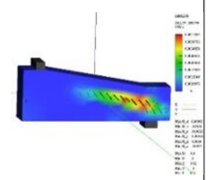 Shear Failure	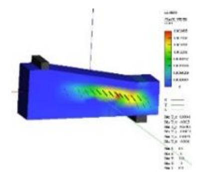 Shear Failure	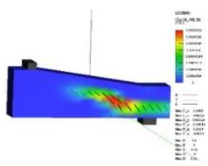 Shear Failure
B12-H10-1.0-20	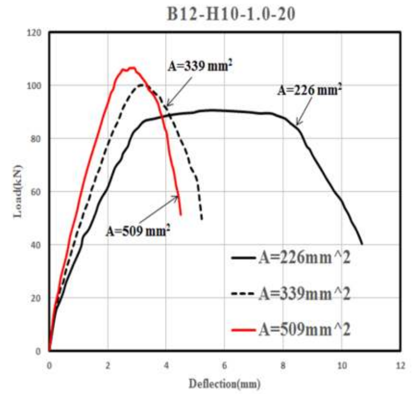	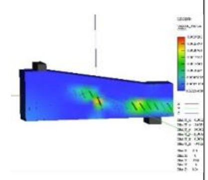 Shear Failure	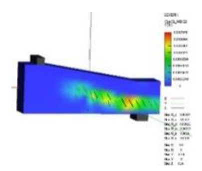 Shear Failure	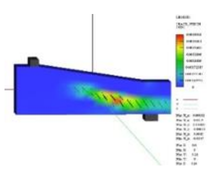 Shear Failure

<table>
<tr><th rowspan="2">Name</th><th rowspan="2">Load-deflection Relationship</th><th colspan="3">Mode and Type of Failure</th></tr>
<tr><th>2ϕ 12</th><th>3ϕ 12</th><th>2ϕ 18</th></tr>
<tr><td rowspan="2">B13-H10-0-40</td><td rowspan="2">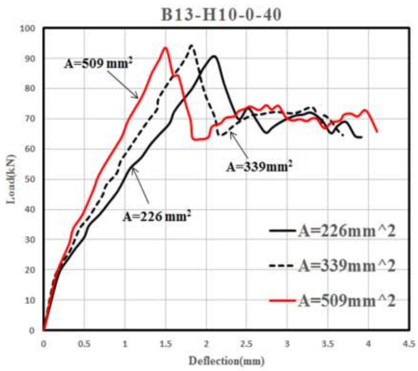</td><td>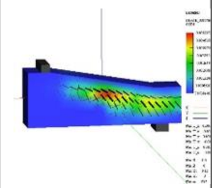</td><td>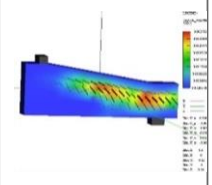</td><td>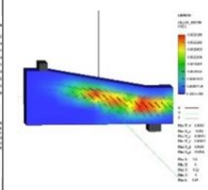</td></tr>
<tr><td>Shear Failure</td><td>Shear Failure</td><td>Shear Failure</td></tr>
<tr><td rowspan="2">B14-H10-0.5-40</td><td rowspan="2">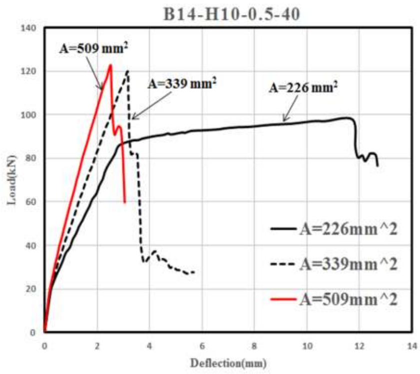</td><td>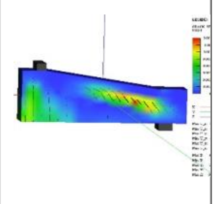</td><td>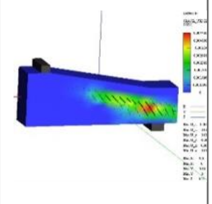</td><td>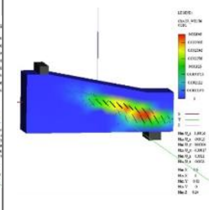</td></tr>
<tr><td>Shear & Flexural Failure</td><td>Shear Failure</td><td>Shear Failure</td></tr>
<tr><td rowspan="2">B15-H10-1.0-40</td><td rowspan="2">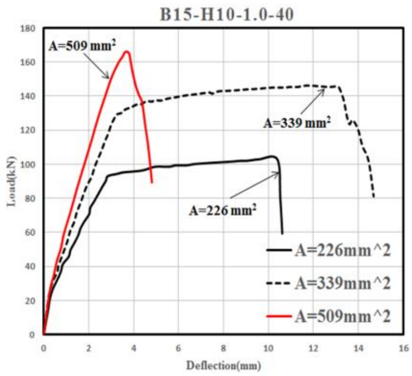</td><td>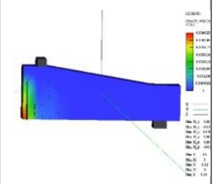</td><td>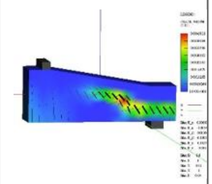</td><td>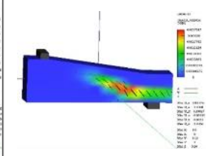</td></tr>
<tr><td>Flexural Failure</td><td>Shear Failure</td><td>Shear Failure</td></tr>
<tr><td rowspan="2">B16-H10-0-60</td><td rowspan="2">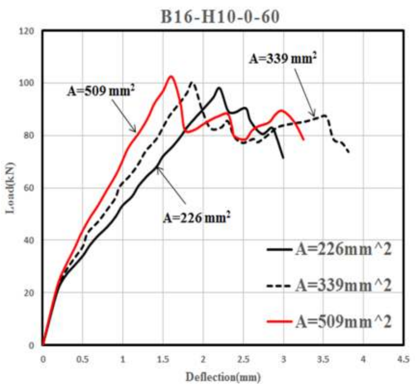</td><td>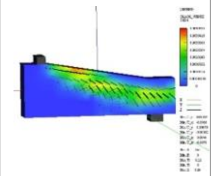</td><td>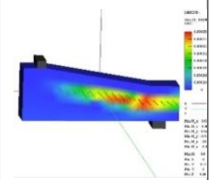</td><td>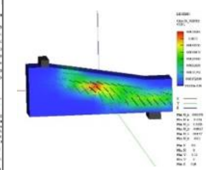</td></tr>
<tr><td>Shear Failure</td><td>Shear Failure</td><td>Shear Failure</td></tr>
</table>

<table>
<tr><th rowspan="2">Name</th><th rowspan="2">Load-deflection Relationship</th><th colspan="3">Mode and Type of Failure</th></tr>
<tr><th>2 ϕ 12</th><th>3 ϕ 12</th><th>2 ϕ 18</th></tr>
<tr><td rowspan="2">B17-H10-0.5-60</td><td rowspan="2">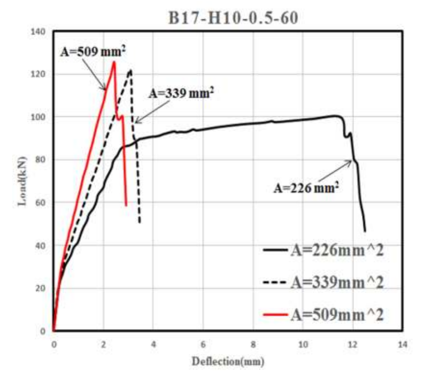
</td><td>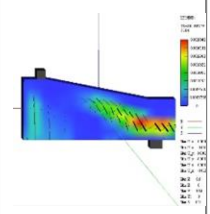</td><td>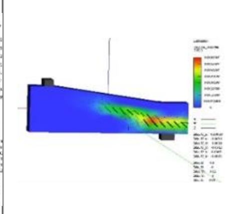</td><td>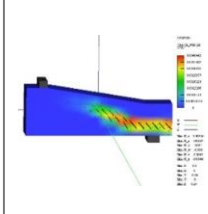</td></tr>
<tr><td>Shear & Flexural Failure</td><td>Shear Failure</td><td>Shear Failure</td></tr>
<tr><td rowspan="2">B18-H10-1.0-60</td><td rowspan="2">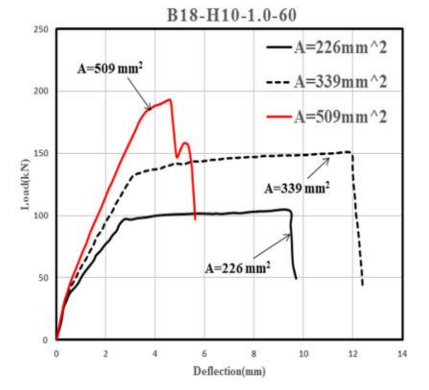
</td><td>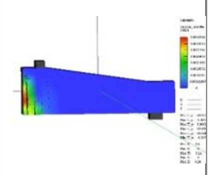</td><td>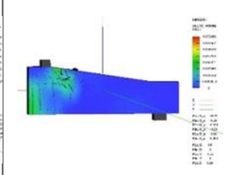</td><td>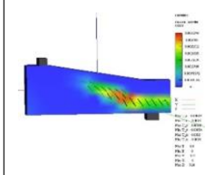</td></tr>
<tr><td>Flexural Failure</td><td>Flexural Failure</td><td>Shear Failure</td></tr>
<tr><td rowspan="2">B19-H15-0-20</td><td rowspan="2">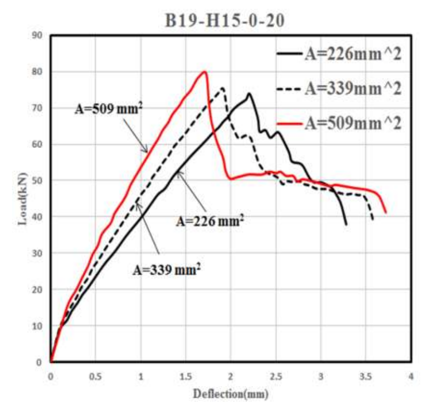
</td><td>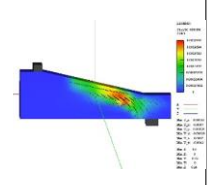</td><td>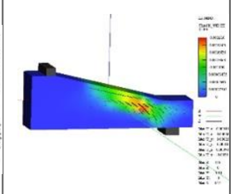</td><td>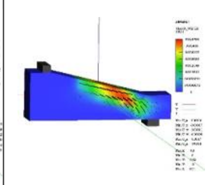</td></tr>
<tr><td>Shear Failure</td><td>Shear Failure</td><td>Shear Failure</td></tr>
<tr><td rowspan="2">B20-H15-0.5-20</td><td rowspan="2">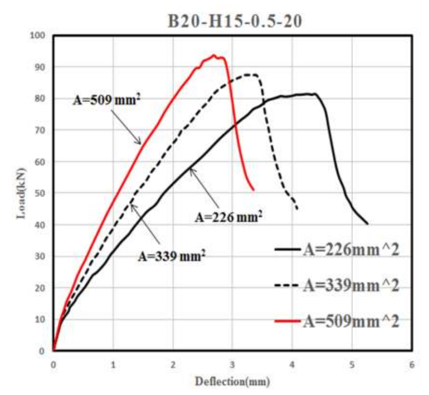
</td><td>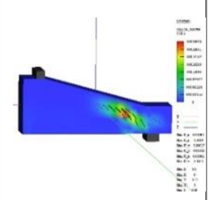</td><td>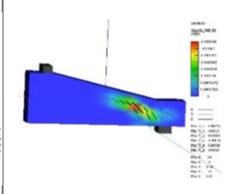</td><td>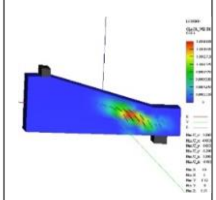</td></tr>
<tr><td>Shear Failure</td><td>Shear Failure</td><td>Shear Failure</td></tr>
</table>

<table>
<tr><th rowspan="2">Name</th><th rowspan="2">Load-deflection Relationship</th><th colspan="3">Mode and Type of Failure</th></tr>
<tr><th>2 ϕ 12</th><th>3 ϕ 12</th><th>2 ϕ 18</th></tr>
<tr><td rowspan="2">B21-H15-1.0-20</td><td rowspan="2">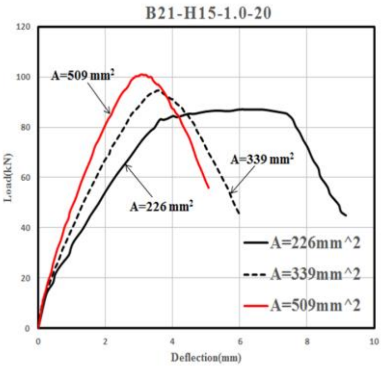
</td><td>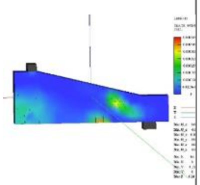</td><td>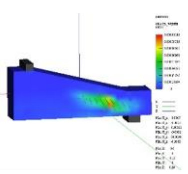</td><td>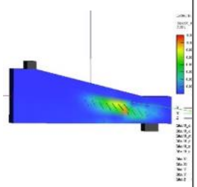</td></tr>
<tr><td>Shear & Flexural Failure</td><td>Shear Failure</td><td>Shear Failure</td></tr>
<tr><td rowspan="2">B22-H15-0-40</td><td rowspan="2">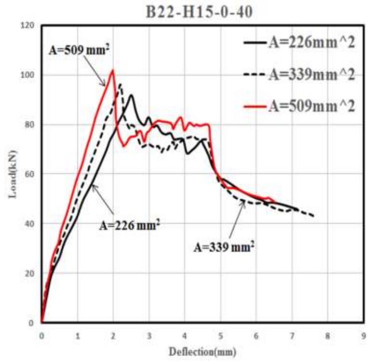
</td><td>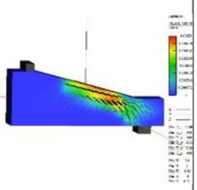</td><td>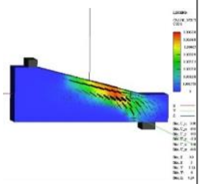</td><td>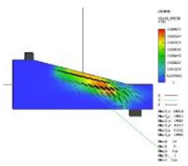</td></tr>
<tr><td>Shear Failure</td><td>Shear Failure</td><td>Shear Failure</td></tr>
<tr><td rowspan="2">B23-H15-0.5-40</td><td rowspan="2">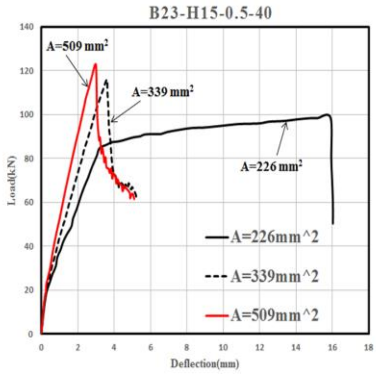
</td><td>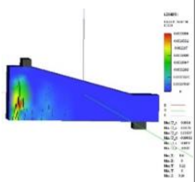</td><td>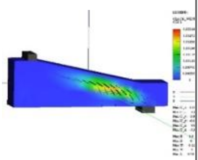</td><td>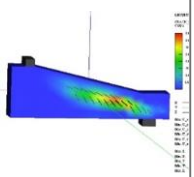</td></tr>
<tr><td>Flexural Failure</td><td>Shear Failure</td><td>Shear Failure</td></tr>
<tr><td rowspan="2">B24-H15-1.0-40</td><td rowspan="2">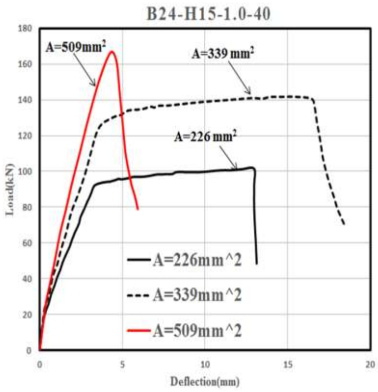
</td><td>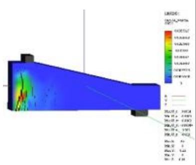</td><td>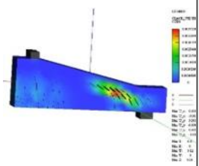</td><td>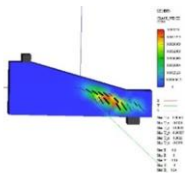</td></tr>
<tr><td>Flexural Failure</td><td>Shear & Flexural Failure</td><td>Shear Failure</td></tr>
</table>

<table>
<tr><th rowspan="2">Name</th><th rowspan="2">Load-deflection Relationship</th><th colspan="3">Mode and Type of Failure</th></tr>
<tr><th>2ϕ 12</th><th>3ϕ 12</th><th>2ϕ 18</th></tr>
<tr><td>B25-H15-0-60</td><td>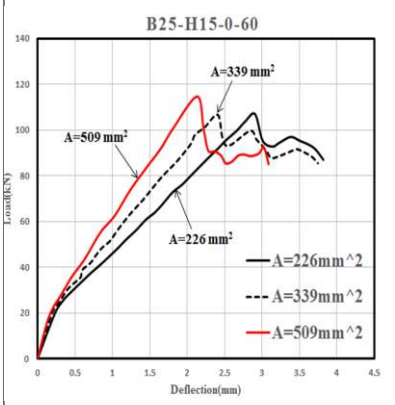
</td><td>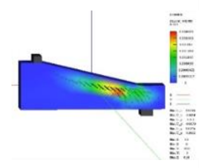
Shear Failure</td><td>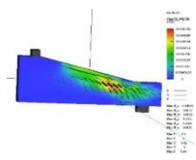
Shear Failure</td><td>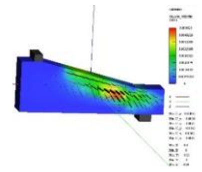
Shear Failure</td></tr>
<tr><td>B26-H15-0.5-60</td><td>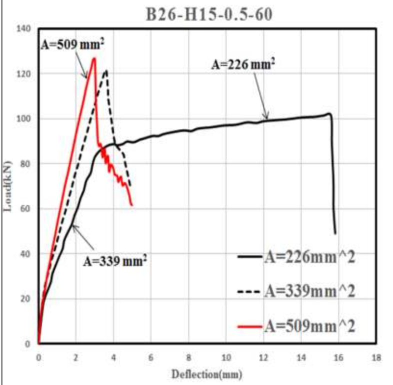
</td><td>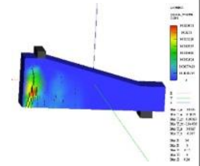
Flexural Failure</td><td>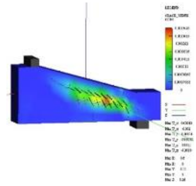
Shear Failure</td><td>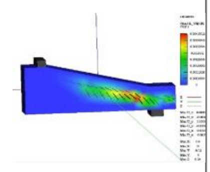
Shear Failure</td></tr>
<tr><td>B27-H15-1.0-60</td><td>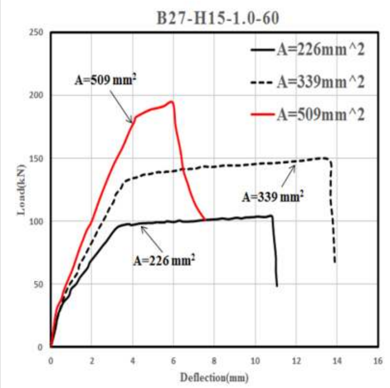
</td><td>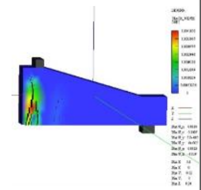
Flexural Failure</td><td>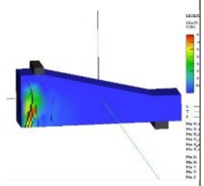
Flexural Failure</td><td>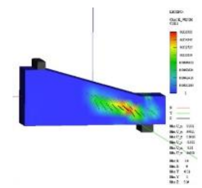
Shear Failure</td></tr>
</table>

Based on the results in Table 6.9; several crucial points can be concluded regarding failure mode:

1. If the compressive strength (f_c) is less than or equal to 20 MPa and with any values of other parameters (A_s, Vf and α); the failure mode will be shear failure.
2. If the compressive strength is between 20 and 60 MPa and the steel fiber ratio is 1%, the failure mode of under reinforced (226 mm^2) RCHBs without

stirrups will be flexure. This means that sufficient amount of steel fiber can convert the failure mode of these beams from shear to flexural failure.

3. If the main steel reinforcement over reinforcement 509 mm^2, and with any values of other parameters (f_c, Vf and α); the failure mode will be shear failure.
4. If the compressive strength (f_c) is equal to 60 MPa, steel fiber ratio is equal to 1%, and area of main steel reinforcement is equal to 339 mm^2; the failure mode will be flexural failure.

The greatest advantage of this study is to conclude the role of steel fiber, which converts the mode of failure from shear to flexural failure with the ideal ratio of 1.0%.

6.4.2.1 Parametric study on Finite Element Results of FE RCHBs

In order to interpret the effective role of each parameter (Area of main reinforcement (A_s), compressive strength (f_c), steel fiber ratio (Vf %), and angle of RCHBs (α)) on the mechanical behavior of RCHBs without stirrups, the parametric study was carried out to verify the generalization of the proposed models and to study the influence of each parameter on the predicted value of shear load capacity.

Main effect plots extracted as a result of the parametric study are shown in Figure 6.6. These plots give further insight to researchers regarding the effect of considered parameters on ultimate shear capacity of SF RCHBs. Each value of A_s, f_c, Vf% and is examined by the parametric analysis. The minimum and maximum values of each parameter are utilized as identified by the FE database. It can be identified from Figure 6.6 that all considered parameters have a significant influence on the shear capacity of the SF RCHBs. However, the influence of the inclination angle (α) after is negligibly small on the shear capacity of SF RCHBs. On the other hand, the effect of steel fiber ratio on the shear capacity is highest among all considered parameters. Moreover, a remarkable effect is observed on the shear capacity when values of compressive strength between (20 MPa to 40 MPa). However, the less influence is observed when the range of f_c is between (40 MPa to 60 MPa).

Two-dimensional interaction diagrams extracted as a result of the parametric study are shown in Figure 6.7 in order to compare the proportional effect of each parameter on the shear capacity of SF RCHBs comprehensively. According to Figure 6.7, it can be concluded that the two-way interaction graphs are compatible with the outcomes of the main effect plots. The comparison also shows that all parameters considered in the proposed model have considerable influence on the shear load capacity of SF RCHBs.

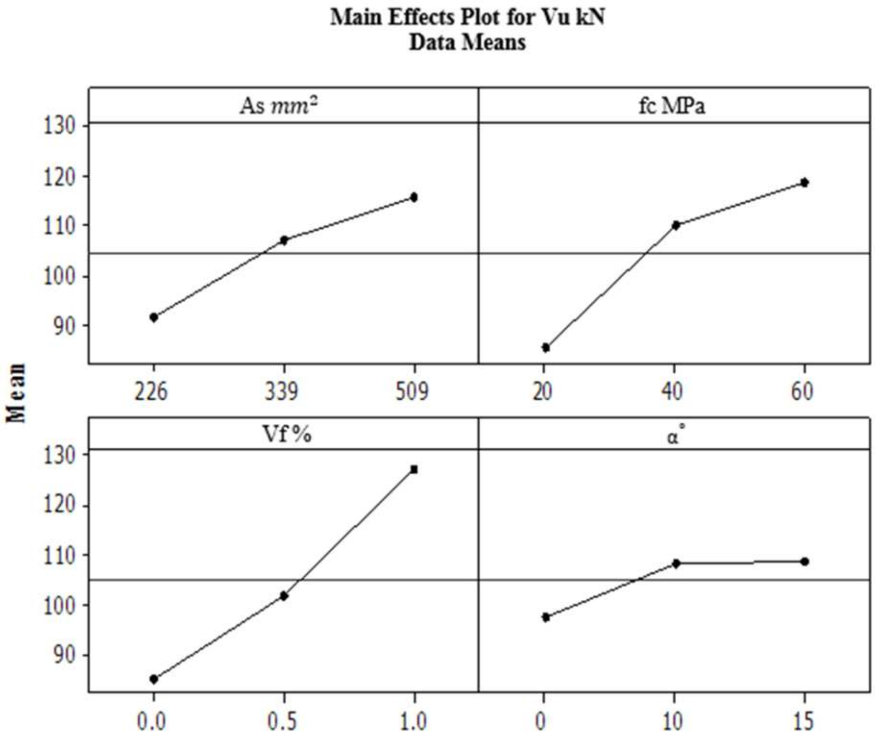

Figure 6.6 Main effect graphs resulted from parametric studies

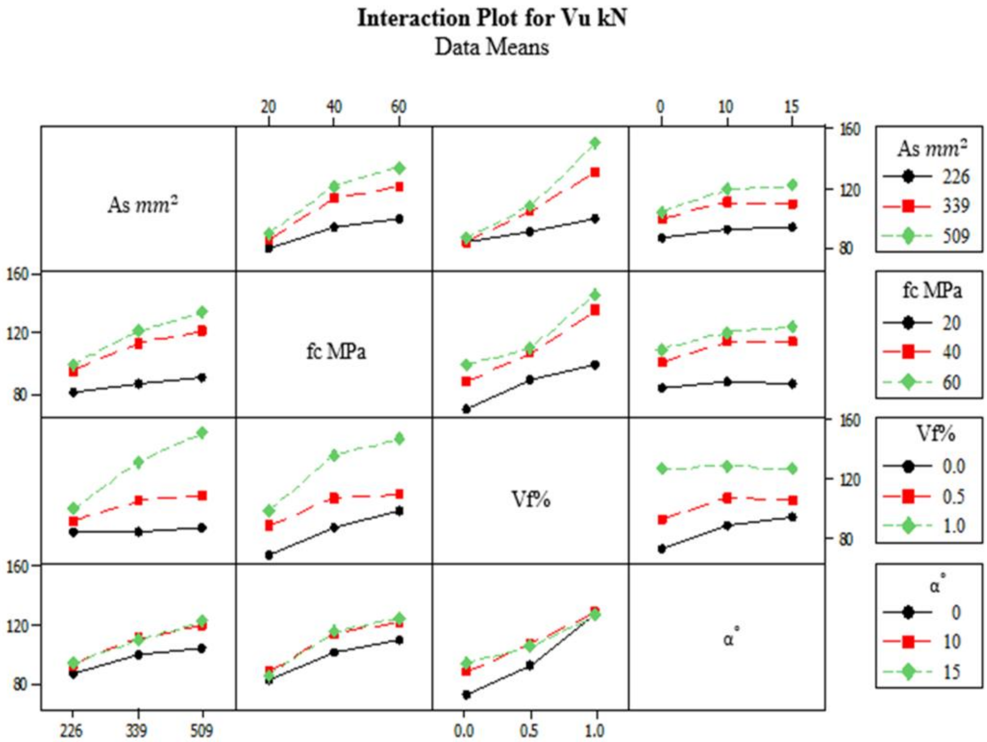

Figure 6.7 Two-dimensional interaction diagrams resulted from parametric studies

3D interaction plots resulted from parametric analysis are also given in Figures 6.8–6.13 to point out the combined effect of each parameter on the load capacity of SF RCHBs without stirrups. These graphs dependably visualize the effect of each parameter on other parameters as wells as on the shear capacity. As can be seen in Figures 6.8–6.13, all combinations of the parameters (A_s, f_c, Vf and α) are sketched in three-dimensional spaces with respect to the essential parameter of ultimate shear capacity (V_u). It is obvious to see the roles of each two parameters on the main parameter (V_u) with a significant increase in the value of V_u when the other values of parameters increased in all cases of the 3D parametric analysis. When all of the graphs are analyzed, it can be seen that there is no extraordinary values which disarrange the trend of changes between parameters. This condition also proves the reliability and accuracy of parametric analysis.

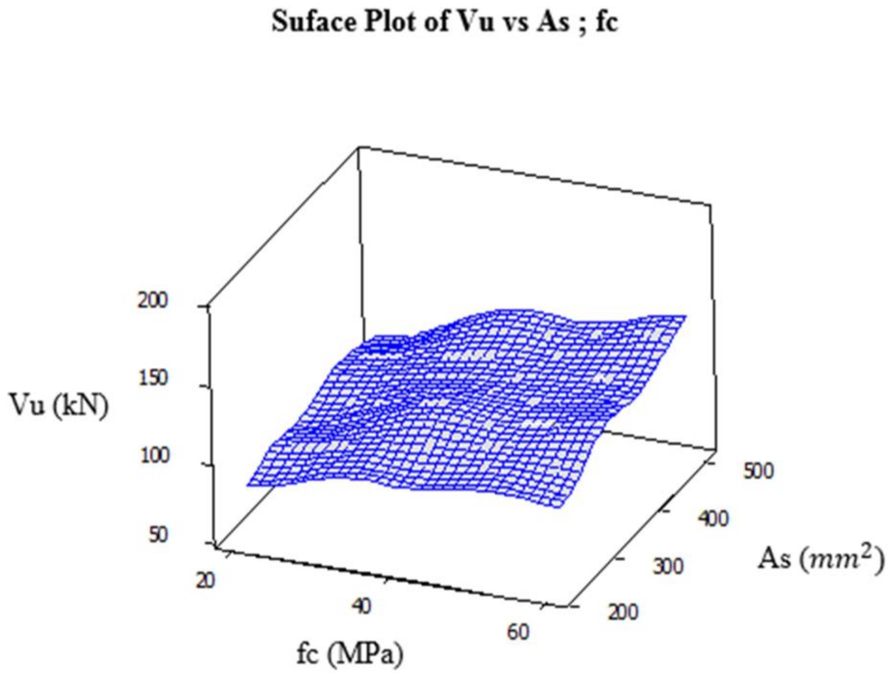

Figure 6.8 3D Interaction Diagram for shear capacity, area of steel and compressive strength

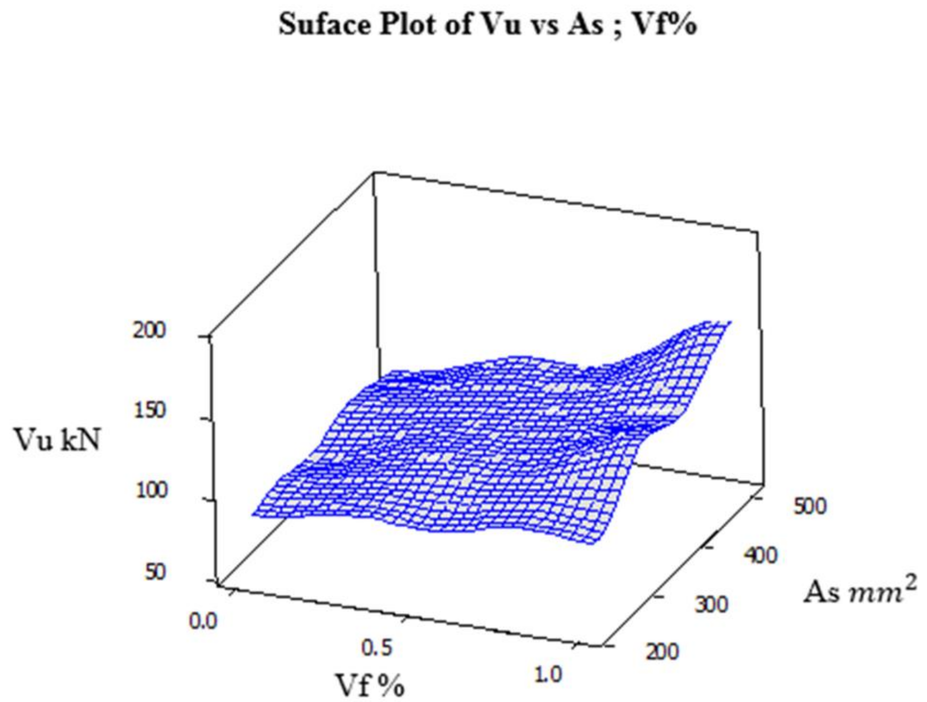

Figure 6.9 3D Interaction Diagram for shear capacity, area of steel and steel fiber ratio

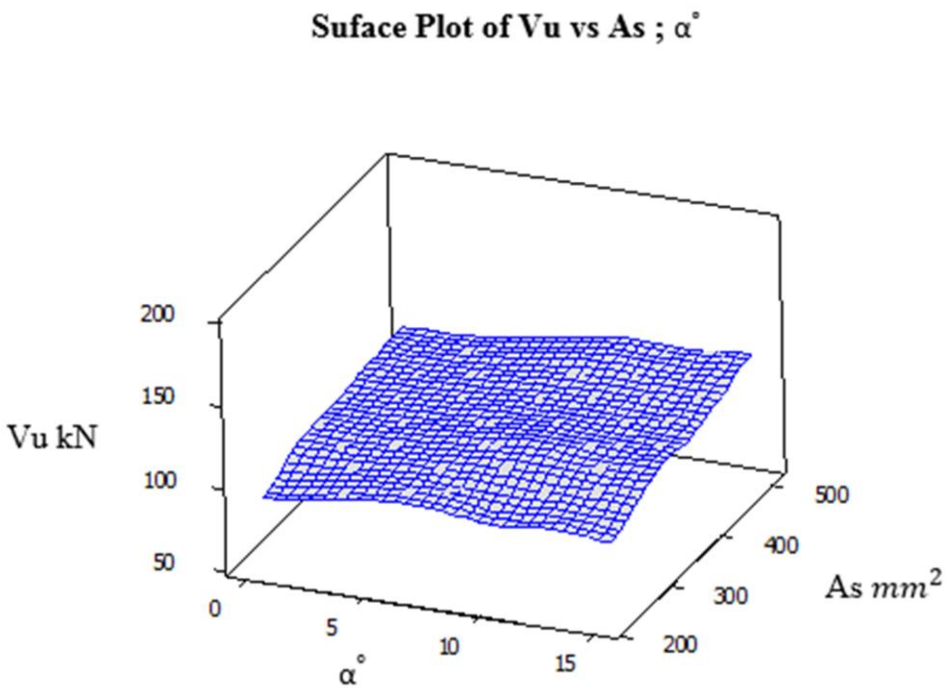

Figure 6.10 3D Interaction Diagram for shear capacity, area of steel and inclination angle of haunched beam

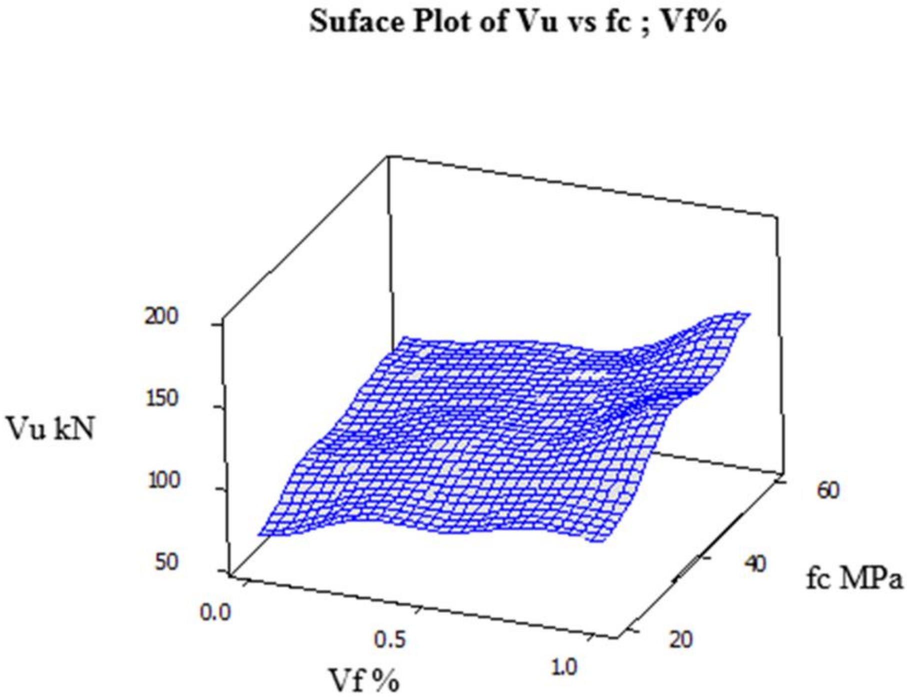

Figure 6.11 3D Interaction Diagram for shear capacity, compressive strength and inclination angle of haunched beam

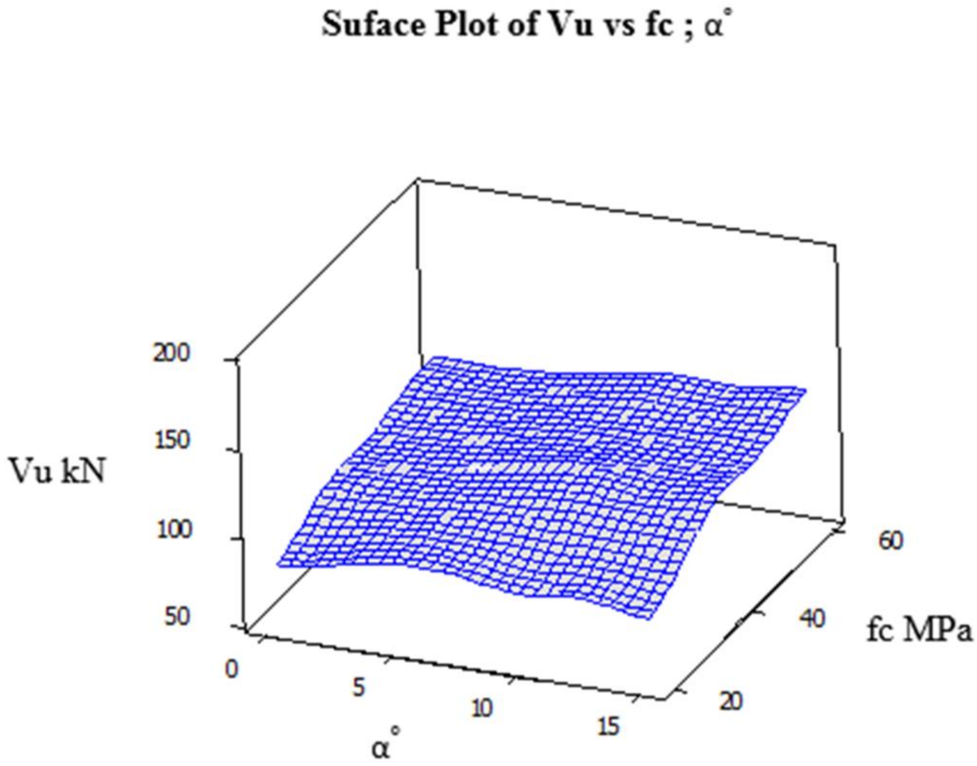

Figure 6.12 3D Interaction Diagram for shear capacity, compressive strength and inclination angle

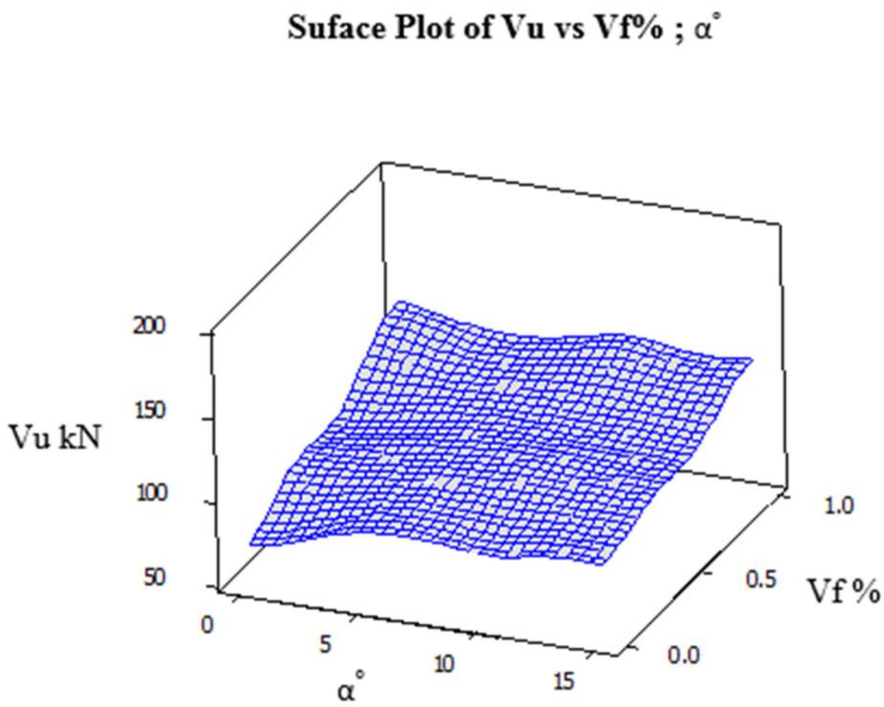

Figure 6.13 3D Interaction Diagram for shear capacity, steel fiber ratio and inclination angle of RCHBs

The effective role of steel fiber ratio on load-deflection relationship can be observed in Table 6.10 of all proposed groups of SF RCHBs, comparing the curves with respect to the steel fiber ratios when keeping other parameters constant. It can be concluded from curves that the effective ratio of steel fiber is 1%, which increases the load capacity and ductility more than other ratios.

Table 6.11 shows the effect of inclination angle on the mechanical behaviour of SF RCHBs via load-deflection curves of the beams. It can be extracted from the table that the influence of inclination angle on the shear load capacity of SF RCHBs is negligibly small after the angle exceeds 10^{o}.

As well as Table 6.12 shows load-deflection relationship exhibits the effective role of compressive strength at the load capacity when its increase from 20, 40 and 60 MPa besides to keep other parameters constant. It can be seen from curves that the load capacity increases when the compressive strength increases from 20 to 40 MPa with less influence when it increases from 40 to 60 MPa.

Table 6.10 Load-deflection relationship of three different ratios (0, 0.5, 1) % of steel fiber proposed models of RCHBs

Code of Beams	A=226 mm^2	A=339 mm^2	A=509 mm^2
B1-P-0-20 B2-P-0.5-20 B3-P-1.0-20	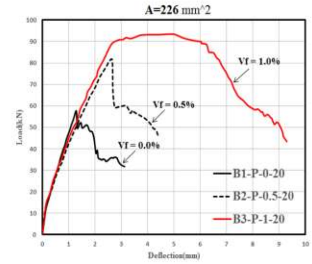	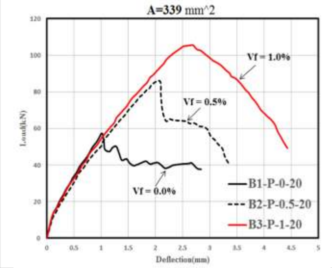	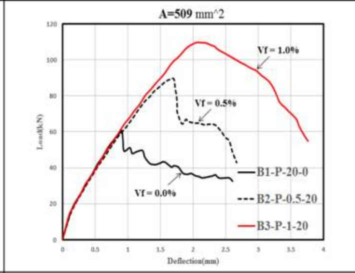
B4-P-0-40 B5-P-0.5-40 B6-P-1.0-40	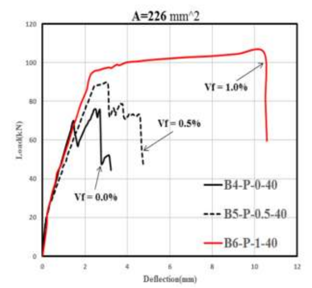	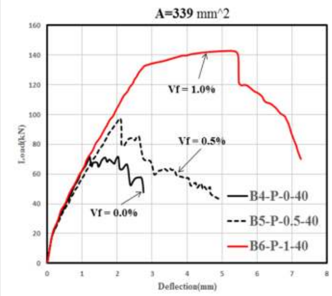	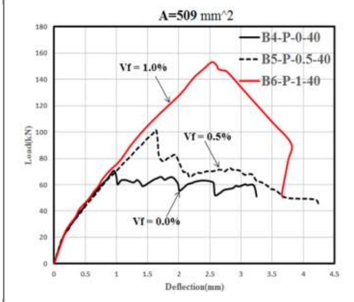
B7-P-0-60 B8-P-0.5-60 B9-P-1-60	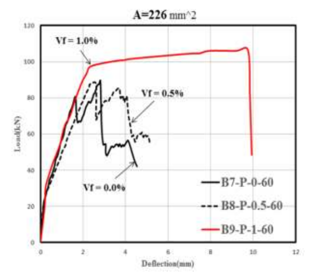	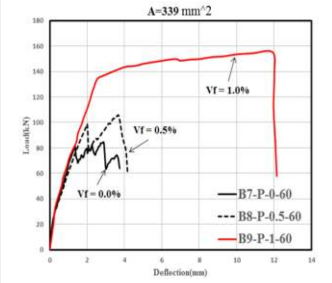	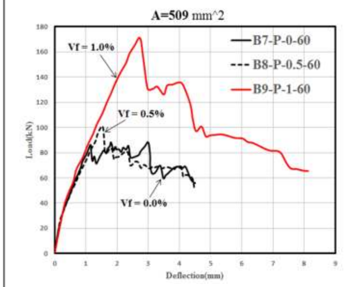
B10-H10-0-20 B11-H10-0.5-20 B12-H10-1.0-20	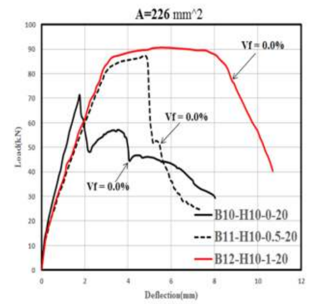	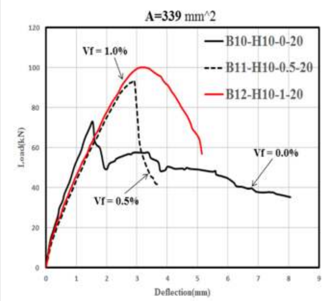	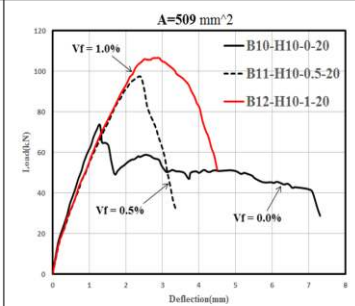
B13-H10-0-40 B14-H10-0.5-40 B15-H10-1.0-40	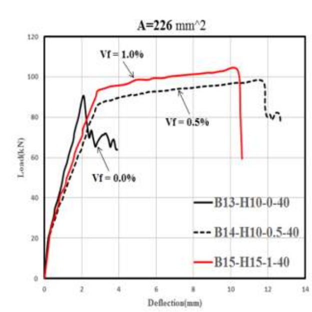	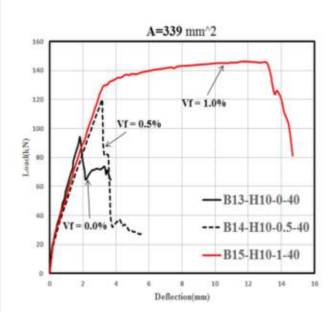	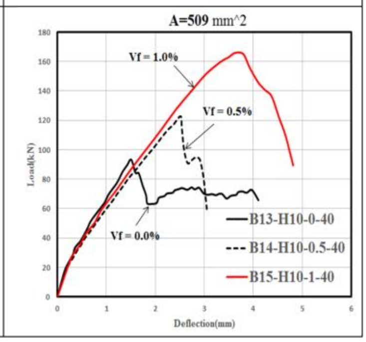

Code of Beams	A=226 mm^2	A=339 mm^2	A=509 mm^2
B16-H10-0-60 B17-H10-0.5-60 B18-H10-1.0-60	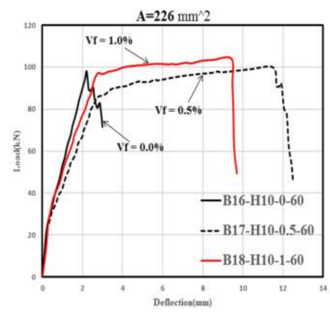	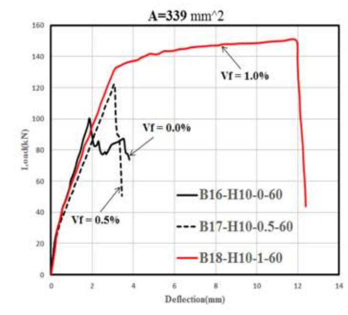	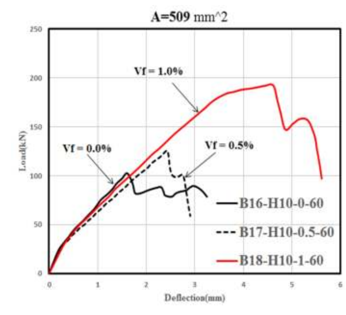
B19-H15-0-20 B20-H15-0.5-20 B21-H15-1.0-20	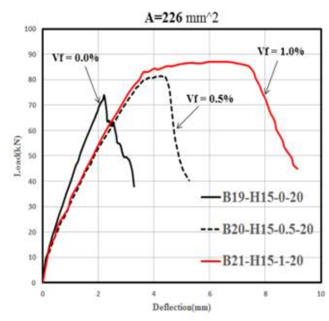	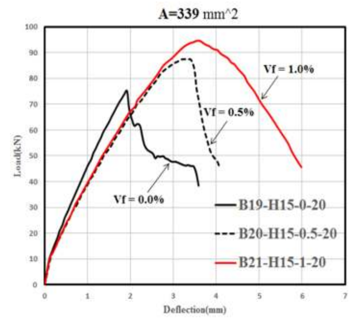	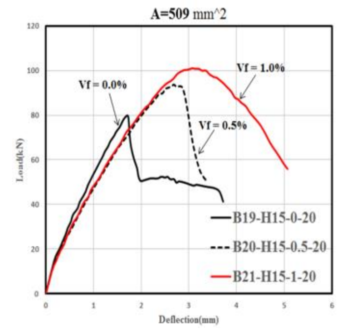
B22-H15-0-40 B23-H15-0.5-40 B24-H15-1.0-40	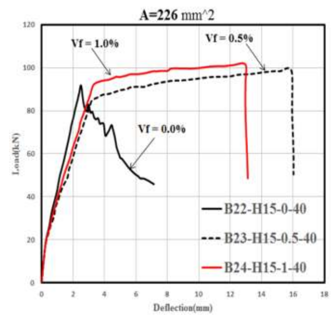	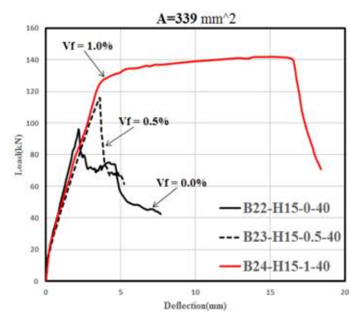	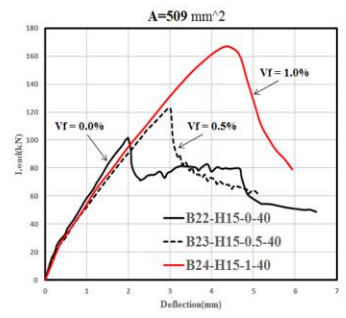
B25-H15-0-60 B26-H15-0.5-60 B27-H15-1.0-60	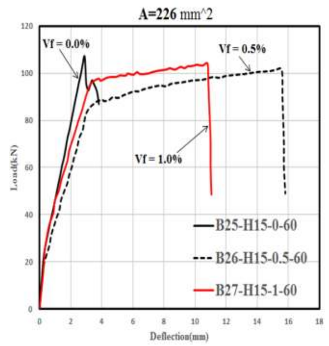	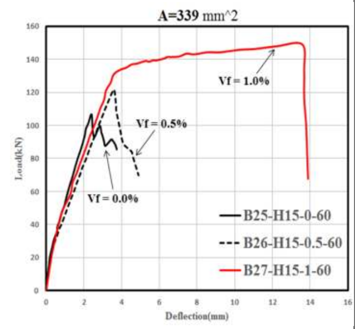	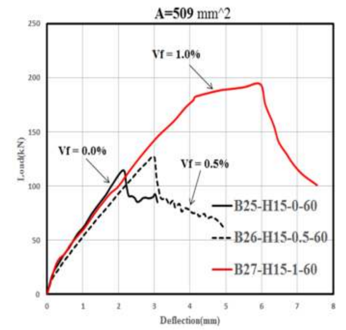

Table 6.11 Load-deflection relationship of three different values (0, 10, 15)° of inclination angle of proposed models of SF RCHBs

Code of Beams	A=226 mm^2	A=339 mm^2	A=509 mm^2
B1-P-0-20 B10-H10-0-20 B19-H15-0-20	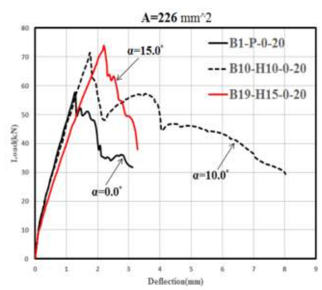	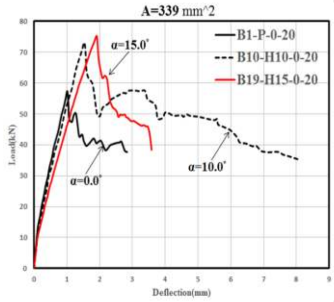	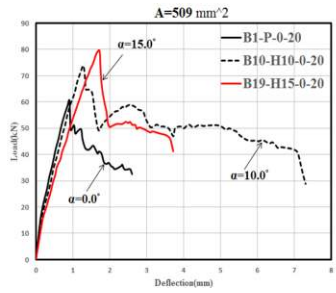
B2-P-0.5-20 B11-H10-0.5-20 B20-H15-0.5-20	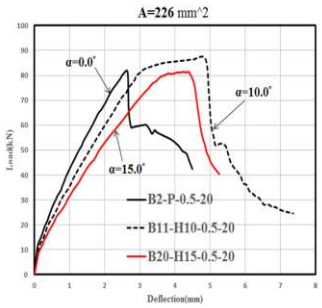	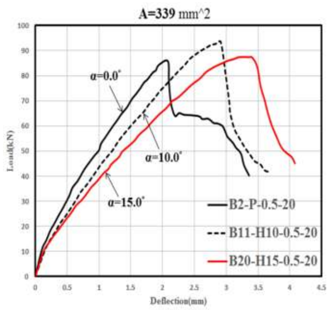	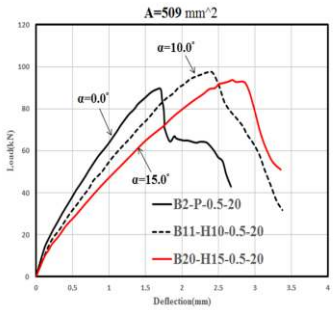
B3-P-1.0-20 B12-H10-1.0-20 B21-H15-1.0-20	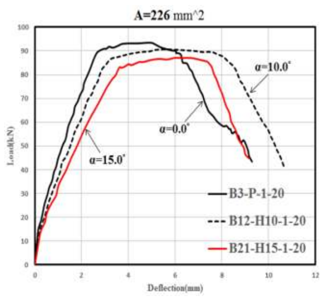	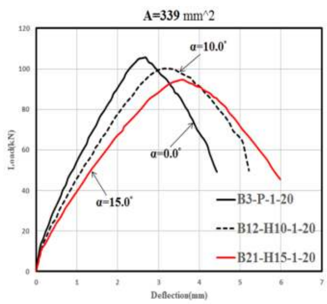	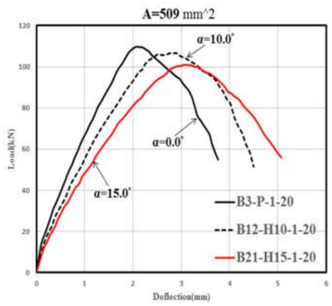
B4-P-0-40 B13-H10-0-40 B22-H15-0-40	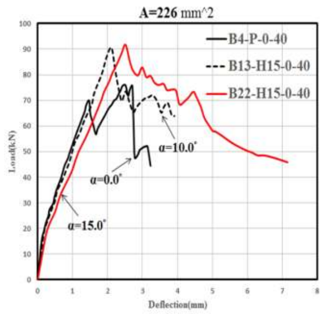	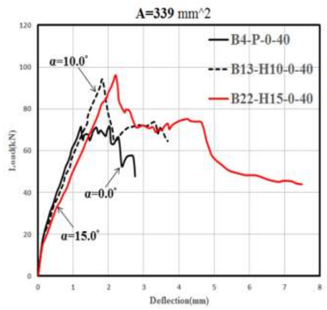	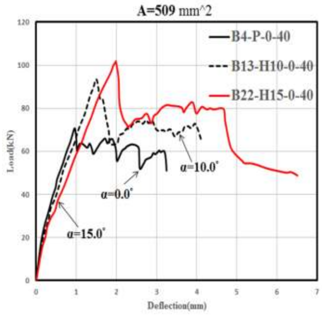
B5-P-0.5-40 B14-H10-0.5-40 B23-H15-0.5-40	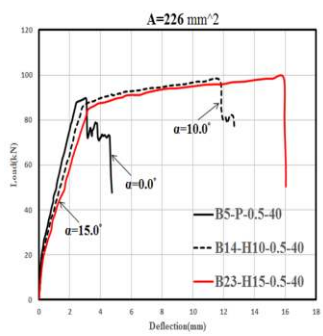	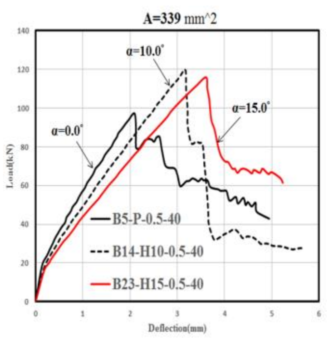	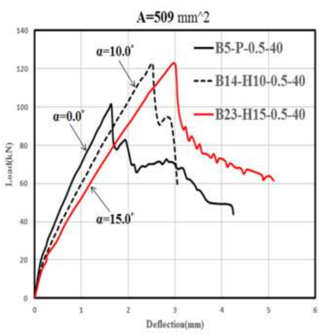

<table>
<tr><th>Code of Beams</th><th>A=226 mm^2</th><th>A=339mm^2</th><th>A=509mm^2</th></tr>
<tr><td>B6-P-1.0-40

B15-H10-1.0-40

B24-H15-1.0-40</td>
<td>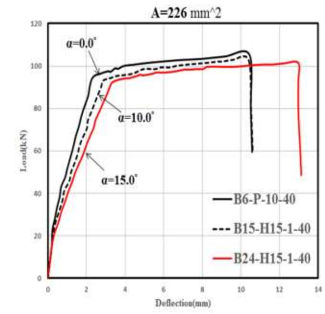</td>
<td>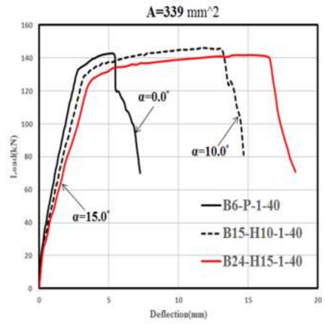</td>
<td>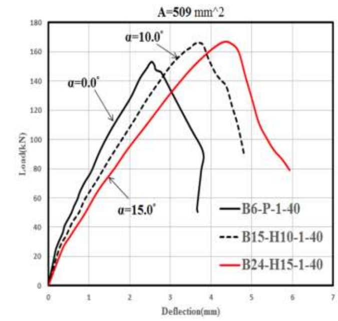</td></tr>
<tr><td>B7-P-0-60

B16-H10-0-60

B25-H15-0-60</td>
<td>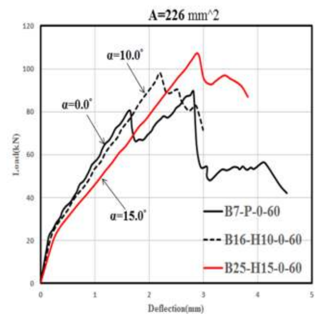</td>
<td>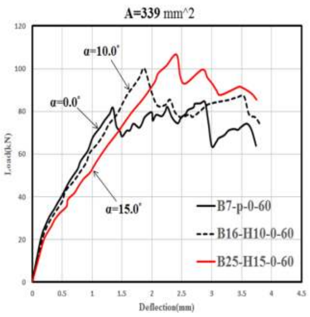</td>
<td>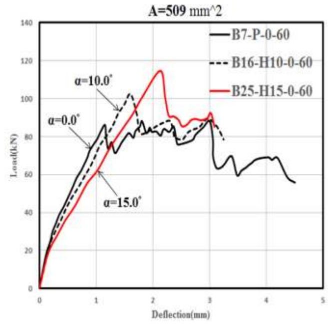</td></tr>
<tr><td>B8-P-0.5-60

B17-H10-0.5-60

B26-H15-0.5-60</td>
<td>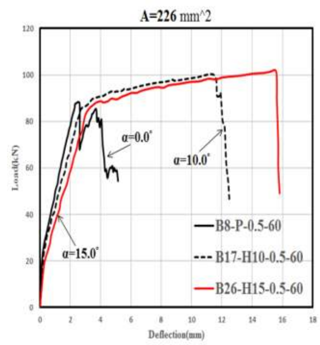</td>
<td>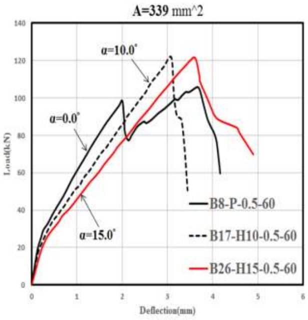</td>
<td>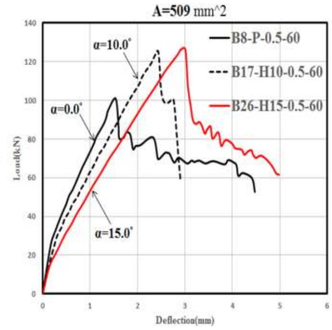</td></tr>
<tr><td>B9-P-1.0-60

B18-H10-1.0-60

B27-H15-1.0-60</td>
<td>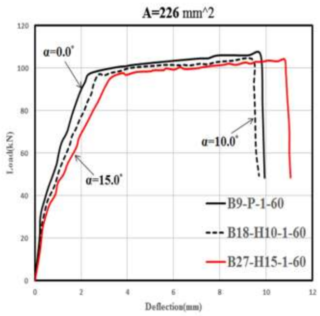</td>
<td>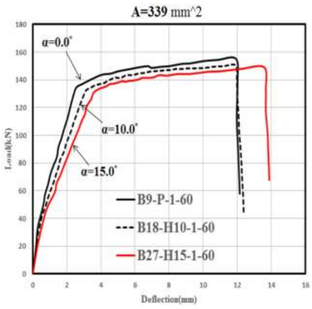</td>
<td>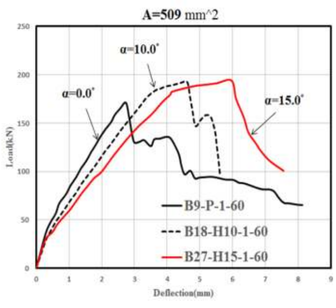</td></tr>
</table>

Table 6.12 Load-deflection relationship of three different values (20, 40, 60) MPa, of compressive strength of proposed models of SF RCHBs

<table>
<tr><th>Code of Beams</th><th>A=226 mm²</th><th>A=339 mm²</th><th>A=509 mm²</th></tr>
<tr><td>B1-P-0-20

B4-P-0-40

B7-P-0-60</td>
<td>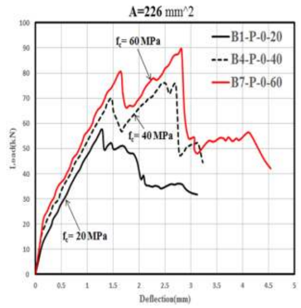</td>
<td>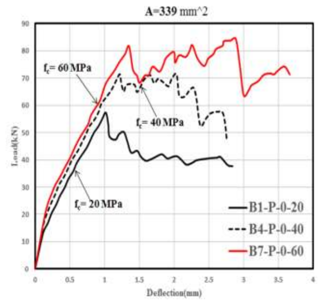</td>
<td>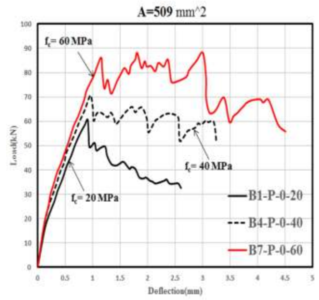</td></tr>
<tr><td>B2-P-0.5-20

B5-P-0.5-40

B8-P-0.5-60</td>
<td>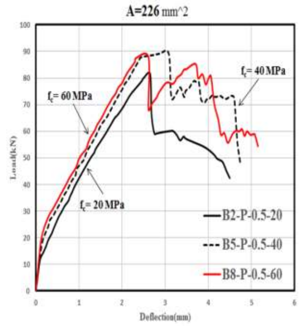</td>
<td>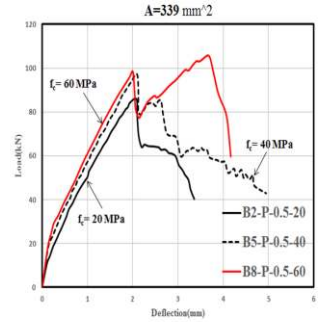</td>
<td>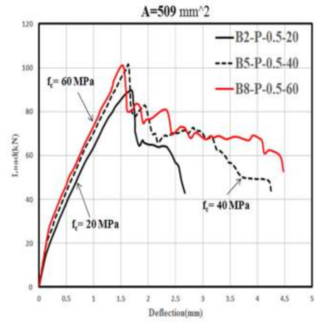</td></tr>
<tr><td>B3-P-1.0-20

B6-P-1.0-40

B9-P-1.0-60</td>
<td>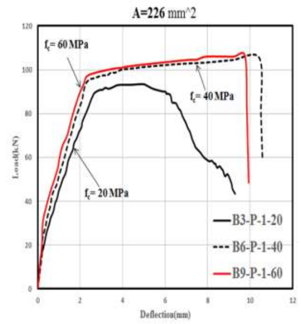</td>
<td>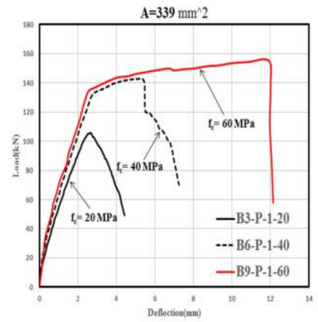</td>
<td>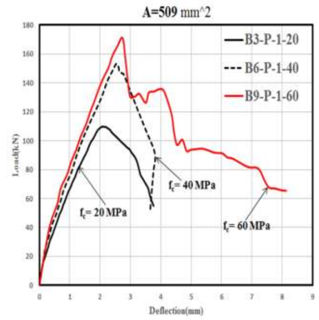</td></tr>
<tr><td>B10-H10-0-20
B13-H10-0-40

B16-H10-0-60</td>
<td>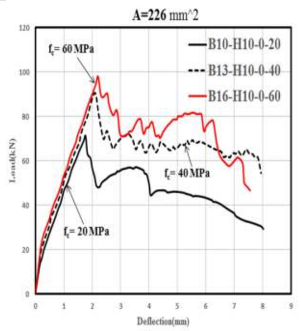</td>
<td>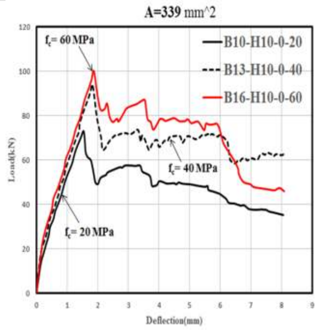</td>
<td>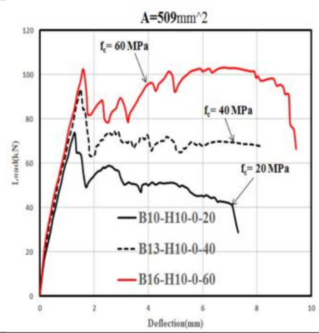</td></tr>
<tr><td>B11-H10-0.5-20
B14-H10-0.5-40

B17-H10-0.5-60</td>
<td>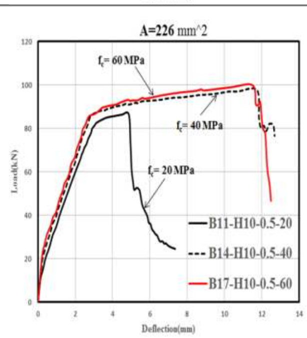</td>
<td>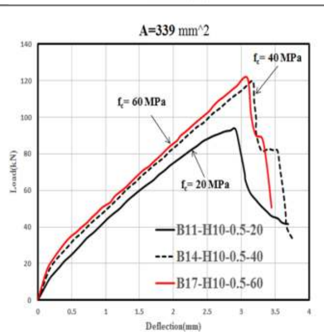</td>
<td>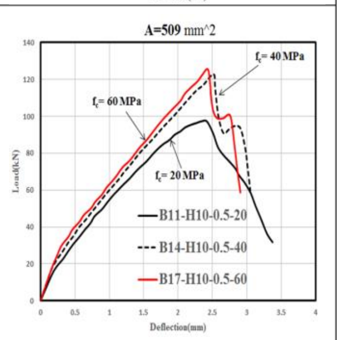</td></tr>
</table>

Code of Beams	A=226 mm^2	A=339mm^2	A=509mm^2
B12-H10-1.0-20 B15-H10-1.0-40 B18-H10-1.0-60	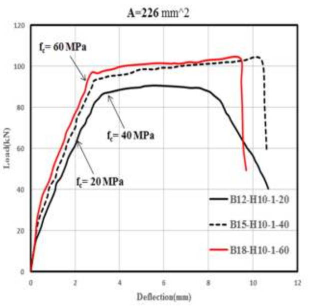	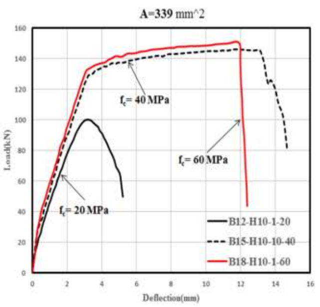	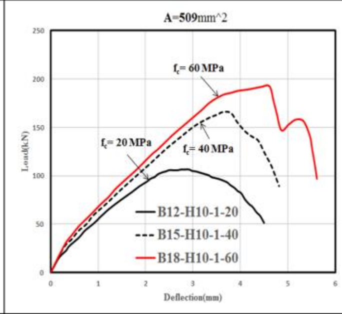
B19-H15-0-20 B22-H15-0-40 B25-H15-0-60	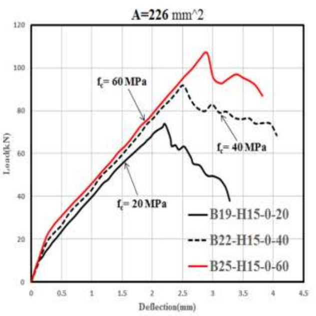	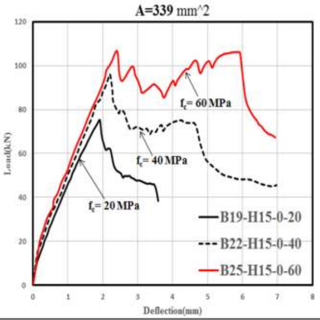	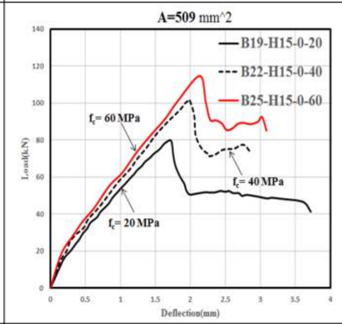
B20-H15-0.5-20 B23-H15-0.5-40 B26-H15-0.5-60	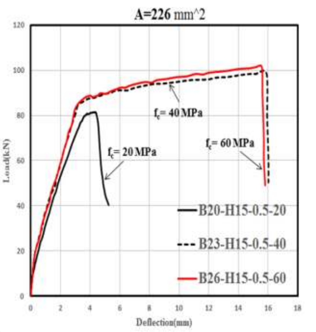	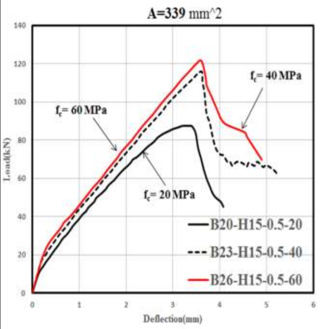	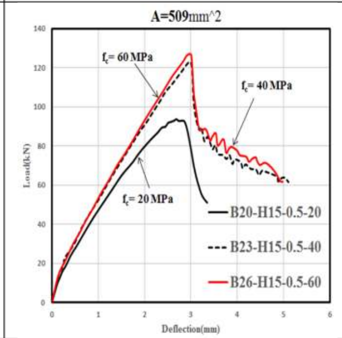
B21-H15-1.0-20 B24-H15-1.0-40 B27-H15-1.0-60	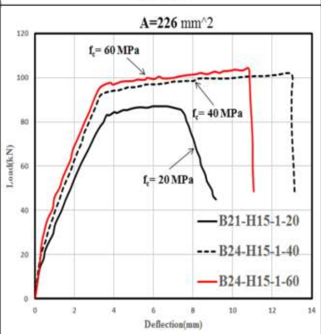	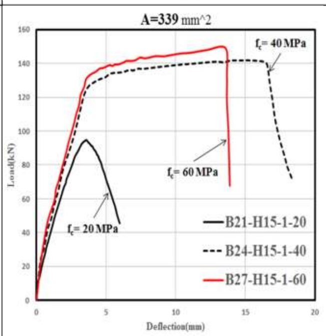	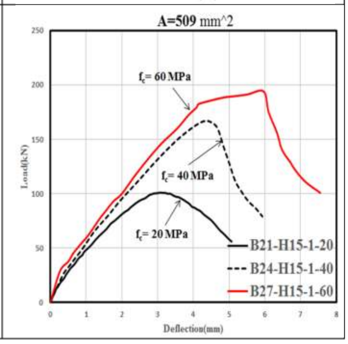

6.5 Conclusions

This study has been pointed out to figure out the mechanical behaviors and shear capacity of steel fiber RCHBs without stirrups. Atena-GiD 3D software was used to analyze the models. This study consists of 81 FE models which are divided into the three groups within 27 models. The difference between each group is in the quantities of main reinforcement (A_s) which are 226, 339, and 509 mm^2, respectively. Each group has different amounts of steel fiber ratio (0.0, 0.5, and

1.0%), inclination angles (0.0^o, 10.0^o, and 15.0^o), and different three values of compressive strength (20.0, 40.0, 60.0 MPa). Nine experimental results of steel fiber haunched beams were used to verify the accuracy of proposed finite element models. The correlation coefficient between numerical and experimental results is (R^2 = 0.9793).

Based on the results of this study, the following conclusions can be shortly summarized below:

- As a result of FE analyses, it is concluded that steel fiber has a noticeable influence on the shear capacity of RCHBs. Moreover, 1% amount of steel fiber is the most efficient ratio regarding the shear capacity.
- The effective angle on the shear behavior of RCHBs is 10°, which is considered as a remarkable angle that resists shear strength.
- When the compressive strength between 20 MPa and 60 MPa, steel fiber ratio is 1%, and main steel reinforcement of RCHBs is equal to 226 mm^2 (under reinforcement); the failure of RCHBs will be a flexural failure if the RCHBs without stirrups reinforcement. In this case, flexural failure means that there is a combined role between steel fiber and compressive strength to resist shear strength of beam.
- When a compressive strength equal 60 MPa, steel fiber ratio equal 1%, and area of main steel reinforcement equal to 339 mm^2 (higher reinforcement); the failure mode will be flexural failure.
- The role of steel fiber to resist shear strength can be played by combining the compressive strength of concrete to eliminate the role of stirrups reinforcement in the beam.
- Comparison of numerical and experimental results shows that FE method is an efficient and reliable tool for the prediction of mechanical behaviour of RCHBs without stirrup reinforcement containing steel fiber or not.

CHAPTER 7

CONCLUSIONS

7.1 Conclusions

This study has pointed out the need to improve the knowledge of the load-deflection behavior of damaged RCHBs after being rehabilitated by Basalt Fiber Fabric and Carbon Fiber Reinforced Polymer strips (CFRP). Besides understanding the shear behaviors and shear capacity of steel fiber RCHBs without stirrups reinforcement. As well as to figure out the behaviour of damaged corbels after being rehabilitated by Basalt Fiber Fabric and Basalt Fiber Mesh.

From the experimental test and nonlinear FE Modeling results presented, the following general conclusions can be drawn:

- Basalt Fiber Fabric material appeared to perform well to rehabilitate the shear and flexural strength. After being damaged; in which the rehabilitated of RCHBs increase the shear and flexural capacities as compared to the original values.
- The most significant and interesting outcome of the crack pattern was when the depth of haunched beams decreases at support, the major crack will propagate upward leading to a decrease in the requirement of the distance of FRP strips above the major crack (requirement of less distance to ensure the bonding between FRP and the surface of the sample). Therefore, the bond of strips on the surface of the sample will decrease, leading to a reduction in ultimate shear capacity when compared with prismatic beams. However, the failure of Basalt Fiber Fabric was a debonding failure. While the position of debonding failure of Basalt Fiber Fabric depended on the shape of the haunched beam.
- In general, the rehabilitation by using Basalt Fabric in addition to repair of cracks will return the load capacity value (shear or flexural) at least to the original load capacity.

- The nonlinear FE models by ATENA-GiD programs predicted quite precisely the behavior of load-deflection of the all tested pre-rehabilitated haunched.
- All values of load capacity of experimental haunched beams after being rehabilitated by Basalt Fabric and carbon fiber polymer located between the values of strengthening nonlinear FE analysis of undamaged haunched beams (max. limit) and the values of strengthening nonlinear FE analysis of damaged haunched beams (min. limit) without injection material in the cracks. And the experimental rehabilitated haunched beams loads suffered a small deviation from the max. limit.
- In general, there is an acceptable agreement between the crack patterns of nonlinear FE analysis and the crack patterns of an experimental test of haunched beams which is considered the second confirmation of accuracy of the proposed model of FE analysis by ATENA-GiD.
- Carbon Fiber Reinforced Polymer (CFRP) material appeared to perform very well regarding the rehabilitation of damaged RCHBs.
- The most important point about the crack patterns is that, when the depth of haunched beams at the support decreases, the major crack will propagate upward.
- The most significant and interesting outcomes of rehabilitation of haunched beams which were repaired only by epoxy without CFRP is that the ultimate shear capacities were found to be higher than the original values.
- The vertical strengthening strips of CFRP were more efficient than inclined strengthening strips of CFRP to increase the shear capacities of damaged haunched beams, which were debonding failure mode for all status of strengthening.
- The zone of all possible load capacities of rehabilitated RCHBs via nonlinear FE analysis models will help the structural engineers to figure out and predict the behavior of rehabilitated damaged haunched beams beside the effect of injection material in the cracks.
- A significant influence of steel fiber ratio was shown from results of FE database, which affects shear load capacity of RCHBs. 1.0% of steel fiber ratio consider the effective ratio to resist shear strength among the other ratios.
- The effective angle on the shear behavior of RCHBs is 10°, which is

considered a remarkable angle that resists the shear strength.

- When the compressive strength between 20MPa and 60 MPa, steel fiber ratio is 1%, and main steel reinforcement of RCHBs equal to 226 mm^2; the failure of RCHBs will be a flexural failure if the RCHBs without stirrups reinforcement. Flexural failure in this case, means that there is a combination role between steel fiber and compressive strength to resist shear strength of beam.
- The role of steel fiber to resist shear strength can be played by combining with the compressive strength of concrete to eliminate the role of stirrups reinforcement in the beam.
- The FE analysis by using Atena-GiD 3D software package showed a good predicting of shear behavior of SF RCHBs. Besides setting it as a reliable software package to analyze and predict the behavior of SF RCHBs.
- For both types of concrete corbels (Normal and Self-Compacting Concrete); Basalt Fiber Mesh cannot improve the ultimate load capacity without epoxy injecting regarding the rehabilitation of damaged corbels.
- For both types of concrete (normal and SCC), the mode of failure of Basalt Fiber Mesh was observed to be a rupture of Basalt Mesh which is considered to be the most important and significant failure mode for FRP.
- Test results showed that it is not reliable to use Basalt Fiber Mesh alone without injection epoxy in high-compressive strength SCC-SFRC corbels for rehabilitation.
- In general, rehabilitation with only epoxy injection gives better results for medium strength corbels as compared to high strength corbels.
- The existence of steel fiber plays an important role in both of the investigated rehabilitation techniques for both medium strength and high strength concrete corbels. It increases the effectiveness of the rehabilitation due to partial restoring of bridging effect of steel fibers. Moreover, the possibility of restoring the original load capacity by repairing with only epoxy injection increases for steel fiber reinforced concrete corbels. This situation leads to an economical alternative for rehabilitation.

7.2 Recommendations for Future Research

It can be recommending the following topics for future works:

- FE analysis of mechanical behavior of rehabilitated RCHBs for other types of concrete such as fiber reinforced concrete can be studied.
- Mechanical behavior of rehabilitated RCHBs for different types of loading, such as a uniformly distributed load, cyclic loading, and impact loading can be studied in addition to the FE analysis studies.
- Mechanical behavior of rehabilitated full-scale RCHBs for the normal concrete and other types of concrete can be studied besides the FE analysis studies.
- Experimental and FE analysis of behavior of rehabilitated other non-prismatic concrete members such as columns, slabs and deck slabs can be investigated.
- Parametric study on the effective width of FRP on the rehabilitation of damaged RCHBs and corbels.
- More experimental studies on the mechanical behavior of SF RCHBs with different shape and different scales.
- Further studies on the rehabilitation of RC-corbels after exposure to elevated temperatures besides the FE analysis studies.

REFERENCES

Abdulhaleem, K. (2018). Mechanical Behavior of Self-Compacting Fiber Reinforced Concrete at Elevated Temperatures. Ph.D. Thesis. Gaziantep Unversity.

Abdulhaleem, K.N., Gülşan, M.E., Çevik, A. (2018). Mechanical Behavior of Steel Fiber-Reinforced Self- Compacting Concrete Corbels at Elevated Temperatures. *Structural Concrete*, **19 (2)**, 1–14.

ACI 224. (2008). *Control of Cracking in Concrete Structures*. American Concrete Institute; Farmington Hills, MI, USA.

ACI 440. (2008). *Guide for the design and construction of externally bonded FRP systems for strengthening concrete structures*. Farmington Hills, MI, USA.

ACI 546. (2006). *Guide for the selection of materials for the repair of concrete*. Farmington Hills, MI, USA.

ACI Committee 318. (2011). *Building Code Requirements for Structural Concrete ACI 318-11 and Commentary*. American Concrete Institute.

Adebar, P., Mindess, S., Pierre, D.S., Olund, B. (1997). Shear tests of fiber concrete beams without stirrups. *Structural Journal*, **94 (1)**, 68–76.

Ahmad, S., Elahi, A., Kundi, S., Haq, W. (2013). Investigation of shear behavior of Corbel beams strengthened with CFRP. *Life Science Journal*, **10**, (12s).

AL-DARRAJI, S.Y. (2018). Self-Compacting Steel Fiber Reinforced Concrete (SCSFRC) Haunched Beam Without Shear Stirrups. M.Sc. Thesis. Gaziantep university.

Al-Rousan, R., Haddad, R. (2013). NLFEA sulfate-damage reinforced concrete beams strengthened with FRP composites. *Composite Structures*, **96**, 433–445.

Al-Sulaimani, G.J., Sharif, A., Basunbul, I.A., Baluch, M.H., Ghaleb, B.N. (1994). Shear repair for reinforced concrete by fiberglass plate bonding. *Structural Journal*, **91 (4)**, 458–464.

ALBEGMPRLI, H. (2017). Experimental Investigation and Stochastic FE Modeling of Reinforced Concrete Haunched Beams. Ph.D. Thesis. Gaziantep Unversity.

Aldahdooh, M.A.A., Muhamad Bunnori, N., Megat Johari, M.A., Jamrah, A., Alnuaimi, A. (2016). Retrofitting of damaged reinforced concrete beams with a new green cementitious composites material. *Composite Structures*, **142**, 27–34.

Alexander, M.G., Beushausen, H.-D., Dehn, F., Moyo, P. (2008). *Concrete Repair, Rehabilitation and Retrofitting II*. ©2009 Taylor & Francis Group, London, UK. Concrete Repair, Rehabilitation and Retrofitting II – Alexander et al (eds) ©2009 Taylor & Francis Group, London, ISBN 978-0-415-46850-3.

ALSHAWAF, A. (2017). Rehabilitation of Heated and Damaged High Strength Self Compacting Steel Fiber Reinforced Concrete Corbels. MS.c. Thesis. Gaziantep Unversity.

Altun, F., Haktanir, T., Ari, K. (2006). Experimental investigation of steel fiber reinforced concrete box beams under bending. *Materials and Structures*, **39 (4)**, 491–499.

Alwan, J.M., Naaman, A.E., Hansen, W. (1991). Pull-out work of steel fibers from cementitious composites: analytical investigation. *Cement and Concrete Composites*, **13 (4)**, 247–255.

Amin, A., Foster, S.J. (2016). Shear strength of steel fibre reinforced concrete beams with stirrups. *Engineering Structures*, **111**, 323–332.

Aoude, H., Belghiti, M., Cook, W., Mitchell, D. (2012). Response of steel fiber-reinforced concrete beams with and without stirrups. *ACI Structural Journal*, **109 (3)**, 359.

Ashour, S.A., Hasanain, G.S., Wafa, F.F. (1992). Shear behavior of high-strength fiber reinforced concrete beams. *Structural Journal*, **89 (2)**, 176–184.

Assih, J., Ivanova, I., Dontchev, D., Li, A. (2015). Concrete damaged analysis in strengthened corbel by external bonded carbon fibre fabrics. *Applied Adhesion Science*, **3 (1)**, 21.

Ayyub, B.M. and McCuen, R.H. (2011). *Probability, statistics, and reliability for engineers and scientists*. CRC press.

Banthia, N., Trottier, J.-F. (1994). Concrete reinforced with deformed steel fibers, part I: bond-slip mechanisms. *ACI Materials Journal*, **91 (5)**, 435–446.

Batson, G., Jenkins, E., Spatney, R. (1972). Steel fibers as shear reinforcement in beams. *ACI Structural Journal*, **69 (10)**, 640–644.

Benyahia, A., Ghrici, M., Mansour, M.S., Omran, A. (2017). Elaboration and characterization of fiber-reinforced self-consolidating repair mortar containing natural perlite powder. *Advances in Concrete Construction*, **5 (1)**, 1–15.

Bousselham, A., Chaallal, O. (2009). Maximum shear strength of RC beams retrofitted in shear with FRP composites. *Journal of Composites for Construction*, **13 (4)**, 302–314.

Casanova, P., Rossi, P. (1997). Can steel fibers replace transverse reinforcements in reinforced concrete beams. *Materials Journal*, **94 (5)**, 341–354.

Cervenka, V., Cervenka, J., Janda, Z., and Pryl, D. (2017). ATENA Program Documentation, Part 8: User's Manual for ATENA-GiD Interface. *Cervenka Consulting, Prague*.

Cervenka, V., Jendele, L., and Cervenka, J. (2016). ATENA Program Documentation, Part 1: Theory. *Praha, Czech Republic*.

Chajes, M.J., Januszka, T.F., Mertz, D.R., Thomson, T.A., Finch, W.W. (1995). Shear strengthening of reinforced concrete beams using externally applied composite fabrics. *Structural Journal*, **92 (3)**, 295–303.

Chen, J.F., Teng, J.G. (2003). Shear capacity of FRP-strengthened RC beams : FRP debonding. *Construction and Building Materials*, **17 (1)**, 27–41.

Chunxiang, Q., Patnaikuni, I. (1999). Properties of high-strength steel fiber-reinforced concrete beams in bending. *Cement and Concrete Composites*, **21 (1)**, 73–81.

Corry, R.W., Dolan, C.W. (2001). Strengthening and Repair of a Column Bracket Using a Carbon Fiber Reinforced Polymer (CFRP) Fabric. *PCI Journal*, **46 (1)**, 54–63.

Cucchiara, C., La Mendola, L., Papia, M. (2004). Effectiveness of stirrups and steel fibres as shear reinforcement. *Cement and concrete composites*, **26 (7)**, 777–786.

Cuenca, E., Serna, P. (2013). Shear behavior of prestressed precast beams made of self-compacting fiber reinforced concrete. *Construction and Building Materials*, **45**, 145–156.

Dancygier, A.N., Savir, Z. (2011). Effects of steel fibers on shear behavior of high-strength reinforced concrete beams. *Advances in Structural Engineering*, **14 (5)**, 745–761.

Debaiky, S.Y. and Elniema, E.I. (1982). Behavior and strength of reinforced concrete haunched beams in shear. *In*: *Journal Proceedings*. 184–194.

Deniaud, C., Cheng, J.J.R. (2001). Shear behavior of reinforced concrete T-beams with externally bonded fiber-reinforced polymer sheets. *Structural Journal*, **98 (3)**, 386–394.

DIN, 1045-1. (2001). EN-Concrete reinforcement and prestressed concrete structures. *Design and construction*, (part 1).

Dinh, Hai H., Parra-Montesinos, Gustavo J and Wight, J.K. (2010). Shear strength model for steel fiber reinforced concrete beams without stirrup reinforcement. *Journal of Structural Engineering*, **137 (10)**, 1039–1051.

Dinh, H.H. (2009). Shear Behavior of Steel Fiber Reinforced Concrete Beams Without Stirrup Reinforcement. Ph.D. Thesis. University of Michigan.

Dinh, H.H., Parra-Montesinos, J.G., Wight, J.K., M.ASCE. (2010). Shear strength model for steel fiber reinforced concrete beams without stirrup reinforcement. *Journal of structural engineering*, **137 (10)**, 1039–1051.

Elgwady, M.A., Rabié, M., and Mostafa, M.T. (2005). Strengthening of corbels using CFRP an experimental program. *Cairo University, Giza, Egypt*.

Erfan, A.M., Abdel-Rahman, G.T., Nassif, M.K., Hammad, Y.H. (2010). Behavior of reinforced concrete corbels strengthened with CFRP fabrics. *Benha University*.

Faisal, F.W., Ashour, S.A. (1992). Mechanical properties of high-strength fiber reinforced concrete. *ACI Material journal*, **89 (5)**, 449–455.

Fattuhi, N.I. (1990). Strength of SFRC Corbels Subjected to Vertical Load. *Journal* *of Structural Engineering*, **116 (3)**, 701–718.

Foster, S.J., Malik, A.R. (2002). Evaluation of efficiency factor models used in strut-and-tie modeling of nonflexural members. *Journal of Structural Engineering*, **128 (5)**, 569–577.

Foster, S.J., Powell, R.E., Selim, H.S. (1996). Performance of high-strength concrete corbels. *Structural Journal*, **93 (5)**, 555–563.

Godat, A., Neale, K.W., Labossière, P. (2007). Numerical modeling of FRP shear-strengthened reinforced concrete beams. *Journal of Composites for Construction*, **11 (6)**, 640–649.

Godínez-Domínguez, E.A., Tena-Colunga, A., Juárez-Luna, G. (2015). Nonlinear finite element modeling of reinforced concrete haunched beams designed to develop a shear failure. *Engineering Structures*, **105**, 99–122.

Haddad, R.H., Al-Mekhlafy, N., Ashteyat, A.M. (2011). Repair of heat-damaged reinforced concrete slabs using fibrous composite materials. *Construction and Building Materials*, **25 (3)**, 1213–1221.

Haddad, R.H., Shannag, M.J., Hamad, R.J. (2007). Repair of heat-damaged reinforced concrete T-beams using FRC jackets. *Magazine of Concrete Research*, **59 (3)**, 223–231.

Haddad, R.H., Shannag, M.J., Moh'd, A. (2008). Repair of heat-damaged RC shallow beams using advanced composites. *Materials and Structures*, **41 (2)**, 287–299.

Harba, I.S.I., Abdulridha, A.J. (2017). Finite Element Analysis of RC Tapered Beams under Cyclic Loading. *Al-Nahrain Journal for Engineering Sciences*, **20 (2)**, 378–396.

hasssan, A.C. (2015). Reliability analysis of reinforced concrete haunched beams shear capacity based on stochastic nonlinear FE analysis. *Computers and Concrete*, **15 (2)**, 259–277.

He, Z.-Q., Liu, Z., Ma, Z.J. (2012). Investigation of load-transfer mechanisms in deep beams and corbels. *ACI Structural Journal*, **109 (4)**, 467.

Hollaway, L.C., Teng, J.-G. (2008). *Strengthening and rehabilitation of civil infrastructures using fibre-reinforced polymer (FRP) composites*. Elsevier.

Hussein, T. (2017). Rehabilitation of Heated and Damaged Normal Strength Self Compacting Steel Fiber Reinforced Concrete Corbels. MS.c. Thesis. Gaziantep Unversity.

Hwang, J.H., Lee, D.H., Ju, H., Kim, K.S., Kang, T.H.K., Pan, Z. (2016). Shear Deformation of Steel Fiber-Reinforced Prestressed Concrete Beams. *International Journal of Concrete Structures and Materials*, **10**, 53–63.

Hwang, S.-J., Lee, H.-J. (2002). Strength prediction for discontinuity regions by softened strut-and-tie model. *Journal of Structural Engineering*, **128 (12)**, 1519–1526.

Hwang, S.-J., Lu, W.-Y., Lee, H.-J. (2000). Shear strength prediction for reinforced concrete corbels. *Structural Journal*, **97 (4)**, 543–552.

Islam, M.S. Alam, S. (2013). Principal Component and Multiple Regression Analysis for Steel Fiber Reinforced Concrete (SFRC) Beams. *International Journal of Concrete Structures and Materials*, **7 (4)**, 303–317.

Ivanova and Assih, J. (2015). Static and dynamic experimental study of strengthened inforced short concrete corbel by using carbon fabrics, crack path in shear zone. *Frattura ed Integrita Strutturale*, (34).

Ivanova, Assih, J., Li, A., Delmas, Y. (2014). Influence of Fabrics Layers on Strengthened Reinforced Concrete Short Corbels.". *International Journal of Civil Engineering and Technology*, **5**, 33–43.

Ivanova, I., Assih, J. (2015). Experimental Study of Local Behavior of Strengthened Reinforced Concrete Short Corbel by Bonding Carbon Fiber Fabrics. *International Journal of Structureal and Civil Engineering Research*, **4 (1)**.

Ivanova, I., Assih, J. (2016). The effect of fatigue test on short reinforced-concrete corbel strengthened by externally bonded composite fibre fabrics. *Engineering Fracture Mechanics*, **167**, 167–175.

Ivanova, I., Assih, J., Dontchev, D. (2016). Mechanical Pathologies of Reinforced and Damaged Concrete Corbels by Gluing Composite Carbon Fabrics Under Static and Dynamic Tests. *In*: *Sustainable Construction*. Springer, 185–211.

Ivanova, I., Assih, J., Li, A., Dontchev, D., Delmas, Y. (2015). Experimental investigation into strengthened short reinforced concrete corbels by bonding carbon fiber fabrics. *Journal of Adhesion Science and Technology*, **29 (20)**, 2176–2189.

Janda, Z., Prochazkova, Z., Cervenka, J., Pryl, D., and Mikolášková, J. (2016). ATENA Program Documentation Part 4-6 ATENA Science – GiD Tutorial. *Cervenka Consulting, Prague*.

Jolly, A., Vijayan, V. (2016). Structural Behaviour of Reinforced Concrete Haunched Beam A Study on ANSYS and ETABS. *IJISET - International Journal of Innovative Science, Engineering & Technology*, **3 (8)**, 495–500.

Kara, I.F. (2013). Empirical modeling of shear strength of steel fiber reinforced concrete beams by gene expression programming. *Neural Computing and Applications*, **23 (3–4)**, 823–834.

Karl, K.-W., Lee, D.-H., Hwang, J.-H., Kim, K.-S., Choi, I.-S. (2011). Revision on material strength of steel fiber-reinforced concrete. *International Journal of Concrete Structures and Materials*, **5 (2)**, 87–96.

Khalifa, A., Gold, W.J., Nanni, A., M.I., A.A. (1998). Contribution of Externally Bonded FRP to Shear Capacity of RC Flexural Members. *Journal of Composites for Construction*, **2 (4)**, 195–202.

Khalifa, A. Nanni, A. (2000). Improving shear capacity of existing RC T-section beams using CFRP composites. *Cement and Concrete Composites*, **22 (3)**, 165–174.

Khuntia, M., Stojadinovic, B., Goel, S.C. (1999). Shear strength of normal and high-strength fiber reinforced concrete beams without stirrups. *ACI Structural Journal*, **96 (2)**, 282–289.

Kumar, R.A., Selvamony, C., Seeni, A., Sethuraman, T.R. (2015). Retrofitting Of RCC Piles By Using Basalt Fiber Reinforced Polymer (BFRP) Composite, Part : 1 Review Papers On RCC Structures And Piles Retrofitting Works. *Internatıonal journal of scıentıfic & technology research volume*, 4 (01).

Kumar, R.A., Selvamony, C., Seeni, A., Sethuraman, T.R. (2015). Retrofitting Of RCC Piles By Using Basalt Fiber Reinforced Polymer (BFRP) Composite, Part: 1

Review Papers On RCC Structures And Piles Retrofitting Works. *International Journal of Technology Enhancements and Emerging Engineering Research*, **4 (1)**, 103–115.

Lee, K., Al-Mahaidi, R., Taplin, G. (2000). Non-Linear Finite Element Modelling of Shear-Damaged Concrete T-Beams Repaired with CFRP Laminates. *In*: *(ACUN-2) International composites conference, Sydney, New South Wales, Australia, February*.

Lee, S.C., Cho, J.Y., Vecchio, F.J. (2013). Simplified diverse embedment model for steel fiber-reinforced concrete elements in tension. *ACI Materials Journal*, **110 (4)**, 403–412.

Leonardi, A., Meda, A., Rinaldi, Z. (2011). Fire-damaged R/C Members Repair With High-Performance Fibre-Reinforced Jacket. *Strain*, **47 (s2)**, 28–35.

Li, V.C., Ward, R., Hamza, A.M. (1992). Steel and synthetic fibers as shear reinforcement. *ACI Materials Journal*, 499–508.

Lim, T.Y., Paramasivam, P., Lee, S.L. (1987). Shear and moment capacity of reinforced steel-fibre-concrete beams. *Magazine of concrete research*, **39 (140)**, 148–160.

MacLeod, I.A., Houmsi, A. (1994). Shear strength of haunched beams without shear reinforcement. *Structural Journal*, **91 (1)**, 79–89.

Mansoori, I. (2017). Shear Rehabilitation of Reinforced Concrete Haunched Beam with CFRP. M.Sc. Thesis. Gaziantep University.

Mansur, M.A., Ong, K.C.G., Paramasivam, P. (1986). Shear strength of fibrous concrete beams without stirrups. *Journal of structural engineering*, **112 (9)**, 2066–2079.

Megahid, A.E.-R., Rashwan, M.M., Sayed, A.M. (2010). Static behaviour of reinforced high strength concrete haunched beams strenghened by using epoxy bonded external steel plates. *Journal of Engineering Sciences*, **38 (6)**, 1391–1428.

Menetrey, P. Willam, K.J. (1995). Triaxial failure criterion for concrete and its generalization. *Structural Journal*, **92 (3)**, 311–318.

Michels, J., Christen, R., Waldmann, D. (2013). Experimental and numerical investigation on postcracking behavior of steel fiber reinforced concrete. *Engineering Fracture Mechanics*, **98 (1)**, 326–349.

Mofidi, A., Chaallal, O. (20100. Shear strengthening of RC beams with EB FRP: Influencing factors and conceptual debonding model. *Journal of Composites for Construction*, **15 (1)**, 62–74.

Naaman, A.E., Najm, H. (1991). Bond-slip mechanisms of steel fibers in concrete. *ACI Materials Journal*, **88 (2)**, 135–145.

Narayanan, R., Darwish, I.Y.S. (1987). Use of steel fibers as shear reinforcement. *Structural Journal*, **84 (3)**, 216–227.

Nghiep, V.H. (2011). Shear design of straight and haunched concrete beams without stirrups. Ph.D. Thesis. Technische Universität Hamburg.

No, I., n.d. 03730, and to the satisfaction of the Engineer.

pellegrino C., Modena. (2002). Fiber reinforced polymer shear strengthening of reinforced concrete beams with transverse steel reinforcement. *composites for construction*, **6 (2)**, 101–111.

pellegrino C., Modena. (2006). Fiber-reinforced polymer shear strengthening of reinforced concrete beams: Experimental study and analytical modeling. *ACI Structural Journal*, **15 (5)**, 720–728.

Di Prisco, M., Plizzari, G., Vandewalle, L. (2009). Fibre reinforced concrete: new design perspectives. *Materials and Structures*, **42 (9)**, 1261–1281.

Romualdi, J.P. Mandel, J.A. (1964). Tensile strength of concrete affected by uniformly distributed and closely spaced short lengths of wire reinforcement. *In*: *Journal Proceedings*, **61 (6)**, 657–672.

Roy, A., Sharma, U., Bhargava, P. (2014). Strengthening of heat damaged reinforced concrete short columns. *Journal of Structural Fire Engineering*, **5 (4)**, 381–398.

Roy, A.B.D., Sharma, U.K., Bhargava, P. (2015). Confinement strengthening of heat-damaged reinforced concrete columns. *Magazine of Concrete Research*, **68 (6)**, 291–304.

Russo, G., Venir, R., Pauletta, M., Somma, G. (2006). Reinforced concrete corbels-shear strength model and design formula. *ACI Structural Journal*, **103 (1)**, 3.

Sahoo, D.R. Kumar, N. (2015). Monotonic behavior of large-scale SFRC beams without stirrups. *Engineering Structures*, **92**, 46–54.

Sahoo, D.R. Sharma, A. (2014). Effect of steel fiber content on behavior of concrete beams with and without stirrups. *ACI Structural Journal*, **111 (5)**, 1157–1166.

Sajdlová, T. (2016). ATENA Program Documentation Part 4-9 ATENA Science – GiD Strengthening of concrete structures. *Cervenka Consulting, Prague*.

Sasmal, S., Kalidoss, S., Srinivas, V. (2012). Nonlinear Finite Element Analysis of FRP Strengthened Reinforced Concrete Beams. *Journal of The Institution of Engineers (India): Series A*, **93 (4)**, 241–249.

Shadhan, Khalid K., Kadhim, M.M.M. (2015). Use of CFRP Laminates For Strengthening of Reinforced Concrete Corbels. *International Journal of Civil Engineering and Technology*, **6 (11)**, 11–20.

Sharma, A. (1986). Shear Strength of Steel Fiber Reinforced Concrete Beams. *ACI Structural Journal*, **83 (4)**, 624–628.

Shoaib, A., Lubell, A.S., Bindiganavile, V.S. (2014). Size Effect in Shear for Steel Fiber Reinforced Concrete Members without Stirrups. *ACI Structural Journal*, **111 (5)**, 1081.

Shoaib, A., Lubell, A.S., Bindiganavile, V.S. (2014). Size effect in shear for steel fiber-reinforced concrete members without stirrups. *ACI Structural Journal*, **111 (5)**, 1081.

Sika Company. (2014). Product Sheet of Sikadur-52 Injection Type N [online]. Available from: https://www.sika.com.

Slater, E., Moni, M., Alam, M.S. (2012). Predicting the shear strength of steel fiber reinforced concrete beams. *Construction and Building Materials*, **26 (1)**, 423–436.

Song, P.S. Hwang, S. (2004). Mechanical properties of high-strength steel fiber-reinforced concrete. *Construction and Building Materials*, **18 (9)**, 669–673.

Soroushian, P. Lee, C. D. (1990). Distribution and orientation of fibers in steel fiber reinforced concrete. *Materials Journal*, **87 (5)**, 433–439.

Spinella, N., Colajanni, P., La Mendola, L. (2012). Nonlinear Analysis of Beams Reinforced in Shear with Stirrups and Steel Fibers. *ACI Structural Journal*, **109 (1)**, 53.

Tekno Construction Chemicals. (2016). Product Sheets of Tekno Bond 200 and 300 [online]. Available from: https://www.teknoyapi.com.tr.

Tena-Colunga, A., Archundia-Aranda, H.I., González-Cuevas, Ó.M. (2008). Behavior of reinforced concrete haunched beams subjected to static shear loading. *Engineering Structures*, **30 (2)**, 478–492.

Tena-Colunga, A., Urbina-Californias, L.A., Archundia-Aranda, H.I. (2017). Assessment of the shear strength of continuous reinforced concrete haunched beams based upon cyclic testing. *Journal of Building Engineering*, **11**, 187–204.

Tena-Colunga, A., Urbina-Californias, L.A., Archundia-Aranda, H.I. (2017). Cyclic behavior of continuous reinforced concrete haunched beams with transverse reinforcement designed to fail in shear. *Construction and Building Materials*, **151**, 546–562.

Tena, A. Hernández, O. (2009). Reinforced concrete haunched beams deficient in shear rehabilitated with jacketing of mortar and welded wire mesh. *BOLETÍN TÉCNICO*, **47 (2)**, 37–56.

The European Project Group. (2005). The European Guidelines for Self-Compacting Concrete. *The European Guidelines for Self Compacting Concrete*, (May), 63.

Toumi, B., Resheidat, M., Guemmadi, Z., Chabil, H. (2009). Coupled effect of high temperature and heating time on the residual strength of normal and high-strength concretes. *Jordan Journal of Civil Engineering*, **3 (4)**, 322–330.

Triantafillon, T.C, A. (2000). Design of concrete flexral members strengthened im shear with FRP. *Journal of Composites for Construction*, **4 (4)**, 198–205.

Triantafillou, T.C. (1998). A new possibility for the shear strengthening of concrete, masonry and wood. *composites for construction*, **4 (4)**, 198–205.

Voo, Y.L., Foster, S.J., Gilbert, R.I. (2006). Shear strength of fiber reinforced reactive powder concrete prestressed girders without stirrups. *Journal of Advanced Concrete Technology*, **4 (1)**, 123–132.

Vora, P.J. Patel, P.C.D. (2014). Basalt Fibers Used in Structural Retrofitting. *IJSRD - International Journal for Scientific Research & Development*, **2 (10)**, 387–389.

Wong, R.S.Y. Vecchio, F.J. (2003). Towards modeling of reinforced concrete members with externally bonded fiber-reinforced polymer composites. *ACI Structural Journal*, **100 (1)**, 47–55.

Yaqub, M. Bailey, C.G. (2011). Repair of fire damaged circular reinforced concrete columns with FRP composites. *Construction and Building Materials*, **25 (1)**, 359–370.

Yaqub, M. Bailey, C.G. (2011). Cross sectional shape effects on the performance of post-heated reinforced concrete columns wrapped with FRP composites. *Composite Structures*, **93 (3)**, 1103–1117.

Yaqub, M., Bailey, C.G., Nedwell, P. (2011). Axial capacity of post-heated square columns wrapped with FRP composites. *Cement and Concrete Composites*, **33 (6)**, 694–701.

Yaqub, M., Bailey, C.G., Nedwell, P., Khan, Q.U.Z., Javed, I. (2013). Strength and stiffness of post-heated columns repaired with ferrocement and fibre reinforced polymer jackets. *Composites Part B: Engineering*, **44 (1)**, 200–211.

Yong, Y.-K. Balaguru, P. (1994). Behavior of reinforced high-strength-concrete corbels. *Journal of Structural Engineering*, **120 (4)**, 1182–1201.

Yoo, D.Y., Yoon, Y.S., Banthia, N. (2015). Flexural response of steel-fiber-reinforced concrete beams: Effects of strength, fiber content, and strain-rate. *Cement and Concrete Composites*, **64**, 84–92.

CURRICULUM VITAE

PERSONAL INFORMATION

Name Surname: Mohammed Shakib Mohammed AL JAWAHERY

Nationality: Iraqi

Place of birth/Date of birth: Mosul / 20 April 1982

Marital status: Married

Phone: +90 5343722664/+9647508454001

Email: mohammed.shakib@dpu.edu.krd - phdcivilengineering82@gmail.com

EDUCATION INFORMATION

M.Sc. Degree in Civil Engineering-Structures-University of Mosul 2009

B.Sc. Degree in Civil Engineering-University of Mosul 2005

WORK EXPERIENCE

2005 – 2011/ Site Engineer in many engineering projects

2011- present / Assist. Lecturer at Duhok Polytechnic university - Akrea technical Institute

Duhok / Iraq.

FOREIGN LANGUAGE

English, Arabic, and Kurdish

JOURNAL ARTICLES

Gülşan, M. E., **Al Jawahery, M. S.**, Alshawaf, A. H., Hussein, T. A., Abdulhaleem, K.N., Çevik, A. (2018). Rehabilitation of Normal and Self-Compacted Steel Fiber Reinforced Concrete Corbels via Basalt Fiber. *Advances in Concrete Construction,* **6 (5)**, 423-463, doi.org/10.12989/acc.2018.6.5.423.

Gülşan, M. E., **Al Jawahery, M. S**., Albegmprli, H. M. A., Çevik, A. (2018). Rehabilitation of RC Haunched Beams via Basalt Fabric: Experimental Study and FE Modeling. *Steel and Composite Structures*, (**Under review)**.

Al Jawahery, M. S., Çevik, A., Gülşan, M. E. (2018). 3D FE Modeling of Steel Fiber Reinforced Concrete Haunched Beams. *Structural Engineering and Mechanics*, (**Under review**).

Al Jawahery, M. S., Gulsana, M. E., Mansoorib, I. A. H., Albegmprlic, H. M., Çevik, A. (2018). Experimental Investigation and 3D-FE modeling of Rehabilitation RC Haunched Beams by CFRP, (**Sending processing**).